Inelastic Lateral Instability Of Beams And Their Bracing Requirements.

INELASTIC LATERAL INSTABILITY OF BEAMS AND THEIR BRACING REQUIREMENTS

by

George Chao-Chi Lee

A DISSERTATION

Presented to the Graduate Faculty
of Lehigh University
in Candidacy for the Degree of
Doctor of Philosophy

Lehigh University
1960

Approved and recommended for acceptance as a dissertation in partial fulfillment of the requirement for the degree of Doctor of Philosophy.

Aug. 12, 1960
(Date)

Theodore V. Galambos
Theodore V. Galambos
Professor in Charge

Accepted, Sept. 6, 1960
(Date)

Special committee directing the doctoral work of Mr. George C. Lee

Lynn S. Beedle
Professor Lynn S. Beedle, Chairman

George C. Driscoll, Jr.
Professor George C. Driscoll, Jr.

Samuel L. Gulden
Professor Samuel L. Gulden

William J. Eney
Professor William J. Eney

Theodore V. Galambos
Professor Theodore V. Galambos

ACKNOWLEDGMENT

The author is deeply indebted to Dr. Theodore V. Galambos, professor in charge of this dissertation, for his encouragement, advice and suggestions during the preparation of this report. The guidance of Professors Lynn S. Beedle, George C. Driscoll, Jr., and Samuel L. Gulden, chairman and members respectively of the Special Committee directing the author's doctoral work, and of Dr. David M. Parke, guest member of the Special Committee, is greatly appreciated. The author also wishes to express his sincere gratitude to Dr. Robert L. Ketter and Dr. Bruno Thürlimann for their helpful advice during the period of development, and to Dr. Akira Nitta for his valuable suggestions and criticisms during the preparation of Chapter 5, of this dissertation.

The work is part of a project on "Welded Continuous Frames and Their Components" being carried out under the general direction of Dr. Lynn S. Beedle. The project is sponsored jointly by the Welding Research Council and the United States Navy Department under an agreement with the Institute of Research of Lehigh University. Funds are supplied by the American Institute of Steel Construction, Office of the Naval Research, Bureau of Ships, and the Bureau of Yards and Docks. The Column Research Council of the Engineering Foundation acts in an advisory capacity. Technical guidance for this project is furnished by the Lehigh Project Subcommittee, Welding Research Council. Mr. T. R. Higgins is Chairman of the Lehigh Project Subcommittee. Valuable suggestions offered by Mr. Higgins

and the Subcommittee members are sincerely appreciated.

The author wishes to acknowledge all his associates working on the same research project of plastic design for fruitful discussions throughout this investigation. He also wishes to express his thankfulness to Mr. Samuel J. Errera, Engineer of Tests, and to Mr. Kenneth R. Harpel, Foreman, of the Fritz Engineering Laboratory, for their cooperation in the preparation of experiments. Professor William J. Eney is Director of the Fritz Engineering Laboratory and the Head of the Department of Civil Engineering.

Various calculations and drawings in this dissertation were made efficiently by Mr. D. P. Jen. The experiments and the calculations of test data were assisted by Mr. Yukio Ueda. Their cooperation is greatly appreciated. The author is also grateful to Miss Grace E. Mann for her careful typing and proofreading of the manuscript.

TABLE OF CONTENTS

Page

Page

A B S T R A C T

This dissertation presents the results of a theoretical and experimental study of the inelastic load-deformation behavior of structural steel beams subjected to uniform moment.

An upper bound solution for the critical buckling length of simply supported wide-flange beams subjected to full plastic moment ($L_{cr} = 40r_{yy}$) is obtained. The theoretical solutions are substantiated by experiments on simply supported beams with idealized supports.

From the results of these experiments it is concluded that a beam can develop satisfactory plastic hinge rotations in the post-buckling range provided the slenderness ratio is not more than 40. These tests show also, that the usefulness of the plastic strength of such beams is controlled by the local instability of the compression flange, and that the rotation capacity does not depend upon the occurrence of lateral buckling.

Further experiments on beams supported by bracing members of practical proportions are performed. These beam-purlin tests indicate that the flexible bracing members are fully as adequate as rigid lateral braces to insure the development of a plastic hinge provided that their lateral stiffness is above a certain critical value.

A theory considering the interaction of deformation variables is developed for obtaining the post-buckling behavior of beams governed by lateral-torsional instability. The theory also accounts for initial imperfection of loading and member geometry (biaxial bending).

I. INTRODUCTION

1.1 THE DEFINITION OF LATERAL-TORSIONAL INSTABILITY AND ITS IMPORTANCE IN STRUCTURAL DESIGN

The phenomenon of lateral buckling is illustrated by the behavior of the single-span wide-flange beam shown in Fig. 1.1a. This beam is subjected to two equal end moments M_{xx} which are applied about the strong axis, and the beam is assumed to be free from any initial deformations. If the moments are increased from zero to their maximum value, the schematic moment versus deformation behavior of the beam will be as shown in Fig. 1.1b. This curve represents the relationship between M_{xx} and the deflection v of the beam in the direction of the applied moments. It would be expected that the M-v behavior would follow the dashed curve, and that the value of the maximum moment would approach the full plastic moment M_p as an asymptote. However, this M-v equilibrium relationship will bifurcate at a certain critical moment value which is less than M_p; at this point of bifurcation lateral deflection associated with twist will take place in addition to the vertical flexural deformation of the beam cross sections. After some lateral-torsional deformations have taken place, the moment is reduced and the beam is considered to have failed by lateral-torsional buckling (or simply lateral buckling).

Lateral buckling has been under investigation for the past 60 years (pertinent references summarizing this work will be given in appropriate sections of this dissertation). However, certain problems related to lateral buckling in the inelastic range need further study and clarification. More specifically,it is desirable to obtain an answer to the following two questions:

(a) At what spacing must lateral supports be placed so that failure by lateral buckling of the member is postponed until the desired strength and rotation of the member can be achieved?

(b) How should lateral supports be designed so that they provide adequate strength and stiffness in order to permit the braced member to reach its desired carrying capacity?

In this dissertation these and several related problems will be studied in order to determine the scope and the applicability of recently developed methods in plastic design of metal structures, and to provide new information useful to the research worker and to the structural designer.

1.2 PROBLEMS ASSOCIATED WITH THE LATERAL-TORSIONAL INSTABILITY OF BEAMS

The various problems connected with the inelastic lateral instability of beams may be classified in the following categories:

(A) Determination of the buckling strength (Initial motion solution).

(a) Lower bound buckling solution.

(b) Upper bound buckling solution.

(B) Determination of the ultimate strength.

(a) Post-buckling solution.

(b) Biaxial bending solution.

(c) Initial imperfection solution.

(C) Bracing requirements.

(a) Stiffness requirement.

(b) Strength requirement.

The various problems contained in categories A and B can be explained with the aid of Figs. 1.1 and 1.2. In Fig. 1.1a is shown a simply supported beam which is subjected to end moments M_{xx} applied about the strong axis. As these moments increase, but before the critical buckling moment $(M_{xx})_{cr}$* has been reached, the beam sections remain symmetrical with respect to the plane of bending. At this stage, the only deformation of the beam is in the direction of the applied moments (denoted by v). The M_{xx}-v curve is shown in Fig. 1.1b. At point A, yielding of the member starts at some portions of the cross section. (It will be assumed here that lateral buckling does not start in the elastic range.) Further increase of moment will cause a nonlinear relationship between M_{xx} and v (see Fig. 1.1b). This, however, does not mean

---

*The critical moment is defined here as the point of bifurcation of the equilibrium.

that the beam is useless. In fact, the beam may continue to carry a considerable amount of additional moment after first yield. The moment carrying capacity of the beam is limited only by its full plastic moment M_p, or if lateral buckling (or local buckling) sets in first, by the maximum lateral buckling (or local buckling) moment $(M_{xx})_{max}$.

At the critical buckling moment the beam will begin to deflect laterally (u) and at the same time twist (β). When this moment is exceeded, deformations u and β will increase. The schematic relationship between the applied moment and these deformations is shown in Fig. 1.1c. In this figure point A represents initiation of yielding of the material. Point B corresponds to the point of the bifurcation of the equilibrium. (The beam buckles at point B.) The moment value corresponding to point D in Fig. 1.1c is the maximum carrying capacity of the beam. After this point the moment will decrease as deformations further increase (point E) and the beam is considered to have failed.

The moment-deformation phenomenon represented by curve BDE corresponds to the post-buckling behavior of the beam. It is important to determine this curve not only for the purpose of obtaining the true maximum strength, but also for the purpose of finding the rotation capacity of the member.

The curves in Fig. 1.1 represent the behavior of an ideally straight member. Generally a beam is not free of imperfections, and the load is not applied precisely in the plane of one axis

alone. These imperfections in beam geometry and loading lead to the problem of moments applied about both of the principal axes of the cross section.

The phenomena of biaxial bending and initial imperfections are very similar to the earlier mentioned post-buckling problem of a beam failing by lateral instability. In Fig. 1.2a is shown a single span wide-flange beam subjected to end couples in two directions. In this case the moment-deformation relationships are different from those that result when the beam is bent by couples in one direction only, since the lateral-torsional deformation components u and β occur as soon as the moments are applied. The moment-deformation curves are plotted in Fig. 1.2b. When a beam is subjected to bending in one direction only but has initial deformations, the moment-deformation curves are similar to that given in Fig. 1.2b.

The various problems described above will be defined more specifically.* Those included in category A (See page 4.) are initial motion or buckling problems. Solutions will result in relationships between the critical buckling load and the unsupported length only. As with the buckling phenomena of an axially loaded column,[1] the two different concepts of tangent modulus and reduced modulus can be used to obtain lower bound and upper bound solutions. The lower bound solution is obtained by

*In this dissertation only the problems of inelastic instability will be considered.

considering no unloading in fiber stress, whereas the upper bound solution includes the unloading effect for calculating the effective rigidities of elastic-plastic cross sections. (See Chapter I of Ref. 1.)

Problems related to the category of ultimate strength solutions are basically different. (Category B on page 4). To solve such a problem a particular length of the member will be given first. Sufficient repetitions on this process for various lengths will then give the final solution for the maximum load versus length relationship. Problems of such nature are termed "ultimate strength solutions" throughout this dissertation. It will be noted that this solution is handicapped by the interaction of the three deformation components: u, v and β; furthermore, in a three-dimensional deformed equilibrium state the yielded configuration in the cross section is unsymmetrical and the combined flexural and torsional resistance of such sections had not been determined as yet. To attempt a solution for any of these ultimate strength problems it is necessary to use a step-by-step trial procedure. Problems in this category are usually referred to as instability problems without bifurcation. This implies that on any load-deformation curve at ultimate load is the point of instability (that is, the point of indifferent equilibrium). However, as mentioned earlier, buckling problems also possess equilibrium in the load-deformation behavior in the post-buckling range. (See Fig. 1.1c.) Therefore in this dissertation the term "instability"

is used for both buckling and ultimate strength problems. In more specific cases the terms "buckling solution" or the "ultimate strength solution" will be used appropriately.

All the previously described instability problems can be explained by typical moment versus length curves as shown in Fig. 1.3. In this figure, failure by lateral instability is considered in three different ranges. For large slenderness ratios buckling takes place when the material is in the elastic range.* This range is represented by the curve PQ. Point Q is the proportional limit. In the elastic-plastic range QR three curves are shown. The lower curve B is obtained on the basis of the tangent modulus concept and is the lower bound solution[3] (point B in Fig. 1.1b), and the upper curve C represents the upper bound or the reduced modulus buckling load.[4] Curve D in Fig. 1.3 is the ultimate strength curve, which can be either a post-buckling solution, or a biaxial bending solution, or an initial imperfection solution depending on the degree of precision in the solution.

For small slenderness ratios lateral instability may occur in the strain-hardening range, where the curves B, C and D denote the same types of solutions as they do in the elastic-plastic range. Of special interest are the points R_B, R_C, and R_D. These

---

*The problems of elastic buckling have been largely solved. A summary of solutions is given in Ref. 2.

points signify respectively the critical unsupported lengths determined by the different methods at the full plastic moment. In Ref. 5 a solution for the determination of point R_B is presented which represents a lower bound of the slenderness ratio for beams subjected to plastic moment. One further remark may be made about the curves RS in Fig. 1.3: Curve R_BS (the lower bound buckling curve) and R_CS (the upper bound buckling curve) do not have as much significance as they do in the elastic-plastic range. For failure in the strain-hardening range a member must be very short; if the member is so porportioned that local buckling cannot occur, the maximum load carrying capacity of the member would be considerably higher than the lower bound lateral buckling load but much less than the upper bound value. (See Fig. 1.3) Thus in the strain-hardening range the maximum strength curve D is the only one of practical importance.

1.3 THE EQUATIONS OF EQUILIBRIUM

In establishing the equilibrium equations, the deformations of the member are referred to two sets of coordinate axes (x,y,z) and (ξ, η, ζ) as shown in Fig. 1.1a or Fig. 1.2a. The (x,y,z) system applies prior to and the (ξ, η, ζ)system after, the occurrence of lateral deformations of the beam cross sections. The ξ - and η- axes are chosen to correspond to the principal

axes at the shear center of any section S-S with lateral-torsional deformations. The ξ axis is in the direction of the tangent to the center line at this section. For a member of thin-walled open cross section subjected to bending moments in the strong direction only, the equilibrium equation can be written in the following form (Refs. 6, 7 and 8).

$$-B_{xx}\frac{d^2v}{dz^2} = M_{xx} \qquad \text{(a)}$$

$$-B_{yy}\frac{d^2u}{dz^2} = -M_{xx}\cdot\beta \qquad \text{(b)} \qquad (1.1)$$

$$-C_w\frac{d^3\beta}{dz^3} + C_T\frac{d\beta}{dz} = -M_{xx}\frac{du}{dz} \qquad \text{(c)}$$

where M_{xx} = Applied moment about the strong axis

B_{xx} = Flexural rigidity in the strong direction

B_{yy} = Flexural rigidity in the lateral direction

C_w = Warping torsional rigidity

C_T = St. Venant's torsional rigidity

It is seen that the deflection in the vertical direction is independent of the other two deformations, whereas the deflections u and β are dependent on each other. Equations 1.1b and 1.1c are the governing equations for lateral-torsional buckling of beams subjected to equal terminal moments M_{xx}. For any given set of boundary conditions Eq. 1.1 will yield the critical moment

and the critical length as the eigenvalue of the differential equations.[9] For simply supported ends (as shown in Fig. 1.1a) the buckling solution is given by[1]

$$(M_{xx})_{cr} = \sqrt{\frac{\pi^2}{L} C_T B_{yy} \left[1 + \frac{\pi^2}{L^2} \frac{C_w}{C_T}\right]} \qquad (1.2)$$

where $(M_{xx})_{cr}$ is the critical buckling moment and L is the unsupported length. Because of the nature of the method of approach, the deformation components are indeterminate.

Equation 1.2 may be written in terms of the critical buckling length as given in Ref. 5,

$$L_{cr} = \frac{\pi}{M_{xx}} \sqrt{C_T B_{yy}} \left[1 - \frac{\pi^2}{L_{cr}^2} \frac{C_w}{C_T}\right]^{\frac{1}{2}} \qquad (1.3)$$

when St. Venant's torsion is governing (long critical lengths), or

$$L_{cr} = \pi \sqrt{\frac{C_w B_{yy}}{M_{xx}^2}} \left[1 + \frac{1}{\frac{\pi^2}{L_{cr}^2} \frac{C_T}{C_w}}\right]^{\frac{1}{4}} \qquad (1.4)$$

when warping torsion is governing (short beams).

The equilibrium equations for beams subjected to inclined end couples as shown in Fig. 1.2a (that is, moments about both principal axes) can be written in the following form: (Refs. 10 and 11.)

$$-B_{xx}\frac{d^2v}{dz^2} = -M_{xx} + M_{yy}\cdot\beta \qquad \text{(a)}$$

$$-B_{yy}\frac{d^2u}{dz^2} = -M_{xx}\cdot\beta - M_{yy} \qquad \text{(b)} \quad (1.5)$$

$$-C_w\frac{d^3\beta}{dz^3} + C_T\frac{d\beta}{dz} = -M_{xx}\frac{du}{dz} + M_{yy}\frac{dv}{dz} \qquad \text{(c)}$$

where the nomenclature is the same as for Eq. 1.1.

Equation 1.5 cannot yield eigenvalue solutions because of the nature of these differential equations. Instead, this type of solution involves the relationship between the applied moment, the unsupported length and the deformation components. For any given length of the beam, the moment versus deformation relationships are uniquely defined. This is similar to the problem of beam-columns. By contrast, Eqs. 1.1 represent a bifurcation problem. Detailed presentation of these two types of solutions will be treated in the subsequent chapters in this dissertation.

1.4 THE PROBLEM OF LATERAL BRACING

Thus far only the buckling problems and the ultimate strength problems have been discussed. Solutions to these problems will provide sufficient information to structural engineers in answering the question of lateral bracing spacing. As described in Art. 1.1 the problem of the stiffness and strength of the lateral bracing is of equal importance (Category C on page 4).

The equilibrium equations for solving such a problem are similar to Eqs. 1.5. However, the formulation of the required boundary conditions is extremely complicated. A rigorous analysis of such problems should consider at least the following major factors:

(a) Beam size, length and loading.

(b) Bracing size, length and loading.

(c) Beam deformations.

(d) Position and method of bracing attachment.

(e) Design procedure requirements (rotation requirements of beams).

A limited number of investigations have considered a few of these factors.[12][13][14] It was concluded that in conventional design the lateral bracing forces are small and the problem of lateral bracing in structural design is not critical. This

conclusion, however, may not be valid for plastic design, since the deformations which must be sustained by the beam at failure are considerably larger. No theoretical solution has yet been found; thus an experimental approach followed.

1.5 THE REQUIREMENTS OF PLASTIC ANALYSIS AND DESIGN*

One basic assumption made in plastic design is that at certain sections of a structure, plastic hinges can occur. These hinges rotate through finite angles until the structure becomes a failure mechanism. The required rotation capacity of a given plastic hinge depends upon its location in the structure and on the loading.[17] To achieve these large inelastic rotations it is necessary to impose more severe design restrictions with respect to lateral instability. As can be seen from Fig. 1.3, the requirement of plastic design concerning the lateral-torsional strength of a member covers all the QRS curves.

Three solutions are available for bracing spacing design in the inelastic range: They are the lower bound curve B[3], the upper bound curve C[4], and the lower bound slenderness ratio

* In Ref. 15 the basic concept as well as the basic methods of analysis of plastic design are given. Theoretical and experimental results of investigations for the design of continuous frame structures are also presented together with an up-to-date (1958) design guide. A compact presentation of the entire subject of plastic design is also given in Ref. 16.

R_B[15]. For a complete understanding of the problem there is a need to investigate the upper bound slenderness ratio (point R_C) for members subjected to the plastic hinge moment and the ultimate strength (or post-buckling strength curve D). From this study, not only the true maximum carrying capacity, but also the deformation behavior of a member may be obtained. Furthermore, the requirements of the stiffness and strength of the bracing members need also be determined.

1.6 PURPOSES OF THIS INVESTIGATION

The purposes of this investigation are:

(a) To study theoretically the lateral buckling strength of beams under plastic moment. More specifically, to obtain the upper bound for the critical spacing length for wide-flange beams. It is desired to compare this solution with an existing lower bound solution and thereby to verify the current plastic design spacing rule[18] which was deduced from the lower bound results only.[19]

(b) To observe experimentally the inelastic lateral-torsional buckling behavior of beams. In particular, the lateral restraint from adjacent spans, the post-buckling strength of the beam, and the plastic hinge rotation capacities

will be examined.

(c) To investigate experimentally the lateral bracing requirements for plastically designed beams in the region of plastic hinges.

(d) To study, both theoretically and experimentally, the ultimate lateral-torsional strength (post-buckling strength) of beams subjected to equal end moments about the two principal axes (biaxial bending).

2. INELASTIC LATERAL-TORSIONAL BUCKLING

A number of inelastic lateral buckling solutions of wide-flange beams are available (Refs. 3,4 and 5). However, as pointed out in the previous chapter, there is still need for information about the upper bound critical slenderness ratio for beams buckling under full plastic moment. In this chapter the factors affecting inelastic buckling strength will be discussed, existing solutions will be summarized, and an upper bound solution for buckling under full plastic moment will be presented. The discussions will be limited to A7 structural steel wide-flange beams.

2.1 FACTORS AFFECTING BUCKLING STRENGTH IN THE INELASTIC RANGE

Inelastic lateral buckling can be shown to be dependent on the stress-strain relationship of the material, the cross sectional shape, the residual stresses, and the variations of the stiffnesses due to yielding of the material. In the following, each of these parameters will be briefly discussed.

2.1.1 The Stress-Strain Relationship

In Fig. 2.1 is shown a typical stress-strain curve for structural steel from a tension coupon test. This diagram can

be conveniently idealized as shown in Fig. 2.2. Three important assumptions are made in this idealization.

(a) Stress and strain are proportional in the elastic range and at the beginning of the strain-hardening range. Stress remains constant at $\sigma = \sigma_y$ in the plastic range.

(b) The start of yielding and the start of strain-hardening are distinct discontinuities in the stress-strain diagram.

(c) The stress-strain behavior under tension is identical to that of the material under compression.

The following average material constants will be used in the subsequent calculations.[20][21]

$$\sigma_y = 33{,}000 \text{ psi}$$
$$E = 30 \times 10^6 \text{ psi}$$
$$E_{st} = 0.9 \times 10^6 \text{ psi}$$
$$G = 11.5 \times 10^6 \text{ psi}$$
$$G_{st} = 2.4 \times 10^6 \text{ psi}$$
$$\epsilon_{st} = 12\,\epsilon_y$$

2.1.2 Cross-Sectional Shape

The nominal dimensions of wide-flange shapes given in the

AISC Steel Handbook[22] are used in the calculations. Fillets and the taper of the flanges are neglected for convenience.

2.1.3 The Residual Stresses

Residual stresses in rolled or built-up structural shapes and their influence on the carrying capacity of compression members have been extensively studied in recent years (Refs. 23, 24, 25, 26 and 27). Residual stresses are due to one or a combination of the following factors:

(a) Differential cooling rate of each individual element of the cross section of a member after rolling.

(b) Differential heating and cooling due to welding.

(c) Cold working.

The magnitude and distribution of residual stresses depend on the following factors:

(a) Metallurgical composition of the steel.[28]

(b) Condition and method of fabrication.[24]

(c) Dimensions of the cross section.[20]

Figure 2.3 shows a typical residual stress distribution pattern in a rolled wide-flange shape. Combining Figs. 2.2 and

2.3 the average stress-strain curve (considering the cross section as a whole) would be in a shape as indicated in Fig. 2.4.

2.1.4 Variations of Stiffness Parameters due to Yielding

Equilibrium considerations demand that the externally applied loads are resisted by the internal resistance of the member. The following stiffnesses resist the various external loads:

B_{xx} = strong axis bending stiffness

B_{yy} = weak axis bending stiffness

C_T = St. Venant's torsional stiffness

C_w = Warping stiffness

In the elastic range these terms are constant; however, in the inelastic range they will vary because certain portions of the cross sections are yielded. It will be assumed that the yielded portions of a cross section do not contribute to any of the above mentioned stiffness parameters. This is essentially the assumption made in many investigations, for the determination of the effective modulus (Refs. 3, 4, 23, 24, 26, 27 and 28). Based on the assumption that $(E_{eff})\ I = E\ (I_{eff})$, the problem is to obtain the effective constants of the cross sections. For bending and axial compression, this assumption is precisely true.[23][24][27][29]

The bending rigidity B_{xx} is equal to EI_{xx} in the elastic

range. In the elastic-plastic range it is equal to the slope of the moment-curvature curve. A description of the construction of moment-curvature relationships for wide-flange sections is given in Ref. 30. Typical examples of such curves are shown in Fig. 2.5. The two curves in this figure represent bending about the strong and the weak axis respectively. These curves were computed for $\sigma_{rc} = 0.3\sigma_y$, and they can be used for any rolled wide-flange shape.[30] Since the slope of the M-Ø curves decreases as loading increases (that is, yielding increases), the bending rigidity of a partially yielded cross section reduces as yielding increases. The reductions for both B_{xx} and B_{yy} vary according to the change of slopes of the M-Ø curves in Fig. 2.5.

It has been shown[31] that St. Venant's torsional resistance C_T remains at its elastic value GK_T (where G is the shear modulus and K_T is the St. Venant's torsional constant) prior to buckling for an initially perfect member regardless of the extent of yielding in the cross section. In Ref. 31 this has been shown theoretically and experimentally for circular and rectangular members. This theory is also shown to be applicable for wide-flange shapes in Ref. 4 and is further substantiated in Ref. 3. It has been demonstrated that the influence of St. Venant's torsion on the buckling strength of such relatively short beams is so small that it may be ignored for all practical purposes. For buckling in the inelastic range the lengths of the beams are relatively short, and generally the slenderness ratio in the

weak direction is less than 120.[3] An error of about 10% in estimating the inelastic buckling strength of beams[5] results in the larger slenderness ratios. For the lengths under consideration here ($\frac{L}{r_{yy}} < 50$), the error is negligible.

The warping stiffness is the principal factor governing the inelastic buckling strength of a member.[5] Since the phenomenon of warping is the differential bending of the flanges of the wide-flange section, the assumption made in determining the bending stiffness of a yielded section can also be adopted for the calculation of the warping stiffness of a partially yielded member[3][4] (that is, use the warping stiffness of the unyielded section). The warping stiffness for a wide-flange section of elastic homogeneous material is given by:

$$C_w = E\, I_w = \frac{E}{4}\, I_{yy} \cdot d^2 \qquad (2.1)$$

2.2 SUMMARY OF EXISTING INELASTIC BUCKLING SOLUTIONS

Solutions to the inelastic lateral buckling problem are based on the concepts that the rigidities of a yielded member are reduced according to the degree of plastification of the cross section, and that equilibrium is satisfied at all times. These concepts are well developed for axially compressed member buckling

in the inelastic range.[32][33]

There are basically three inelastic buckling solutions for I-shaped beams found in the literature.[2] In Fig. 2.6 the basic assumptions are indicated for each of these investigations, and the solutions are briefly described in the following articles.

2.2.1 Upper Bound Solution (Ref. 4)

In Fig. 2.6a is shown a stress-strain relationship used in this solution. Since the influence of residual stresses is neglected, and bending is about the major axis only, yielding will commence parallel to this axis from the outer surface of both flanges. At buckling the stresses in the plastic region unload elastically. The yielded configuration of the cross section at buckling is shown next to the stress-strain diagram in Fig. 2.6a. The criterion for determining the stiffness is that when an infinitesimal amount of lateral curvature is introduced, the total moment in the loading direction remains unchanged. This consideration enables the determination of the unloading zones of the cross section and the effective cross sectional constants can be evaluated. The resulting curves are those represented by curve C in Fig. 1.3.

The solution in Ref. 4 was performed for simply supported beams. A simple support is the weakest type of end condition, and it is merely an idealization for the convenience of theoretical

analysis. The buckling load will be increased due to the restraints from the adjacent spans in a continuous member. Based on Ref. 4, Ref. 34 gives calculated lateral restraints of various degrees, and presents a table of critical lengths for British Standard rolled steel beams.

Although the solution presented in Ref. 4 is an upper bound (reduced modulus concept) and neglects the influence of residual stresses (which may lead to unconservative results), it is the first attempt to solve the inelastic lateral buckling problem for wide-flange beams.

2.2.2 Lower Bound Solution (Ref. 3)

The basic stress-strain relationship is indicated in Fig. 2.6b for this solution. Due to the effect of the residual stresses the neutral axis will shift toward the tension flange as yielding progresses; it will not, however, rotate with respect to the shear center because of the symmetry of the residual stresses and the section geometry. For each yielded configuration of the cross section, the moment and the effective cross sectional constants are calculated. It is found that the presence of residual stresses may reduce the inelastic lateral buckling strength of a rolled wide-flange structural member considerably. The solutions, which are achieved by considering no unloading in the yielded portion of a

cross section, are compared with existing experimental results; the correlation seems to be satisfactory.

This approach gives the inelastic buckling load at which the equilibrium bifurcates. Since strain reversal is not considered, the solution yields a lower bound value for the critical load. (Represented by curve B in Fig. 1.3.) According to the conclusion in Ref. 32, the lower bound solution is more suitable for designers than an upper bound solution.

2.2.3 Buckling Under Full Plastic Moment (Lower Bound, Ref. 5)

In this analysis it is assumed that under general loading (that is, any inclination of moment gradient) the material in the beam is either elastic or strain-hardened. Under uniform plastic moment, then, the whole beam is strain-hardened and the solution differs from an elastic analysis only in that instead of the elastic moduli E and G, the corresponding strain-hardening moduli E_{st} and G_{st} are used. (See Art. 2.1.1.) This solution thus assumes that the member will rotate plastically until the strains have reached strain-hardening, and that lateral buckling will take place only after this has occurred. This insures sufficient rotation for plastic hinges to form; moreover, unloading is not considered, and the method therefore provides a lower bound for the bracing spacing of plastically designed structures.

The solution is more general with regard to loading than the previously mentioned two solutions. Furthermore, various additional practical factors have been considered. It is basically different from the other two solutions in the following points:

(a) Solutions in Refs. 3 and 4 may predict the inelastic buckling strength for any given length of a member before full plastification of the cross section is reached. These solutions are not capable of estimating the buckling strength when a plastic hinge is formed in the member.

(b) The solution in Ref. 5 can provide the critical buckling length of members subjected to moment gradient of various inclination.

For a member subjected to constant moment, the material becomes entirely strain-hardened along its length, and thus the buckling Eq. 1.6 can be written as

$$L_{cr} = \pi \sqrt{\frac{E_{st}\sqrt{I_{yy} \cdot I_w}}{M_p}} \left[1 + \frac{1}{\frac{\pi^2 E_{st} I_w}{L_{cr}^2 G_{st} K_T}} \right]^{\frac{1}{4}} \qquad (1.6)$$

This equation is simplified if it is assumed that the St. Venant's torsional resistance $G_{st}K_T$ is small compared with the

warping torsional resistance $E_{st} I_w$. This is true for relatively short members, as mentioned earlier. The above equation is then reduced to the following simple form:

$$L_{cr.} = \pi \sqrt{\frac{E_{st} \sqrt{I_{yy} \cdot I_w}}{M_P}} \qquad (2.2)$$

with $E_{st} = 900$ ksi

$\sigma_y = 36$ ksi

$I_w = \frac{1}{4} d^2 (I_{yy})$

$z = \frac{1}{2} d - A$

Equation 2.2 can be written as

$$\frac{L_{cr}}{r_{yy}} = 18 \qquad (2.3)$$

Equation 2.3 implies that, for a simply supported wide-flange beam under constant moment about the major axis only, the critical unsupported length is $18\ r_{yy}$ if buckling starts at the beginning of the strain-hardening range.

2.3 BUCKLING UNDER FULL PLASTIC MOMENT (UPPER BOUND)

In this section an upper bound solution for the critical unsupported length under full plastic moment will be presented.

Since it is desired to compare this with the lower bound solution described in Art. 2.2.3, the same assumptions will be used in this reduced modulus solution. The method of determining the effective stiffness parameters, however, will be different from that which is used for the tangent modulus solution.(5)

Figure 2.7 shows the stress-strain diagram that is assumed (Compare with Fig. 2.6c). As treated in Ref. 5 for the lower bound solution, lateral buckling will be prohibited until the material has reached the onset of strain-hardening; but at the moment of buckling, unloading in the yielded zones of the cross section will be permitted. The effective area of the cross section (that is, the unyielded portion in the cross section) thus increases, and the effective cross sectional constants calculated on this basis would be greater than those when unloading is not permitted (that is, the tangent modulus concept). Consequently, it is clear from Eq. 2.2 that the critical buckling length based on the reduced modulus concept will be higher. This is illustrated in Fig. 2.8. In this figure the points R_B, R_C and R_D (see Fig. 1.3) are again scaled on a set of slenderness ratio-versus-deflection coordinate axes. Points R_B and R_C (lower and upper bound slenderness ratios under plastic moment respectively) are the buckling solutions and R_D (slenderness ratio corresponding to the true ultimate carrying capacity with a finite value of deformation) is the ultimate strength solution. δ in this sketch represents either the

lateral deflection u or the twisting angle β. It is the purpose of this section to develop a solution for the point R_C.

2.3.1 The Determination of Unloading Zones

In Fig. 2.9a is shown a typical wide-flange cross section, which is subjected to a bending moment M_{xx}. The member is deformed only in the plane of the applied moment, and therefore it has only the curvature ϕ_{xx} in the strong direction. If, at the inception of lateral buckling, an infinitesimal curvature $d\phi_{yy}$ is introduced in the lateral direction, (Fig. 2.9b) this disturbance will cause a change of curvature $d\phi_{xx}$ in the direction of the applied moment and an infinitesimal bending moment dM_{yy} about the weak axis. However, in accordance with the reduced modulus concept, there is no change of magnitude of the applied moment M_{xx}.[1] This definition, that $dM_{xx} = 0$, makes it possible to define a neutral axis NN along which the strain is unaltered. Line NN thus defines the unloading zones of the cross section as shown in Fig. 2.9b.

By equilibrium the change of moment dM_{xx} due to a small moment dM_{yy} is the following:

$$dM_{xx} = \int_{(1-q)b_1}^{b_1} E\left[x(d\phi_{yy}) - \frac{d}{2}(d\phi_{xx})\right]\frac{t\cdot d}{2}(dx)$$

$$+ \int_{-b_1}^{(1-q)b_1} E_{st}\left[x(d\phi_{yy}) - \frac{d}{2}(d\phi_{xx})\right]\frac{t\cdot d}{2}(dx)$$

$$+ \int_{0}^{\frac{d}{2}} E_{st}\left[y(d\phi_{xx})\right]w\cdot y\cdot(dy) = 0 \quad (2.4)$$

where dM_{xx} = change of moment about the x-x axis

$d\phi_{xx}$ = change of curvature about the x-x axis

$d\phi_{yy}$ = change of curvature about the y-y axis

b = flange width = $2b_1$

t = flange thickness

d = depth of section

w = web thickness

q = non-dimensional parameter, expressing the extent of unloading along the flange

E = Young's Modulus of Elasticity

E_{st} = strain-hardening modulus

x,y = coordinate axes with the origin coincides with the shear center of the cross section

In formulating Eq. 2.4, the variation of strain along the

thickness of the flanges has been assumed to be negligible (see Fig. 2.9).

Equation 2.4 can be readily integrated provided that the relationship between $d\phi_{xx}$ and $d\phi_{yy}$ is given. From geometry in Fig. 2.9b this relationship is given by

$$\frac{(d\phi_{yy})}{(d\phi_{xx})} = \frac{d}{2(1-q)b_1} \tag{2.5}$$

After integration and substituting b for $2b_1$, Eq. 2.4 can be written in the following form.

$$dM_{xx} = (1-n)q^2 + 4nq - 4n + \frac{2}{3}n\frac{wd}{bt}(1-q) = 0 \tag{2.6}$$

where n is the ratio of the strain-hardening modulus E_{st} and Young's modulus E. From Eq. 2.6 and ignoring the higher power term in n the unloading zones of the cross section can be determined as

$$q = \frac{2}{1-n}\left[\sqrt{n\left(1-\frac{R}{3}\right)} - n\left(1-\frac{R}{3}\right)\right] \tag{2.7}$$

where $R = \frac{A_W}{A_F}$ is the ratio of the areas of the web and the flanges. If the material values given in Art. 2.2.3 are used, (E=30,000 ksi, E_{st} = 900 ksi) Eq. 2.7 can be written as:

$$q = 0.206\left[\sqrt{3-R} - 0.1(3-R)\right] \qquad (2.8)$$

It is seen that the value of q depends on R only.

Equation 2.8 gives the degree of unloading in the cross section for given wide-flange shapes. It is only applicable when lateral buckling takes place at the onset of strain-hardening.

2.3.2 St. Venant's Torsional Rigidity

St. Venant's torsional rigidity of a thin-walled open cross section can be approximated by[6]

$$GK_T = G\frac{1}{3}\sum_{i=1}^{g} l_i t_i^3 \qquad (2.9)$$

where l_i and t_i are, respectively, the length and the thickness of each of the elements of the cross section, and g is the total number of elements of the cross section. For a fully strain-hardened section, the St. Venant's torsional rigidity has been assumed to be $G_{st}K_T$ in the lower bound solution in Ref. 5.

As described in Art. 2.2.1, the value GK_T remains unchanged at the inception of buckling, regardless of the strain conditions in a cross section. This idea may also be used for this calculation. However, since the influence of St. Venant's torsion is

small for very short members, this resistance is entirely neglected in this calculation.

2.3.3 The Lateral Flexural Rigidity

For an elastic-strain-hardened cross section, the bending rigidity is calculated based on the assumption that the thicknesses of the strain-hardened elements are reduced by a factor E_{st}/E, since in both the elastic and the strain-hardening ranges material behaves linearly. This assumption is similar to that which is commonly used in the analysis of members composing two different materials.(35)

Based on this assumption, the lateral bending stiffness can be written as: (See Fig. 2.11.)

$$B_{yy} = E(I_{yy})_{eff} = E\left\{\frac{(2b_1)^3 t}{12}\left[1.03 - 0.97(1-q)^3\right] + \frac{1}{12} w d_w^3\right\} \qquad (2.10)$$

where the nomenclature is defined in Fig. 2.11.

2.3.4 The Warping Torsional Rigidity

Based on the same effective cross sectional area the warping constant $(I_w)_{eff}$ for a wide-flange shape is derived in

Appendix A. The expression for the effective warping torsional rigidity takes the following form: (See Fig. 2.11.)

$$C_w = E(I_w)_{eff}$$

$$= \frac{\bar{C}_w \cdot n}{8\left[2+R+\left(\frac{1}{n}-1\right)q\right]}\left\{ 2(2+R)\left[4-2q^2\left(\frac{1}{n}-1\right)(3-q)\right] \right.$$

$$\left. +\left(\frac{1}{n}-1\right)q\left[q^3\left(\frac{1}{n}-1\right)+4(8+3R)\right]\right\} \qquad (2.11)$$

where the nomenclature is defined as before, and $\bar{C_w} = EI_w$ = the warping stiffness in the elastic range as defined by Eq. 2.1.

2.3.5 The Critical Slenderness Ratio

The necessary modified constants in Eq. 2.2 may be determined for any given cross section from Eqs. 2.8, 2.10 and 2.11. The critical lengths for a number of wide-flange shapes have been calculated, and the results are plotted in Fig. 2.12. This figure also compares the solution obtained in Ref. 5 with the upper bound solutions. The vertical axis indicates the ratio R and the horizontal axis denotes the slenderness ratio $\frac{L_{cr}}{r_{yy}}$.

It is seen that the value $\frac{L}{r_{yy}} = 40$ is an upper bound of the critical unsupported length for simply supported beams subjected to uniform plastic moment when lateral buckling takes place in the strain-hardening range.* If the last integral in Eq. 2.4 is ignored, a value of $\frac{L}{r_{yy}} = 38$ is obtained (See Fig. 2.12).

2.4 SUMMARY AND CONSLUSIONS

2.4.1 Discussion of the Lower and the Upper Bound Solutions

Three existing inelastic solutions are summarized and discussed in this chapter. The first two solutions (Refs. 3 and 4) are studies of the inelastic lateral-torsional buckling of beams before full plastification of any cross section of a member is reached. The last solution (Ref. 5) is aimed at determining design procedure for the spacing of bracing near plastic hinges. For uniform plastic moment, the lower bound critical length is equal to 18 r_{yy}. The new work in this chapter presents an upper bound solution which is based on the reduced modulus concept. It is found that for beams subjected to constant plastic moment, the upper bound critical length is approximately equal to 40 r_{yy}.

---

* The upper bound slenderness ratio, which is approximately twice as much as the lower bound value, has been also discussed in Ref. 38 with regard to axially compressed members of a rectangular cross section.

2.4.2 The Concept of Buckling Under Full Plastic Moment

Both in Ref. 5 and in this chapter strain hardening moduli are used in the theoretical calculations. This is purely an assumption for achieving a possible solution rather than implying that lateral buckling can be postponed until the material has become fully strain-hardened. In the field of mathematical theory of plasticity it is possible to solve problems corresponding to any strain value on an assumed stress-strain diagram, either using the deformation theory or the flow theory.[39] However, for a buckling problem such as this, the stiffness parameters, and not the strain, come directly into the picture. Strictly speaking, this assumption of effective stiffnesses is by no means related to strain, and therefore the strain that corresponds to lateral buckling can be anywhere in the plastic range of the stress-strain diagram shown in Fig. 2.2.

According to the above discussion it is clear that due to the assumption made, the big difference between the lower and the upper bounds is possible (Points R_B and R_C in Figs. 1.3 or 2.8). Furthermore, using this approach, to relate rotation capacity (that is, strain parameter) in the full plastic range to the buckling solution in a rational way, is not possible because of the nature of the buckling solution.

The problem of rotation capacity is very important in the

field of plastic design of lateral instability of beams. There is definitely a need to understand the strain behavior as well as the stiffness in connection with the lateral buckling problem. Carefully conducted experiments could rationally furnish the desired information.

3. INELASTIC LATERAL BUCKLING EXPERIMENTS

3.1 INTRODUCTION

To gain deeper understanding of the problem of lateral buckling of beams subjected to the full plastic moment experimental information is essential. It is desired to determine an exact optimum spacing length in which a plastic hinge can form and the beam can rotate sufficiently before failure takes place because the lower and the upper bound theoretical results yield a wide range of unsupported lengths. (L/r_{yy} = 18, and 40 respectively.)

In the theoretical solutions of lateral buckling it is usually assumed for reason of simplicity that the ends of a member are either simply supported or fixed. In some investigations the influence of various degrees of end fixity of a member have been studied (Refs. 40, 41, 42 and 43); however, these papers consider only the effect of the end restraints on the critical lateral buckling load. The reason for this is that the beam is commonly assumed to have failed once lateral buckling has started.* This concept is realistic for single span members, but it is too conservative for estimating the usefulness of continuous members found in actual cases. In a continuous beam the

*This philosophy is carried over from the behavior of axially loaded columns, where the tangent modulus buckling load is taken as the limit of structural usefulness, even though the member may still carry some small additional load.

critical span may have sufficient lateral torsional restraint provided by the adjacent spans such that not only the buckling load can be increased, but also the maximum load can be maintained while the critical span goes through rather large inelastic deformations. Indeed the termination of the usefulness of a beam can be defined as that point at which unloading starts. This definition is used throughout this investigation.

The main purposes for the experiments are:

(a) To determine the most suitable and economical unsupported length between lateral bracing, (that is, to verify the theoretical results presented in Chapter 2) and

(b) To investigate the behavior of the beam in the post-buckling range.

3.2 RESULTS OF PREVIOUS EXPERIMENTS

Experiments on elastic lateral buckling of beams have been conducted by many investigators. (Refs. 11, 43, 44, 45, 46, 47, 48, 49, 50 and 51). The elastic buckling theories;[52][53] which have been adopted by the steel industry,[22] are verified satisfactorily.[54]*

*More detailed discussion on elastic buckling tests may be found in Ref. 55.

Experiments on inelastic lateral buckling of wide-flange beams are described in the following:

3.2.1 Lehigh Test Results (Refs. 19, 56)

Test results obtained from these two papers are plotted in Fig. 3.1. In this figure test points are indicated by solid points; the coordinates are the nondimensional ratios $\frac{M_{max}}{M_p}$ (ordinate) and $\frac{L_{cr}}{r_{yy}}$ (abscissa). In the strain-hardening range the moment at the initiation of lateral buckling has much less meaning than the maximum moment; therefore, in Fig. 3.1 the latter values are used for ordinates.

Only one test ($\frac{L_{cr}}{r_{yy}} = 50.5$) is reported in Ref. 56. This test was performed for demonstration purpose; the result, however, was not reliable because of the restraint provided by the setup. Eight tests are described in Ref. 19. The end conditions of the critical span in some of these tests were not defined well because of lateral movement of the supports. Two conclusions, however, may be drawn:

(a) These test results confirm that the most severe loading case is that of constant moment in the inelastic range as already known for elastic buckling.[40] The steeper the moment gradient, the higher the maximum load.

(b) These test results indicate that the beams contain a considerable post-buckling strength reserve.

3.2.2 Connecticut Test Results (Ref. 57)

The test results described in Ref. 57 are also shown in Fig. 3.1. All tests were conducted for a moment gradient equal to zero. All observed maximum moments are higher than M_p. It should be pointed out that the maximum observed moment values greater than M_p do not necessarily imply that lateral buckling took place in the strain-hardening range. If a very short beam is tested with sufficient lateral supports in order to achieve failure in the strain-hardening range, the member will fail eventually as a result of local buckling.[58] Thus the high maximum loads observed in this test series can be explained as the result of restraints and as the result of the dynamic effect due to high strain rate, in addition to the effect due to strain-hardening.*

3.2.3 Discussions on Inelastic Experiments

The following can be summarized with regard to inelastic lateral buckling tests:

(a) Purpose for Investigation.

According to the description given in Chapter I

* The development of solid state physics in recent years has shown that shear force can cause strain-hardening of the material. This explains the phenomenon of the variation of maximum load for different moment gradient in inelastic experiments. (See Ref. 59.)

(Fig. 1.3), there are a variety of problems involved in lateral buckling in the inelastic range, many of which do not have a theoretical solution yet. Each of these problems again contain various cases due to different loading or support conditions. Furthermore, the behavior of the material in the inelastic range is less known than in the elastic range.[60] It is therefore most desirable to program experiments by keeping the number of variables to a minimum.

(b) Support Conditions.

Besides the restraints provided by the adjacent spans which will increase both the lateral buckling load and the post-buckling strength, a test specimen may be subjected to certain restraints due to the loading devices or the supporting fixtures which are usually of unknown magnitude. With specimens loaded by testing machine, the loading points (or point) were considered as supporting points. Lateral movement at these points can not usually be avoided particularly in the post-buckling range when the friction between the loading device and the specimen cannot overcome the lateral bending moment due to lateral deformations of the cross sections of the critical span.

It is not essential to have support conditions exactly corresponding to the situations that are assumed in theoretical analysis, but it is necessary to have known and constant end conditions by which the planned variables (or variable) of the experiments can be differentiated and compared.

(c) The Influence of Strain Rate.

The influence of strain rate on the stress-strain relationships is discussed in Ref. 20. For higher strain rates the yield stress is considerably higher than for slow strain rates for the same strain interval. Consequently, testing with faster loading speeds results in higher maximum loads. Besides, the strain rate in all tests may not be equally controlled and hence test results cannot be compared.

3.3 DESCRIPTION OF THE TEST PROGRAM

Two series of tests were performed within the framework of the current program:

(a) Beam tests with lateral supports.

(b) Tests of beam-purlin assemblies.

In the rest of this chapter the first of these two series

of tests will be discussed. The beam-purlin assembly experiments will be examined in detail in Chapter 4.

A schematic view of the test setup is shown in Table 3.1. All beam specimens were divided by lateral supports into three equal spans. In each beam the center span was subjected to constant moment and this was the critical span. The beam specimens were 10WF25 as-rolled, wide-flange beam sections of ASTM A7 structural steel. All specimens were obtained from the same ingot and the same rolling, and each piece was subjected to cooling and straightening processes that were as identical as possible.

The main variables for these series of tests are the following:

(a) Beam size.

(b) Unsupported length.

(c) Loading condition.

(d) Number of critical braced spans.

(e) Stiffness of purlin.

(f) Type of purlin.

(g) Method of purlin attachment.

(h) Length of adjacent spans.

In accordance with the previous discussion of other test programs, and according to the principal purposes given in the beginning of this chapter, it is desirable to leave all conditions

identical for the first series of tests, with the exception of the length. A summary of the test numbers, the support conditions and the variables of each of the tests is given in Table 3.1.

Four beam tests were performed: LB-9 ($\frac{L}{r_{yy}} = 40$), LB-10 ($\frac{L}{r_{yy}} = 45$), LB-11 ($\frac{L}{r_{yy}} = 35$) and LB-15 ($\frac{L}{r_{yy}} = 40$). Test LB-15 was a repetition of test LB-9. This test was repeated because of unsatisfactory lateral support conditions in the first test. This error was subsequently corrected, and no noticeable lateral movement occurred at the supports for the remaining three experiments.

3.4 DESCRIPTIONS OF TEST SETUP

3.4.1 Fixtures

Figure 3.2 shows the over-all view of the test setup; the details of the lateral support system are shown in Fig. 3.3. The load was applied downward through jacks at the ends of the test beam. The vertical supports, which corresponded to the ends of the critical span, were constructed in the following manner (see Fig. 3.3b). The test beam was suspended from a supporting girder by means of two high strength steel rods of 1-1/4" diameter. At the ends of each rod, clevises connected the rod to the supporting girder and to the specimen by two inch round pins. This vertical connection permits free rotation of the test specimen in the plane

of loading. The supporting girder (see Fig. 3.2) was a 12WF99 beam of a 20-ft. span and it was bolted at its ends to the centers of the cross beams of two parallel rectangular frames. These frames were fixed to the laboratory floor at their bases by bolts fitting into already existing holes.

This loading and supporting system provided statically simply supported conditions for the beam specimen in the loading direction. The magnitude of the constant moment in the critical span is equal to the product of the applied load at the specimen ends, times the overhanging span length. This loading condition placed the test specimen in an inverse position (that is, with the compression flange at the bottom) to the normal beam tests. The purpose of adopting such a testing position was to overcome the unknown restraints at the interior support points due to loading at these points.

The four sets of lateral supports were placed at the two sections of vertical support (third points) and at the two loading sections (at the ends). Each lateral support (as shown in Fig. 3.3) consisted of two 1/2" thick knife-edge plates which were bolted to the webs of two 5" channels. The distance between the two knife-edges was made adjustable by slotted holes in the channels. The test specimen was guided between these knife-edges; they permitted lateral rotation but not twisting and lateral motion

of the section at the support point. The two channels were welded to a base plate, thereby providing one unit which is called the "lateral support system". The four lateral supports were fastened to the top flange of a 14WF314 base beam which was fixed to the floor by bolts. Stiffeners were attached to the web of this base beam at positions underneath the lateral supports to assure lateral fixity.

The above mentioned fixtures thus provide known support conditions. Figure 3.4 shows the overall setup and Fig. 3.5 is a closer view indicating the details of the test setup as specimen LB-9 was in place prior to testing.

3.4.2 The Loading System

The concentrated loads at the specimen ends were applied by means of two hydraulic jacks. Each jack had a capacity of 55,000 lbs. These jacks apply equal loads, because they were connected to one hydraulic system and they were controlled by a single valve. The magnitude of the load was recorded by an Amsler indicator and the load can be estimated to the closest 10 lbs. The base plates of the jacks were bolted to the same supporting girder to which the vertical rods were attached. The distances between the rods and jacks were adjustable for the purpose of testing specimens of various lengths. At the loading ends

of the jacks were located spherical bearing heads with flat lower surfaces (See Fig. 3.3). The load was transmitted to the specimen by a two inch roller to assure a knife-edge loading condition (Fig. 3.5).

3.4.3 Instrumentation

The following data were taken during each test:

(a) Concentrated load at ends (end moments).

(b) Deflections along the length of the beam in the plane of the web, at the quarter points in each span.

(c) Lateral deflections along the length of the beam, taken both on the compression and the tension flanges at the quarter points in each span.

(d) Strain readings at locations indicated in Fig. 3.6.

The following instruments were used in taking the above mentioned data:

(a) An Amsler indicator.

(b) A surveyor's level. This level was fixed in elevation and the telescope can rotate only in a horizontal plane. A 1/100" scale was held vertically at each of the previously laid out marks on the tension flange (top flange) in the plane of the web. (See Fig. 3.5) Readings along the length were taken as

the vertically held scale was moved from point to point and the telescope of the level rotated.

(c) A 1/100" scale and a transit were used, same as the level above, except that the transit was fixed to rotate only in a vertical plane, and the scale was held horizontally, to measure lateral deflections.

(d) SR-4 strain gages of type A-11 (one inch gage length) were put on the specimen at locations as shown in Fig. 3.6b, and the readings were recorded by a Baldwin strain indicator.

3.5 DESCRIPTION OF THE TEST SPECIMENS AND THEIR MATERIAL PROPERTIES

In Fig. 3.7 a sketch of the typical test specimen is shown. Stiffeners of 3/8" thickness were used at the two loading sections and under the two vertical supports. At the end sections 1/2" plates were welded to the beam. These plates extended one inch above the surface of the upper flange and they also served as a stop to the loading roller for large deflections.

On the surface of the tension flange, two 6" x 4" x 12" plates were welded to the beam at each vertical support position. These plates were parallel to the web, and they have 2-1/8" pin holes for the purpose of hanging up the specimen. The lengths for each test specimen are given in Fig. 3.7. All specimens were

painted with a solution of hydrated lime before testing: white for the critical span, and light blue for the adjacent spans. This afforded a means of observing the yielding process during the test.

Four tension coupons were tested: two cut from the flanges and two cut from the web of the test material. A summary of coupon data and all the measured dimensions of the test specimens are given in Table 3.2. The calculations based on the measured results in this table assume that the inner surface of the flanges is parallel to the outer surfaces.*

A stub column test was carried out to check the static yield stress level with that obtained from the tension coupon tests. Close correlation between these two test results was obtained. The stress-strain diagram plotted from the stub column test is given in Fig. 3.8.

3.6 TEST PROCEDURE

3.6.1 Elastic Range

Prior to the application of the loads, zero reference readings were taken on all instruments and gage locations. After three or four load increments, before the proportional limit was

*According to the steel designer's handbook, the 10WF25 sections have tapered flanges with a five degrees inclination of the inner surfaces of the flanges. (See Ref. 61.) This is neglected in the calculations, and an average thickness is used.

reached the load was released and all zero readings were checked. Identical values were obtained. This implies that the friction between the knife-edges of the lateral supports and the specimen were negligible. The load increments were selected to give approximately four to six load readings in the elastic range.

3.6.2 Proportional Limit to Lateral Buckling

Flaking off of the whitewash on the compression flange and the creeping of the strain indicator needle occur simultaneously when the proportional limit was exceeded. In the inelastic range, load applications were controlled by strain increments. (That is, to keep the deflection increments approximately the same.) After the application of each load, time was allowed for the load to settle down, and readings were recorded when the plastic flow had nearly ceased. Time versus load decrement curves were used for this purpose.

In all the tests lateral buckling was initiated in the inelastic range when the curvature in the middle section of the critical span reached a value from three to five times its value at first yield.

Load increments were relatively small in this range. It was intended to find the transition curve of the stress-strain curve due to the influence of residual stresses and the load at

which lateral buckling started as closely as possible.

3.6.3 Post-Buckling Range

After lateral buckling, the lateral deflections increased steadily at a near constant moment level. This was due to the restraint of the adjacent spans which remain elastic. When the moment versus curvature curve, which was plotted as a control curve during the whole test, indicated definite unloading, the test was terminated. A set of final readings was taken after complete removal of the load.

The hydraulic jacks had a maximum stroke of five inches. This length was not enough for the total maximum deflections at the specimen ends. In each test, it was necessary to adjust the stroke once in the post-buckling range by releasing the load completely.

The average time necessary to conduct one experiment ranged from six to eight hours. Figure 3.4 shows a general view of a test in progress; (LB-9) at the time of photographing, strain readings and vertical deflection readings were being made, and the yield lines on the compression flange were being inspected.

3.7 DISCUSSION OF TEST RESULTS

3.7.1 The Moment-Curvature Relationships

The curvature at mid-span was measured by two SR-4 strain gages of one inch gage length which were attached to the outer surfaces of the flanges. (See Fig. 3.6.) At each load increment the absolute value of the difference of the strain increments at the two flanges is added, and the curvature ϕ is obtained by dividing this sum by the distance between these two gages. (That is, the measured total depth of the cross section). In all tests, the absolute values of these two strain readings were approximately the same, implying that the neutral axis was at mid-depth. This relationship between the fiber strains and the curvature is illustrated in Fig. 3.9. In this figure the experimental M-ϕ curve of test LB-10 is plotted for explanation. The deviation of the experimental points from the theoretical line in the elastic range is due to the variations of the cross sectional depth, since the calculations use the average measured value. The beam entered the inelastic range at load number 5 (marked "initiation of yielding"). However, lateral buckling did not occur until load number 11, as indicated in the M-ϕ curve of Fig. 3.9. From the start of lateral buckling, the moment can be seen to be at a nearly constant value while the test beam was undergoing large rotations in the post-buckling range. When ϕ/ϕ_y reached a value of more than 12* the test specimen begins to unload as local buckling of the

---

*The SR-4 strain gages are warranted by the producer for accurate strain recording up to 2% strain. This strain value corresponds approximately to $\frac{\phi}{\phi_y} = 14$.

compression commences. Similar behavior was observed in all the tests. All four M-Ø curves are shown in Fig. 3.10. It should be mentioned that in test LB-9 after lateral buckling had taken place, one of the two interior lateral supports moved because of the relative movement of the knife-edge plate and the channel. Therefore in the next two load increments, unloading immediately commenced. (See Fig. 3.10.) The load was then released to zero and all lateral supports were fixed in the deformed position by tightening bolts which held the knife-edge plates in position. The channels were further fixed by using additional clamps. After this, the test beam was able to rotate at a constant moment level which was about 5% less than the full plastic moment. These additional clamping devices were used throughout the rest of the experiments, and no other movement was observed.

There are possibly three factors that may influence the recorded magnitude of load in the test setup:

(a) The friction provided by the lateral supports in the vertical direction.

(b) The decreasing of the moment arm due to increased deflections.

(c) Moment gradient due to unequal adjacent span lengths.

The first question is answered automatically (See Fig. 3.9) as explained earlier. The other two questions are answered

by the curves in Figs. 3.11 and 3.12. Figure 3.11 is a plot of the moment-curvature relationship at sections having equal moment arms in the elastic spans, and Fig. 3.12 is the moment-curvature plot of the two quarter point sections in the critical span. In both figures the M-ϕ curves at section 1-1 and section 2-2 should be consistent, since they are symmetrical with respect to mid-span section. That this is true is shown. The lengths of the adjacent spans have slight variations due to inaccurate specimen fabrication (See Fig. 3.7); the effects of such small differences as seen from Fig. 3.11, can be ignored.

The change of the moment arms where deflections become large is relatively important. The change of length at each load interval was not measured in all tests. However, the total change of length was recorded after each test. The table in Fig. 3.13 contains this information. To illustrate quantitatively this effect, the M-ϕ curve at mid-span of test LB-15 is given. The maximum reduction of moment due to this effect is approximately 1% just before the termination of the tests.

3.7.2 The Moment-Vertical Deflection Relationships

In Fig. 3.14 the M-v curves are shown for the four tests. Curves in this figure only indicate the maximum deflection at the mid-span. The overall deflection of the critical span were found

to be smooth curves for all the tests. Since the supporting girder and the vertical suspending rods have elastic deflections as the load was applied, the deflection readings plotted in Fig. 3.14 have been adjusted by the average deflections at points (2) and (3). Therefore in Fig. 3.14, the abscissa indicates the vertical deflection of the mid-span with respect to the ends of the critical span. In this figure corresponding points of lateral buckling and local buckling are also indicated.

The overall deflections of the test specimen at various stages of loading are shown in Fig. 3.15 for test LB-9. Very similar situations were prevalent in other tests.

The vertical deformations are of primary interest since they are directly related to the problem of rotation capacity of the beams. In all tests the total inelastic rotation was found to be sufficient and satisfactory. As can be seen from Fig. 3.15, lateral buckling of the critical span starts rather early (before large deflection takes place, or at about 20% of the total deflection at the termination of tests). This implies that the post-buckling strength, which is the ability of further deformation without unload after buckling, is quite large and it can be utilized for the type of beam investigated.

With regard to the load carrying capacity, however, there are some differences observed in the tests. Since the

original purpose of this investigation is to study the behavior of beams having plastic hinges, it is necessary for the moments to reach their full plastic value and then to rotate at this moment level. For test specimens with slenderness ratios equal to 35 and 40, (LB-9, LB-11 and LB-15) the full plastic moment value was achieved. (See Fig. 3.10.) However in test LB-10 ($L/r_{yy} = 45$) the maximum moment value is about 0.95 M_p. In all tests the lateral buckling loads are approximately the maximum loads as also can be seen in Fig. 3.10.

3.7.3 The Moment-Lateral Deflection Relationships

In Fig. 3.16 lateral deflections for both the compression and the tension flange at mid-span are shown. The initiation of lateral movement of the compression flange in each test is indicated in Fig. 3.15. In all tests lateral buckling occurred in the inelastic range and no effect on the load carrying capacity was observed. Instead, a slight increase of load had been recorded. Furthermore, lateral buckling did not influence the rotation capacity of a member. Test beams started to unload when the warping torsional resistance of the sections began to decrease as the lateral deflections of the tension flange grew large, and eventually failure took place as a result of local buckling of the compression flange. These phenomena were observed in all the tests without exception. Therefore, for beams proportioned as in this investigation, local buckling of the compression flange is the major factor

controlling the termination of the full usefulness in the post-buckling range. Lateral buckling, on the other hand, has very little significance with respect to the inelastic rotation capacity of a beam so proportioned.

A quantitative picture of the lateral deflections for test LB-10 is shown in Fig. 3.17. In Fig. 3.18 a general view of test specimen LB-15 in place after completion of the test is shown. The load has been released and the deflected shape indicates the permanent deformations. In this figure the twisting at the center portion of the cross section can also be seen.

For short beams the warping torsional stiffness of the cross section in the critical span contributes almost the entire resistance of the beam to withstand large inelastic rotations. This differential bending of the flanges can be observed in Fig. 3.19, where three test specimens after the completion of the test are shown.

3.8 THE CURRENT SPACING RULE IN PLASTIC DESIGN

As given in Ref. 18, current rules for the spacing of lateral bracing in plastic design are:

$$\begin{aligned} \frac{L_{cr}}{r_{yy}} &= 60 - 40\ \frac{M}{M_p} && \text{for} \quad \frac{M}{M_p} \leq 0.625 \\ &= 35 && \text{for} \quad \frac{M}{M_p} > 0.625 \end{aligned} \qquad (3.1)$$

Equations 3.1 are the simplified results of the following recommended design rules given in Ref. 19.

$$\frac{1}{\eta_r}\frac{L_{cr}}{r_{yy}} = 48 - 30\frac{M}{M_p} \qquad \text{for } 0.6 \geq \frac{M}{M_p} \geq -1.0$$

$$= 30 \qquad \text{for } 1.0 \geq \frac{M}{M_p} \geq 0.6 \tag{3.2}$$

where η_r is the correction factor due to end restraints, it is equal to unity for simply supported end conditions. Hence the value $L_{cr}/r_{yy} = 30$ corresponds to the situation discussed in this chapter, which is "in between" the values of 18 and 40. The upper bound solution developed in Chapter 2 supports the adequacy of the design rules given by Eq. 3.2.

Based on the experimental results presented in this chapter, it may be concluded that for a laterally continuous beam the unsupported length of the critical span could be 40 r_{yy}.

3.9 CONCLUSIONS

(a) The currently recommended plastic design rule $L_{cr}/r_{yy} = 35$, for beams subjected to a moment gradient $M/M_p > 0.625$, (Eq. 3.1) is a safe lower limit for the bracing spacing.

(b) For buckling under full plastic moment, these test results verify satisfactorily the lower and upper

bound theoretical solutions given in Chapter 2.

(c) Initiation of lateral buckling is immaterial with respect to the rotation capacity of beams having slenderness ratios of the critical span L/r_{yy} equal to or less than 45.

(d) The rotation capacity of beams so proportioned is sufficient to provide satisfactory plastic hinge rotations.

(e) The termination of the post-buckling strength is due to the local buckling of the compression flange.

(f) In order to determine the influence of lateral restraints, tests with various adjacent span lengths may be desirable.

(g) Several inelastic buckling solutions have been developed but few experimental verifications have been made.[55] It may be desirable to conduct some future lateral buckling tests at slenderness ratios ranging from 50 to 120 for the completeness of the knowledge of inelastic lateral-torsional buckling.

3.10 DESIGN RECOMMENDATION

Based on the above given conclusions the following design

recommendation is suggested:

> The spacing of the lateral bracing for a critical span to develop sufficient hinge rotation under constant moment should be equal to or less than 40 r_{yy}, provided that (a) the critical span is laterally continuous, and (b) the geometry of the beam sections meet the requirements of local buckling.[21]

4. EXPERIMENTS ON THE PERFORMANCE OF THE LATERAL BRACING

4.1 INTRODUCTION

4.1.1 The Necessity of Obtaining Information on Bracing Requirements

In the previous two chapters the problem of bracing spacing is treated both theoretically and experimentally. As described in the beginning of Chapter 1, the question of bracing requirements also should be considered in a study of the lateral buckling of beams. This study is important because it is the bracing which provides the necessary support between the unsupported critical lengths of the beam. The combined result of the two studies can then be applied to actual cases in designing economical and safe structures, since in the considerations of the first problem (bracing spacing) the bracing points are idealized for convenient theoretical analysis. Furthermore, in the experimental verifications, the support conditions are made to simulate idealized conditions as closely as possible.(55) The idealized support conditions do not actually exist in structures. Thus without proper information on the bracing requirement, it is impossible to achieve a safe design, even if the bracing spacing is adequate.

4.1.2 Consideration of Theoretical Approaches

It has been noted in Chapter 1 that a rigorous theoretical analysis of the problem of bracing requirement is highly

complicated because many variables are involved. The intrinsic difficulty occurs at the point of lateral support, where both the beam and the bracing member are continuous in two perpendicular directions. There are possibly two physical models that may be used for theoretical considerations.

Model (a) A simply supported beam with end restraints of various degrees in three directions (transversely, laterally and torsionally).

Model (b) A continuous beam with continuous bracing members in the perpendicular direction. This is illustrated in Fig. 4.1.

Model (a) is commonly used in traditional elastic analysis as described in Chapter 3. Some investigations considered the restraint in the loading direction, others considered it in the lateral direction. No investigation has, however, considered the restraints in all three directions. This is of small concern, since the studies made for Model (a) can only show the influence of end fixities on the buckling load. At the present time there seems to be no way to correlate the restraints with the stiffness and strength of a bracing member except by experimental means.

Model (b) (Fig. 4.1), however, can give information on the bracing requirement if an analytical solution were possible.

Since, in this case, the bracing members are part of the structure, their influence on the carrying capacity of the beam can be taken into consideration. It should be noted that this beam-purlin structure shown in Fig. 4.1 is statically indeterminate. For a complete post-buckling solution, the required analytical procedures are more involved than those which are presently available. A particular solution might be possible if drastic simplifications were made; however, the trustworthiness of the solution would not be comparable with that obtained by carefully conducted experiments. In theoretical considerations, it is best to obtain the post-buckling strength solution for idealized support conditions first, before any attempt is made to find a solution for Model (b).

4.1.3 The Test Program

According to the conclusion of Chapter 3, the optimum slenderness ratio is $L/r_{yy} = 40$. This length is used for all the tests with purlins given in Table 3.1. In this program the loading, beam size, beam length, purlin length and method of purlin attachment are kept constant. The only variable is the size of purlins. The purlin sizes and the constant parameters are listed below:

For All Tests

Loading: Constant Moment

Unsupported Length: $L = 40\ r_{yy}$ (52.4")

Beam Specimen: 10WF25

Purlin Span Length: L_b = 7'0" = 84"

Purlin Attachment: Purlins are continuous and are welded to the compression flange. (Fig.4.9)

For Test LB-12

Purlin size: 4 I 7.7 (d_b/d = 0.40)

For Test LB-13

Purlin size: 3 I 5.7 (d_b/d = 0.3)

For Test LB-14

Purlin size: M 2362* (d_b/d = 0.26)

Table 4.1 contains detailed information about the purlins and Table 4.2 summarizes the material properties of the beam sections.

4.2 DESCRIPTION OF THE TEST SETUP

The test setup in this program was kept identical with that of the first series of tests, with the exception of two additional fixtures.

In the first series of tests (presented in Chapter 3), the ends of the critical span were guided by lateral supports and

---

*This is a special small 2" I section produced by the Bethlehem Steel Company. See Table 4.1 for details.

twisting of the beam at these sections was prevented. In this second test series the two lateral supports were removed and actual bracing members were substituted. The vertical rods were connected to the test specimen by double clevises (See Fig. 4.9) which permitted the beam specimen to twist and to rotate vertically. Thus, the only resistance to twisting and lateral movement was provided by purlins.

All purlins were 14' in length. They were welded directly to the outside face of the compression flange of the beam specimen at the ends of the critical span. Thus in all tests the purlin span was 7 ft. The ends of the purlins were pin-connected to the flange of the cross beams, (See Fig. 4.2b) so that the end conditions of the purlins were as follows: vertical rotations are free; and both the horizontal rotations and twisting of the purlin sections are prevented. The cross beams were clamped to stub columns, which were bolted to the laboratory floor at already existing holes. Each stub column was a 8WF67 section, 36" long. With different purlin section depths only the level of the cross beams needed to be adjusted through clamping devices. Fig. 4.2 shows the details of this setup. The setup of a typical test is shown in Fig. 4.9.

4.3 DISCUSSION OF TEST RESULTS

4.3.1 The Moment-Curvature Relationships

The method of taking various readings and the positions where readings were taken in these tests were identical with those used in the first series of tests. (See Chapter 3.) The moment-curvature curves at the center of the critical span for all three tests are shown in Fig. 4.3. From this figure it is seen that very similar M-ϕ relationships were obtained in this series of tests. Comparisons can also be made between these M-ϕ curves and those with lateral supports of the same length (Chapter 3, Fig. 3.10), since all of the M-ϕ relationships in these two figures are plotted with the same scale. It is observed that very small differences exist between the M-ϕ curves and these two series of tests. In Fig. 4.3 test LB-12 and LB-13 indicate sufficient post-buckling strength, while test LB-14, which had the weakest purlins, could not maintain the maximum load after lateral buckling. The performance of test LB-14 is considered to be inadequate.

Throughout this dissertation the termination of the useful post-buckling strength is defined as that point at which the moment in an M-ϕ curve begins to drop. According to this definition, test LB-14 would have no post-buckling strength. For LB-13, this point is at $\phi/\phi_y = 10.5$ and for LB-12, it is at $\phi/\phi_y = 13$.

It will be noted from Fig. 4.3 that prior to lateral buckling the M-ϕ curves for these three tests are identical.

Furthermore, lateral buckling starts at almost the same time. The behavior indicates that the bracing members which are necessary in order to reach the lateral buckling load of a beam need be very small. This has been shown both theoretically and experimentally to be true for elastic lateral buckling. (Refs. 12, 13 and 14). Test results observed in this series of tests strongly support an extension of this theory to the case of inelastic buckling. The post-buckling strength, on the other hand, depends on the strength of the bracing members.

The local buckling behavior (as can be seen from Fig. 4.3) does not seem to depend on the purlin strength. Similar behavior to that in the first series of tests was observed.

Since the beam-purlin assembly constitutes an indeterminate structure, a question may be raised concerning the magnitude of the moment values. The constant moment in the critical span is equal to the product of the concentrated end loads and the adjacent span length modified by a correction factor. This correction factor contains the following:

(a) Frictions between the test specimen and the lateral supports.

(b) Change in the moment arms due to large deflections in the adjacent spans.

(c) Moment gradient due to unequal adjacent span lengths.

(d) Elastic deformations of the vertical rods and the supporting girder. These deflections were taken by the purlins in bending and this may decrease the moment value.

(e) Since the purlin ends were fixed against twisting, there was a twisting moment existing at the bracing points when the adjacent span deforms as a cantilever. These twisting moments of the purlins become bending moments to counteract the applied moments, since the beam and the purlins were rigidly connected.

(f) The pivot point of twisting of the beam cross section at bracing points (that is, the center of the pin of the clevis connecting the vertical rods) was two inches above the upper flange. This means that the loads were applied two inches from the tension flange and may offer restraints against lateral torsional deformations of the beam cross sections.

The first three factors are shown to be negligible in Chapter 3.

The maximum total elastic deflections of the high-strength steel rod and the supporting girder at the bracing points of the beam specimen were calculated to be 0.3" which was negligibly small. This value was also observed from level readings during testing.

The twisting moment of the purlin due to the rotations of the beam can be calculated based on the vertical deflection readings along the beam, and the rotations of the beam at the bracing sections can be obtained from the following expression[62]

$$\psi = \frac{4\delta_1 - \delta_2}{2\tau} \qquad (4.1)$$

where ψ = rotation in radians at the bracing section

δ_1 = deflection at a section which is a τ distance from the bracing point

δ_2 = deflection at a section which is 2τ distance from the bracing point

τ = equal interval between the sections where vertical deflections were measured.

Based on Eq. 4.1 the end rotations of the critical span can be obtained. Figure 4.4* shows the moment versus end rotation

---

*This M-ψ curve may also be obtained by integration of the M-ϕ curve given in Fig. 4.3.

relationships for test LB-12 which has the largest purlin section.

Due to rigid purlin attachment at bracing points, at any stage of loading the rotation value is the applied twisting angle at the center span of the purlin. The corresponding twisting moment is given by:[6]

$$T = \frac{(d_{wb} w_b^3 + 2 b_b t_b^3)}{3 \ell_b} G \psi \qquad (4.2)$$

where T = twisting moment

ψ = total twisting angle

G = shear modulus

ℓ_b = one-half purlin span length

d_{wb} = purlin web depth

w_b = purlin web thickness

b_b = purlin flange width

t_b = purlin flange thickness

The free body for Eq. 4.2 is shown in Fig. 4.5.

For test LB-12, the maximum twisting moment based on Eq. 4.2 at $\psi = 0.202$ (see Fig. 4.4) is only 1.405 k-in. This is approximately 0.14% of the maximum applied moment. This influence can be considered to be negligible.

Finally the problem of the loading position is discussed. The influence of a loading point other than at the shear center on the lateral buckling load has been studied by a number of investigators* In these studies only the influence on elastic buckling loads are treated. There is no information concerning this effect in the post-buckling range. With the test setup of these experiments, this influence on the rotation capacity is believed to be small, since in all the tests no lateral movement at the braced section was observed. This is reasonable because the purlins are continuous, and they are rigid enough to prevent any lateral deformations. Nevertheless, further tests conducted with supporting points on the compression flange are planned in order to evaluate the effect of loading positions on the post-buckling strength of beams.

4.3.2 The Behavior of Purlins

During the tests the deflections of the purlins were also measured. Purlins remained straight prior to lateral buckling in all the tests. After lateral movement of the compression flange, the purlins started to deflect into "S" shapes in their lateral direction in addition to twisting. However, no appreciable deformations in the vertical direction were observed even at the end of the post-buckling range. It was noted

*A summary of these investigations is contained in Chapter 4 of Ref. 1.

that the stiffness in the weak direction of the purlin section is one of the primary factors that directly affect the post-buckling strength of the beam. Test LB-12 had the strongest purlin section ($r_{yy} = 0.59$) and it was able to produce the greatest post-buckling strength. On the other hand, test LB-14 had the weakest purlin section ($r_{yy} = 0.174$) and it could establish no post-buckling strength. Based on the observations made in these three tests, it is concluded that in order to develop sufficient post-buckling strength of a beam, the bracing members must have enough lateral rigidity in addition to the depth and area requirements which are usually considered.[14][15]

In all experiments, the purlins remained within the proportional limit. No yielding of the purlins was observed.

Thus based on Table 4.1 and Fig. 4.3, a relationship between the slenderness ratio of purlins and the rotation capacity of beams may be formulated:

$$\frac{\phi}{\phi_y} = 1.0 + 40 \frac{\frac{L}{r_{yy}}}{\left(\frac{\ell}{r_{yy}}\right)_b} \qquad (4.3)$$

where ϕ/ϕ = required curvature of plastic hinges

L/r_{yy} = slenderness ratio of beam between bracing points

$(\ell/r_{yy})_b$ = slenderness ratio of bracing members

The basis for this approximation is shown in Fig. 4.6.

It is emphasized that Eq. 4.3 is not suggested as a design rule for checking the purlin strength. There should be considerably more investigations made in order to compose a design recommendation. Equation 4.3, however, may be consulted as a guide for selecting bracing members in future experiments of this kind.

4.3.3 The Moment-Deflection Relationships

The moment versus vertical deflection curves for the three beam-purlin tests are given in Fig. 4.7 and the moment versus lateral deflection relationships are shown in Fig. 4.8. It will be noted that all these relationships are similar to those presented in Chapter 3. (Compare with Figs. 3.14 and 3.16 respectively.) Lateral buckling and local buckling behavior is identical to that explained in Chapter 3.

The influence of purlin strength may be realized by comparing the three beam-purlin tests. Similar to the explanations made about the M-ϕ curves, it is seen from Figs. 4.7 and 4.8 that the post-buckling strength decreases as the strength of the bracing member decreases. In test LB-14 the lateral rigidity of the bracing members is too weak to restrain the beam section from deflecting laterally. The large deflections of the compression flange will also introduce deflections of the tension flange through the web. This phenomenon can also be seen from Fig. 4.8.

In Fig. 4.10 is shown a view of the entire beam-purlin structure of test LB-12 after testing. Figure 4.11 shows the critical spans of all the test beams. Purlins were burned off for comparison of their cross sectional areas. It is noted that the yielding configurations are very similar for all the beam specimens.

4.4 CONCLUSIONS

(a) The strength of the bracing has very little influence on inelastic lateral buckling loads of the braced beam.

(b) The strength of the bracing has great influence on the post-buckling strength of a beam designed to sustain plastic hinge rotations.

(c) If the bracing members are adequate in size and length, the termination of the usefulness of the beam is governed by the local buckling of the compression flange. If the bracing members are too weak, the lateral rigidity of purlins controls the post-buckling strength of a beam.

(d) If the required hinge rotation is given, the adequacy of the slenderness ratio of bracing

members may be checked by using Eq. 4.3.

(e) The optimum bracing spacing concluded from the previous chapters is satisfactory for the full development of plastic hinge rotations if the requirement of bracings is adequate.

It is obvious that adequate design information cannot be concluded from a limited number of tests. Further possible experiments are suggested in the following:

(a) Tests with the same setup and same loading conditions, but with various purlin shapes and various methods of purlin attachment.

(b) Tests with the same setup, but with the loads applied on the compression flange.

(c) Tests of two parallel beams connected by purlins and subjected to both constant moment and moment gradient.

(d) Repeat of tests in (b), except that the ends of the beams would be connected to plastically designed corner connections.[63] The extension of this study may be tests on parallel purlin-connected frames.

5. INELASTIC LATERAL-TORSIONAL STRENGTH OF BEAMS SUBJECTED TO BIAXIAL FLEXURE

5.1 INTRODUCTION

Thus far in this dissertation only the problems of symmetrical loading have been considered. As described in Chapter 1, problems with symmetrical loading (that is, buckling problems) are different in nature from the maximum carrying capacity problems (that is, ultimate strength problems). These latter problems, although extremely difficult to analyze, can give adequate explanation of member behavior throughout the full history of a structure with regard to loading and deformations. This is a necessary and sufficient background on which plastic design procedures can be rationally based. It is therefore necessary to develop a method of analyzing such ultimate strength problems. These problems include the biaxial bending problem, the initial imperfection problem, and the post-buckling strength problem, as mentioned in Chapter 1. It will be noted that the maximum carrying capacity obtained from a post-buckling solution should be an upper bound solution to those obtained from the other two solutions. As can be seen from Fig. 1.2, the maximum moment value on the biaxial bending curve (or an initial imperfection solution) approaches the maximum moment point on the post-buckling strength curve as the lateral bending moment M_{yy} (or the initial imperfections $\bar{u}$ and $\bar{\beta}$) approaches zero. The

basic method of solution to all such inelastic instability problems is the same.

In this dissertation a method is developed for the solution of the maximum carrying capacity of biaxially bent beams. This solution may be represented by the curve QR_D in Fig. 1.3.

In conventional design (or elastic design) such problems have been considered by a number of investigators (Refs. 10, 11, 64, 65, 66, 67, 68, and 69) on various cross sections and for different loadings, theoretically and experimentally. In some of these references the "ultimate load" of a beam is defined as that load which causes the maximum fiber stress at any cross section to reach the proportional limit. This terminology is quite misleading. If a member is subjected to bending in two directions, portions of the cross section will be yielded when the ultimate load of the member is reached and as deformations become large, regardless of whether the member is long or short. Solutions in these references are therefore "critical stress problems" in elastic design, in which no instability of any type will take place (Point A in Fig. 1.1). A few inelastic investigations on biaxial bending (Refs. 70, 71, 72, 73, and 74), on the contrary, treat the problem without considering the length parameter. In other words these solutions are limited to the study of the behavior of the neutral axis when the cross sections are partially yielded. Strictly speaking, solutions of such a type again can not be called

instability solutions, since the deformations of a member are not predicted. These are essentially studies of the full plastic moment under inclined loads.

The method presented in this chapter considers the interaction between the deformations as well as the related stiffness parameters. Their influence on the load versus deformation relationships are included, and the maximum carrying capacity of biaxially bent beams is predicted.

To illustrate the method of solution, a simply supported beam of rectangular cross section will be treated in detail in this chapter. Solutions for wide-flange beams are presented in Appendix B.

5.2 THE EQUATIONS OF EQUILIBRIUM

The differential equations presented in Chapter 1 for biaxial bending of wide-flange members are as follows (see Fig. 1.2):

$$-B_{xx}\frac{d^2v}{dz^2} = -M_{xx} + M_{yy}\cdot\beta \qquad \text{(a)}$$

$$-B_{yy}\frac{d^2u}{dz^2} = -M_{xx}\cdot\beta - M_{yy} \qquad \text{(b)} \qquad (1.5)$$

$$-C_w\frac{d^3\beta}{dz^3} - C_T\frac{d\beta}{dz} = -M_{xx}\frac{du}{dz} + M_{yy}\frac{dv}{dz} \qquad \text{(c)}$$

For beams of rectangular cross section, these equations can be written as:(6)(10)(11)

$$-B_{xx}\frac{d^2v}{dz^2} = -M_{xx} + M_{yy}\cdot\beta \qquad (a)$$

$$-B_{yy}\frac{d^2u}{dz^2} = -M_{xx}\cdot\beta - M_{yy} \qquad (b) \qquad (5.1)$$

$$C_T\frac{d\beta}{dz} = -M_{xx}\frac{du}{dz} + M_{yy}\frac{dv}{dz} \qquad (c)$$

The end conditions for simple supports are:

$$\begin{aligned} &\text{at} \quad z = 0 \qquad u = v = \beta'' = 0 \\ &\text{at} \quad z = L \qquad u = v = \beta'' = 0 \end{aligned} \qquad (5.2)$$

The solution of the differential equations (5.1) is obtained by differentiating Eq. 5.1c first with respect to z and then substituting Eqs. 5.1a and 5.1b into this new equation to yield a second order equation in β:

$$\frac{d^2\beta}{dz^2} + \left(\frac{M_{xx}^2}{C_T B_{yy}} + \frac{M_{yy}^2}{C_T B_{xx}}\right)\cdot\beta = M_{xx}M_{yy}\left(\frac{1}{C_T B_{xx}} - \frac{1}{C_T B_{yy}}\right) \qquad (5.3)$$

The general solution of Eq. 5.3 is given by(10)

$$\beta = A\cos q_1 z + B\sin q_1 z + \frac{q_2}{q_1} \qquad (5.4)$$

where A and B are constants determined by the boundary conditions, and

$$q_1 = \sqrt{\frac{M_{xx}^2}{C_T B_{yy}} + \frac{M_{yy}^2}{C_T B_{xx}}} \tag{5.5}$$

$$q_2 = M_{xx} M_{yy} \left(\frac{1}{C_T B_{xx}} - \frac{1}{C_T B_{yy}} \right) \tag{5.6}$$

Substituting the boundary conditions of Eq. 5.2 into Eq. 5.4 solving for A and B, the final expression for β is:

$$\beta = \frac{q_2}{q_1} \left[1 - \left(\cos q_1 z + \sin q_1 z \tan \frac{q_1 L}{2} \right) \right] \tag{5.7}$$

Substitution of Eq. 5.7 into Eq. 5.1a, integrating with respect to z, and using the conditions v = 0 at z = 0 and at z = L, the vertical deflection v is obtained.

$$\begin{aligned} v = -\frac{1}{B_{xx}} \Bigg\{ & \frac{M_{xx}}{2} \left[Lz - z^2 \right] \\ & + M_{yy} \frac{q_2}{q_1^2} \Bigg[\frac{1}{2} (z^2 - Lz) \Bigg[\left(\cos q_1 z - \frac{z}{L} \cos q_1 L \right) \\ & + \tan \frac{q_1 L}{2} \left(\sin q_1 z - \frac{z}{L} \sin q_1 L \right) - \frac{1}{q_1^2} \left(1 - \frac{z}{L} \right) \Bigg] \Bigg] \Bigg\} \end{aligned} \tag{5.8}$$

Similarily from Eq. 5.1b and from the condition that, $u = 0$ at $z = 0$ and at $z = L$, the lateral deflection u is equal to:

$$u = \frac{1}{B_{yy}} \left\{ M_{yy} \cdot \frac{1}{2}(z^2 - Lz) + M_{xx} \cdot \frac{q_2}{q_1^2} \left[\frac{1}{2}(z^2 - Lz) - \frac{1}{q_1^2} \left[\left(\cos q_1 z - \frac{z}{L} \cos q_1 L \right) + \tan \frac{q_1 L}{2} \left(\sin q_1 z - \frac{z}{L} \sin q_1 L \right) + \frac{1}{q_1^2} \left(\frac{z}{L} - 1 \right) \right] \right] \right\} \quad (5.9)$$

Since the applied moment is constant along the beam the maximum deflections occur at $z = \frac{L}{2}$. Therefore, at the center section

$$\beta_o = \frac{q_2}{q_1^2} \left\{ 1 - \frac{1}{\cos \frac{q_1 L}{2}} \right\} \quad (5.10)$$

$$u_o = \frac{1}{B_{yy}} \left\{ -\frac{L^2}{8} \left(M_{xx} \frac{q_2}{q_1^2} + M_{yy} \right) + \frac{q_2}{q_1^4} \left[-\frac{1}{2} + \left(\cos \frac{q_1 L}{2} - \frac{1}{2} \cos q_1 L \right) + \tan \frac{q_1 L}{2} \left(\sin \frac{q_1 L}{2} - \frac{1}{2} \sin q_1 L \right) \right] \right\} \quad (5.11)$$

$$v_o = -\frac{1}{B_{xx}} \left\{ \frac{L^2}{8} \left(-M_{yy} \frac{q_2}{q_1^2} + M_{xx} \right) + \frac{q_2}{q_1^4} M_{yy} \left[-\frac{1}{2} + \left(\cos \frac{q_1 L}{2} - \frac{1}{2} \cos q_1 L \right) + \tan \frac{q_1 L}{2} \left(\sin \frac{q_1 L}{2} - \frac{1}{2} \sin q_1 L \right) \right] \right\} \quad (5.12)$$

where q_1 and q_2 are defined in Eqs. 5.5 and 5.6 respectively.

5.3 ASSUMPTIONS

(a) The stress-strain diagram of the material in compression is identical to that in tension. Furthermore the effect of strain-hardening is neglected. (See Fig. 2.2.)

(b) Residual stresses are not considered.

(c) Plane sections remain plane (that is, linear strain).

(d) The St. Venant's torsional constant of a solid parallelogram section can be approximated by Eq. 5.23.

5.4 THE ELASTIC SOLUTIONS

In elastic analysis the determination of the maximum fiber stresses is required. According to the formula of general unsymmetrical bending, the stresses at any point in the cross section are:

$$\sigma = \frac{M_{\xi\xi}(\eta)}{I_{\xi\xi}} + \frac{M_{\eta\eta}(\xi)}{I_{\eta\eta}} \qquad (5.13)$$

where $M_{\xi\xi}$ and $M_{\eta\eta}$ are components of the applied moments about the principal axes. In the elastic range the ξ - and η - axes coincide with the x'- and y'- axes. (See Fig. 5.1.) However,

$$\begin{aligned} M_{\xi\xi} &= - M_{xx} + \beta \cdot M_{yy} \\ M_{\eta\eta} &= \beta \cdot M_{xx} + M_{yy} \end{aligned} \tag{5.14}$$

Thus Eq. 5.13 can be written as:

$$\sigma = \frac{\eta}{I_{\xi\xi}} \left(- M_{xx} + \beta M_{yy} \right) + \frac{\xi}{I_{\eta\eta}} \left(\beta M_{xx} + M_{yy} \right) \tag{5.15}$$

The term $- \frac{\beta \cdot M_{yy} \cdot \eta}{I_{\xi\xi}}$ in Eq. 5.15 is much smaller than the other terms if $M_{xx} \gg M_{yy}$. Neglecting this term, Eq. 5.15 can be simplified to:

$$\sigma = \frac{M_{xx}(\eta)}{I_{\xi\xi}} + \frac{M_{yy}(\xi)}{I_{\eta\eta}} + \beta \frac{M_{xx}(\xi)}{I_{\eta\eta}} \tag{5.16}$$

Equation 5.16 is the basis for elastic design of beams subjected to equal end moments in two directions.*

---

*In Ref. 10 beam curves which show the influence of various types of cross sections and various degrees of imperfection on the critical stresses of slender beams are presented.

5.5 THE BEHAVIOR OF PARTIALLY YIELDED SECTIONS SUBJECTED TO INCLINED LOADING

It should be pointed out that regardless of whether the material is entirely elastic or partially plastic, equilibrium between the externally applied load and the internal resistance of a member must be maintained. The fundamental difference between an elastic cross section and a partially yielded one is that the stiffness coefficients B_{yy}, B_{xx}, and C_T of an elastic section remain constant irrespective of the magnitude of loading, whereas for a yielded section the rigidities decrease as yielding (that is, loading) increases. The reduction of the rigidities for a partially yielded section are considered in following sections.

5.5.1 Symbols and Definition

The yielded and deformed shape of a rectangular beam is shown in Fig. 5.1. The cross-hatched portions are yielded and it is assumed that these portions of the cross section furnish no stiffness against additional loading in the yielded zone. The rest of the cross section remains elastic.[3] The dimensional and deformational parameters of the cross section are explained below:

b = width of the cross section

C = center of twist

NA = neutral axis

u = lateral deflection of the shear center

v = vertical deflection of the shear center

x,y = coordinate axes in the undeformed state

x',y' = principal coordinate axes in the deformed state before yielding starts

α = inclination of the plane of the applied moment with respect to the vertical plane

β = angle of twist

θ = inclination of the neutral axis with respect to the principal axis x'-x' of the elastic section

ϕ = inclination of the principal axes ξ-ξ and η-η with respect to the principal axes of the elastic section x'x' and y'y'

$\lambda_1, \lambda_2, (\text{or } \lambda_3)$ = penetration of yielding parameters of the cross section

ξ, η = principal coordinate axes (variable).

5.5.2 The Bending Rigidities

The bending rigidity of a yielded section is obtained by using the concept that $E_{eff} \cdot I = E \cdot I_{eff}$ as explained in Chapter 2. In Fig. 5.2 are shown two possible cases of yielded configuration for a rectangular cross section. The moment of inertia of the

effective area of the cross section with respect to the x'y' coordinate system are given by the following expressions:

Case I

$$I_{x'x'} = \bar{I}_{xx}\left[1-\lambda_1\lambda_2(3-8\lambda_2+6\lambda_2^2)\right]$$

$$I_{y'y'} = \bar{I}_{yy}\left[1-\lambda_1\lambda_2(3-8\lambda_1-6\lambda_1^2)\right] \qquad (5.17)$$

$$I_{x'y'} = b^2d^2\left[-\frac{1}{4}\lambda_1\lambda_2-\frac{1}{6}\lambda_1\lambda_2(\lambda_1+\lambda_2)-\frac{5}{36}\lambda_1^2\lambda_2^2\right]$$

Case II

$$I_{x'x'} = \bar{I}_{xx}\left[(1-\lambda_2-\lambda_3)^3-\frac{2}{3}(\lambda_2-\lambda_3)^3+12(\lambda_2-\lambda_3)\left[\!\left[\frac{1}{2}-\lambda_3-\frac{1}{3}(\lambda_2-\lambda_3)\right]\!\right]^2\right]$$

$$I_{y'y'} = \bar{I}_{yy}\left[1-(\lambda_2+\lambda_3)\right] \qquad (5.18)$$

$$I_{x'y'} = b^2d^2\left[-\frac{1}{36}(\lambda_2-\lambda_3)^2-\frac{1}{12}(\lambda_2-\lambda_3)\left[\!\left[\frac{1}{2}-\lambda_3-\frac{1}{3}(\lambda_2-\lambda_3)\right]\!\right]\right]$$

where $\bar{I}_{xx} = \frac{1}{12}bd^3$ and $\bar{I}_{yy} = \frac{1}{12}b^3d$ are the moments of inertia of the unyielded cross section.

The inclination of the principal axes is defined as[35]

$$\tan 2\phi = \frac{2 I_{x'y'}}{I_{y'y'} - I_{x'x'}} \tag{5.19}$$

and the moments of inertia with respect to the principal axes are:

$$I_{\xi\xi} = I_{x'x'} \cos^2\phi + I_{y'y'} \sin^2\phi - I_{x'y'} \sin 2\phi \tag{5.20}$$

$$I_{\eta\eta} = I_{x'x'} \sin^2\phi + I_{y'y'} \cos^2\phi + I_{x'y'} \sin 2\phi \tag{5.21}$$

For any yielded configuration of the cross section it is thus always possible to determine the inclination of the prinicpal axes and the moment of inertia about these axes.

Interaction curves constructed for both yielding cases are shown in Figs. 5.3 through 5.6. These curves are presented in a non-dimensionalized form. The vertical axis represents the value of $I_{\xi\xi}$ divided by I_{xx} (or $I_{\eta\eta}/I_{yy}$) on the horizontal axis the non-dimensioned parameter λ_1 (or λ_3) is plotted. The interaction parameter is λ_2/λ_1 for Case I. For Case II this parameter is $\lambda_2 - \lambda_3$. Both λ_2/λ_1 and $\lambda_2 - \lambda_3$ indicate the inclination of yielding surface (that is, the inclination of the neutral axis).

5.5.3 The St. Venant's Torsional Constant

The St. Venant's torsional constant of a rectangular section

is given by:[6]

$$\bar{K}_T = \frac{1}{3} b^3 d \left(1 - 0.63 \frac{b}{d}\right) \tag{5.22}$$

As shown in Fig. 5.7 it is assumed that for a partially yielded section the value K_T can be approximated by

$$K_T = \frac{1}{3} b^3 d_1 \left(1 - 0.63 \frac{b}{d_1}\right) \tag{5.23}$$

where $d_1 = d\,(1 - \lambda_1 \lambda_2)$ for Case I

and $d_1 = d - (\lambda_2 + \lambda_3)\, d$ for Case II.

The effective depth d_1 is obtained by equating the triangular area ABC to the rectangular area AB'DE. This is purely an approximation, further investigation on this subject is essential before a precise solution can be obtained. The purpose of this dissertation, however, is primarily aimed at the development of a basic analytical procedure to solve the ultimate strength problems, and this procedure can be applied with any kind of K_T versus λ_2 and λ_1 (or λ_3) relationships. Since there is some torsional stiffness in the already yielded portion of the cross section, therefore this approximation for St. Venant's torsional constant is believed to be conservative.

Based on this assumption, the effective torsional constant can be written in terms of the yielding parameters as follows:

Case I $$K_T = \bar{K}_T \left[1-\lambda_1\lambda_2\right]\left[1-\frac{0.63}{1-\lambda_1\lambda_2}\frac{b}{d}\right] \tag{5.24}$$

Case II $$K_T = \bar{K}_T \left[1-(\lambda_2+\lambda_3)\right]\left[1-\frac{0.63}{1-(\lambda_2+\lambda_3)}\frac{b}{d}\right] \tag{5.25}$$

The interaction curves for Eqs. 5.24 and 5.25 are given in Fig. 5.8.

5.5.4 The Bending Moment About the Neutral Axis

For any yielded configuration of the cross section, the internal moment about the neutral axis can be evaluated, provided the correct inclination of the neutral axis is known. The direction of the neutral axis is governed by the inclination of the interface between the elastic core and the yielded regions in the cross section. The angle between the x'-x' axis and the neutral axis, θ, can be written in the following form:

Case I: $$\theta = \tan^{-1}\left[\frac{d}{b}\frac{\lambda_2}{\lambda_1}\right] \tag{5.26}$$

Case II: $$\theta = \tan^{-1}\left[\frac{d}{b}(\lambda_2-\lambda_3)\right] \tag{5.27}$$

where d/b is the aspect ratio of the cross section and λ_2 and λ_1 (or λ_3) are the basic parameters of yielding penetration.

In Fig. 5.9 the geometric representation of the relationship between a partially plastic section and its stress and strain distribution in the plane perpendicular to the neutral axis is shown. The bending moment about the neutral axis is defined as

$$M_{NA} = \int_A \sigma \cdot s \cdot dA \qquad (5.28)$$

where s is measured in the direction perpendicular to the neutral axis.

Equation 5.28 is integrated for the two stress distributions in Fig. 5.9. The resulting equations are:

Case I:

$$\frac{M_{NA}}{(M_p)_{xx}} = \frac{4}{bd^2}\left\{\frac{2}{3}\frac{bc_2^2}{\cos\theta} + \frac{c_2^3}{3\sin 2\theta}\left[1+4\left(\frac{c_1}{c_2}\right)-\left(\frac{c_1}{c_2}\right)^4-6\left(\frac{c_3}{c_2}\right)+2\left(\frac{c_3}{c_2}\right)^3\right]\right\} \qquad (5.29)$$

where:

$$c_1 = \frac{b}{2}\left(\frac{d}{b}\cos\theta - \sin\theta\right)$$

$$c_2 = \frac{b}{2}\left[\frac{d}{b}\cos\theta + (1-2\lambda_1)\sin\theta\right]$$

$$c_3 = \frac{b}{2}\left(\frac{d}{b}\cos\theta + \sin\theta\right)$$

and

$$\theta = \tan^{-1}\left(\frac{d}{b}\frac{\lambda_2}{\lambda_1}\right)$$

Therefore

$$\frac{c_1}{c_2} = \frac{\frac{d}{b} - \tan\theta}{\frac{d}{b} + (1-2\lambda_1)\tan\theta}$$

$$\frac{c_3}{c_2} = \frac{\frac{d}{b} - \tan\theta}{\frac{d}{b} + (1-2\lambda_1)\tan\theta}$$

Case II

$$\frac{M_{NA}}{(M_p)_{xx}} = \frac{4}{bd^2}\left\{\frac{b c_1^2}{3\cos\theta}\left[3-\left(\frac{c_4}{c_1}\right)^3\right]\right.$$

$$\left.-\frac{2c_1^3}{3\sin 2\theta}\left[\left(\frac{c_3}{c_1}\right)^3-3\left(\frac{c_3}{c_1}\right)+2\right]\right\} \qquad (5.30)$$

where

$$c_1 = \frac{b}{2}\left(\frac{d}{b}\cos\theta-\sin\theta\right)$$

$$c_4 = \frac{b}{2}\left[\frac{d}{b}(1-2\lambda_3)-\tan\theta\right]\cos\theta$$

$$c_3 = \frac{b}{2}\left(\frac{b}{d}\cos\theta+\sin\theta\right)$$

and

$$\theta = \tan^{-1}\left[\frac{d}{b}(\lambda_2-\lambda_3)\right]$$

Therefore

$$\frac{c_4}{c_1} = \frac{\frac{d}{b}(1-2\lambda_3)-\tan\theta}{\frac{d}{b}-\tan\theta}$$

$$\frac{c_3}{c_1} = \frac{\frac{d}{b}+\tan\theta}{\frac{d}{b}-\tan\theta}$$

Equations 5.29 and 5.30 can be reduced to an identical expression when $\lambda_1 = 1.0$ in Case I and $\lambda_3 = 0$ in Case II respectively.

It is seen that the moment about the neutral axis given by Eqs. 5.29 and 5.30 is determined by the basic yielding parameters only. The interaction curves for these two equations are given in Figs. 5.10 and 5.11 respectively. For any given combination of λ_2 and λ_2/λ_1 (or λ_2 and $\lambda_2 - \lambda_3$) the value of M_{NA} may be obtained from these curves.

5.5.5 The Relationship Between the Neutral Axis and the Twisting Angle

The inclination of the neutral axis depends not only on the yielding parameters but also on the twisting angle and the ratio of M_{xx} and M_{yy}. The ratio of the moment components, $\frac{M_{yy}}{M_{xx}} = \tan\alpha$, is a constant. The value of β is an unknown variable, depending on the loading, the cross sectional geometry, and the beam length as well as on the degree of yielding. The solution of this problem cannot be obtained explicitly, it requires an over-all trial and error procedure. This can be done with the aid of the previously prepared interaction curves (Figs. 5.3 through 5.11).

The rotation of the neutral axis for any given cross section is given by[35]

$$\tan\theta' = \frac{I_{11}}{I_{22}} \tan\alpha' \qquad (5.31)$$

where θ' = inclination of the neutral axis with respect to the principal axes.

α' = inclination of the load with respect to the neutral axis.

I_{11}, I_{22} = moment of inertia about the principal axes of the given cross section.

Thus for a partially yielded cross section, the actual rotation of the neutral axis with respect to x'-x' axis can be obtained from the following equation: (See Fig. 5.1)

$$\tan(\theta+\phi) = \frac{I_{\xi\xi}}{I_{\eta\eta}} \cdot \tan(\alpha+\beta+\phi)$$

or

$$\beta = \tan^{-1}\left[\frac{I_{\eta\eta}}{I_{\xi\xi}} \cdot \tan(\theta+\phi)\right] - (\alpha+\phi) \qquad (5.32)$$

In Eq. 5.32 α is a constant. For any given yielding penetration λ_2, λ_1 or λ_3, the value of θ is defined by Eqs. 5.26 or 5.27, and the values of $I_{\eta\eta}/I_{\xi\xi}$ and ϕ can be found from Figs. 5.12 through 5.15; these figures are plotted using the values obtained in the process of the construction of Figs. 5.3 through 5.6. As a consequence, the unknown value β in Eq. 5.32

can be determined for a given yielding configuration.

For various degrees of yielding, a series of β values can be obtained. The relationships between β and the yielding parameters obtained from Eq. 5.32 are plotted in Fig. 5.16 for $\alpha = 10^{o}$ and for d/b = 2. In this figure the variations of the twisting angle β are shown with respect to λ_2 and with λ_1 as parameter. For given β values, the correct relationships between λ_1 and λ_2 thus are defined by the curves given in Fig. 5.16. For a member of given length, each twisting angle β_o corresponds only to one set of values of λ_1 and λ_2.

5.6 THE MOMENT VERSUS TWISTING ANGLE RELATIONSHIP

5.6.1 Elastic Range

The relationship of moment versus twisting angle β_o at the middle span is given in Fig. 5.17. The ordinate is the component of the applied bending moment about the major axis in non-dimensional form (that is, divided by the full plastic moment $\sigma_y \cdot Z_{xx}$ in the strong direction). The abscissa shows the twisting angle β_o in degrees.

In this calculation the following values are assumed:

b = 2"

d/b= 2

L/b= 30

$$\alpha = 10^{o}$$

These values are substituted into Eq. 5.10. Since in the elastic range the cross sectional constants $\bar{K}_T$, $I_{x'x'}$ and $I_{y'y'}$ remain unchanged, the curve OAB can be plotted directly by using Eq. 5.10.

5.6.2 The Proportional Limit

The portion AB of the curve OAB is not true since at point A, yielding starts in the cross section. This point A is obtained by using Eq. 5.16 in the following form:

$$\sigma_y = \frac{M_{xx} \cdot \frac{d}{2}}{I_{x'x'}} + \frac{M_{yy} \cdot \frac{b}{2}}{I_{y'y'}} + \beta \frac{M_{xx} \cdot \frac{b}{2}}{I_{y'y'}} \qquad (5.33)$$

The plot of Eq. 5.33 intercepts the curve OAB at point A as shown in Fig. 5.17. Point A is therefore the proportional limit.

5.6.3 Inelastic Range

The trial procedure of obtaining an equilibrium point on the moment versus twisting angle curve above the elastic limit is described below. Equation 5.10 is the expression which must be satisfied by the trials.

(a) Starting with Case I, a value of β_o is assumed and then from Fig. 5.16 a family of λ_1 and λ_2 values are obtained. It has been noted that for this particular β_o every combination of λ_1 and λ_2 in this family is a correct set of yielded configurations depending upon the length of the beam.

(b) Taking one set of these λ_1 and λ_2 values and determining the corresponding values of $I_{\xi\xi}$, $I_{\eta\eta}$ and K_T from Figs. 5.3, 5.5 and 5.8, substitutions can be made into Eq. 5.10.

(c) For these same λ_1 and λ_2 values, the moment about the neutral axis can be obtained from Fig. 5.10. The relationship between M_{NA} and M_{xx} (the component about the strong axis in Eq. 5.10) is given by the following equation.

$$M_{xx} = M_{N.A.} \cos (\beta_o - \theta) \qquad (5.34)$$

where θ is the inclination of the neutral axis and β_o is the assumed twisting angle in step (a).
The value of M_{xx} obtained from Eq. 5.34 is again substituted into Eq. 5.10.

(d) The requirement for equilibrium is that the calculated β_o from Eq. 5.10 is equal to the assumed value in step (a).

(e) If the calculated β_o does not equal the assumed value,

the beam is not in equilibrium with the picked λ_2 and λ_1 values in step (b). Therefore steps (b) through (d) are repeated until the calculated value of β_o has reached within 1% of the assumed value. Then the condition of equilibrium is considered to be satisfied.

(f) As is noted in Appendix B, when the twisting angle β_o becomes large the yielded configuration will be governed by Case II. Identical procedures are used with the aid of the appropriate figures. The rectangular beam considered in this example, however, fails simply on the upper margin of Case I.

5.7 THE MOMENT VERSUS DEFLECTION RELATIONSHIPS

The relationships between moment and deflections are obtained by using Eqs. 5.11 and 5.12. Since the correct values for M_{xx} versus β_o are known, a trial procedure is not necessary. These relationships are shown in Figs. 5.18 and 5.19.

5.8 PILOT TEST ON BIAXIAL BENDING

One test was conducted to verify the theoretical solutions presented above on a 4" x 2" rectangular steel bar of 15 ft. length.

5.8.1 Test Specimen and Test Setup

The test setup was the same as used for the tests described in Chapter 3. (See Fig. 5.20.) The 180" long beam was subdivided into three segments of 60" span, corresponding to L/b = 30 (b=2"). The center span, which was subjected to constant moment, was the critical span. The inclination of the moment application was achieved in the following manner:

> At each of the four lateral support sections, two 5" x 5" x 1/2" knife-edge plates were welded to the top and bottom surfaces of the beam specimen. The positions of these two plates were such that the knife-edges of the top and bottom plates defined an inclined plane which made an angle of 10 degrees with the vertical plane. (See Fig. 5.21.) Trapezoidal blocks were then welded to the top plates such that the upper surfaces of these blocks remained horizontal when the beam was in a testing position. Therefore, during testing, the applied moment was kept in the vertical plane and the beam cross sections were inclined by 10 degrees at the points of lateral support.

In all other respects the test assembly, the details of the test setup, and the test procedures were identical with the lateral buckling tests of the wide-flange beams presented in Chapter 3.

5.8.2 Instrumentation

SR-4 strain gages were attached to the beam specimen at positions as shown in Fig. 5.22. The method of measuring the deformations u_o, v_o and β_o at the middle section of the test span is explained in Fig. 5.22. At the middle section of the critical length of the beam, four rigid bars were welded to the four sides of the bar as shown in Fig. 5.22b. The intersection point of the two perpendicular lines AB and CD is the centroid of the cross section. Both vertical and horizontal movements at the ends of these rigid bars were measured by means of a 1/100" scale which was moved from point to point. Readings were taken by a transit and a level. With known distances between these measured points and the centroid, the deformations at the centroid, u_o, v_o and β_o, are given by the expressions indicated in Fig. 5.22.

5.8.3 Test Results and Discussions

Fig. 5.23 shows the correlation between the theoretical curve and the experimental results for vertical deflections. The following two conclusions can be drawn from the pilot test:

(a) Although due to inaccurate deflection measurements* the deformation readings became scattered when compared with

* The 1/100" scale was not accurate enough for deflection readings in this test, since the critical span of L/b = 30 was too short to yield appreciable deformations. For future tests more sensitive measuring devices are suggested.

theory, the prediction of maximum load is nevertheless fairly satisfactory. The observed maximum moment was about 5% higher than the predicted moment. (See Fig. 5.23.)

(b) The lateral restraints due to the adjacent spans are responsible for the larger rotation capacity at the maximum moment level as shown in Fig. 5.23. As concluded in Chapter 3, the post-buckling strength of a symmetrically loaded member is primarily governed by the lateral restraints. The supposition is further verified here experimentally for the case of inclined loading.

5.9 SUMMARY AND CONCLUSIONS

A method is presented in this chapter to obtain the true ultimate carrying capacity of a simply supported beam subjected to end moments applied in two directions. Moment versus deformation relationships are obtained for the whole loading history of the beam. The method is illustrated by solving the problem of a beam of rectangular cross section.

One experiment was conducted to substantiate the theory. From this test it can be concluded that the ultimate load predicted

by the theory was about 5% less than the observed value. This experiment indicated also that the rotation capacity of a member is mainly due to lateral restraints, as it has been concluded in Chapter 3.

Using the same methods, solutions for wide-flange beams are also obtained. The beam sections for which computations were made is the 10WF25 section. The calculations are performed for L/r_{yy}=40, 60, and 80 respectively. In all cases the inclination of the end moments is 10 degrees. The details of the solutions are given in Appendix B. The moment versus deformation relationships are shown in Figs. 5.43 through 5.45. From these figures it is seen that the deformations u_o and β_o at maximum moment increase as the slenderness ratio L/r_{yy} increases, while the vertical deflection v_o at maximum moment decreases as the beam length increases.

As mentioned earlier, the purpose of the theoretical treatment of the problem of biaxial bending in this chapter is the development of a method of solution. Further theoretical and experimental work is necessary before the method can be employed as a design tool.

The proposed theoretical procedures, however, reveal a gleam of light for the solutions of various other problems in biaxial flexure. Those were heretofore handicapped by the complicated interaction of the lateral-torsional deformations.

These problems are briefly pointed out in the following:

(a) The post-buckling strength of beam.

The analytical procedures presented in this chapter can directly be applied to obtain the post-buckling strength of beams if the influence of residual stresses is neglected. In such a case the beam will be loaded about the strong axis only and deflections will be in the plane of loading alone before lateral buckling is initiated. After this initial motion load is reached, lateral and torsional deformations will take place; however, the beam will remain in stable equilibrium until the maximum load is reached. In the post-buckling range the problem becomes identical to that presented in this chapter and the method can directly be adopted without additional difficulties. This problem of post-buckling strength will be further illustrated in Art. 5.10.

(b) Strength of plate girders subjected to eccentric loading.

Solution for lateral-torsional strength of deep beams is more complicated than that of wide-flange beams, since the local strength of plate elements[76][77] involves into the interaction with the lateral-torsional deformations. However, it is desirable to know the behavior of deep beams subjected to eccentric loads (or symmetrical load but with imperfections of fabrication) because such situations exist in actual cases.

(c) Beams subjected to moment gradient.

The analytical procedures developed in this chapter apply only to the case of constant moment. Solutions will become more involved if the curvature along the member varies. The midspan deformations in such a case cannot be treated alone. Instead, they are influenced by the overall deformations of the beam. A numerical integration process, perhaps a method as presented in Ref. 78, might be incorporated into the analytical procedures developed in this chapter for the solution of moment gradient. A method of solution for members subjected to moment gradient is essential for the purpose of solving further important problems.

(d) Biaxially loaded columns.

One of the most important applications of the study of biaxial flexure is to predict the strength of continuous columns in building frames, since an interior column is always subjected to end moments in two directions in addition to axial loads. In this case the column is subjected to moment gradient, furthermore there will be translation of the neutral axis in addition to rotation and hence the problem becomes extremely complicated. However, before this problem is solved, plastic design of building frames will not be able to reach the most economical state.

5.10 THE POST-BUCKLING STRENGTH SOLUTION

A post-buckling strength solution will be illustrated in this section. Again the rectangular beam with the aspect ratio equal to two will be considered. A complete solution is twofold:

(a) The initial motion solution.

(b) The post-buckling solution.

5.10.1 The Initial Motion Solution*

The buckling equation for a beam of rectangular cross section can be written in the following form:[6]

$$(M_{xx})_{cr.} = \frac{\pi}{L}\sqrt{C_T B_{yy}} \tag{5.35}$$

where $(M_{xx})_{cr}$ = The critical bending moment about the strong axis.

C_T = St. Venant's torsional rigidity.

B_{yy} = Lateral bending rigidity.

L = Length of the beam with simple supports.

For calculation of Eq. 5.35, the following quantities in terms of the yielding parameter λ are necessary. (See Fig. 5.46.)

---

*A rigorous treatment of such a lower bound buckling solution is given in Ref. 79. The assumptions made in this reference are essentially the same as in Ref. 31.

The effective moment of inertia in the lateral direction.

$$\frac{I_{yy}}{\bar{I}_{yy}} = (1-2\lambda) \tag{5.36}$$

The effective St. Venant's torsional constant.

$$\frac{K_T}{\bar{K}_T} = \frac{(1-2\lambda)-(0.63\frac{b}{d})}{1-0.63\frac{b}{d}} \tag{5.37}$$

The bending moment about the neutral axis.

$$\frac{M_{xx}}{(M_p)_{xx}} = 1-\frac{1}{3}(1-2\lambda)^2 \tag{5.38}$$

With the aid of Eqs. 3.36 through 3.38, equation 5.35 may be written as:

$$L_{cr} = \frac{4\pi}{\sigma_y bd^2\left[1-\frac{1}{3}(1-2\lambda)^2\right]}\sqrt{\bar{B}_{yy}\,\bar{C}_T\,(1-2\lambda)\left[\frac{(1-2\lambda)-0.63\frac{b}{d}}{1-0.63\frac{b}{d}}\right]} \tag{5.39}$$

where $\bar{I}_{yy}$ and $\bar{C}_T$ are the elastic bending rigidity and the elastic torsional rigidity of the cross section, and λ is the yielding parameter.

The critical moment versus length curve can thus be constructed by using Eqs. 5.38 and 5.39 as λ varies. This is

shown in Fig. 5.47. It should be noted that this is a lower bound buckling curve; all points on this curve correspond to the point B on the schematic plot in Fig. 1.1c, and at every point on this curve the yield penetration λ is known.

5.10.2 Description of the Post-Buckling Strength Solution

After the load-deflection curve reaches point B in Fig. 1.1c, lateral-torsional deformations will take place, and the yielded configuration in the beam cross sections will become anti-symmetrical with respect to the centroid as shown. This is exactly the same situation as Case II of the biaxial bending problem. The procedures are identical to those developed for biaxial bending, with the exception of the following minor correction:

In this case the inclination of the applied moments, α, is a variable. At any stage of loading it is equal to the twisting angle β. Therefore modifications are necessary for calculating Eq. 5.32. This relationship can be rewritten in the following form:

$$\beta = \frac{1}{2}\left\{ \tan^{-1}\left[\frac{I_{\eta\eta}}{I_{\xi\xi}} \tan(\theta+\phi) \right] - \phi \right\} \qquad (5.40)$$

The equilibrium trials of Eq. 5.10 are the same as described before.

Figure 5.48 shows the results of the illustrated solution of the post-buckling strength problem. In this figure the M-β_o relationships for α equals to 0^o, 5^o, and 10^o are plotted for comparison. The curve marked $\alpha = 0^o$ is the post-buckling solution, whereas the other two curves are biaxial bending solutions. In this calculation the following values are assumed:

$$b = 2"$$

$$\frac{d}{b} = 2$$

$$\frac{L}{b} = 30$$

$\alpha = 0^o$, 5^o and 10^o respectively.

It should be mentioned that the M-β_o relationships in Fig. 5.48 serve quantitatively as an example for the initial imperfection solutions. For an initially straight member, the M-β_o curve would correspond to the curve for $\alpha = 0^o$. The larger the initial deformations the lower the maximum moment would be expected.

5.10.3 Solutions Considering Residual Stresses

Solutions considering residual stresses would be more complicated since the yielded configuration of the beam cross sections will no longer be anti-symmetrical and the neutral axis will translate in addition to rotations. A wide-flange cross section is

shown in Fig. 5.49 to illustrate this phenomenon. It should be noted that the additional complications in such a case only lie in the preparations of all the interaction curves. The basic trial procedure again would be the same as presented in this chapter. The initial motion solutions taking into account the effect of residual stresses presented in Ref. 3 can be adopted as a starting point for such solutions.

With the influence of residual stresses, the lower bound initial motion load is lower than that when ignoring the residual stresses.[3] Therefore the total increment of moment ΔM_{xx} would be more appreciable than that of the solution when the influence of residual stresses is ignored.

6. SUMMARY AND CONCLUSIONS

This dissertation deals with the load-deformation behavior of beams subjected to uniform moments. Special attention is paid to the following problems:

(a) The spacing of lateral bracing in the vicinity of plastic hinges.

(b) Lateral bracing requirements in the vicinity of plastic hinges.

(c) The biaxial bending strength and the post-buckling strength of beams.

These subjects are treated both analytically and experimentally for A7 type structural steel beams failing in the inelastic range.

The following list contains the new contributions set forth in this dissertation.

(a) The problems associated with lateral-torsional instability phenomena are explained and differentiated, and the concept of buckling under full plastic moment is analyzed. An upper bound solution is developed by analytical means for predicting the critical unsupported length of a beam failing by lateral buckling under plastic hinge moment.

(b) The critical length of beams is determined by experiments on laterally supported beams. These same experimental observations furnish information about the post-buckling strength, rotation capacity and cause for failure.

(c) The bracing requirement necessary to prevent failure until the beam has performed its intended function is investigated experimentally by testing beam-purlin assemblies.

(d) The biaxial bending strength and the post-buckling strength of beams subjected to equal terminal moments is determined analytically.

The following conclusions may be drawn from this investigation:*

(a) For simply supported beams buckling under constant plastic moment, an upper bound solution of the critical unsupported length is achieved. This critical slenderness ratio L/r_{yy} is equal to 40 (versus a lower bound solution of $L/r_{yy} = 18$).

(b) The optimum unsupported length for the bracing spacing of laterally continuous beams ($L/r_{yy} = 40$) is established experimentally.

*More detailed conclusions are contained at the end of each chapter.

(c) The lateral restraints provided by adjacent spans are of primary importance in order to develop satisfactory post-buckling strength and plastic hinge rotations of a member.

(d) Lateral buckling does not influence the rotation capacity of laterally continuous beams.

(e) Local buckling of the compression flange terminates the post-buckling strength of beams with idealized support conditions.

(f) The lateral bending stiffness of bracing members controls the post-buckling strength of a beam supported by purlins. The relationship of the rotation capacity of a beam and the requirements of bracing members is determined from experimental results of the beam-purlin assembly tests.

(g) A theory taking into account the interactions among deformation variables is developed for obtaining the true ultimate strength of beams governed by lateral-torsional instability. The method of solution is explained by solving the problem of biaxial bending of a beam of rectangular cross section.

(h) The developed analytical procedures are applied to obtain solutions of wide-flange beams. Moment versus deformation relationships are presented. The method developed in this dissertation can be used directly to obtain other types of ultimate strength solutions equally well, (that is, the post-buckling strength solution and the initial imperfection solution) for members subjected to constant moment. Extension of the procedures may lead to the solutions of biaxially loaded columns failing in the inelastic range.

7. NOMENCLATURE

A = Cross sectional area

= Integration constant (Chapter 5)

A_F = Area of flanges for wide-flange section

A_W = Area of web for wide-flange section

dA = Differential area element

B = Integration constant (Chapter 5)

= $4 + 2(\alpha-1)\, q + \beta\Gamma$ (Appendix A)

B_{xx} = Bending stiffness about x-x axis (strong axis stiffness)

B_{yy} = Bending stiffness about y-y axis (weak axis stiffness)

$\bar{B}_{xx}$ = Bending stiffness about x-x axis in the elastic range

$\bar{B}_{yy}$ = Bending stiffness about y-y axis in the elastic range

$B_{\xi\xi}$ = Bending stiffness about ξ - ξ axis in the inelastic range (Strong axis stiffness)

$B_{\eta\eta}$ = Bending stiffness about η - η axis in the inelastic range (Weak axis stiffness)

C = Centroid of a cross section

C_w = Warping stiffness

C_T = St. Venant's torsional stiffness

$\bar{C}_w$ = Warping stiffness in the elastic range

$\bar{C}_T$ = St. Venant's torsional stiffness in the elastic range

E = Young's modulus

E_{st} = Strain-hardening modulus

G = Shear modulus

G_{st} = Shear modulus in the strain-hardening range

I = Moment of inertia

I_{11}, I_{22} = Principal moment of inertia of a cross section

I_{xx} = Moment of inertia about the x-x axis

I_{yy} = Moment of inertia about the y-y axis

$I_{x'x'}$ = Principal moment of inertia about the x'-x' axis in the elastic range

$I_{y'y'}$ = Principal moment of inertia about the y'-y' axis in the elastic range

$I_{\xi\xi}$ = Principal moment of inertia about the ξ -ξ axis in the inelastic range

$I_{\eta\eta}$ = Principal moment of inertia about the η - η axis in the inelastic range

I_w = Warping moment of inertia

$\bar{I}_w$ = Warping moment of inertia in the elastic range

K_T = St. Venant's torsional constant

$\bar{K}_T$ = St. Venant's torsional constant in the elastic range

L = Length of a member

L_{cr} = Critical unsupported length of a beam

$\frac{L_{cr}}{r_{yy}}$ = Weak axis slenderness ratio of a beam

$\left(\frac{L_{cr}}{r_{yy}}\right)_T$ = Lower bound critical slenderness ratio

$\left(\frac{L_{cr}}{r_{yy}}\right)_R$ = Upper bound critical slenderness ratio

M = Moment

M_{NA} = Moment about the neutral axis

M_{xx} = Moment about the x-x axis (strong axis)

M_{yy} = Moment about the y-y axis (weak axis)

$M_{\xi\xi}$ = Moment about the ξ-ξ axis (in the inelastic range)

$M_{\eta\eta}$ = Moment about the η-η axis (in the inelastic range)

$(M)_{max}$ = Maximum moment

$(M)_{cr}$ = Critical buckling moment

M_y = Yield moment = $\sigma_y.S$

M_p = Plastic hinge moment = $\sigma_y.Z$

dM_{xx} = Change of moment about the x-x axis

NA = The neutral axis of a cross section

P = Concentrated load

P_y = Full plastic load = $\sigma_y.A$

R = A_w/A_F = Ratio of the areas of the web to the flanges

R_1 = $\frac{wd}{bt}$ = ratio of the areas of the web to one flange

S = Section modulus

T = Twisting moment

Z = Plastic modulus

b = Width of flange of a WF section

= Width of a rectangular section

b_1 = One half flange width = b/2

b_b = Purlin flange width

b' = Width of the elastic portion of flange

c = Center of twist of a lateral-torsionally deformed cross section

c_o, c_1, c_2, c_3, c_4 Are perpendicular distances measured from the neutral axis to different locations in a partially yielded cross section

d = Depth of a WF section

= Depth of a rectangular section

d_w = Depth of web

d/b = The aspect ratio of a rectangular section

d_1 = Effective depth of a partially yielded section

d_b = Purlin section depth

d_{wb} = Purlin web depth

f = Z/S, the shape factor

g,i,k = Symbols for tensor notations

l_b = Purlin span length

$$m_1^2 = -\frac{C_T}{2C_w} + \sqrt{\frac{C_T^2}{4C_w^2} + \left[\frac{M_{xx}^2}{B_{\eta\eta}\cdot C_w} + \frac{M_{yy}^2}{B_{\xi\xi}\cdot C_w}\right]}$$

$$m_2^2 = \frac{C_T}{2C_w} + \sqrt{\frac{C_T^2}{4C_w^2} + \left[\frac{M_{xx}^2}{B_{\eta\eta}\,C_w} + \frac{M_{yy}^2}{B_{\xi\xi}\,C_w}\right]}$$

n = Ratio of strain-hardening modulus to Young's modulus

$$p_1 = \frac{m_1^2}{m_1^2 + m_2^2}$$

$$p_2 = \frac{m_2^2}{m_1^2 + m_2^2}$$

q = $\dfrac{M_{xx} M_{yy} \left(\dfrac{1}{B_{\eta\eta}} - \dfrac{1}{B_{\xi\xi}} \right)}{\dfrac{M_{xx}^2}{B_{\eta\eta}} + \dfrac{M_{yy}^2}{B_{\xi\xi}}}$ (Chapter 5)

= Penetration of strain-hardening zones along flanges (Chapter 2)

q_1 = $\sqrt{\dfrac{M_{xx}^2}{C_T B_{\eta\eta}} + \dfrac{M_{yy}^2}{C_T B_{\xi\xi}}}$

q_2 = $M_{xx} M_{yy} \left(\dfrac{1}{C_T B_{\xi\xi}} - \dfrac{1}{C_T B_{\eta\eta}} \right)$

r = Radius of gyration

r_{yy} = Radius of gyration of beams in the weak direction

$(r_{yy})_b$ = Radius of gyration of purlins in the weak direction

s = Distance measured along one element of a thin-walled open section (Appendix A)

=Distance perpendicular to the neutral axis (variable) (Chapter 5)

ds = Infinitesimal change of distance from the neutral axis

t = Thickness of flanges of a WF beam section

t_b = Thickness of flange of purlins

u = Deflection in the z-x plane

u_o = Deflection of the midspan section in the z-x plane

$\bar{u}$ = Initial deflection of the midspan section in the z-x plane

v = Deflection in the z-y plane

v_o = Deflection of the midspan section in the z-y plane

$\bar{v}$ = Initial deflection of the midspan section in the z-y plane

w = Thickness of the web of a wide-flange beam section

w_b = Thickness of the web of a purlin section

x,y = Principal coordinates of the cross section in the undeformed state

x',y' = Principal coordinates of the cross section in the deformed state

z = Coordinate along undeformed beam centerline

α = $\frac{t_1}{t_2}$ (Appendix A)

= Inclination of the applied moment (Chapter 5)

β = w/t_2 (Appendix A)

= Twisting angle of the beam sections (Chapter 5)

β_o = Twisting angle at midspan section

$\bar{\beta}$ = Initial twisting angle at midspan section

γ = d/b_1 (Appendix A)

$\delta, \delta_1, \delta_2$ = Deflections of a member

ϵ = Strain

ϵ_y = Strain at first yield

ϵ_{st} = Strain at the onset of strain-hardening

ζ = Deflected longitudinal axis of centroid of cross section

θ = Inclination of the neutral axis with respect to the x'-x' axis of a partially yielded cross section

$\lambda_1, \lambda_2, \lambda_3$ = Yielding parameters of a partially yielded rectangular section

μ_1, μ_2 = Yielding parameters of a partially yielded wide-flange section

ν_r = Lateral restraining factor

ξ, η = Variable coordinate axes corresponding to the x'- and y'- axis respectively, after deformation has taken place.

ρ_o = Distance of tangent at any point on a cross section from the shear center

σ = Stress

σ_y = Yield stress

σ_{rc} = Maximum compressive residual stress

σ_{rt} = Maximum tensile residual stress

τ = Equal interval between the sections where deflections were measured (Chapter 4)

ϕ = Inclination of the principal axes ξ-ξ and η-η with respect to x'-x' and y'-y' axes (Chapter 5)

= Curvature

ϕ_{xx} = Curvature about the strong axis

ϕ_{yy} = Curvature about the weak axis

$\Delta\phi_{xx}$ = Virtual increment of curvature about the x-x axis

$\Delta\phi_{yy}$ = Virtual increment of curvature about the y-y axis

ψ = Rotation in radians at the bracing section

ω_o = $\int \rho_o \, ds$, the unit warping

ω_n = Normalized unit warping

8. APPENDICES

APPENDIX A

CALCULATION OF THE WARPING CONSTANT I_w FOR A WIDE-FLANGE SECTION OF VARIABLE THICKNESSES IN THE FLANGES

Rigorous presentation of warping torsion for thin-walled open cross sections can be found in Refs. 8, 36 and 37. By definition:

$$I_w = \int \omega_n^2 \, t_{ik} \, ds = \sum \frac{1}{3} t_{ik} \ell_{ik} \left[(\omega_{ni} + \omega_{nk})^2 - \omega_{ni} \omega_{nk} \right] \tag{A.1}$$

and

$$\omega_o = \int \rho_o \, ds \tag{A.2}$$

where: I_w = the warping constant

i,k = symbols represent the two end stations of an element in a thin-walled section (see Fig. 2.10)

t_{ik} = thickness of an element between stations i and k

ℓ_{ik} = length of an element between stations i and k

s = distance along element ik measured from point i toward point k

ρ_o = distance of tangent at any point on the section from the shear center of the cross section. It is positive if the direction i-k is counter-clockwise with respect to the shear center.

w_o = unit warping with respect to shear center

w_n = normalized unit warping with respect to shear center

$$= \frac{1}{A}\int w_o t_{ik}\, ds - w_o$$

A = area of the element i-k

$$= \int_i^k t_{ik} ds = t_{ik}\, \ell_{ik}$$

The normalized unit warping can be written as:

$$\omega_n = \frac{1}{2A}\sum (\omega_{oi} + \omega_{ok})\, t_{ik}\, \ell_{ik} - \omega_o \qquad \text{(A.3)}$$

Equation (A.1) can now be calculated by using Eq. (A.3). The result is given by:

$$I_w = \frac{1}{3}\left\{ -\frac{3}{4}\left[(\omega_{oi} + \omega_{ok})\, t_{ik}\, \ell_{ik} \right]^2 \cdot A + \sum (\omega_{oi} + \omega_{ok})^2\, t_{ik}\, \ell_{ik} - \sum \omega_{oi}\, \omega_{ok}\, t_{ik}\, \ell_{ik} \right\} \qquad \text{(A.4)}$$

For a wide-flange shape, Eq. (A.4) may be listed in a tabular form for convenient calculations.

STATION	① $\frac{t_{ik}}{t_2}$	② $\frac{l_{ik}}{b_1}$	③ $\frac{\rho_{ik}}{\frac{d}{2}}$	④ ②×③	⑤ $\frac{\omega_o}{\frac{b_1 d}{2}} = \sum$④	⑥ $\frac{\omega_{oi}+\omega_{ok}}{\frac{b_1 d}{2}}$	⑦ ①×②	⑧ ⑥×⑦
1					0			
1-2	α^*	q	1	q		q	αq	αq^2
2					q			
2-3	1	$1-q$	1	$1-q$		$1+q$	$1-q$	$1-q^2$
3					1			
3-4	1	1	1	1		3	1	3
4					2			
3-5	β^*	r^*	0	0		2	βr	$2\beta r$
5					1			
5-6	1	$1-q$	-1	$-(1-q)$		$1+q$	$1-q$	$1-q^2$
6					q			
6-7	α	q	-1	$-q$		q	αq	αq^2
7					0			
5-8	1	1	-1	1		3	1	3
8					2			

Thus

$$2A = 2\sum⑦ = 2t_2 b_1 \left[4 + 2(\alpha-1)q + \beta r\right]$$

$$\sum⑧ = b_1^2 d t_2 \left[4 + \beta r + q^2(\alpha-1)\right]$$

and Eq. (A.3) is given by:

---

* The expression for α, β and Γ are shown in Fig. 2.11.

$$\omega_n = \frac{1}{2A}\sum ⑧-⑤_i = \frac{k_o}{2} - ⑤_i \qquad \text{(A.5)}$$

With the aid of Eq. (A.5) Eq. (A.4) can be simplified to:

$$I_w = -\frac{3}{4}\frac{[\Sigma ⑧]^2}{A} + \sum ⑦\left[⑥^2 - ⑤_i ⑤_k\right]$$

Substituting the corresponding values from the above given table, the warping constant becomes:

$$I_w = \frac{1}{4B}\left\{(4+\beta r)\left[2q^2(\alpha-1)(q-3)+4\right] + (\alpha-1)q\left[q^3(\alpha-1)+2(16+3\beta r)\right]\right\}\cdot\frac{t_2 b_1^3 d^2}{3} \qquad \text{(A.6)}$$

where

$$B = \left[4 + 2(\alpha-1)q + \beta r\right]$$

$\frac{t_2 b_1^3 d^2}{3} = I_w$ = The warping constant for a wide-flange section of uniform flange thicknesses (See Fig. 2.11).

For $E_{st} = 900$ ksi

$E = 30{,}000$ ksi

$n = \frac{E_{st}}{E} = 0.03$

$R_1 = \frac{d_w w}{2b_1 t}$

$b = 2b_1$

and $\alpha = \frac{t_1}{t_2}$

$\beta = w$

$\gamma = d/b_1$

$\therefore B = 2\left[2 + R_1 + (\alpha-1)q\right]$

Equation (A.6) can be written as

$$E I_w = \frac{n E}{8\left[2+R_1-\left(\frac{1}{n}-1\right)q\right]}\left\{2(2+R_1)\left[4-2q^2\left(\frac{1}{n}-1\right)(3-q)\right] + \left(\frac{1}{n}-1\right)q\left[q^3\left(\frac{1}{n}-1\right)+4(8+3R_1)\right]\right\}\cdot \bar{I}_w \quad (A.7)$$

or, in a form for calculations,

$$\frac{C_w}{\bar{C}_w} = \frac{3}{800\left[2+q\frac{97}{3}+R_1\right]}\left\{2(2+R_1)\left[4-194\,q^2-\frac{194}{3}q^3\right] + \frac{97}{3}q\left[\frac{97}{3}q^3+4(8+3R_1)\right]\right\} \quad (A.8)$$

APPENDIX B

INELASTIC BIAXIAL BENDING OF WIDE-FLANGE BEAMS

B.1 THE DIFFERENTIAL EQUATIONS AND THEIR SOLUTIONS

For thin-walled open cross sections, the equilibrium equations are given by Eqs. 1.5. For simply supported end conditions* the solutions of the differential equations can be written as follows.

$$\beta = q\left[P_2\left(-\sin m_1 z \tan\frac{m_1 L}{2} - \cos m_1 z\right) + P_1\left(\sinh m_2 z \tanh\frac{m_2 L}{2} - \cosh m_2 z\right) + 1\right] \qquad \text{(B.1)}$$

$$u = \frac{1}{B_{\eta\eta}}\left\{-\frac{M_{yy}}{2}(Lz - z^2) + M_{xx} q\left[\frac{P_2}{m_1^2}\left[\tan\frac{m_1 L}{2}\cdot\left(\sin m_1 z - \frac{z}{L}\sin m_1 L\right) + \left(\cos m_1 z - \frac{z}{L}\cos m_1 L\right)\right]\right.\right.$$
$$+ \frac{P_1}{m_2^2}\left[\tanh\frac{m_2 L}{2}\left(\sinh m_2 L - \frac{z}{L}\sinh m_2 L\right) - \left(\cosh m_2 L - \frac{z}{L}\cosh m_2 L\right)\right] + \frac{1}{2}\left[z^2 - Lz\right]\Bigg]$$
$$\left. - M_{xx} q\left[\frac{P_2}{m_1^2}\left(1 - \frac{z}{L}\right) - \frac{P_1}{m_2^2}\left(1 - \frac{z}{L}\right)\right]\right\} \qquad \text{(B.2)}$$

*The necessary boundary conditions for the solution of Eqs. 1.5 are: $u = v = 0$ and $\beta = \frac{d^2\beta}{dz^2} = 0$ at $z = 0$ and at $z = L$, the condition $\beta'' = 0$ implies no warping at both ends.

$$v = -\frac{1}{B_{55}}\left\{\frac{M_{xx}}{2}(Lz-z^2) + M_{yy}\,q\left[\frac{P_2}{m_1^2}\left[\left[\tan\frac{m_1L}{2}\cdot\right.\right.\right.\right.$$

$$\left(\sin m_1 z - \frac{z}{L}\sin m_1 L\right) + \left(\cos m_1 z - \frac{z}{L}\cos m_1 L\right)$$

$$-\frac{P_1}{m_2^2}\left[\left[\tan\frac{m_2L}{2}\left(\sinh m_2 z - \frac{z}{L}\sinh m_2 L\right)\right.\right.\right.$$

$$\left.\left.\left.\left.-\left(\cosh m_2 L - \frac{z}{L}\cosh m_2 L\right) + \frac{1}{2}\left[\left[z^2 - Lz\right]\right]\right]\right.\right.$$

$$\left.\left.-M_{yy}\,q\left[\frac{P_2}{m_1^2}\left(1-\frac{z}{L}\right) - \frac{P_1}{m_2^2}\left(1-\frac{z}{L}\right)\right]\right\} \qquad \textbf{(B.3)}$$

The expression for equilibrium at the center span ($z = \frac{L}{2}$) are given by:

$$P_o = q\left[-P_2\,\mathrm{Sec}\,\frac{m_1L}{2} - P_1\left(\mathrm{Sech}\,\frac{m_2L}{2}\right) + 1\right] \qquad \textbf{(B.4)}$$

$$u_o = -\frac{1}{B_{\eta\eta}} \left\{ -\frac{M_{yy}}{8} L^2 + M_{xx}\, q \left[\frac{P_2}{m_1^2} \left[\left[\tan \frac{m_1 L}{2} \cdot \left(\sin \frac{m_1 L}{2} - \frac{1}{2} \sin m_1 L \right) + \left(\cos \frac{m_1 L}{2} - \frac{1}{2} \cos m_1 L \right) \right] \right. \right. \right.$$

$$\left. - \frac{P_1}{m_1^2} \left[\left[\tanh \frac{m_2 L}{2} \left(\sinh \frac{m_2 L}{2} - \frac{1}{2} \sinh m_2 L \right) \right. \right. \right.$$

$$\left. \left. \left. - \left(\cosh \frac{m_2 L}{2} - \frac{1}{2} \cosh m_2 L \right) \right] - \frac{L^2}{8} \right] \right.$$

$$\left. - \frac{M_{xx}}{2} \cdot q \left[\frac{P_2}{m_1^2} - \frac{P_1}{m_2^2} \right] \right\} \qquad \text{(B.5)}$$

$$v_o = -\frac{1}{B_{ss}} \left\{ \frac{M_{xx}}{8} L^2 + M_{yy} \cdot q \left[\frac{P_2}{m_1^2} \cdot \left[\left[\tan \frac{m_1 L}{2} \cdot \left(\sin \frac{m_1 L}{2} - \frac{1}{2} \sin m_1 L \right) + \left(\cos \frac{m_1 L}{2} - \frac{1}{2} \cos m_1 L \right) \right] \right. \right. \right.$$

$$\left. - \frac{P_1}{m_2^2} \left[\left[\tanh \frac{m_2 L}{2} \left(\sinh \frac{m_2 L}{2} - \frac{1}{2} \sinh m_2 L \right) \right. \right. \right.$$

$$\left. \left. \left. - \left(\cosh \frac{m_2 L}{2} - \frac{1}{2} \cosh m_2 L \right) \right] - \frac{L^2}{8} \right] \right.$$

$$\left. - \frac{M_{xx}}{2} \cdot q \left[\frac{P_2}{m_1^2} - \frac{P_1}{m_2^2} \right] \right\} \qquad \text{(B.6)}$$

where

$$\gamma = -\frac{M_{xx}\, M_{yy}\left(\frac{1}{B_{\eta\eta}} - \frac{1}{B_{\xi\xi}}\right)}{\frac{M_{xx}^2}{B_{\eta\eta}} + \frac{M_{yy}^2}{B_{\xi\xi}}} \tag{B.7}$$

$$m_1^2 = -\frac{C_T}{2C_w} + \sqrt{\frac{C_T^2}{4C_w^2} + \left[\frac{M_{xx}^2}{B_{\eta\eta}\, C_w} + \frac{M_{yy}^2}{B_{\xi\xi}\, C_w}\right]} \tag{B.8}$$

$$m_2^2 = +\frac{C_T}{2C_w} + \sqrt{\frac{C_T^2}{4C_w^2} + \left[\frac{M_{xx}^2}{B_{\eta\eta}\, C_w} + \frac{M_{yy}^2}{B_{\xi\xi}\, C_w}\right]} \tag{B.9}$$

$$P_1 = \frac{m_1^2}{m_1^2 + m_2^2} \tag{B.10}$$

$$P_2 = \frac{m_2^2}{m_1^2 + m_2^2} \tag{B.11}$$

For a wide-flange beam section, the bending stiffness in the strong direction is much greater than that in the weak direction. (That is $B_{\xi\xi} \gg B_{\eta\eta}$.) Furthermore if the inclination of moment is small (that is, $M_{xx} \gg M_{yy}$) Eqs. B.7 through B.9 can be simplified to the following expression: (The error introduced by these simplifications is negligible.)

$$\eta = -\frac{M_{yy}}{M_{xx}} \qquad (B.12)$$

$$m_1^2 = -\frac{C_T}{2C_w} + \sqrt{\frac{C_T^2}{4C_w^2} + \frac{M_{xx}^2}{B_{\eta\eta} C_w}} \qquad (B.13)$$

$$m_2^2 = \frac{C_T}{2C_w} + \sqrt{\frac{C_T^2}{4C_w^2} + \frac{M_{xx}^2}{B_{\eta\eta} C_w}} \qquad (B.14)$$

Equations B.3 through B.5 and B.10 through B.14 are used for solutions in this dissertation. Calculations of the expressions for bending moment about the neutral axis (Eqs. B.24 and B.25) were obtained by a LGP-30 electronic computer furnished by Lehigh University.

B.2 THE INTERACTION CURVES FOR THE REDUCTION OF STIFFNESS PARAMETERS IN PARTIALLY YIELDED CROSS SECTIONS

Symbols and definitions of a partially yielded section in the deformed position are shown in Fig. 5.24. Calculations are performed on a 10WF25 section.

Based on the same assumptions made in the solutions of rectangular beams and Eqs. 5.19 through 5.21, the interaction curves of bending stiffnesses with respect to the yielding parameters are given in Figs. 5.25 through 5.28. The expressions for the

effective moment of inertia in terms of the yielding parameters are given by:

Case I

$$I_{x'x'} = 2\left\{ \frac{1}{12} b\left(1-\frac{1}{2}\mu_1\mu_2\right)^3 t^3 + bt\left(1-\frac{1}{2}\mu_1\mu_2\right)\cdot \left[\frac{d-\left(1-\frac{1}{2}\mu_1\mu_2\right)}{2}\right]^2 + \frac{1}{12}\omega\left[d-2\left(1-\frac{1}{2}\mu_1\mu_2\right)\right]^3 \right\} \quad \text{(B.15)}$$

$$I_{y'y'} = \frac{1}{6} b^3\left(1-\frac{1}{2}\mu_1\mu_2\right) t \quad \text{(B.16)}$$

$$I_{x'y'} = -2\left[-\frac{1}{72}\mu_1^2\mu_2^2 b^2 t^2 + \frac{1}{2}\mu_1\mu_2 bt\left(\frac{b}{2}-\frac{\mu_2 b}{3}\right)\left(\frac{d}{2}-\frac{\mu_1 t}{3}\right)\right] \quad \text{(B.17)}$$

Case II

$$I_{x'x'} = \left[1-\frac{1}{2}(\mu_1+\mu_2)\right]\left[\frac{1}{6} bt^3 + bt\left(\frac{d-t}{2}\right)^2\right] + \frac{1}{12}\omega(d-2t)^3 \quad \text{(B.18)}$$

$$I_{y'y'} = \frac{1}{6} b^3 t\left[\left(1-\frac{\mu_1+\mu_2}{2}\right)^3 + 3\left(1-\frac{\mu_1+\mu_2}{2}\right)\left(\frac{\mu_1+\mu_2}{2}\right)^2\right] \quad \text{(B.19)}$$

$$I_{x'y'} = -\frac{1}{36} b^2 t\left[18\mu_1(1-\mu_1)(d-t) - (\mu_2-\mu_1)^2 t + (\mu_2-\mu_1)(3-4\mu_1-2\mu_2)(3d-2t)\right] \quad \text{(B.20)}$$

In obtaining the expressions for $I_{x'x'}$ and $I_{y'y'}$, simplifications were made as indicated in Fig. 5.29. The same approximations, that is, the area ABC = area ADEF as shown, were also adopted for the calculations of St. Venant's torsional constant (Figs. 5.30 and 5.31) and the warping constant (Figs. 5.32 and 5.33) of partially yielded sections.

The St. Venant's torsional constant is thus given by the following expressions:

$$K_T = \frac{2}{3} b' t^3 + \frac{1}{3} d_w \omega^3 \qquad \text{(B.21)}$$

where

$$b' = \left(1 - \frac{1}{2}\mu_1\mu_2\right) b \qquad \text{for Case I}$$

$$= \left[1 - \frac{1}{2}(\mu_1 + \mu_2)\right] b \qquad \text{for Case II} \qquad \text{(B.22)}$$

$\bar{K}_T$ is defined by Eq. (2.9) and may be found in Ref. 75.

The interaction curves for St. Venant's torsional rigidity are given in Figs. 5.30 and 5.31 for Case I and Case II respectively.

The approximations made for calculating the effective warping constant are shown in Figs. 5.32 and 5.33. In these

figures the interaction curves are also given. The corresponding interaction expression takes the following form:

$$\frac{I_w}{\bar{I}_w} = \frac{1}{8\left[(\alpha+1)+R_1\right]^2}\Bigg\{ 2\left[(1+\alpha)^2+2R_1\right]\left[(1+\alpha)+R_1\right] + 2\alpha\left[(1+\alpha)^2+2\alpha R_1\right]\left[(1+\alpha)+\alpha R_1\right] + (\alpha^2-1)^2(1+\alpha)+3R_1(\alpha^2-1)^2\Bigg\} \qquad \text{(B.23)}$$

where I_w = effective warping constant

$\bar{I}_w = \frac{1}{24} b^3 d^2 t$

= warping constant of a fully elastic wide-flange section

$\alpha = 1 + 1/2\ (\mu_1 - \mu_2)$

= yielding parameter along the flange in the x' direction as shown in Fig. 5.33

$R_1 = \frac{d_w.w}{bt'}$

= ratio of web area and one flange area in which

$t' = (1 - \frac{1}{2}\mu_1\mu_2)\ t$ for Case I (Fig. 5.32)

$= \frac{(1 - \frac{1}{2}\mu_1\mu_2)}{1-\mu_1}\ t$ for Case II (Fig. 5.33).

Equation B.23 is obtained based on the same procedure as presented in Appendix A. In fact, it can be deduced directly

from Eq. A.6.

B.3 THE BENDING MOMENT ABOUT THE NEUTRAL AXIS

The nomenclatures for integrating of Eq. 5.28 are defined in Fig. 5.34. The resultant expressions for the moment about the neutral axis are given as follows:

Case I

$$M_{N.A.} = \frac{2}{3}\sigma_y \left\{ \frac{\omega}{C_2}\cdot\frac{C_d^3}{\cos\theta} + \frac{t}{C_2}\frac{C_3^3}{\sin\theta}\left[1-\left(\frac{C_1}{C_3}\right)^3\right] \right.$$
$$+3(\tan\theta+\cot\theta)\left[\frac{C_o^4}{12C_2}\left[1+3\left(\frac{C_1}{C_o}\right)^4-4\left(\frac{C_1}{C_o}\right)^3\right]\right.$$
$$+\frac{C_4^3}{C_2}\left[\frac{1}{4}\left(\frac{C_3}{C_4}\right)^4-\frac{1}{4}\left(\frac{C_2}{C_4}\right)^4-\frac{1}{3}\left(\frac{C_2}{C_3}\right)^3-\frac{1}{3}\left(\frac{C_3}{C_4}\right)^3\right]$$
$$\left.\left.+\frac{C_4^3}{6}\left[1-3\left(\frac{C_2}{C_4}\right)^2-2\left(\frac{C_2}{C_4}\right)^3\right]\right]\right\} \qquad \text{(B.24)}$$

Case II

$$M_{N.A.} = \sigma_y \left\{ \frac{1}{\cos\theta}\left[\frac{2}{3}b(\mu_2-\mu_1)C_2^2\left[1-\left(\frac{C_1}{C_2}\right)^3\right]\right.\right.$$
$$+bC_3^2(\mu_2-\mu_1)\left[1-\left(\frac{C_2}{C_3}\right)^2\right]+\frac{2}{3}\omega\frac{C_d^3}{C_2}\Bigg]$$
$$+\frac{1}{3}(\tan\theta+\cot\theta)\left[C_4^3\left[1+2\left(\frac{C_3}{C_4}\right)^3-3\left(\frac{C_3}{C_4}\right)^2\right]\right.$$
$$\left.\left.+\frac{C_o^4}{C_2}\left[\frac{1}{2}+\frac{3}{2}\left(\frac{C_1}{C_o}\right)^4-2\left(\frac{C_1}{C_o}\right)^3\right]\right]\right\} \qquad \text{(B.25)}$$

where $\theta = \tan^{-1}\left(\frac{t}{b}\right)\left(\frac{\mu_1}{\mu_2}\right)$ for Case I

$= \tan^{-1}\left(\frac{t}{b}\right)\left(\frac{1}{\mu_1-\mu_2}\right)$ for Case II

$C_d = \frac{1}{2}(d-2t)\cos\theta$

$C_o = \frac{1}{2}(d-2t)\cos\theta - \frac{1}{2} b \sin\theta$

$C_1 = \frac{1}{2}(d\cos\theta - b\sin\theta)$

$C_2 = \left(\frac{d}{2} - \mu_1 t\right)\cos\theta + \frac{b}{2}\sin\theta$ for Case I

$= \frac{1}{2}\left[(d-2t)\cos\theta + b(1-2\mu_1)\sin\theta\right]$ for Case II

$C_3 = \frac{1}{2}\left[(d-2t)\cos\theta + b\sin\theta\right]$

$C_4 = \frac{1}{2}(d\cos\theta + b\sin\theta)$

For $\mu_1 = \mu_2 = 1.0$ in Case I and $\mu_1 = 0$ and $\mu_2 = 1.0$ in Case II, Eq. B.24 and B.25 can be reduced to the following identical expression:

$$M_{N.A.} = \frac{2}{3}\sigma_y\left\{\frac{\omega}{C_2}\cdot\frac{C_d^3}{\cos\theta} + \frac{t C_2^2}{\sin\theta}\left[1-\left(\frac{C_1}{C_2}\right)^3\right]\right.$$

$$+ \frac{1}{\sin 2\theta}\left[\frac{1}{2}\left(\frac{C_o}{C_2}\right)^4\left[1-4\left(\frac{C_1}{C_o}\right)^3+3\left(\frac{C_1}{C_o}\right)^4\right]\right.$$

$$\left.\left. + C_4^3\left[-3\left(\frac{C_2}{C_4}\right)^2+2\left(\frac{C_2}{C_4}\right)^3\right]\right]\right\} \qquad \text{(B.26)}$$

The interaction curves plotted from Eqs. B.24 and B.25 are shown in Figs. 5.35 and 5.36 respectively.

B.4 THE INTERACTION CURVES FOR THE VARIATION OF THE TWISTING ANGLE IN PARTIALLY YIELDED CROSS SECTIONS

In Figs. 5.37 through 5.40 are shown the variations of the ratio of the principal moment of inertia, $I_{\xi\xi}/I_{\eta\eta}$, and the inclinations of the principal axes, ϕ, with respect to the yielding parameters μ_1 and μ_2. The relationships between the twisting angle β and the yielding parameters can then be obtained by trials based on Eq. 5.32 and Fig. 5.37 through 5.40. These relationships are given in Figs. 5.41 and 5.42.

B.5 SUMMARY OF SOLUTIONS FOR WIDE-FLANGE BEAMS

Using the same trial procedures mentioned in Chapter 5, the moment versus twisting relationships at the midspan (Eq. B.4) are obtained as shown in Fig. 5.43. Three different slenderness ratios are calculated. (L/r_{yy} = 40, 60, and 80.) The corresponding moment versus lateral deflection and moment versus vertical deflection are consequently obtained for these different slenderness ratios. They are given in Figs. 5.44 and 5.45 respectively.

It is seen from Figs. 5.43 through 5.45 that the lateral deflection u_o and the maximum twisting angle β_o at maximum moment increase as the slenderness ratio L/r_{yy} increases, while the vertical deflection v_o at maximum moment decreases as the slenderness ratio L/r_{yy} increases. The maximum moment itself, of course, decreases as the slenderness ratio increases.

9. TABLES AND FIGURES

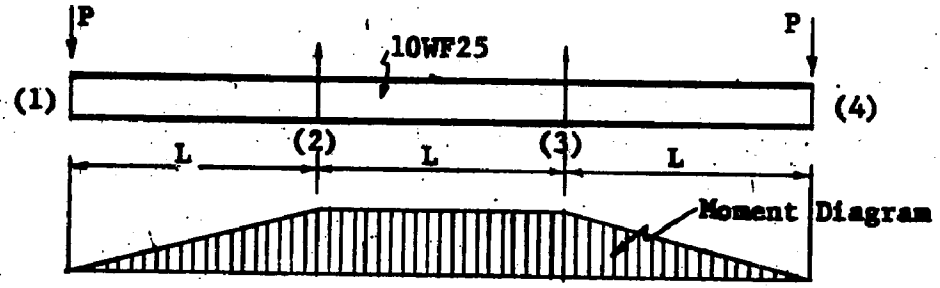

SERIES	TEST NO.	$\frac{L}{r_{yy}}$	SUPPORTING CONDITION AT (2) AND (3)	SUPPORTING CONDITION AT (1) AND (4)	VARIABLES
I (Chapter 3)	LB-9	40	Rotation free in both principal directions but no deflections. Twisting prevented. Warping prevented.	Vertical deflections free. Lateral rotations free. Lateral deflections and twisting prevented.	Critical Span Length
	LB-10	45			
	LB-11	35			
	LB-15	40			
II (Chapter 4)	LB-12	40	Rotations, deflections, warping and twisting are restrained by purlins welded to comp. flange.	Vertical deflection and lateral rotations free. Lateral deflections and twisting prevented.	Purlin size
	LB-13	40			
	LB-14	40			

TABLE 3.1 SUMMARY OF SPECIMEN LENGTHS, VARIABLES AND SUPPORTING CONDITIONS

ITEMS		SPECIMEN				NOMINAL
		LB-9	LB-10	LB-11	LB-12	
TENSION COUPON DATA	σ_y (ksi)	σ_{yf} = 33.95 σ_{ya} = 35.5 σ_{yw} = 38.75 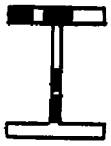				33
	E (ksi)	30,400 (Average)				30,000
	ϵ_{st}/ϵ_y	14				12
STUB COLUMN DATA	σ_y (ksi)	34.81				33
	E (ksi)	29,900				30,000
GEOMETRICAL PROPERTIES	t (in)	0.410	0.410	0.406	0.405	0.430
	w (in)	0.278	0.272	0.276	0.279	0.252
	b (in)	5.779	5.775	5.774	5.783	5.762
	d (in)	10.136	10.123	10.146	10.119	10.080
	A (in^2)	7.296	7.321	7.273	7.274	7.350
	Z (in^3)	28.90	29.000	28.58	28.80	29.50
FULL PLASTIC MOMENT	$Z \cdot \sigma_{ya}$	1025.9	1029.5	1014.6	1022.4	980

TABLE 3.2 SUMMARY OF MATERIAL PROPERTIES

Test No.	LB-12	LB-13	LB-14
PURLIN SECTION	4 I 7.7	3 I 5.7	M 2362
ℓ_b (in)	84	84	84
d_b (in)	4	3	2.6
I_{xx} (in^4)	6.0	2.5	1.25
A_b (in^2)	2.21	1.64	1.04
$(r_{yy})_b$ (in)	0.59	0.53	0.174
A_b/A	0.30	0.22	0.14
d_b/ℓ_b	1/21	1/28	1/32.5
d_b/d	0.40	0.30	0.26
$(\ell/r_{yy})_b$	142.4	158.5	482.8
PROPERTIES OF BEAM SPECIMENS (10WF25)	Area A (in^2)	7.35	
	Depth d (in)	10.08	
	L/r_{yy}	40	

TABLE 4.1 SUMMARY OF PURLIN PROPERTIES

ITEMS		BEAM SPECIMEN			NOMINAL*
		LB-12	LB-13	LB-14	
TENSION COUPON DATA*	σ_y (ksi)	σ_{yf} = 33.95 σ_{ya} = 35.5 σ_{yw} = 38.75			33
	E (ksi)	30,400 (Average)			30,000
	ϵ_{st}/ϵ_y	14			12
STUB COLUMN DATA*	y (ksi)	34.81			33
	E (ksi)	29,900			30,000
GEOMETRICAL PROPERTIES	t (in)	0.408	0.408	0.406	0.430
	w (in)	0.277	0.275	0.278	0.252
	b (in)	5.790	5.814	5.776	5.762
	d (in)	10.119	10.115	10.107	10.080
	A (in^2)	7.235	7.329	7.274	7.350
	Z (in^3)	28.59	29.05	28.75	29.50
FULL PLASTIC MOMENT	$Z \cdot \sigma_{ya}$	1012	1030	1019	980

*These values are identical with those listed in Table 3.2.

TABLE 4.2 SUMMARY OF MATERIAL PROPERTIES OF BEAM SPECIMEN

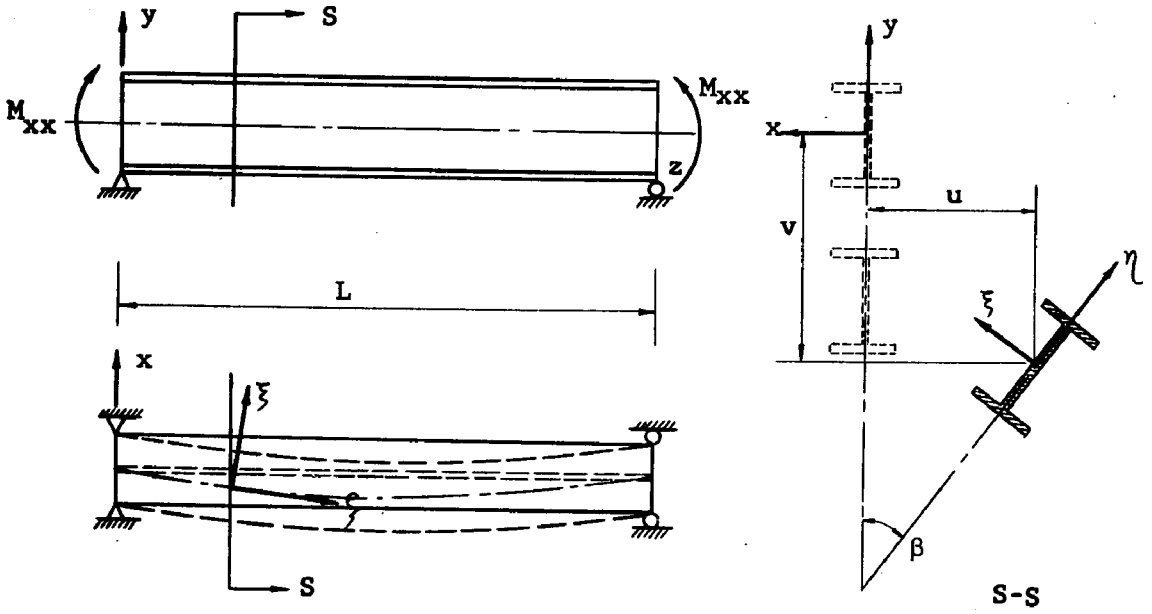

(a)

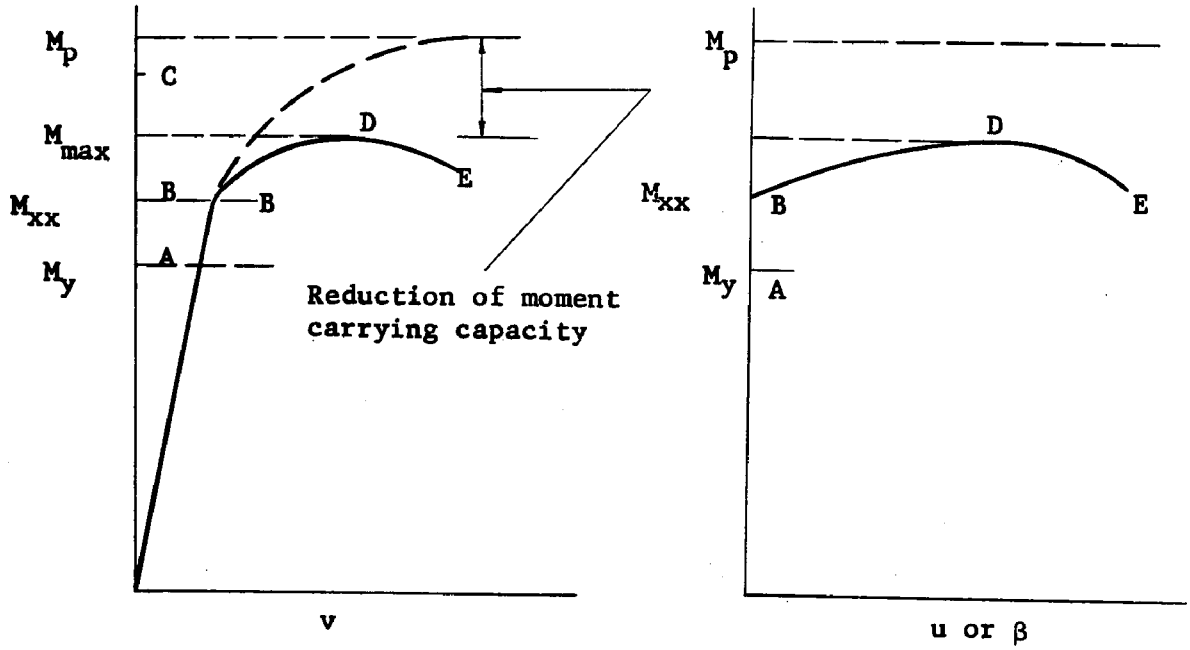

(b) (c)

Fig. 1.1 ILLUSTRATION OF THE PHENOMENA OF LATERAL BUCKLING

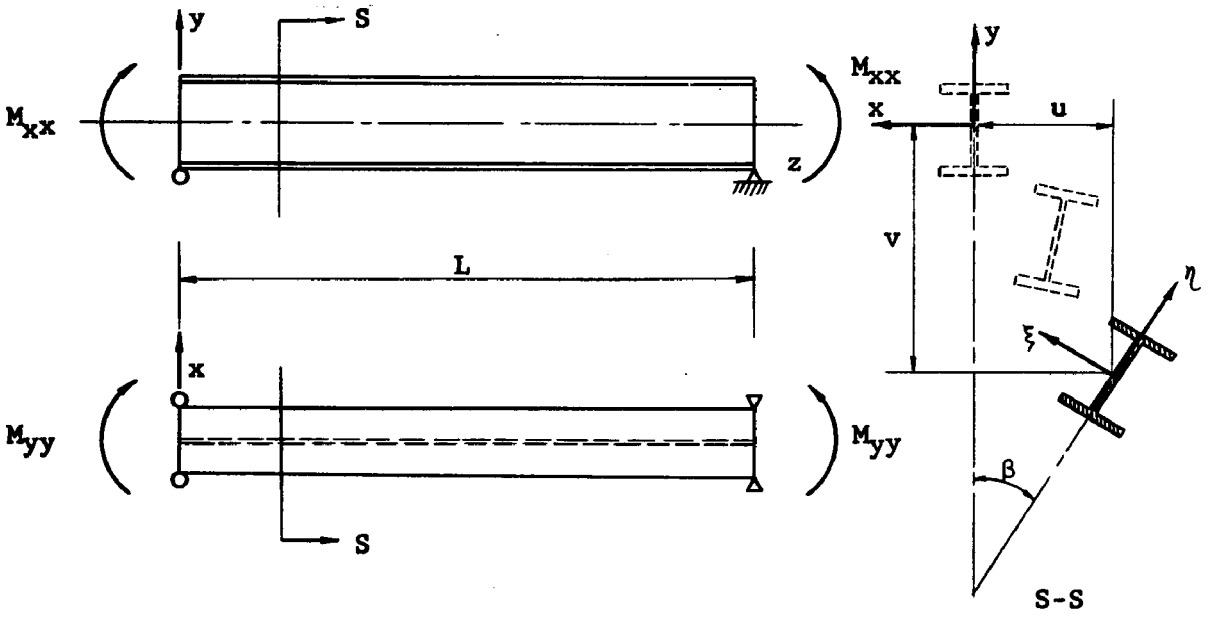

(a)

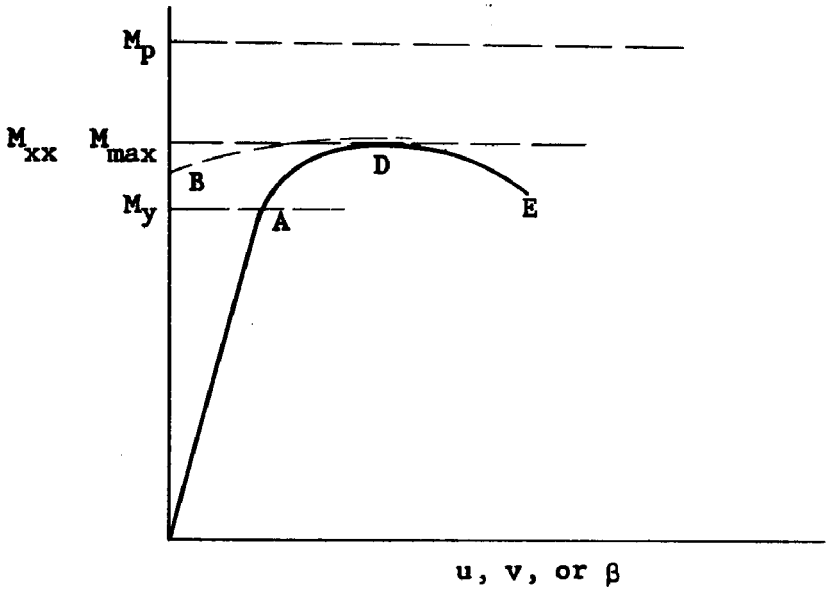

(b)

Fig. 1.2 ILLUSTRATION OF THE PHENOMENA OF ULTIMATE STRENGTH WITH RESPECT TO LATERAL-TORSIONAL INSTABILITY

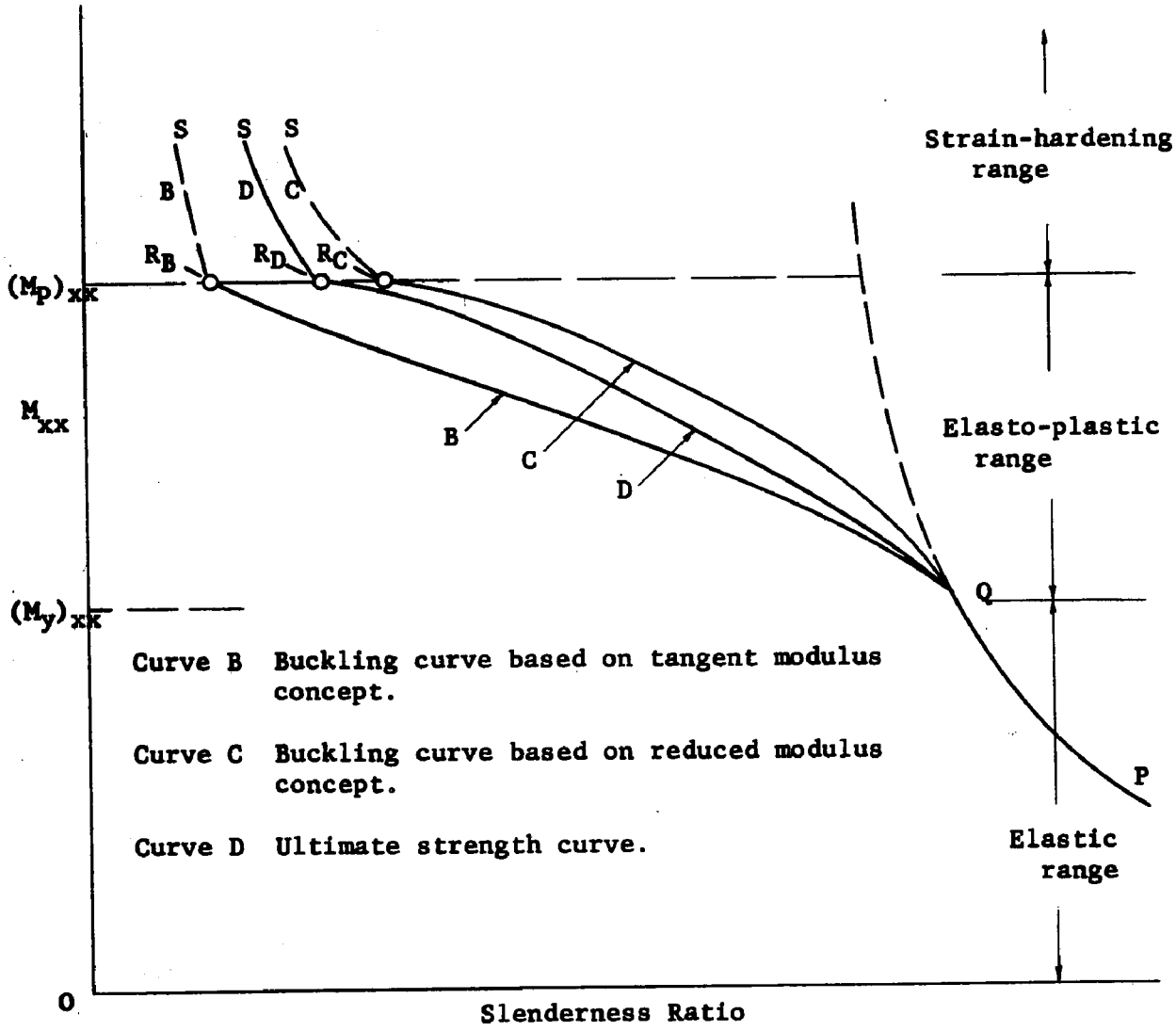

Fig. 1.3 ILLUSTRATION OF THE MOMENT VERSUS SLENDERNESS RATIO RELATIONSHIP IN ELASTIC, ELASTO-PLASTIC, AND THE STRAIN-HARDENING RANGES

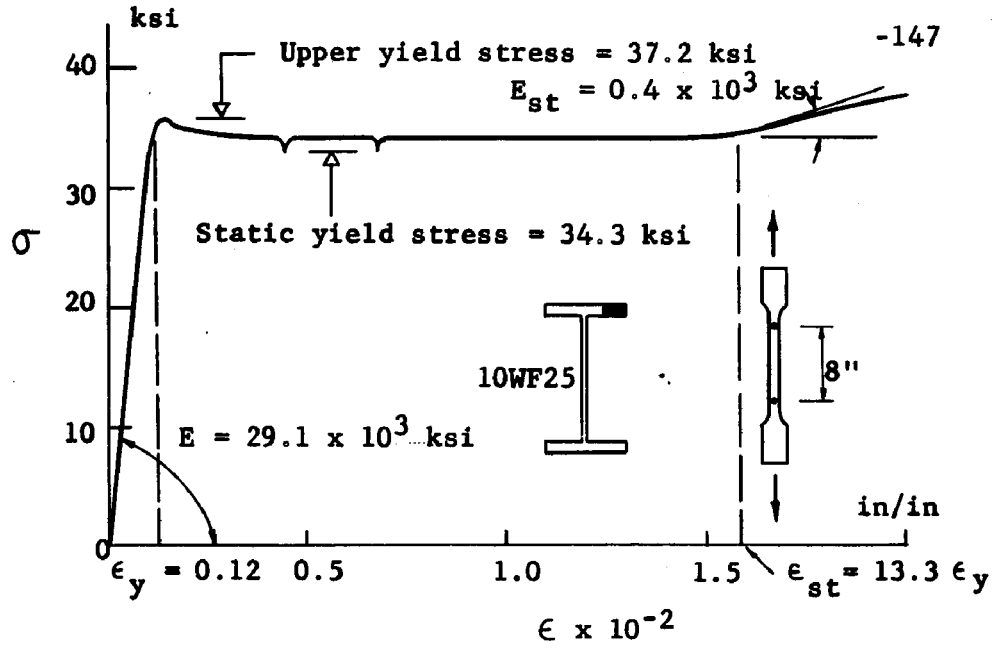

Fig. 2.1 STRESS-STRAIN RELATIONSHIP UNDER TENSION COUPON TEST

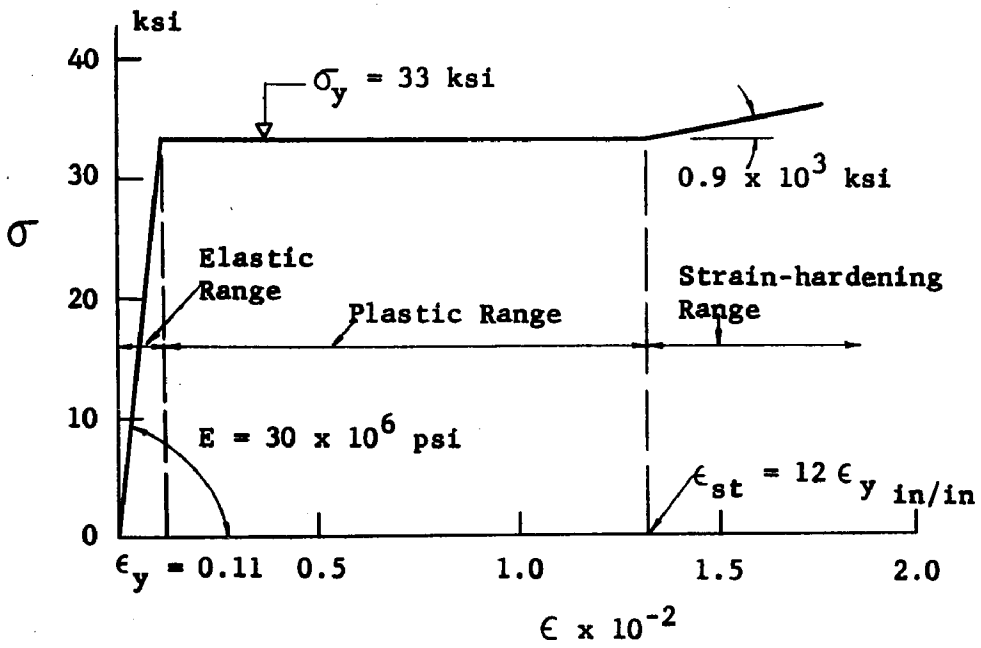

Fig. 2.2 IDEALIZED STRESS-STRAIN RELATIONSHIP

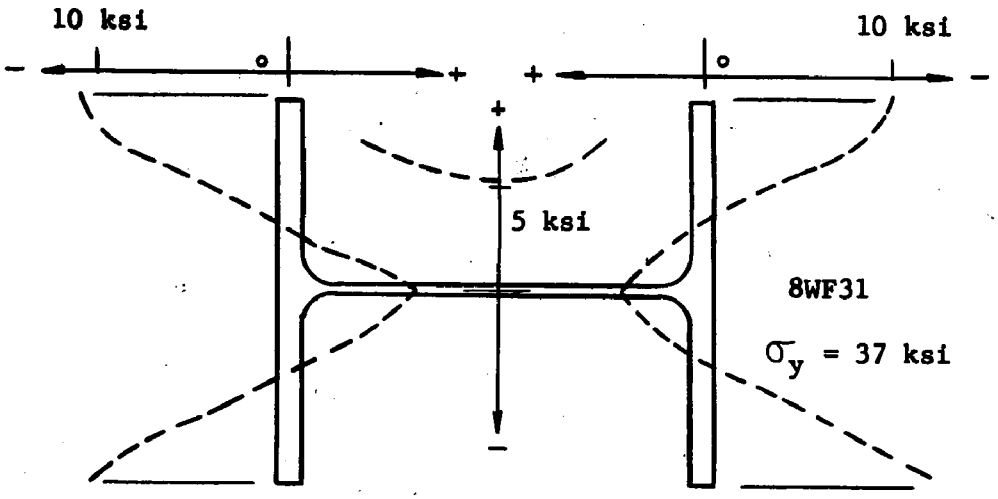

Fig. 2.3 MEASURED RESIDUAL STRESS VARIATION IN A ROLLED WIDE-FLANGE SECTION

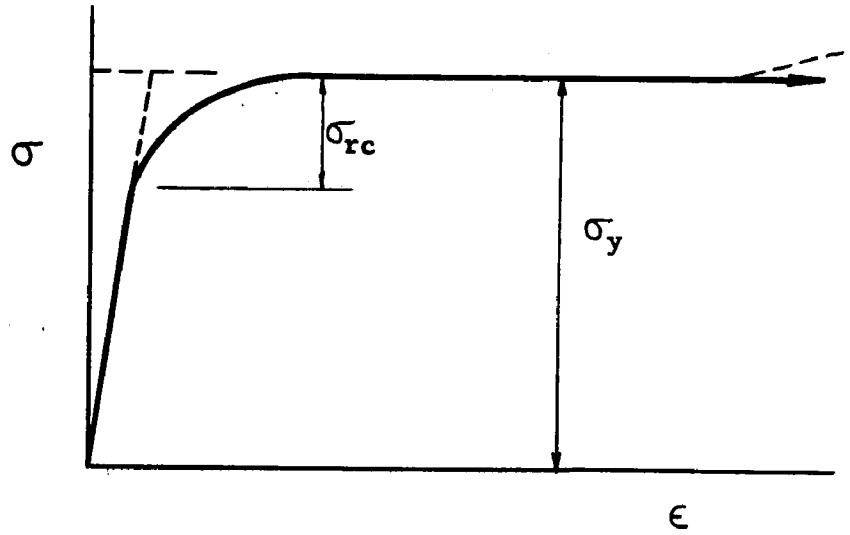

Fig. 2.4 AVERAGE COMPRESSIVE STRESS-STRAIN CURVE CONSIDERING THE CROSS SECTION AS A WHOLE

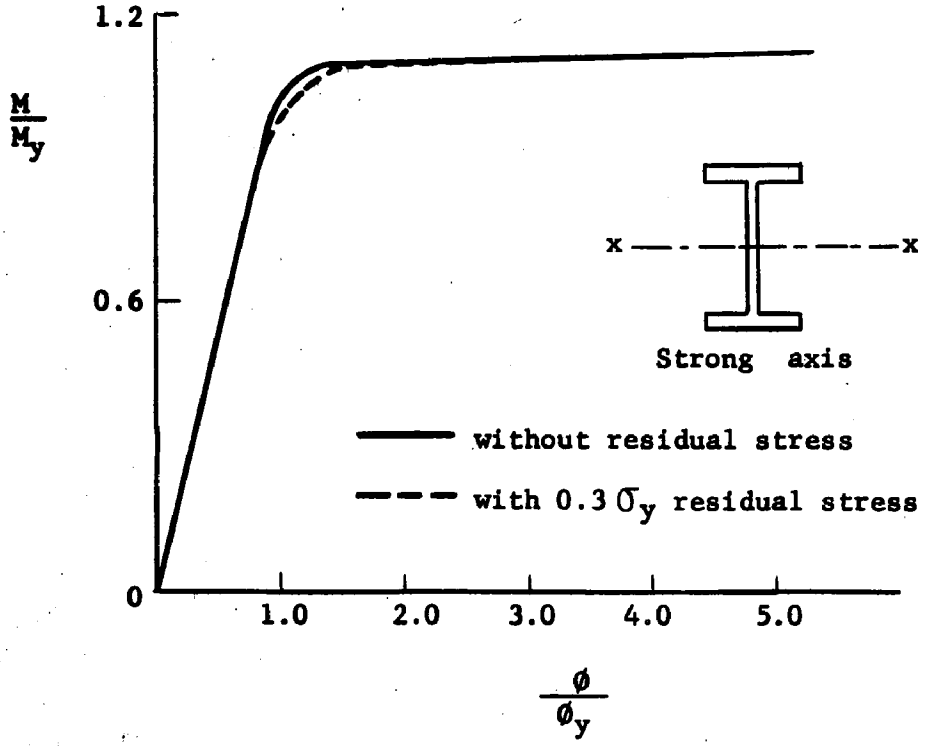

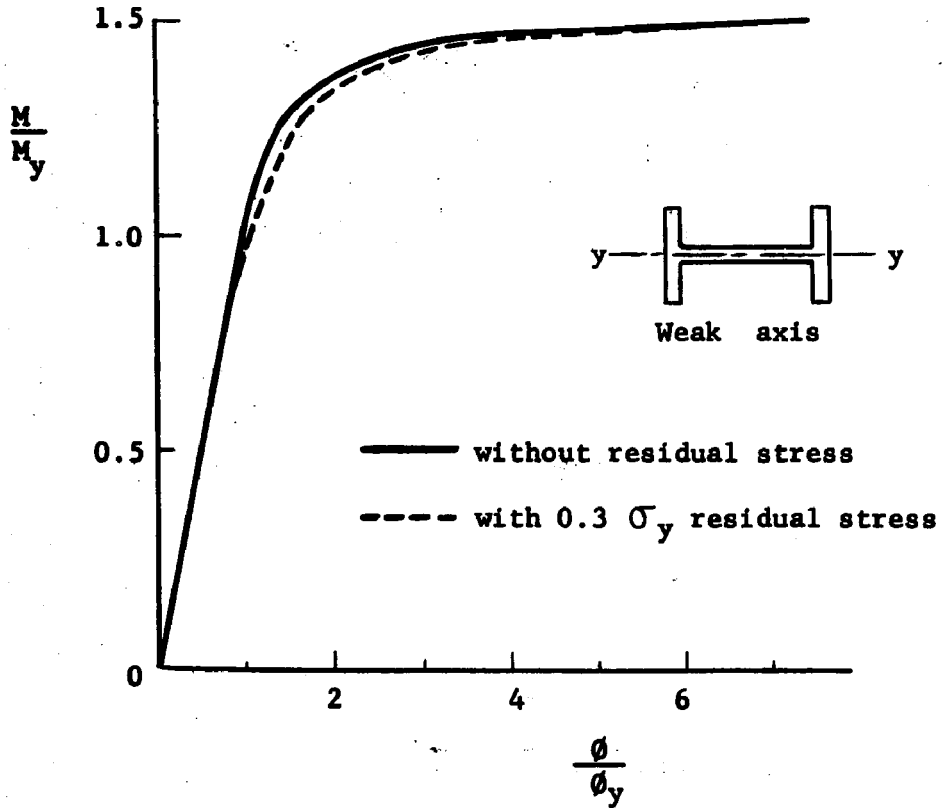

Fig. 2.5 THE MOMENT-CURVATURE RELATIONSHIPS FOR 8WF31

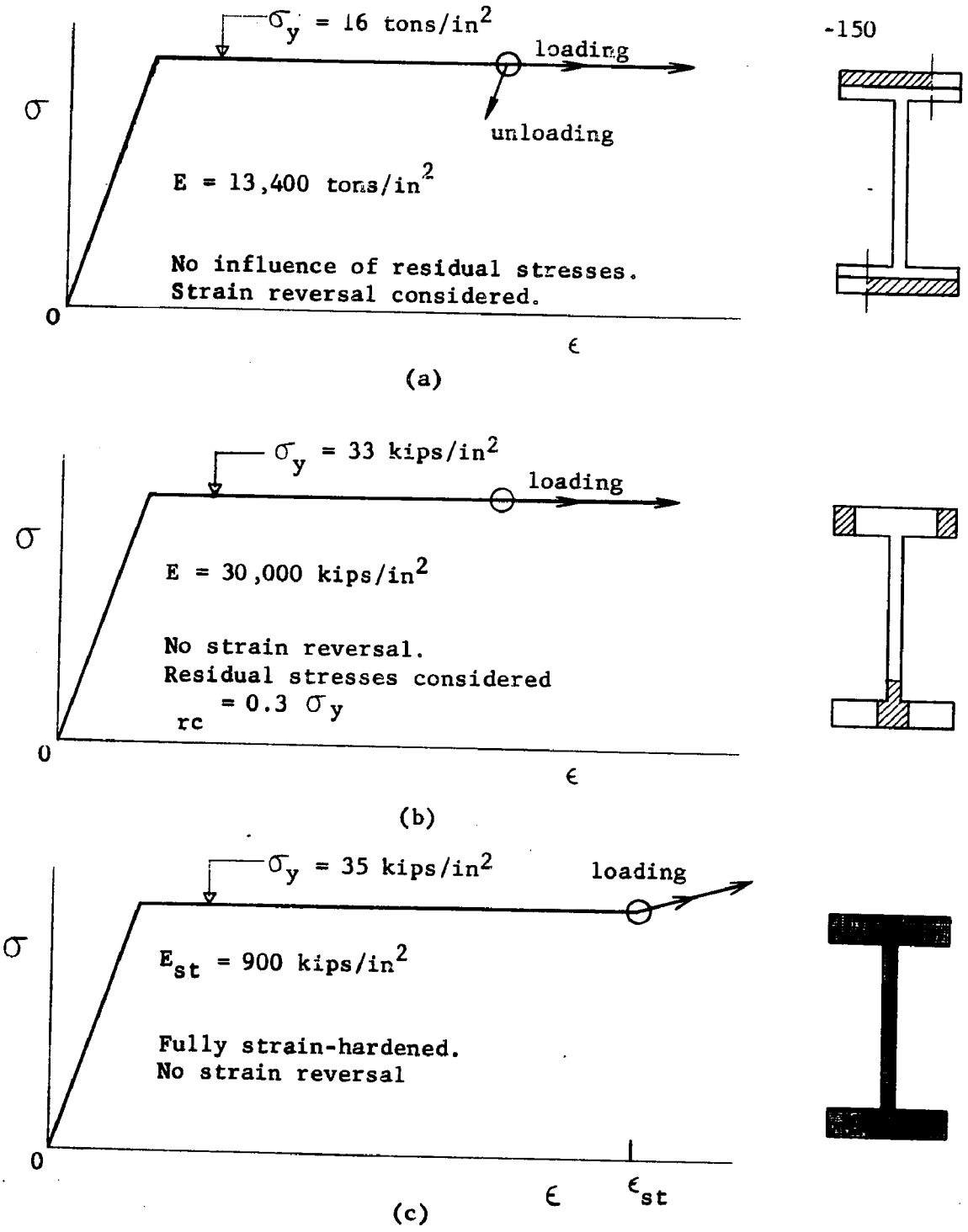

Fig. 2.6 ASSUMED σ - ϵ RELATIONSHIPS IN EXISTING INELASTIC LATERAL-TORSIONAL BUCKLING SOLUTIONS

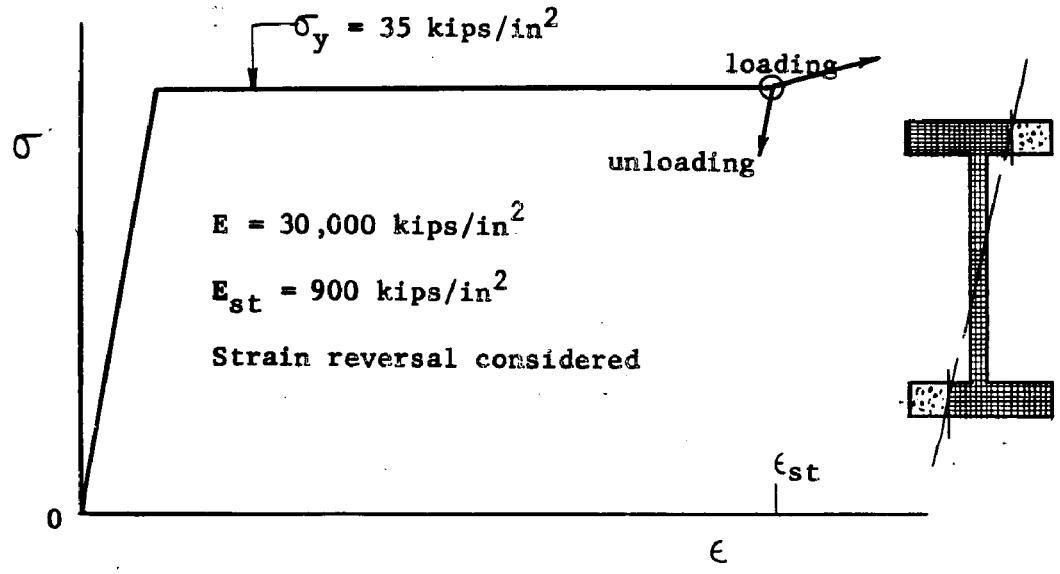

Fig. 2.7 BASIC ASSUMPTIONS FOR BUCKLING UNDER FULL PLASTIC MOMENT (UPPER BOUND SOLUTION)

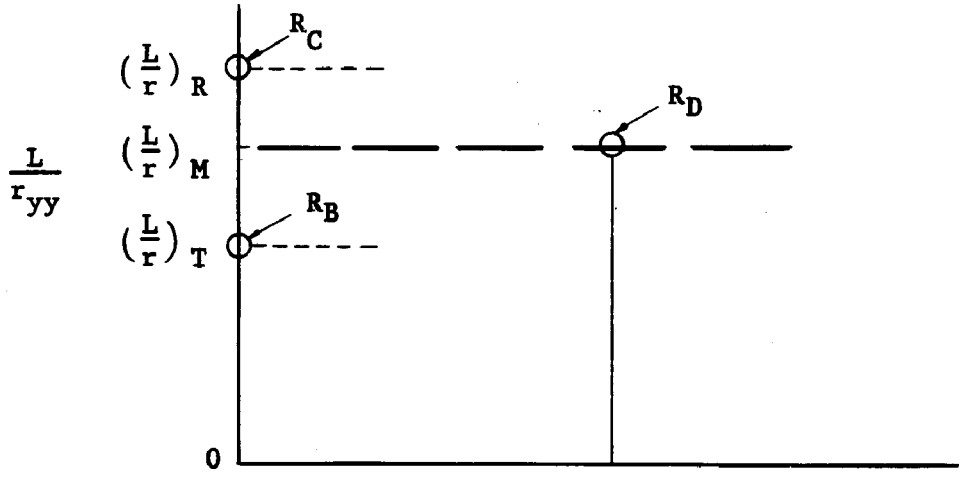

Fig. 2.8 COMPARISON OF SLENDERNESS RATIOS FOR BEAMS SUBJECTED TO FULL PLASTIC MOMENT

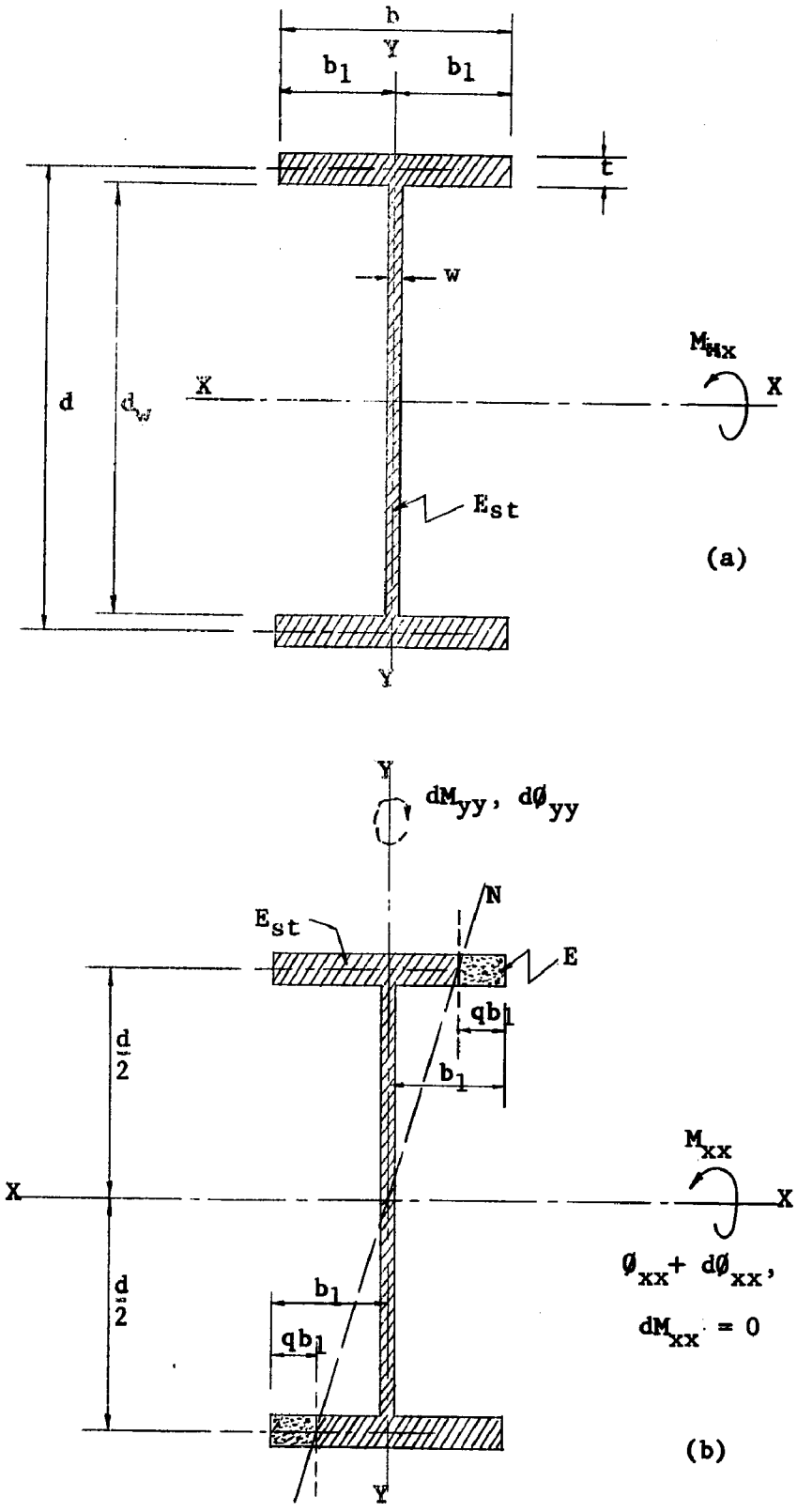

Fig. 2.9 ILLUSTRATION OF STRAIN DISTRIBUTION IN A WIDE-FLANGE SECTION AT REDUCED MODULUS LOAD

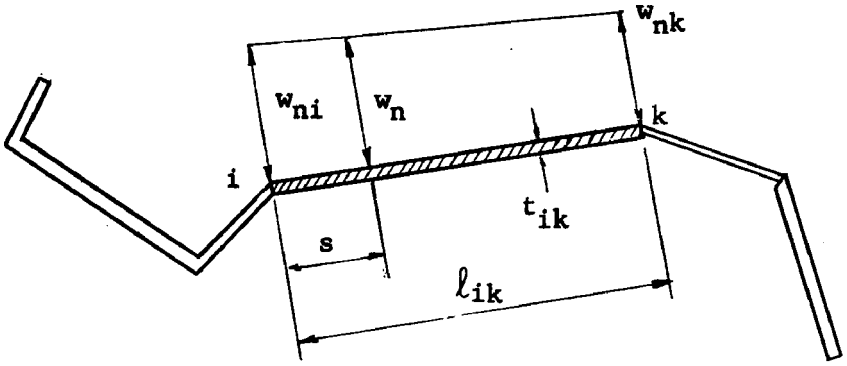

$$w_n = w_{ni} - \left(\frac{w_{nk} - w_{ni}}{\ell_{ik}} \right) \cdot s$$

Fig. 2.10 VARIATION OF THE NORMALIZED UNIT WARPING ALONG AN ELEMENT OF A THIN-WALLED OPEN CROSS SECTION

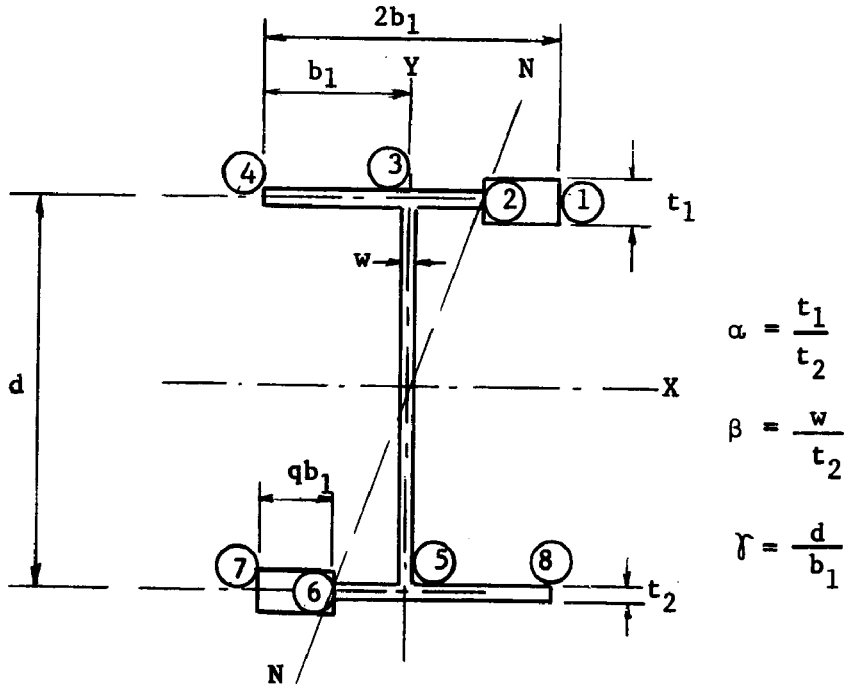

Fig. 2.11 ILLUSTRATION FOR THE CALCULATION OF THE WARPING CONSTANT OF AN ELASTIC-STRAIN-HARDENED CROSS SECTION

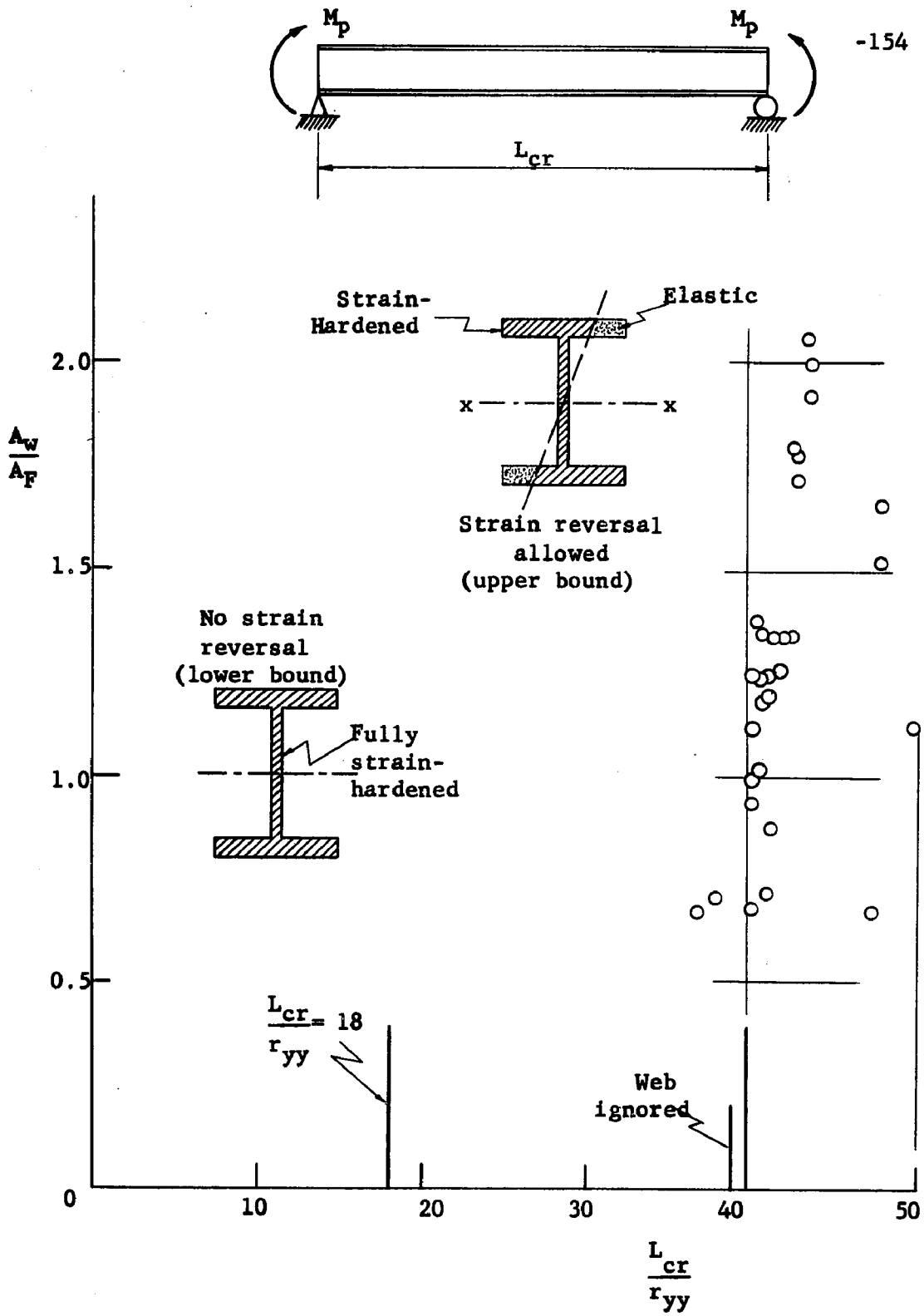

Fig. 2.12 LOWER AND UPPER BOUNDS OF LATERAL BRACING SPACING FOR A SIMPLY SUPPORTED BEAM SUBJECTED TO CONSTANT PLASTIC MOMENT

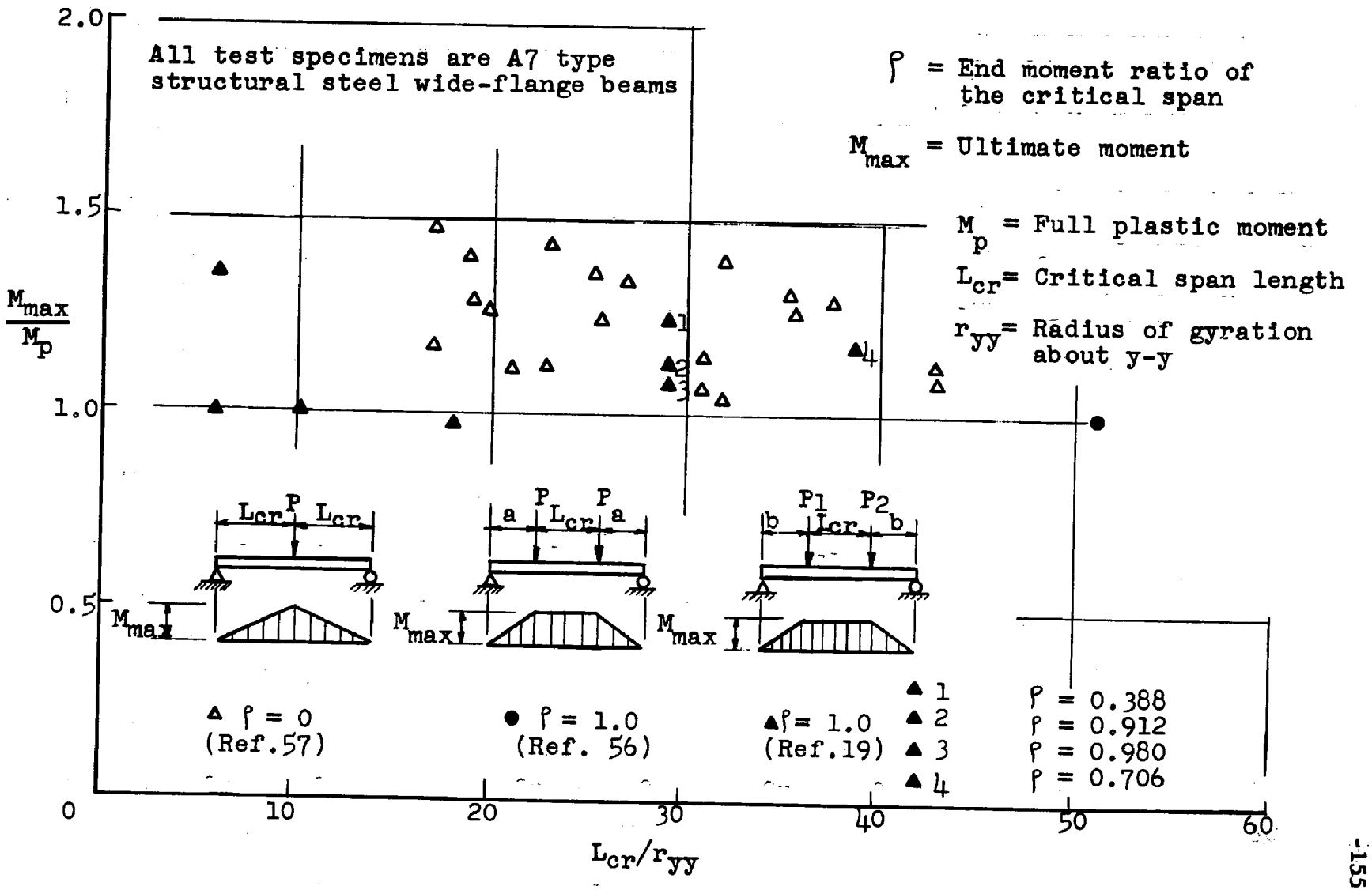

Fig. 3.1 - TEST RESULTS OF INELASTIC LATERAL BUCKLING OF WF STEEL BEAMS

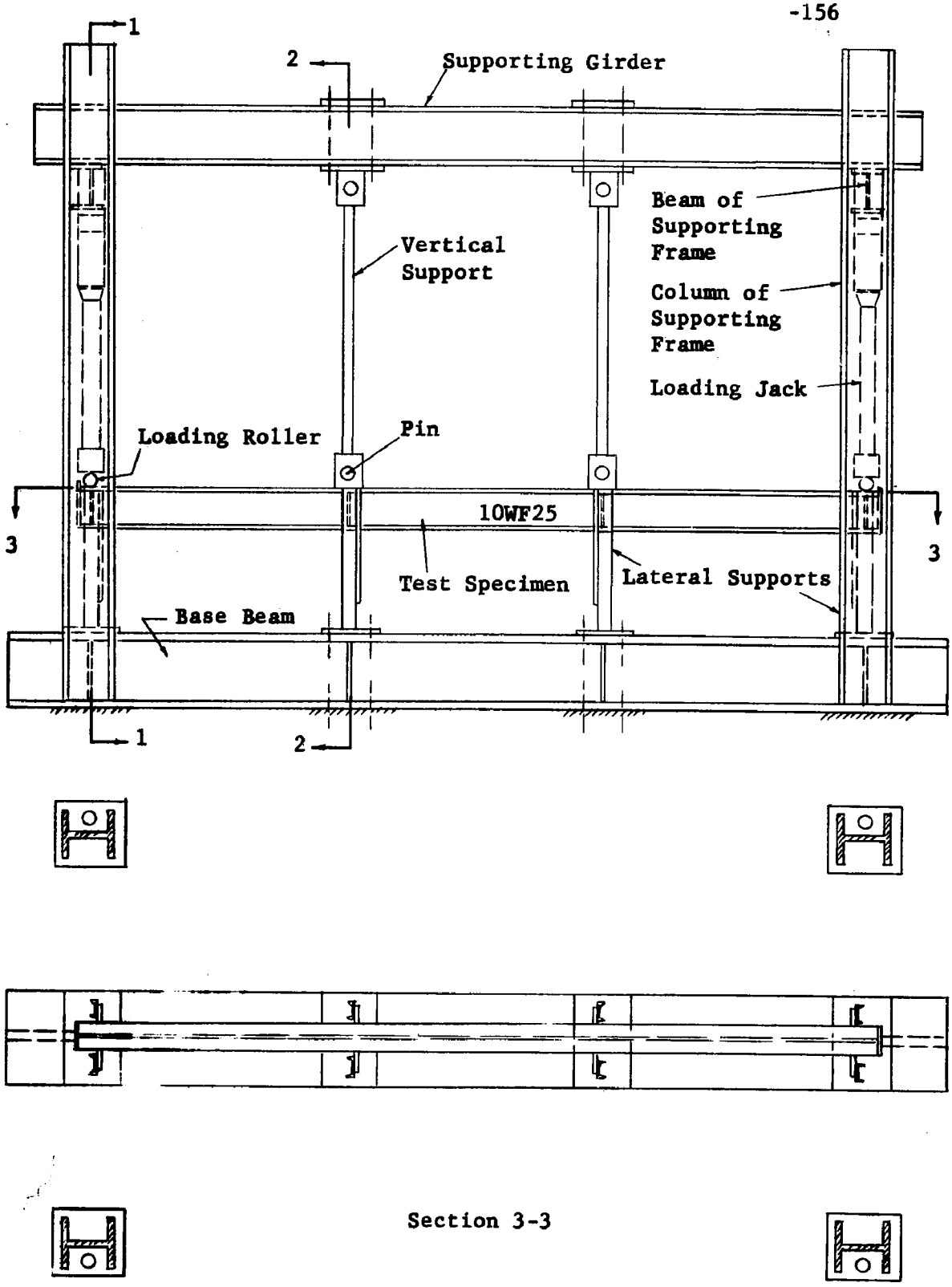

Fig. 3.2 SCHEMATIC SKETCH OF TEST SETUP

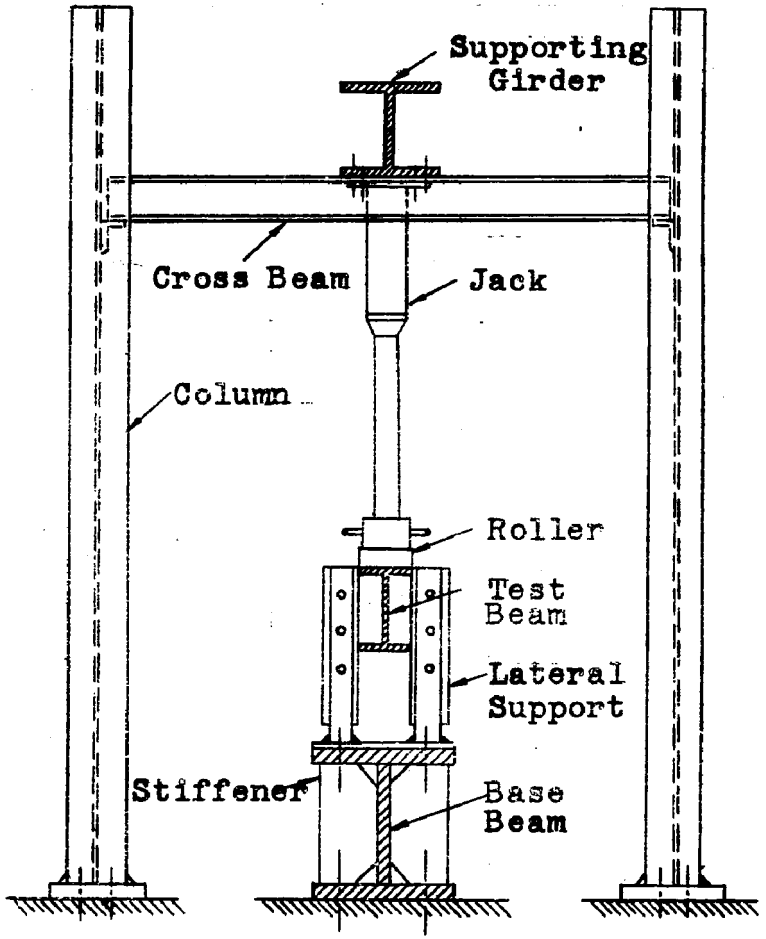

(a) Section 1-1 of Fig. 3.2

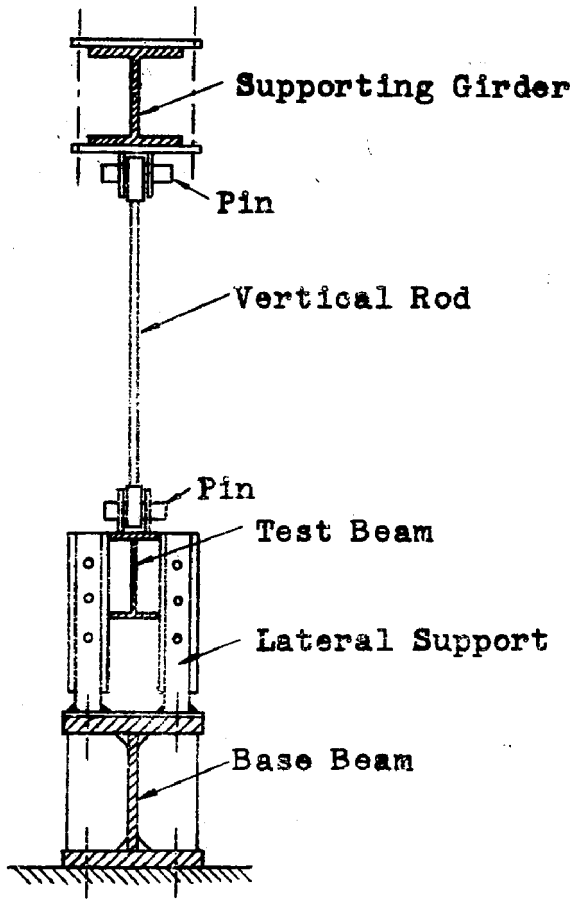

(b) Section 2-2 of Fig. 3.2

Fig. 3.3 - SECTION VIEWS OF FIG. 3.2

Fig.3.4 TEST LB-9 IN PROGRESS

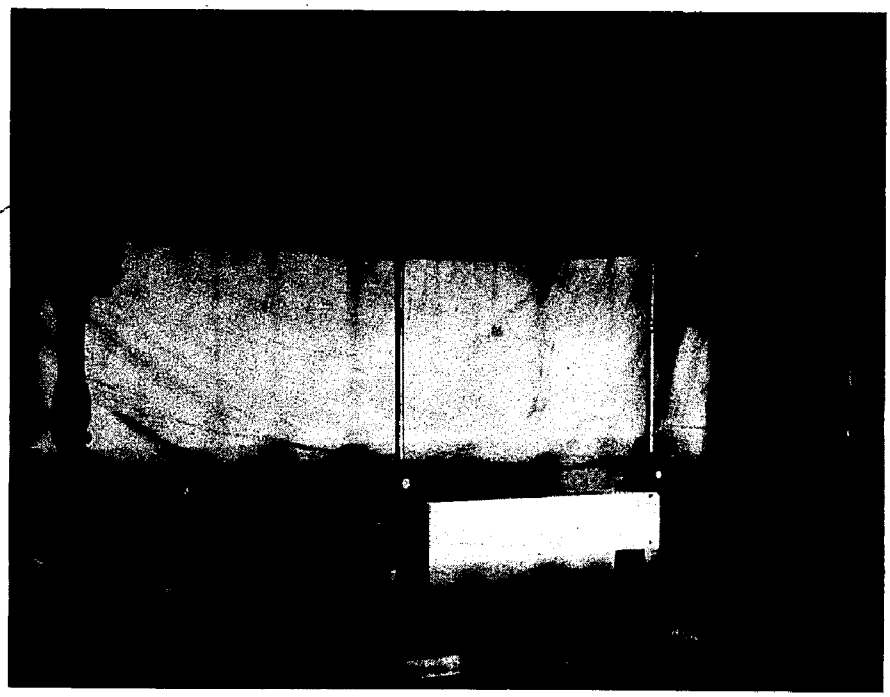

Fig. 3.5 LATERAL BUCKLING TEST SETUP

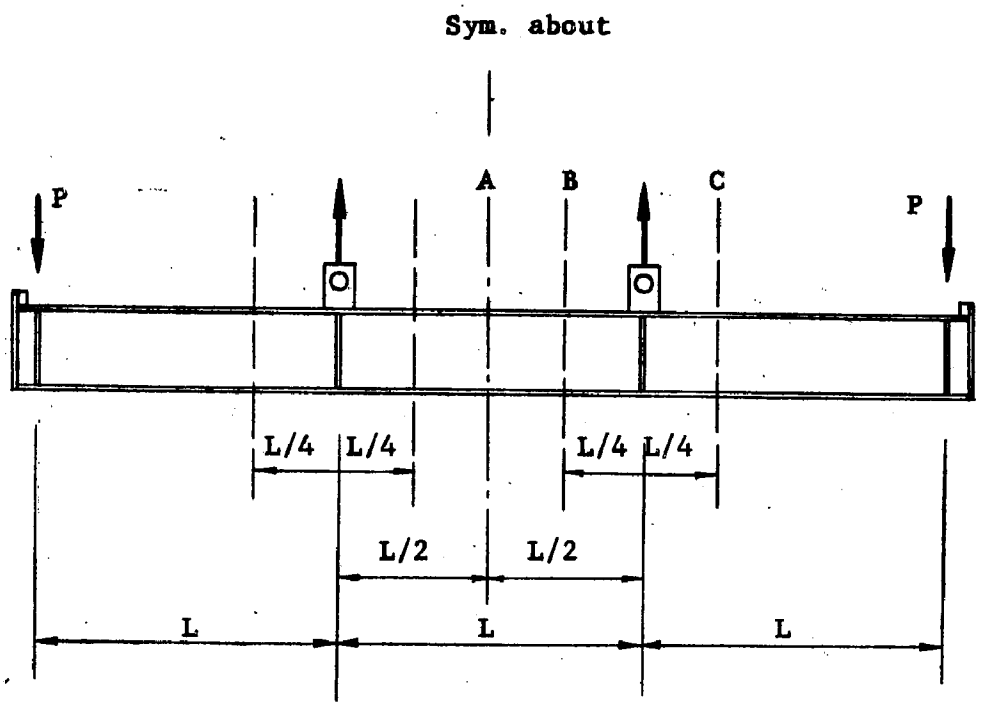

(a) Sections Where Strain Gages are Attached.

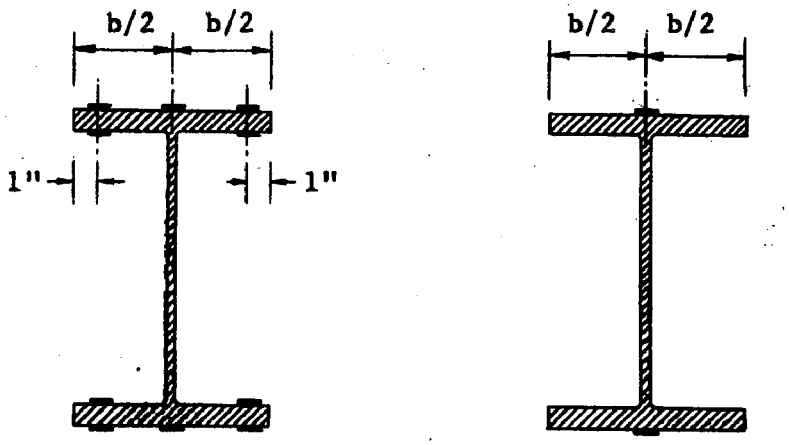

Section A Sections B and C

(b) Locations of Strain Gages

Fig. 3.6 ARRANGEMENT OF SR-4 STRAIN GAGES

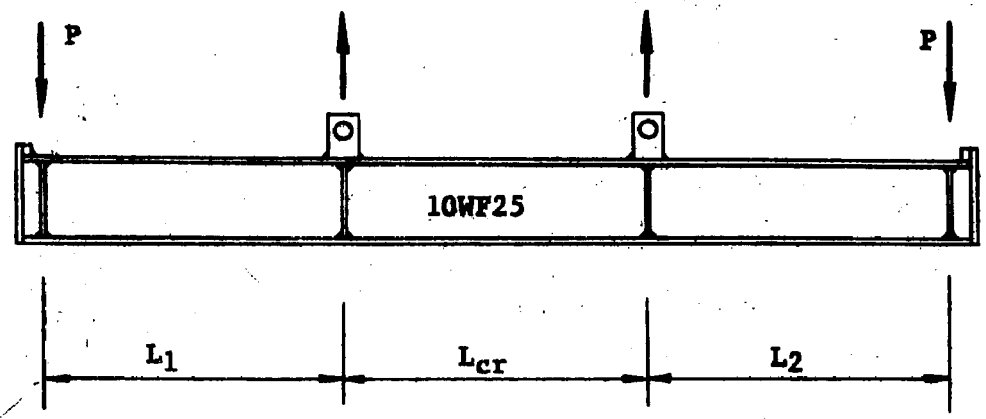

TEST NO.	$\frac{L}{r_{yy}}$	MEASURED			INTENDED
		L_1	L_{cr}	L_2	$L_1 = L_{cr} = L_2$
LB-9	40	52.48"	52.40"	52.50"	52.40"
LB-10	45	59.16"	58.93"	59.14"	58.95"
LB-11	35	46.31"	45.81"	46.39"	45.85"
LB-15	40	52.33"	52.44"	52.28"	52.40"
LB-12	40	52.40"	52.39"	52.40"	52.40"
LB-13	40	52.27"	52.50"	52.22"	52.40"
LB-14	40	52.35"	52.58"	52.45"	52.40"

Fig. 3.7 SAMPLE SPECIMEN SKETCH AND SPECIMEN LENGTHS

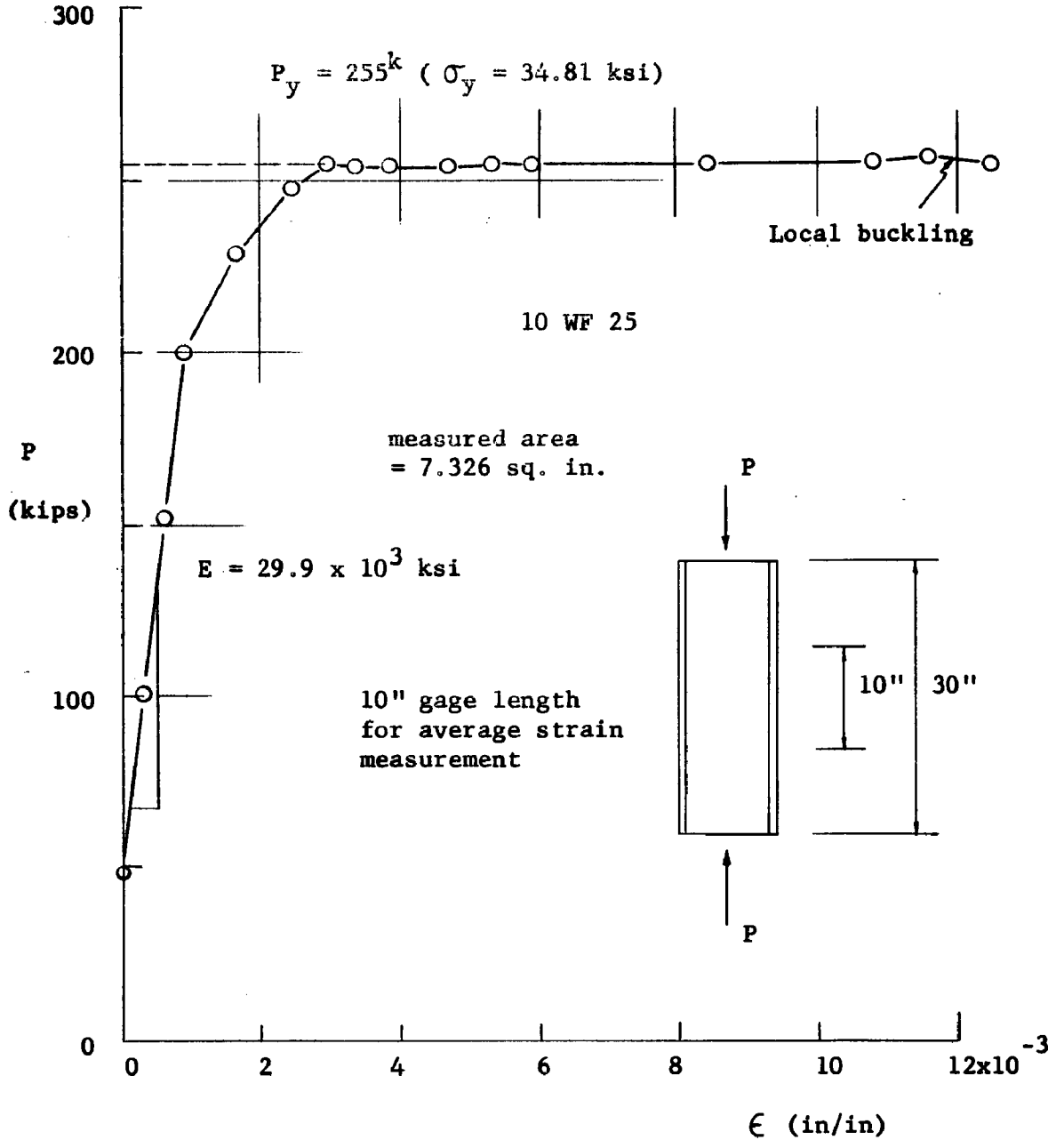

Fig. 3. 8 STUB COLUMN TEST RESULT

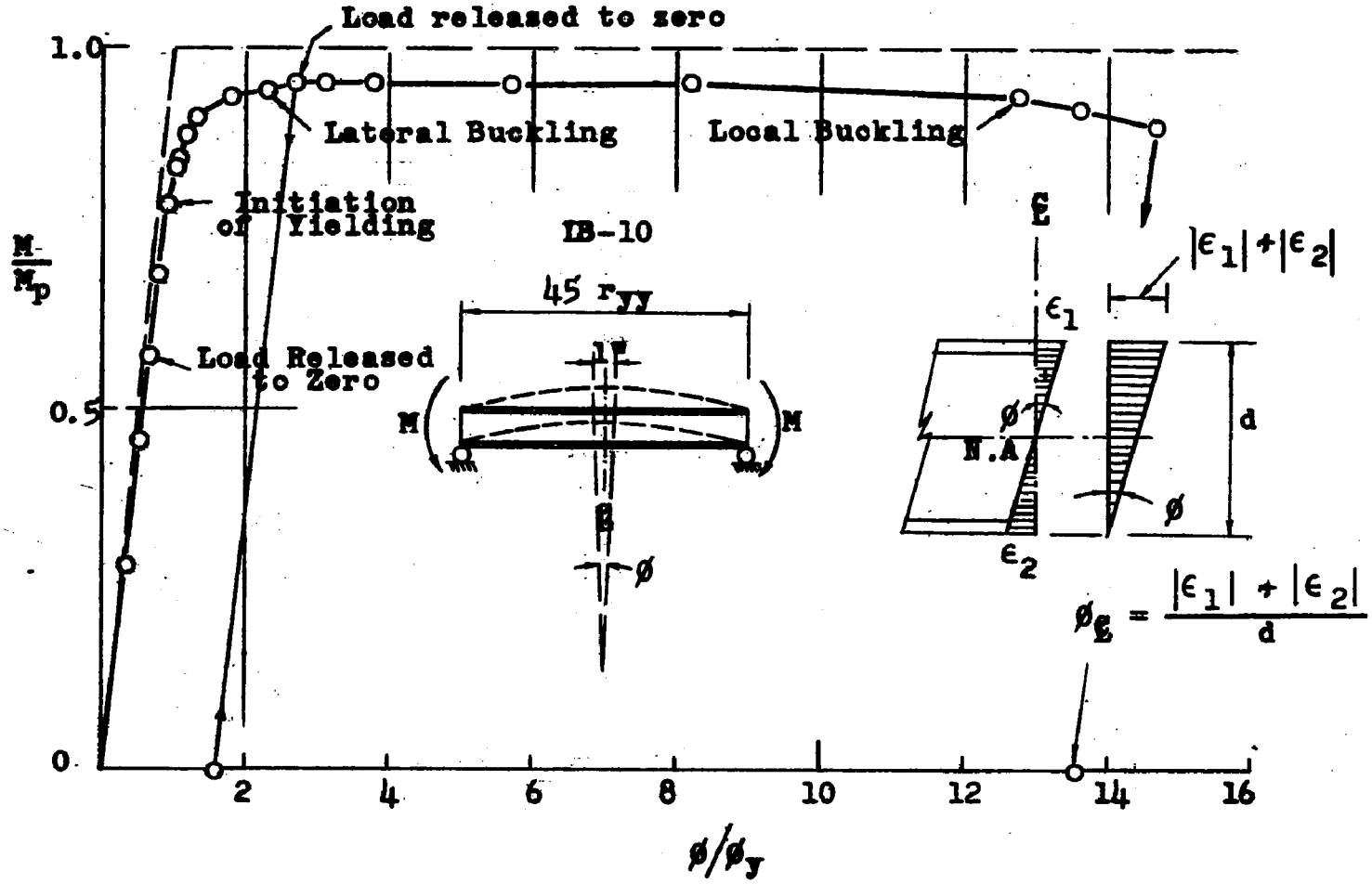

Fig. 3.9 - EXPERIMENTAL M-ϕ CURVE OF TEST IB 10 (L/r_{yy} = 45)

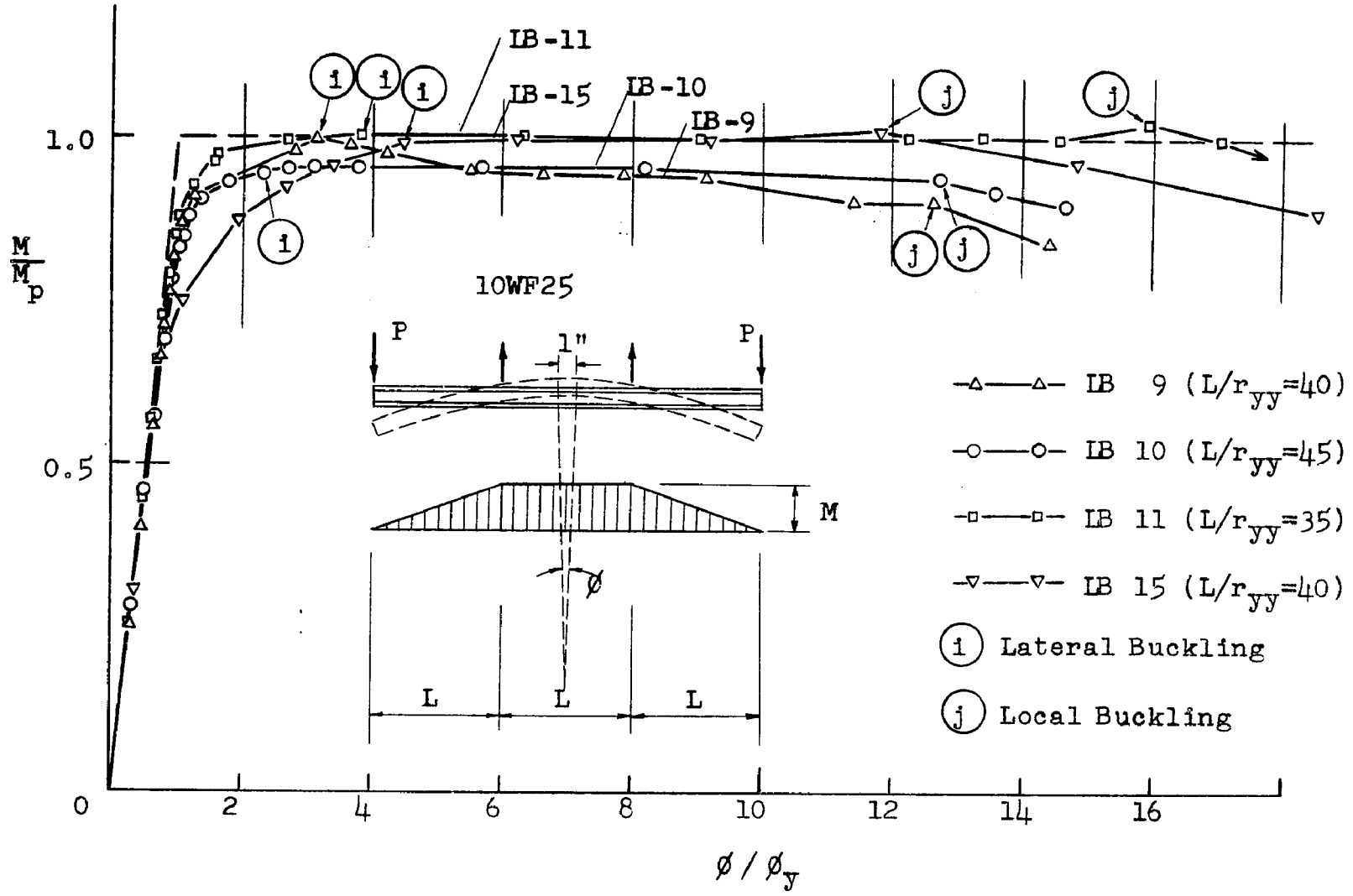

Fig. 3.10 - MOMENT VS. CURVATURE RELATIONSHIPS AT MIDDLE SPAN

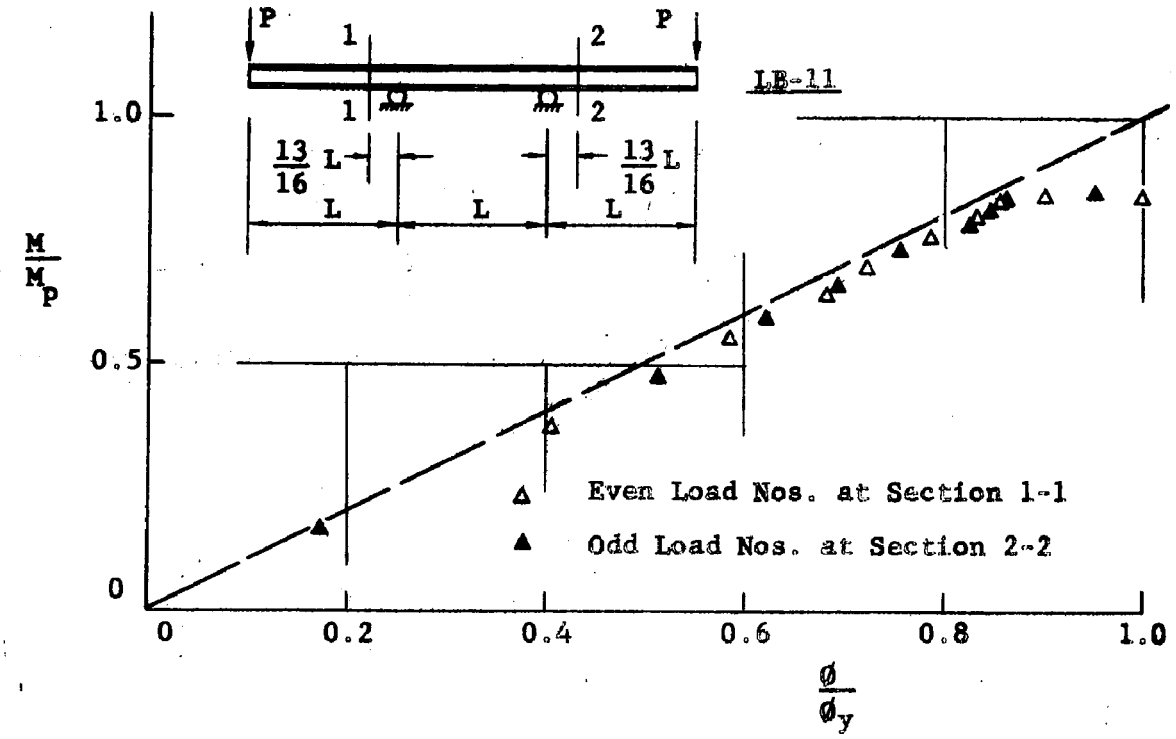

Fig. 3.11 MOMENT-CURVATURE RELATIONSHIPS IN ADJACENT SPANS

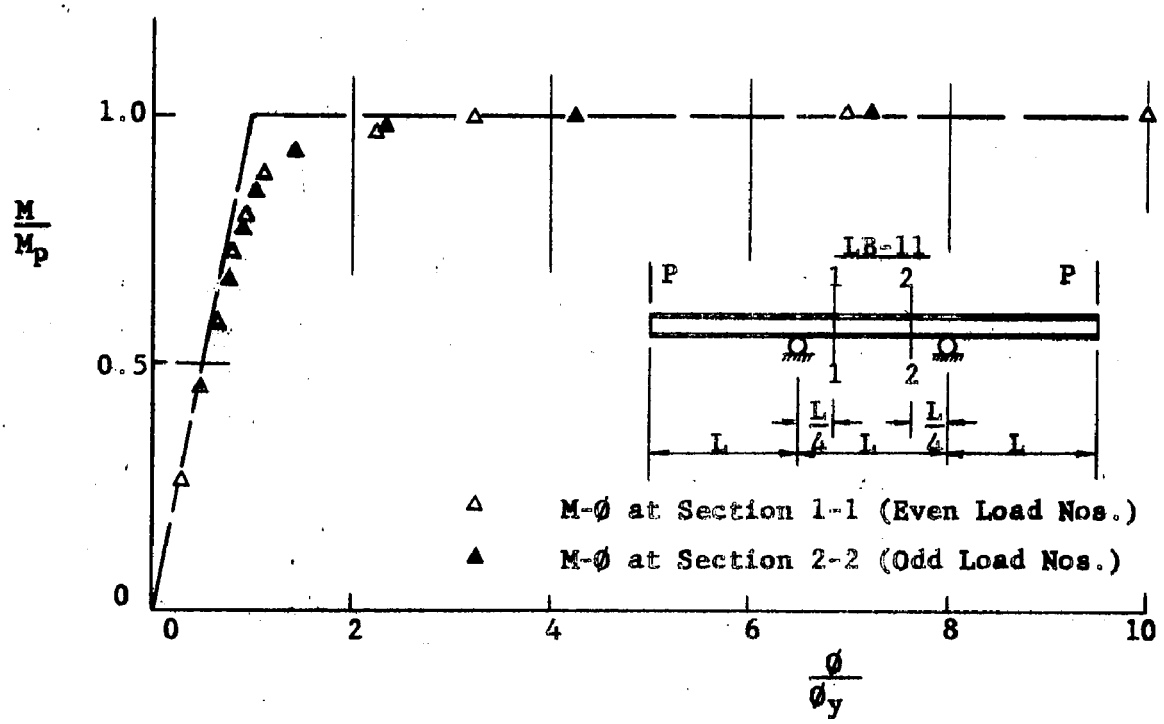

Fig. 3.12 MOMENT-CURVATURE RELATIONSHIPS AT QUARTER POINT SECTIONS OF THE CRITICAL SPAN

	LB-9	LB-10	LB-11	LB-15
ϕ/ϕ_y	14.40	14.60	14.40	14.80
L (in)	52.49	59.15	46.35	52.31
ΔL (in)	0.50	0.50	0.375	0.625
(M/M_p)adj	0.897	0.889	1.004	0.951
M/M_p	0.906	0.897	1.012	0.962
% Reduction	1%	0.9%	0.8%	1.1%

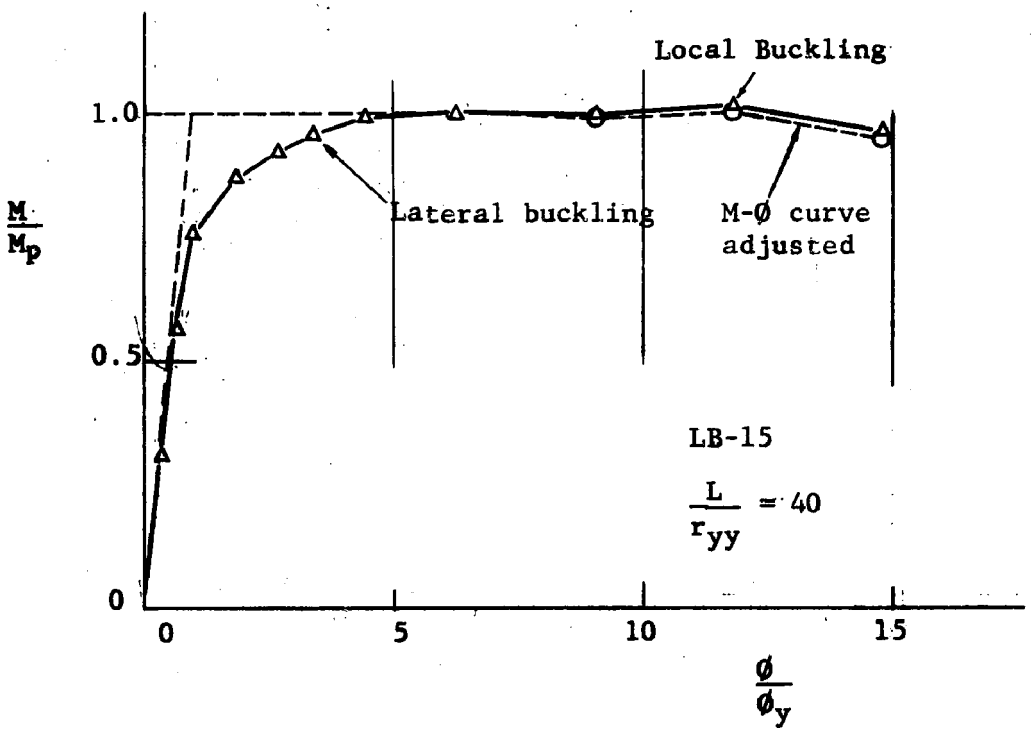

Fig. 3.13 INFLUENCE OF DECREASING MOMENT ARMS ON THE MOMENT-CURVATURE RELATIONSHIPS

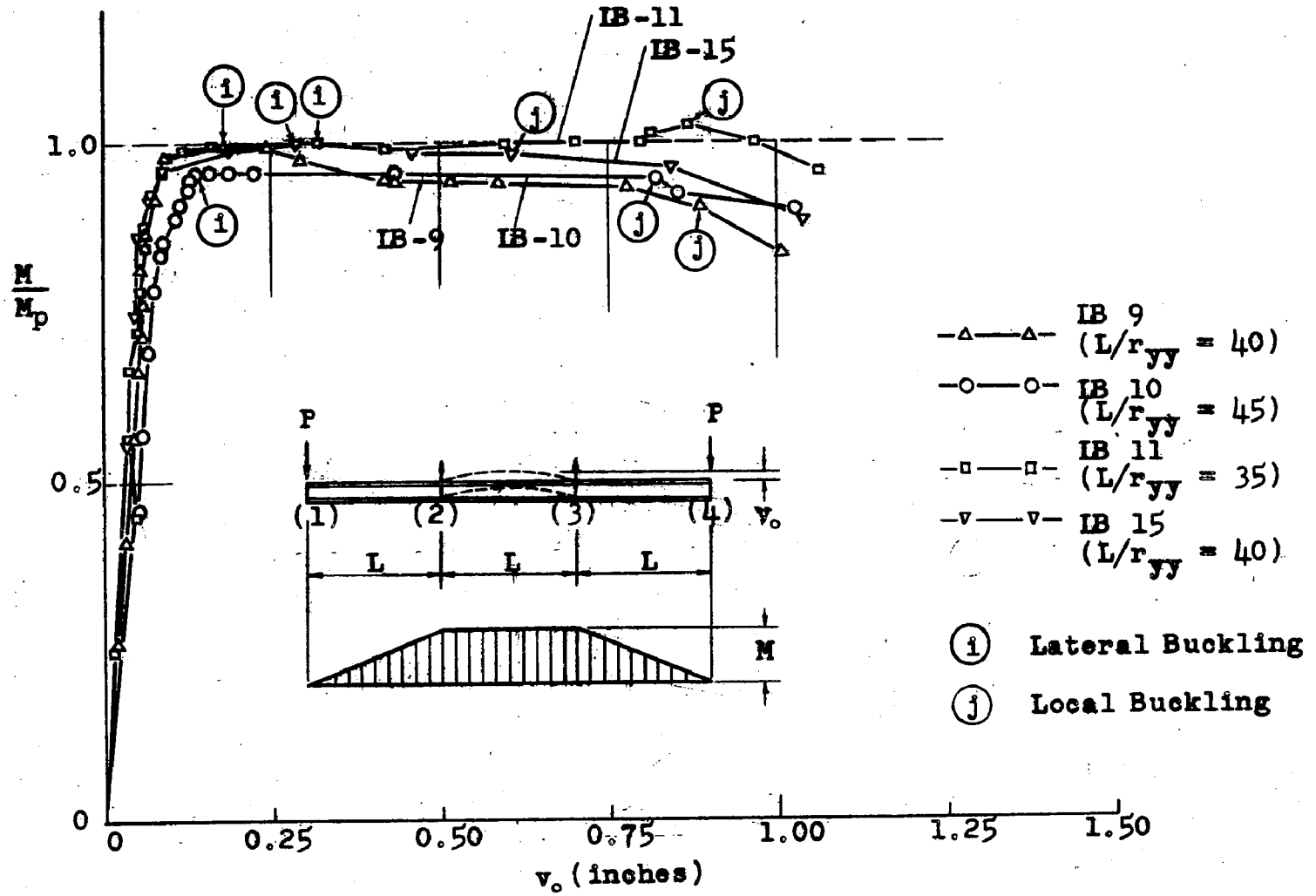

Fig. 3.14 - MOMENT VS. VERTICAL DEFLECTION RELATIONSHIPS AT MID SPAN

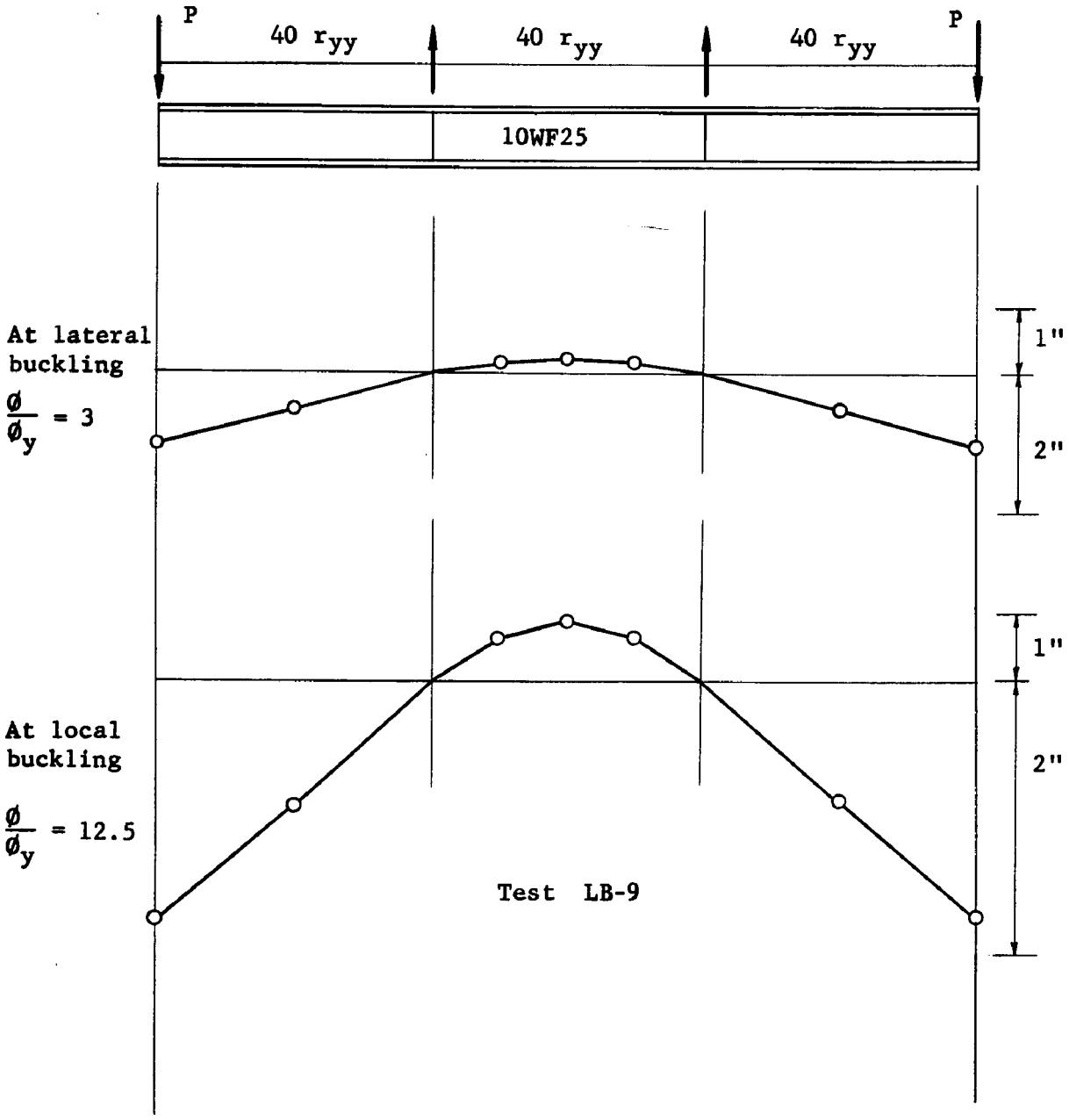

Fig. 3.15 VERTICAL DEFLECTIONS AT LATERAL BUCKLING AND AT LOCAL BUCKLING

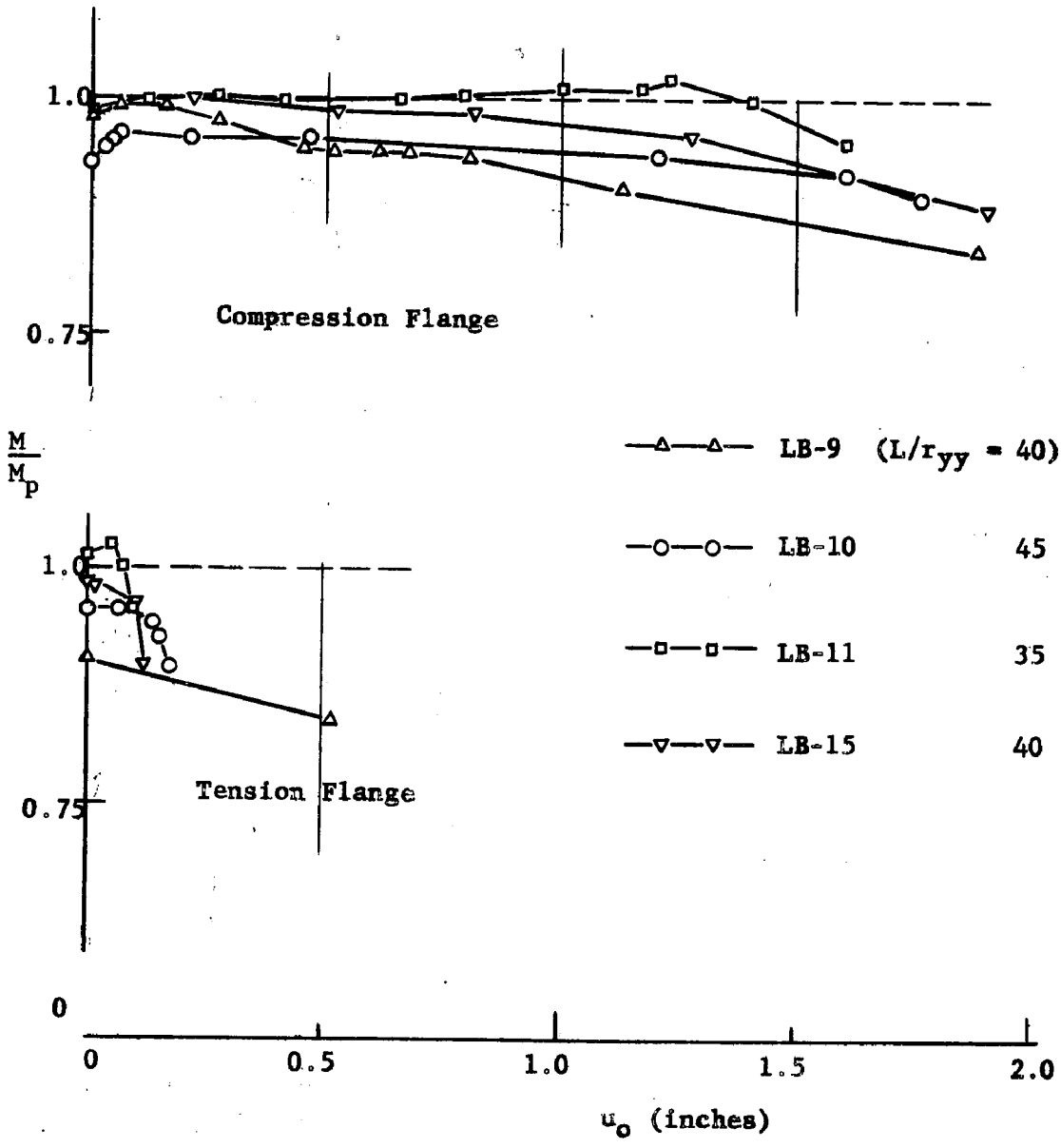

Fig. 3.16 LATERAL DEFLECTIONS AT MIDSPAN

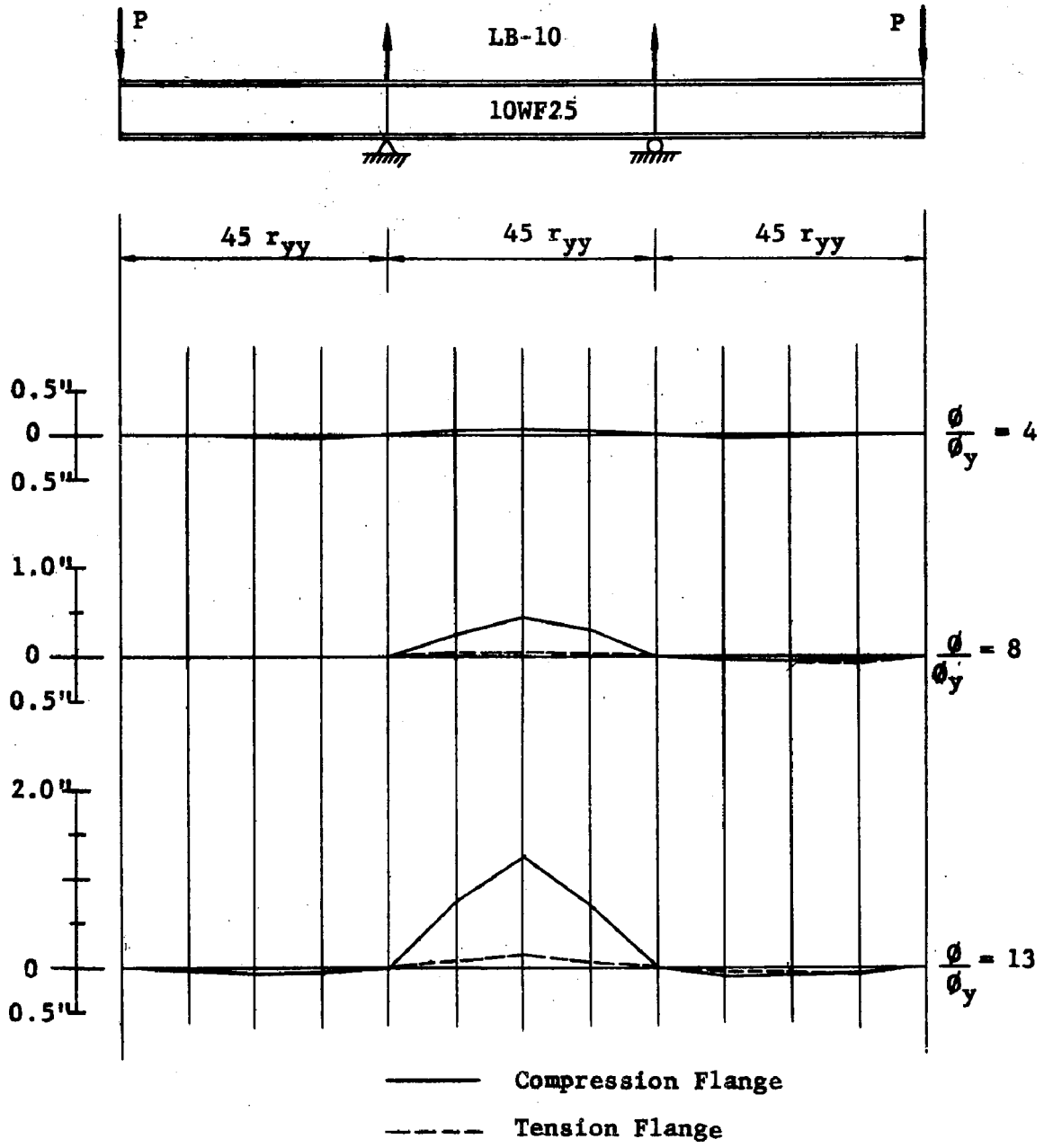

Fig. 3.17 LATERAL DEFLECTIONS OF FLANGES AT VARIOUS LOADING STAGES

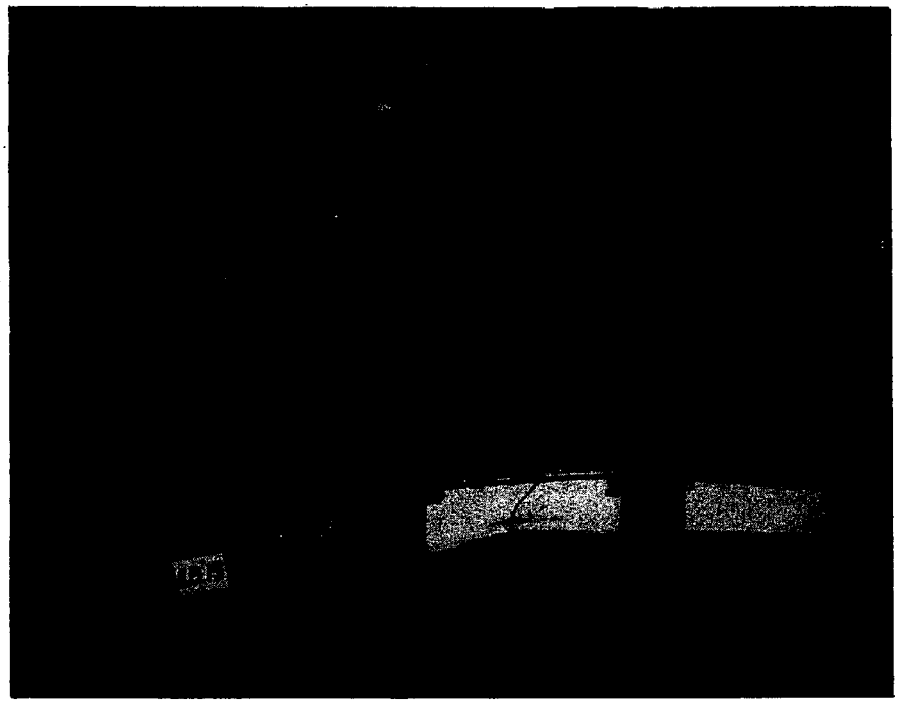

Fig. 3.18 **SPECIMEN LB-15 IN PLACE AFTER TEST COMPLETION**

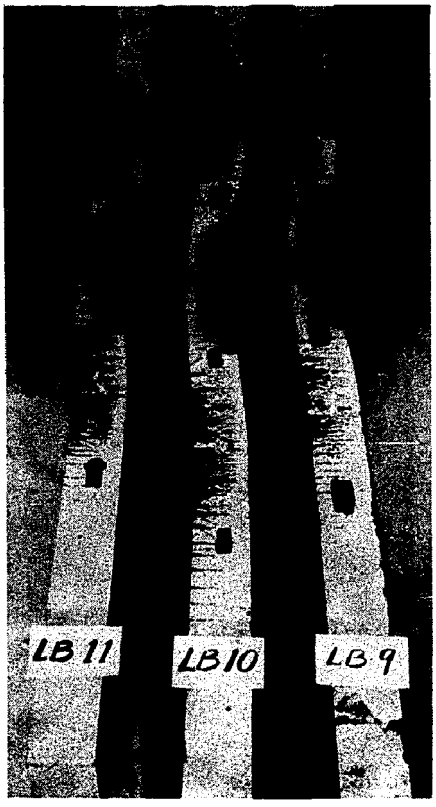

Fig. 3.19 **SPECIMENS LB-9, LB-10 AND LB-11 AFTER COMPLETION OF TEST**

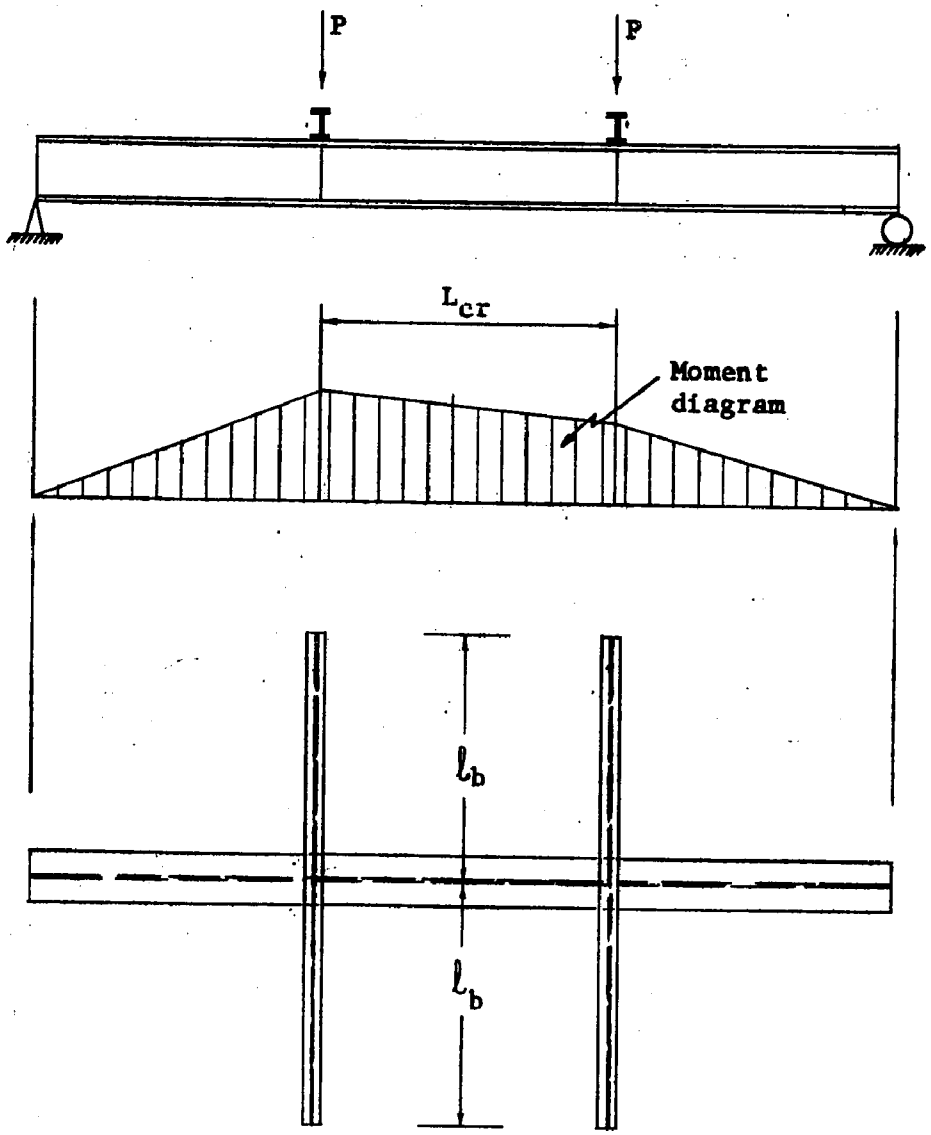

Fig. 4.1 MODEL (b) FOR PURLIN STRENGTH ANALYSIS

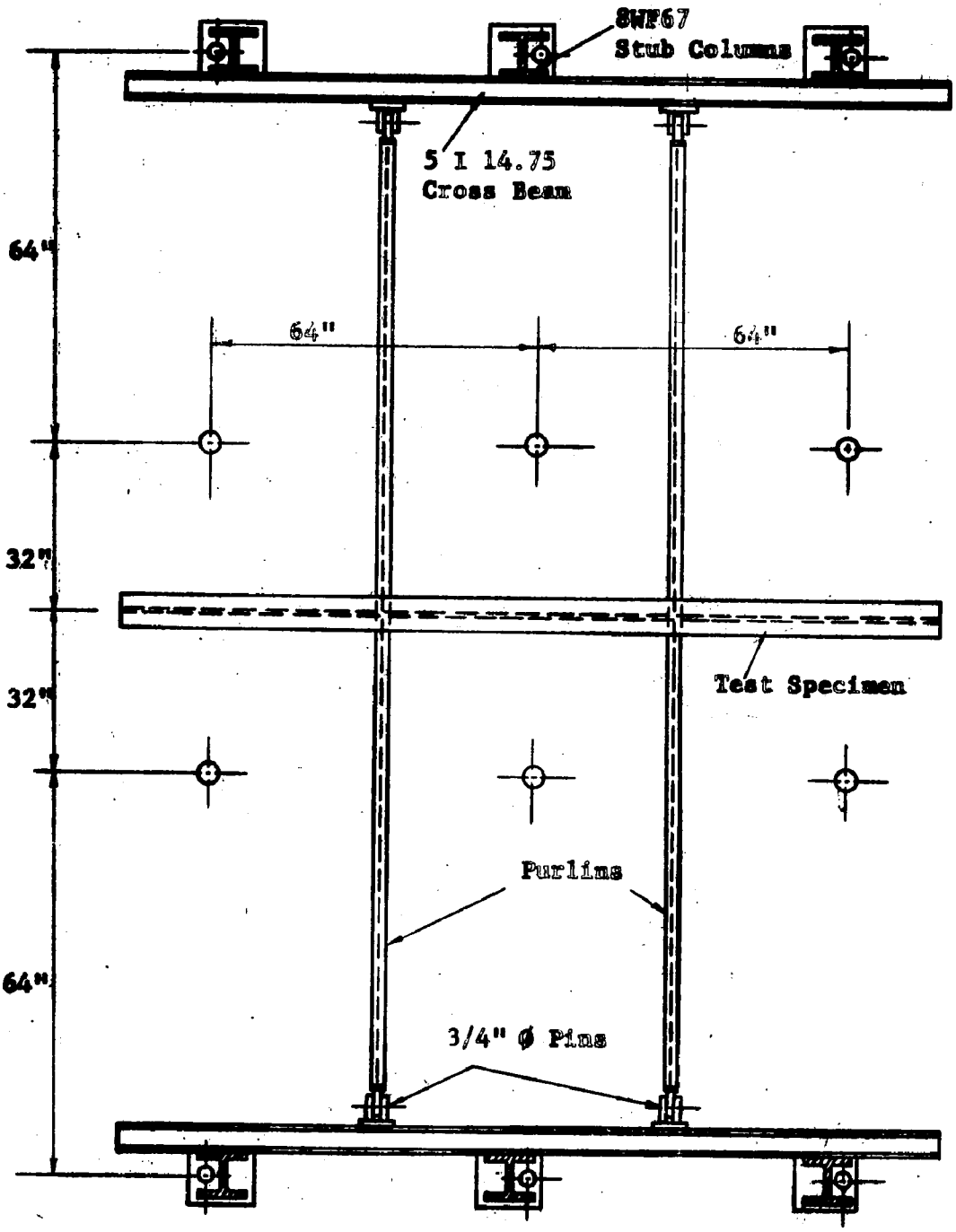

Fig. 4.2(a) PLAN VIEW OF THE BEAM-PURLIN ASSEMBLY

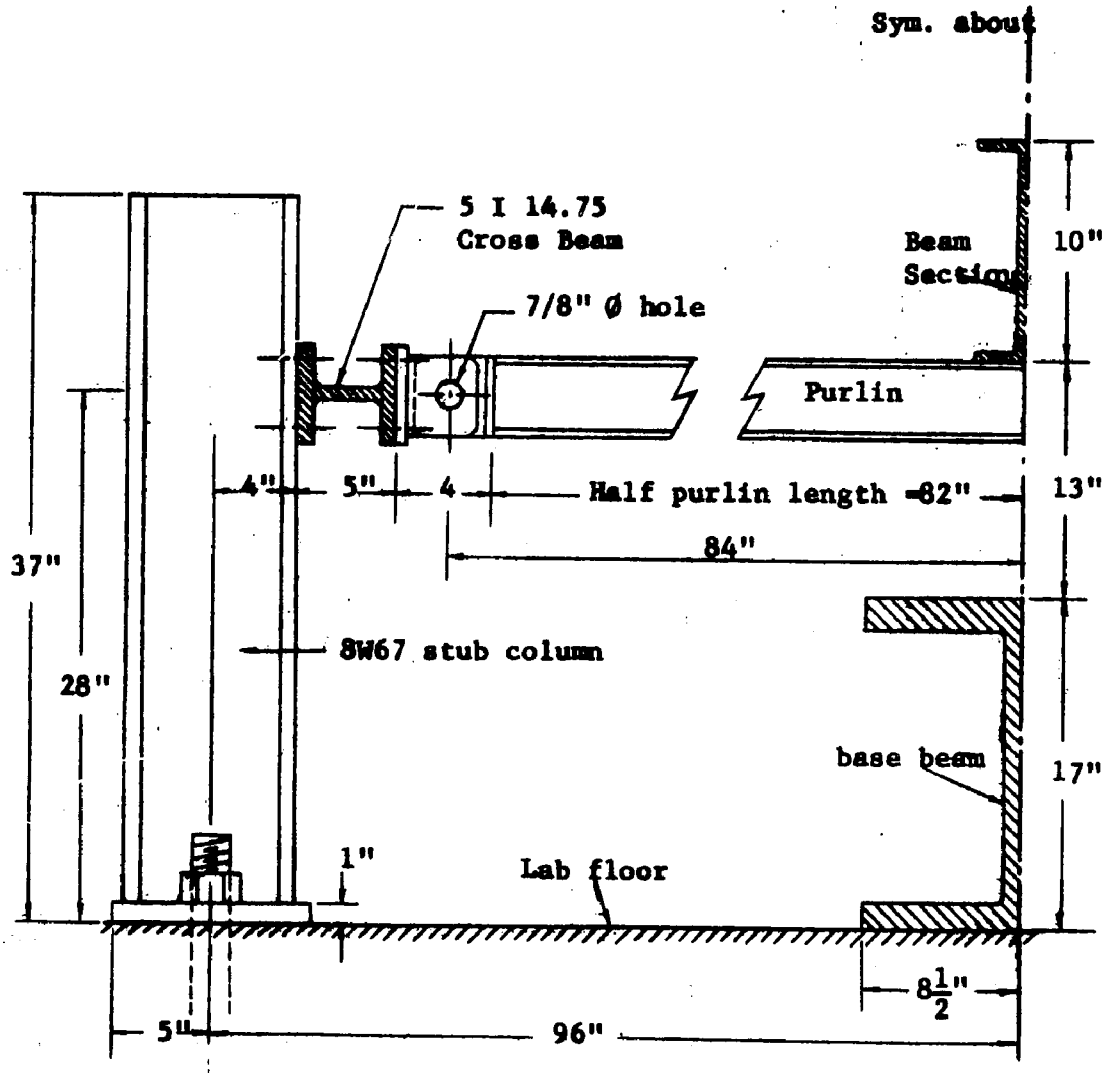

Fig. 4.2(b) SECTION VIEW OF THE BEAM-PURLIN ASSEMBLY

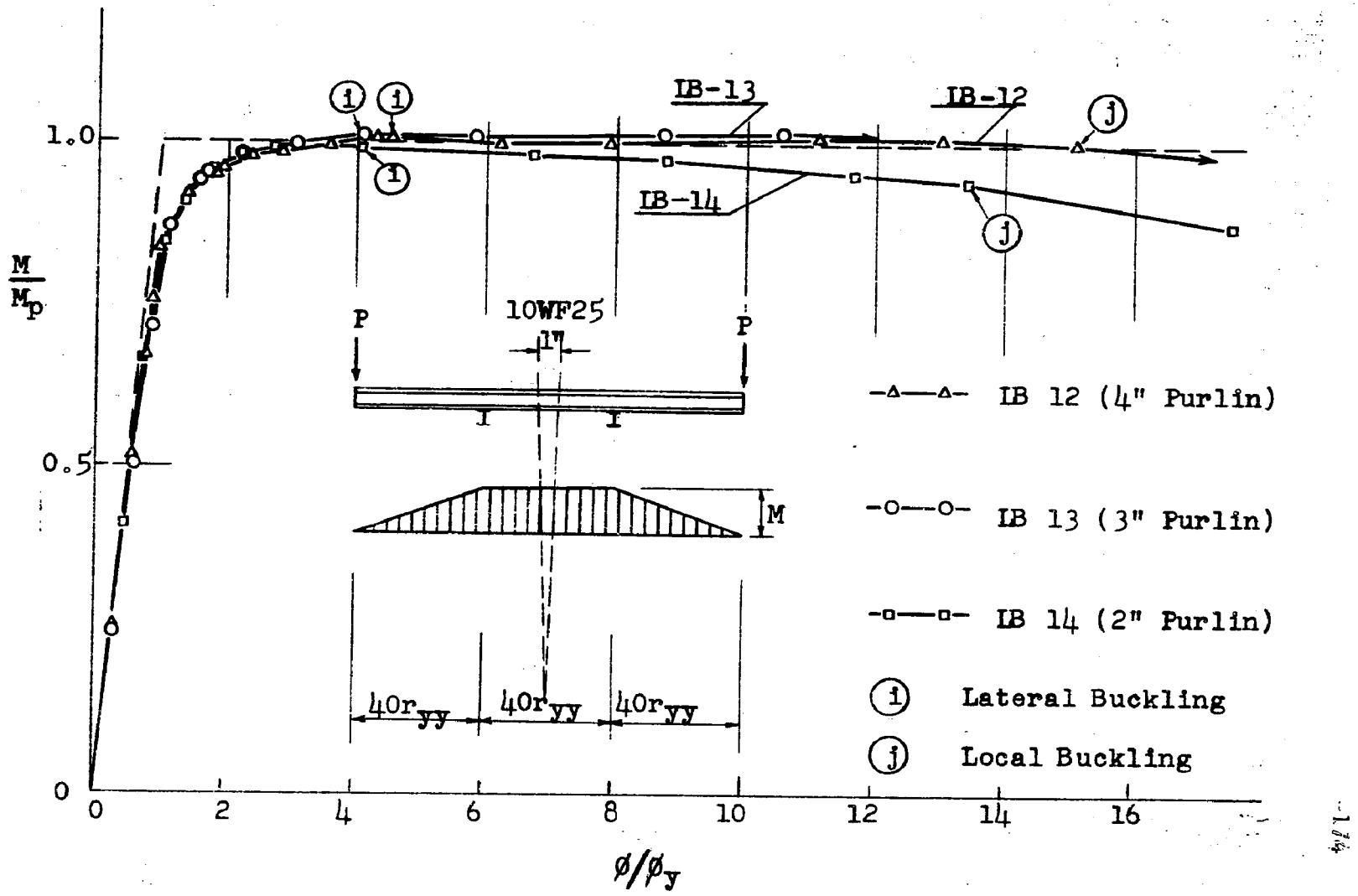

Fig. 4.3 - MOMENT VS. CURVATURE RELATIONSHIPS AT MIDDLE SPAN

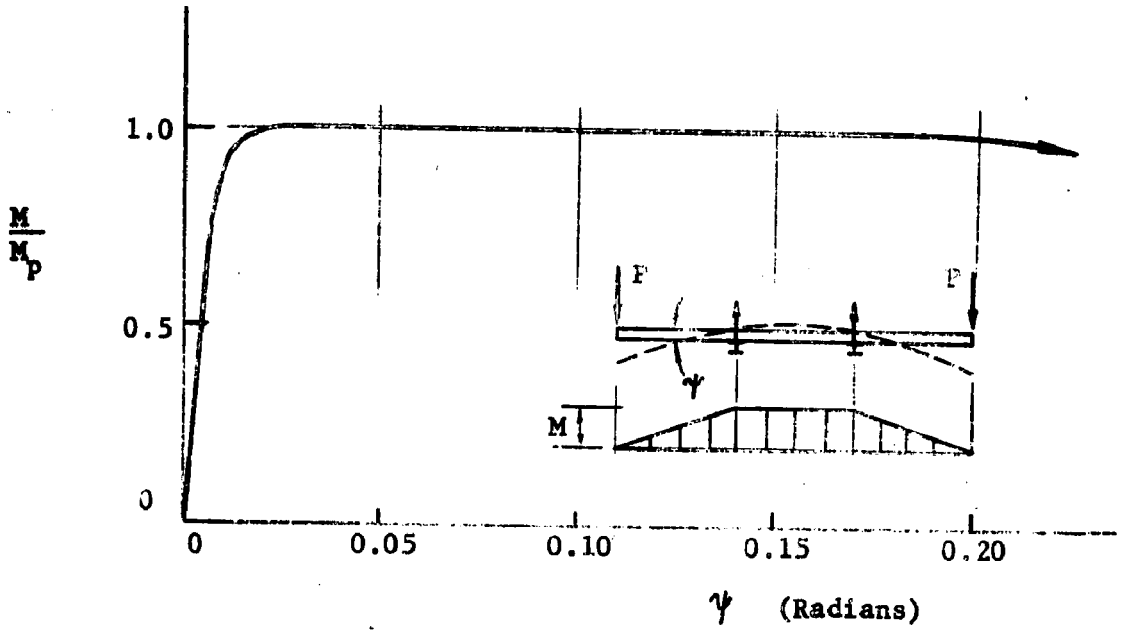

Fig. 4.4 MOMENT VERSUS ROTATION CURVE FOR TEST LB-12

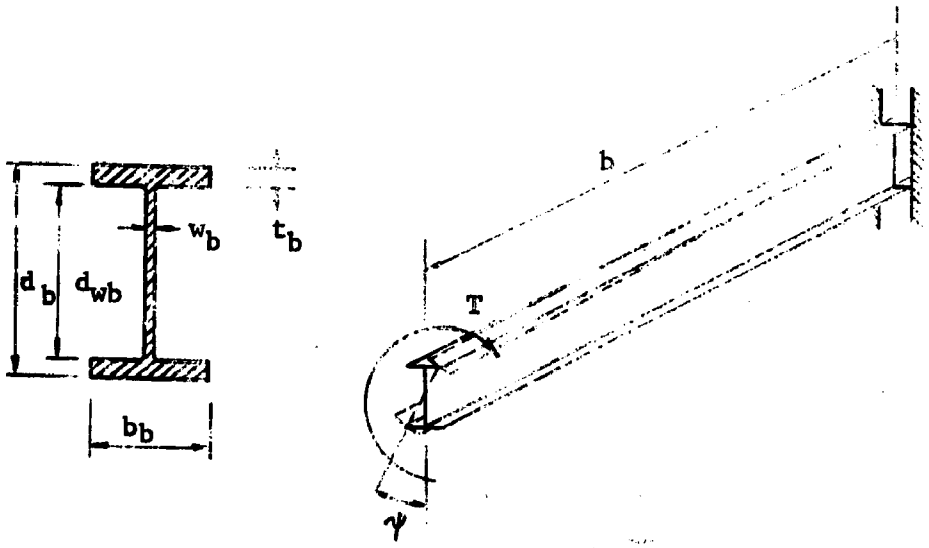

Fig. 4.5 FREE BODY FOR ANALYSIS OF TWISTING OF PURLINS

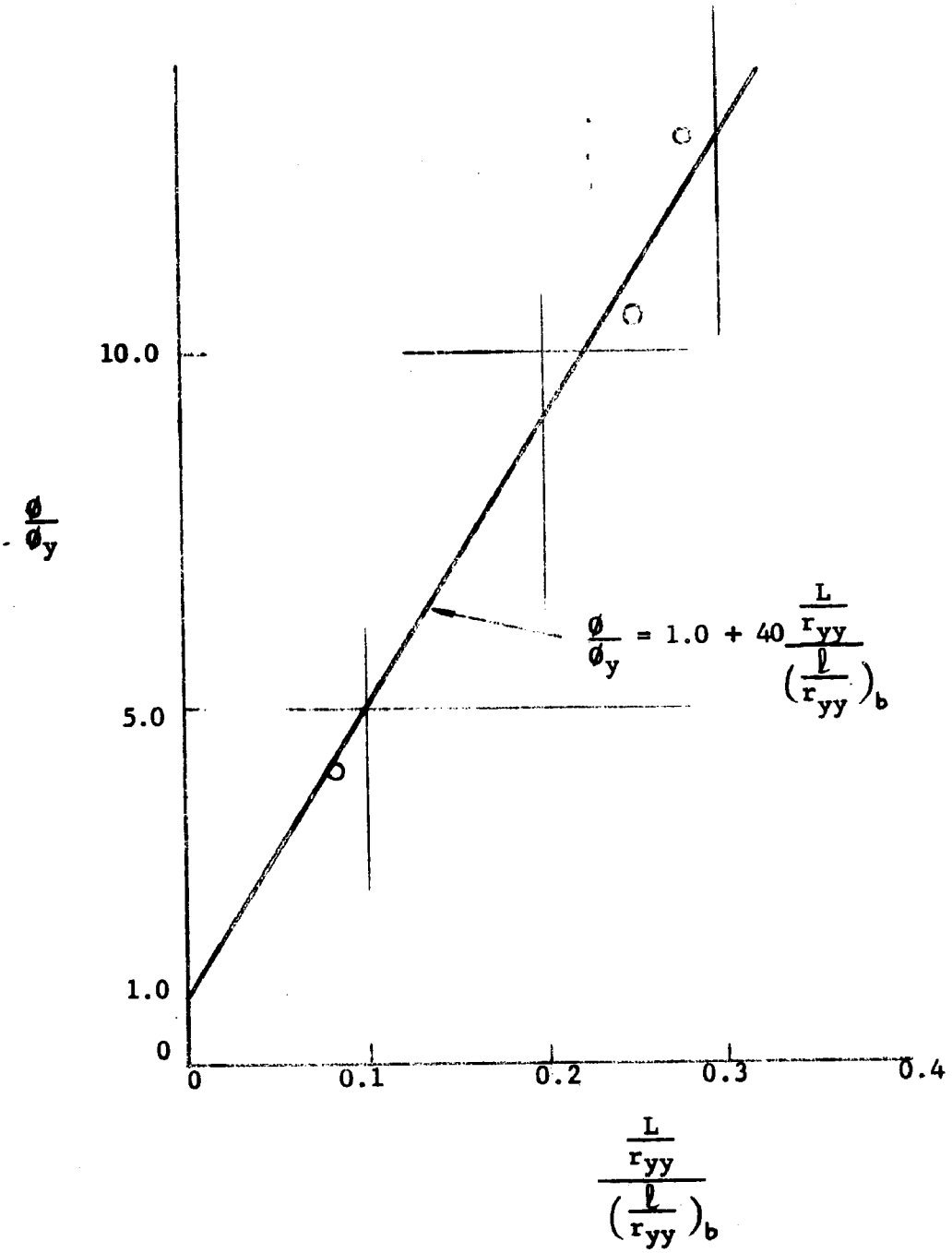

Fig. 4.6 RELATIONSHIPS BETWEEN THE STRENGTH OF PURLINS AND THE ROTATION REQUIREMENT OF BEAMS

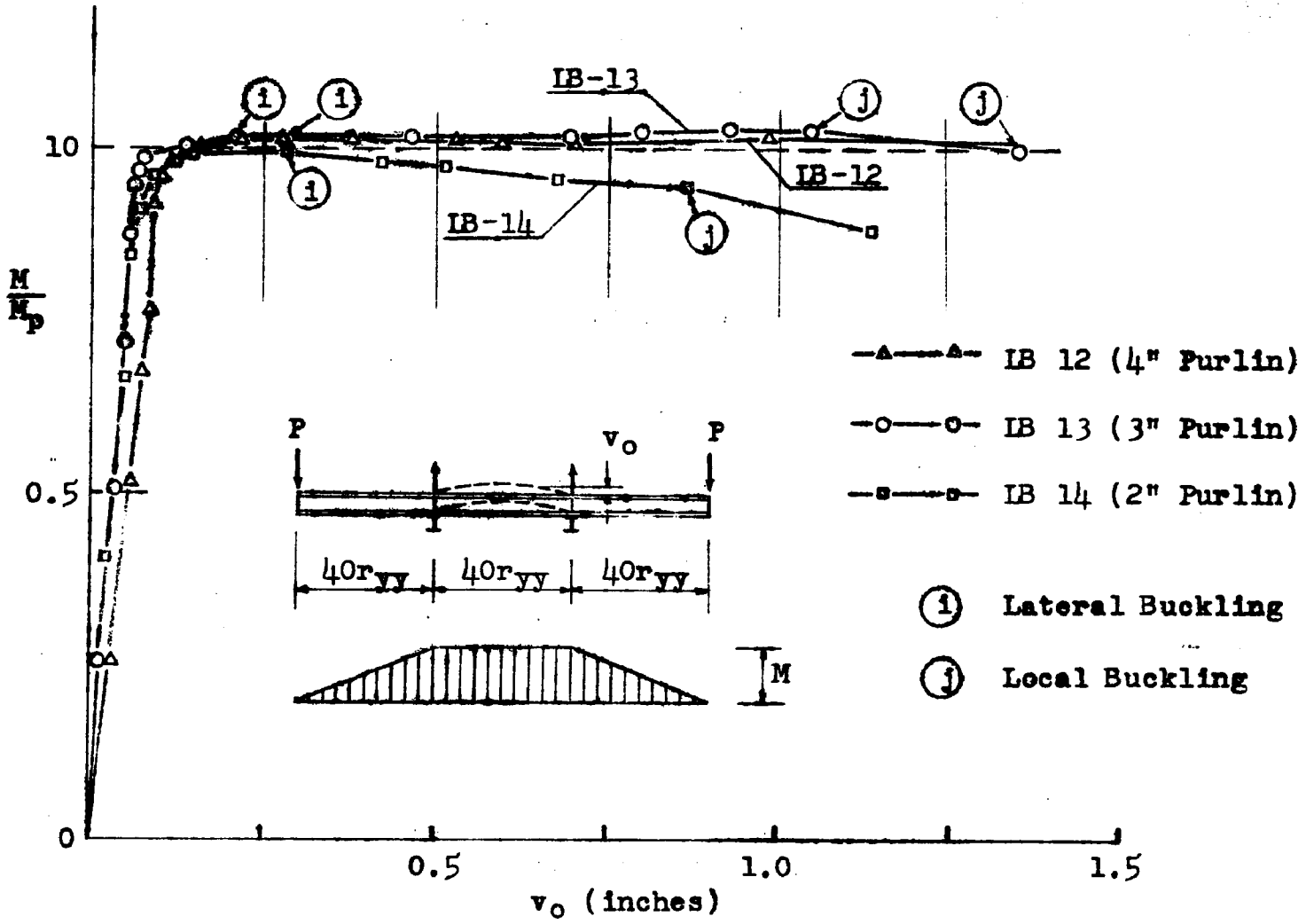

Fig. 4.7 - MOMENT VS VERTICAL DEFLECTION RELATIONSHIPS AT MIDSPAN

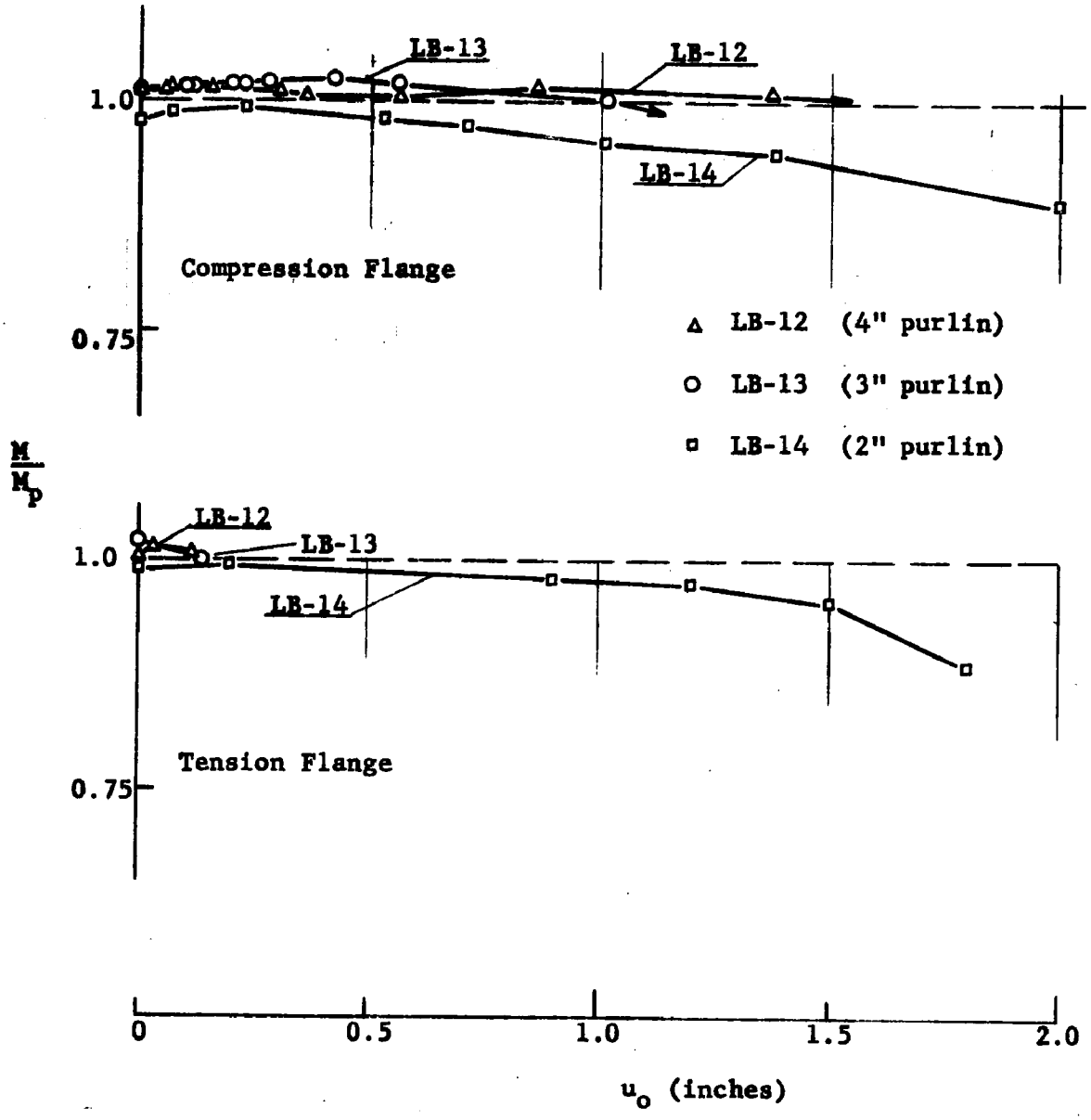

Fig. 4.8 MOMENT VERSUS LATERAL DEFLECTION RELATIONSHIPS AT MIDSPAN

Fig. 4.9 TEST SETUP OF THE BEAM-PURLIN ASSEMBLY (COMPLETION OF TEST LB-13)

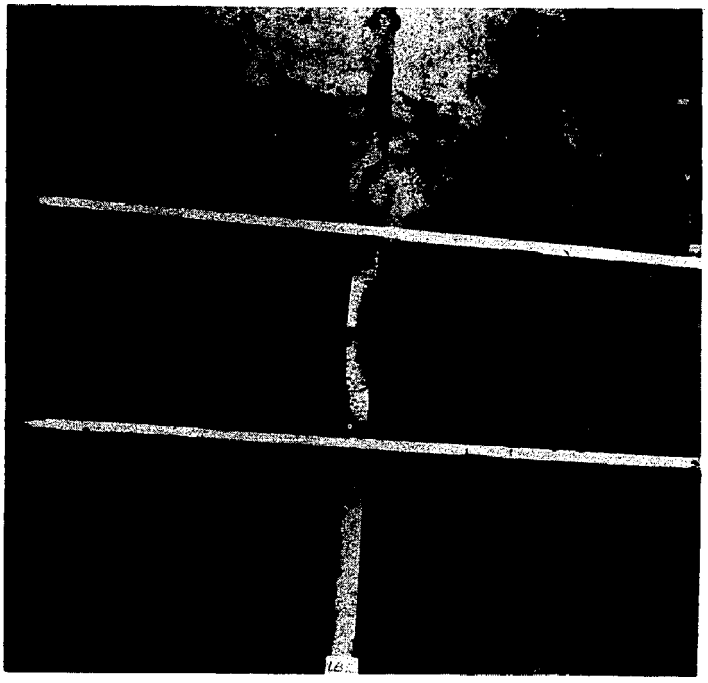

Fig. 4.10 FINAL DEFORMED SHAPE OF THE BEAM-PURLIN STRUCTURE (LB-12)

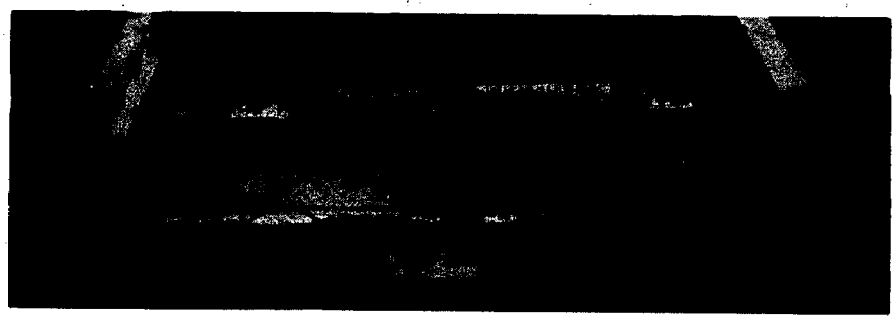

BEAM 10WF25
PURLINS 4I7.7

BEAM 10WF25
PURLINS 3I5.7

BEAM 10WF25
PURLINS M2362

Fig. 4.11 CRITICAL SPANS AFTER TEST. THE PROPORTIONS OF THE PURLIN AREAS ARE SHOWN.

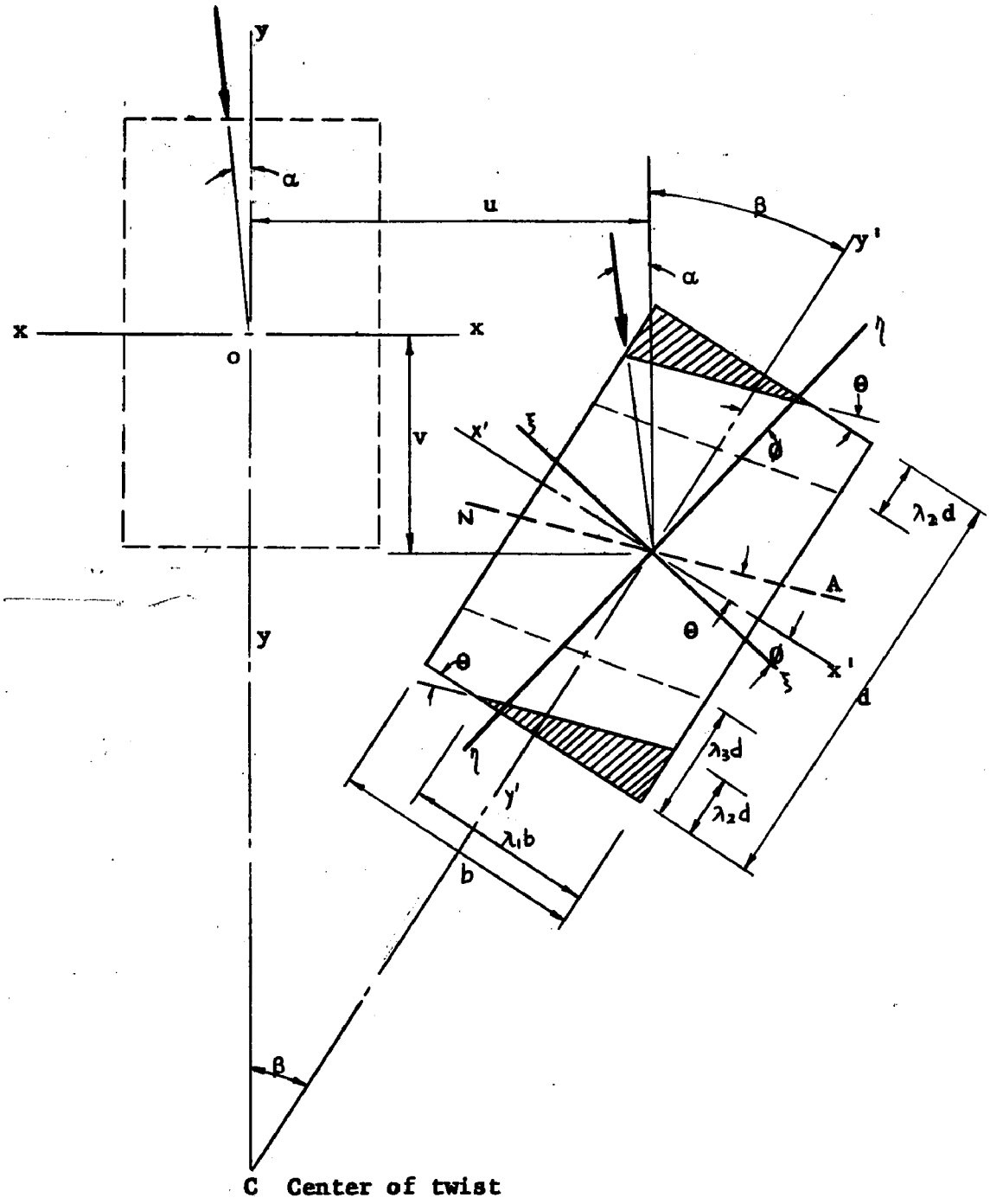

Fig. 5.1 SYMBOLS AND DEFINITIONS FOR A PARTIALLY YIELDED SECTION HAVING DEFORMATIONS u, v AND β.

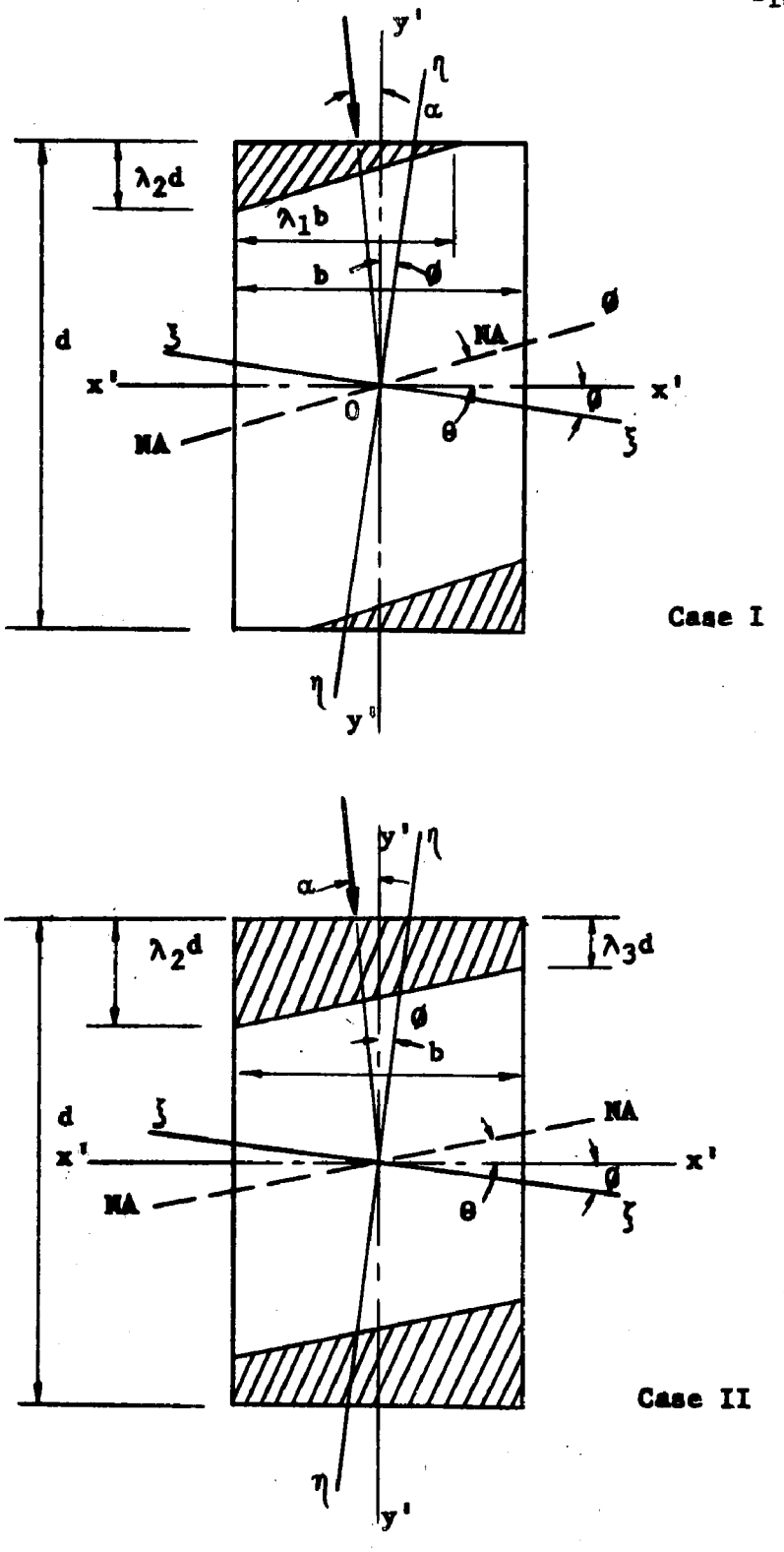

Fig. 5.2 TWO POSSIBLE YIELDING CASES FOR THE CALCULATION OF THE EFFECTIVE MOMENT OF INERTIA

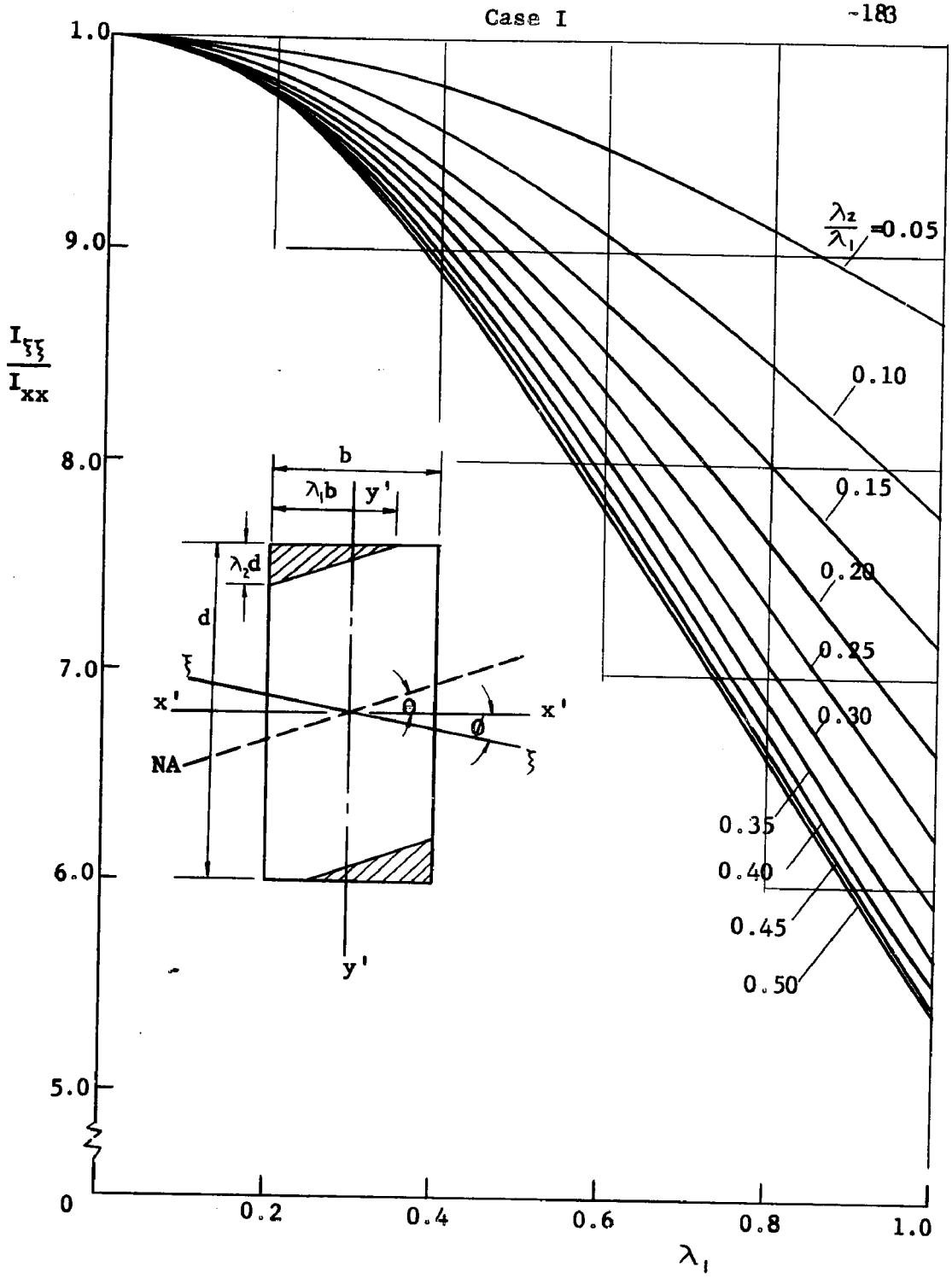

Fig. 5.3 REDUCTION OF MOMENT OF INERTIA ABOUT THE STRONG AXIS

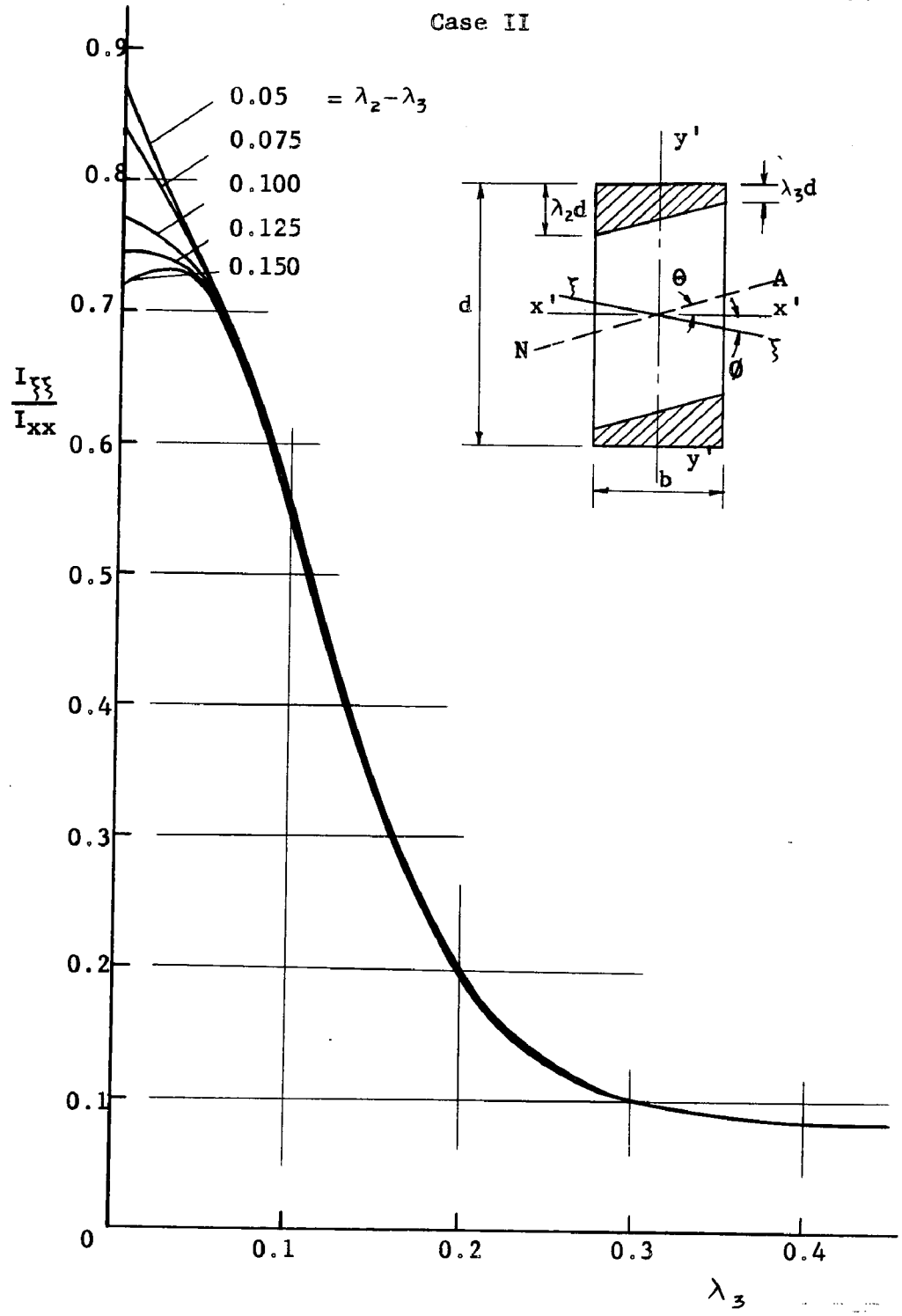

Fig. 5.4 REDUCTION OF MOMENT OF INERTIA ABOUT THE STRONG AXIS

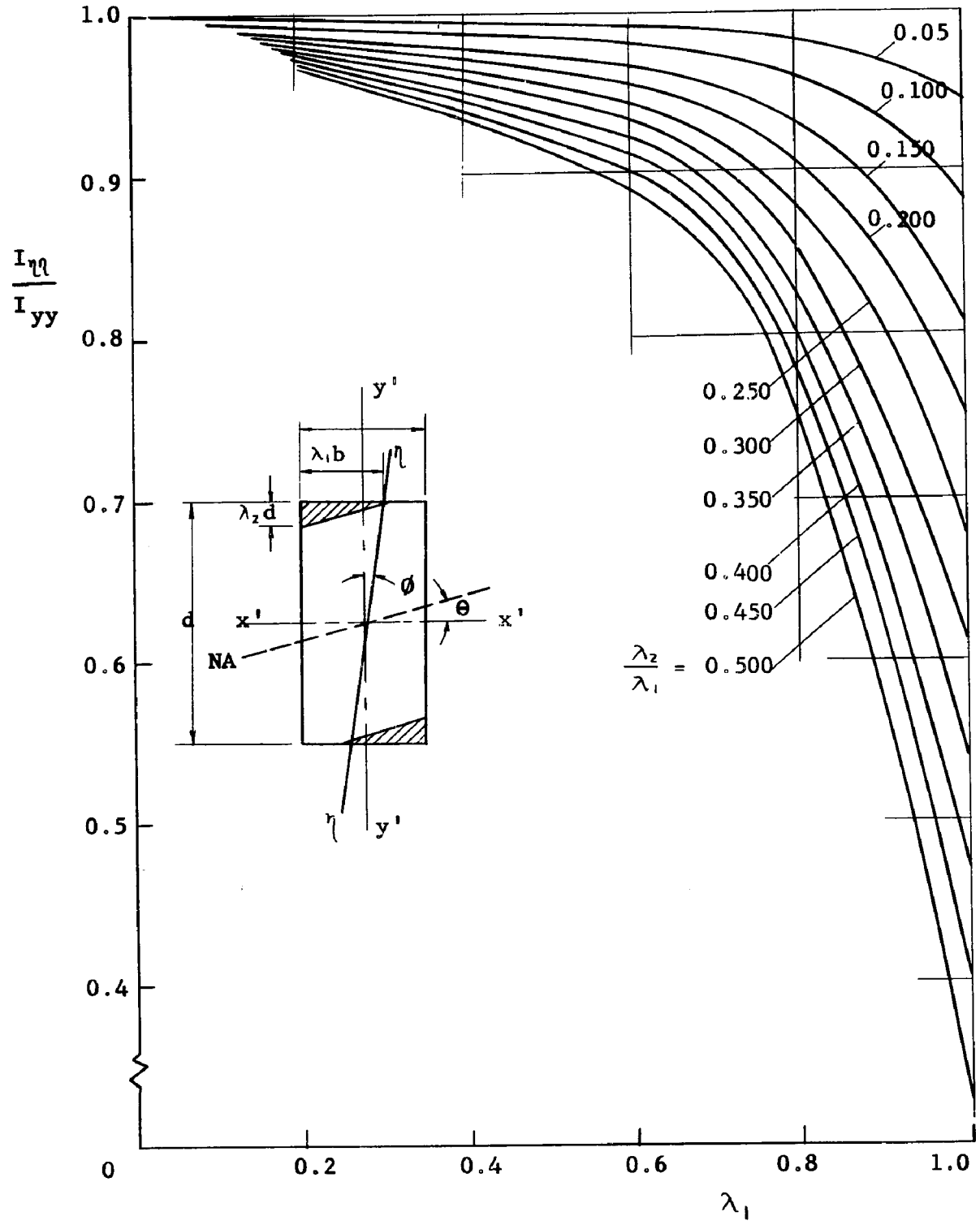

Fig. 5.5 REDUCTION OF MOMENT OF INERTIA ABOUT THE WEAK AXIS

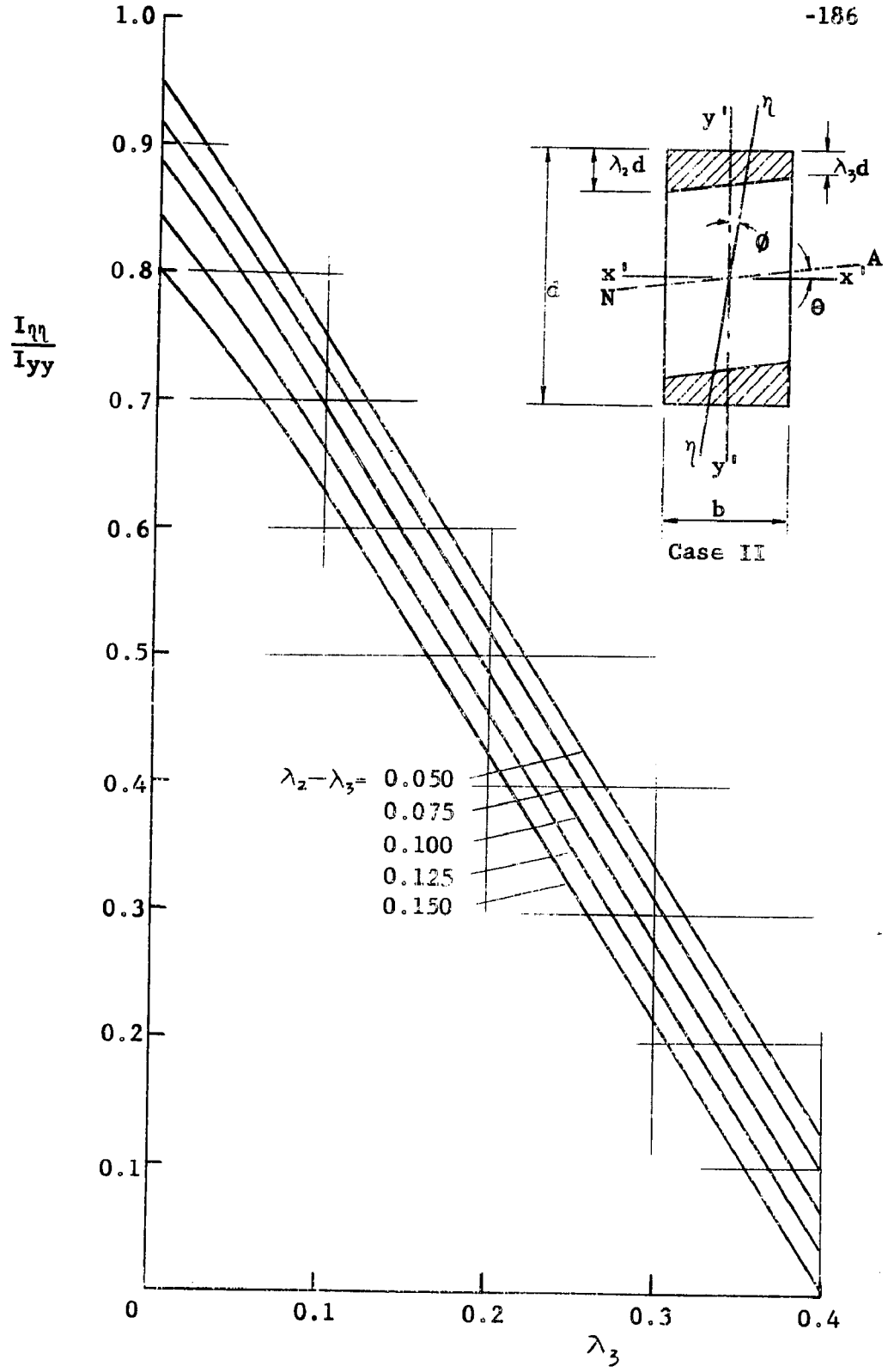

Fig. 5.6 REDUCTION OF MOMENT OF INERTIA ABOUT THE WEAK AXIS

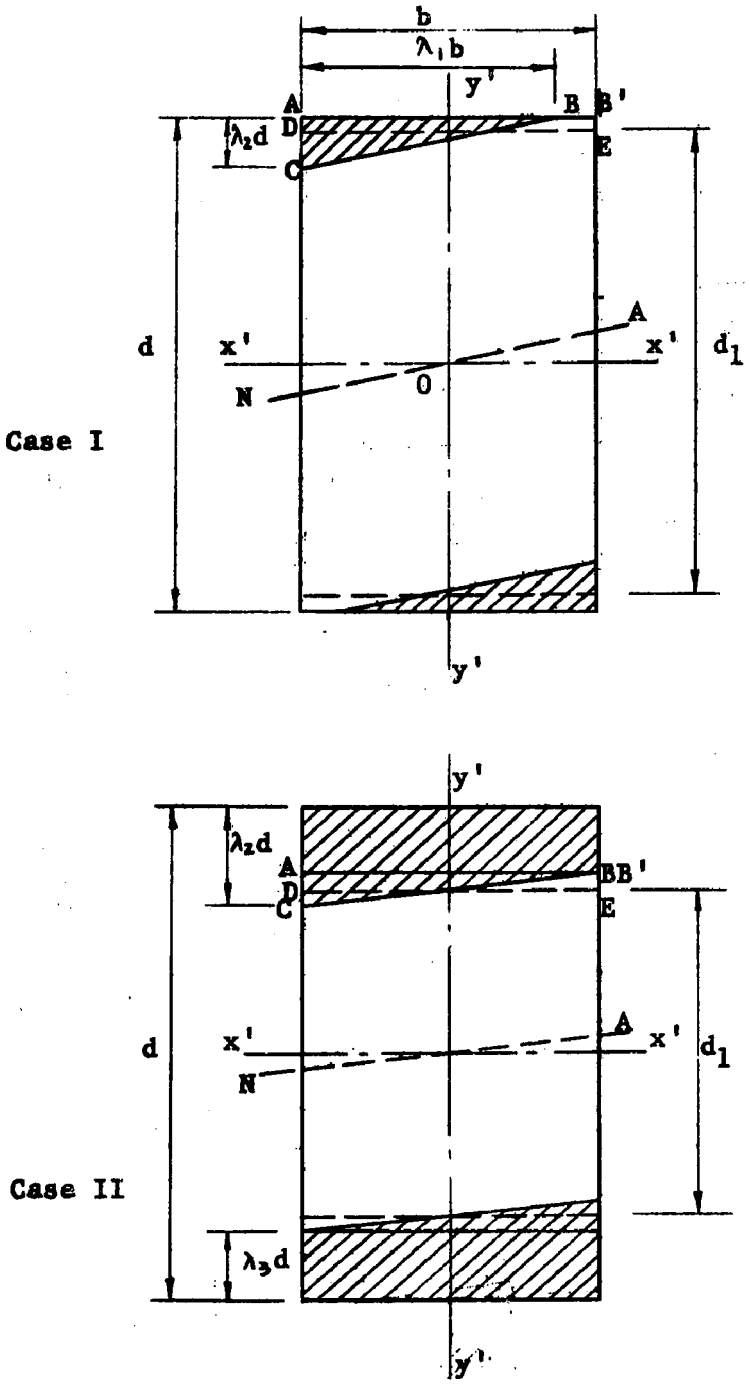

Fig. 5.7 APPROXIMATIONS OF ST. VENANT'S TORSIONAL CONSTANT FOR PARTIALLY YIELDED CROSS SECTIONS

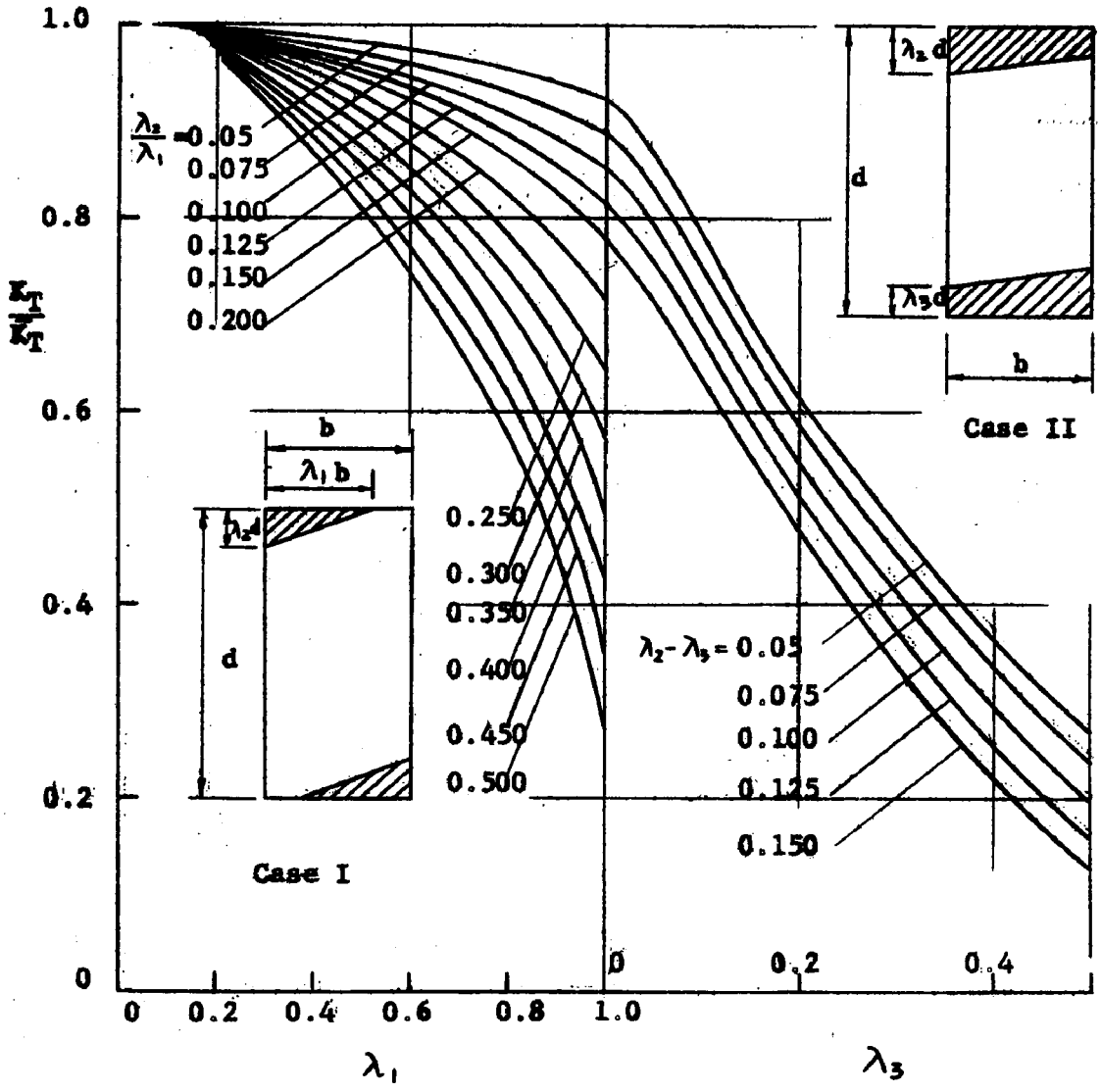

Fig. 5.8 REDUCTION OF THE ST. VENANT'S TORSIONAL CONSTANT FOR PARTIALLY YIELDED SECTIONS

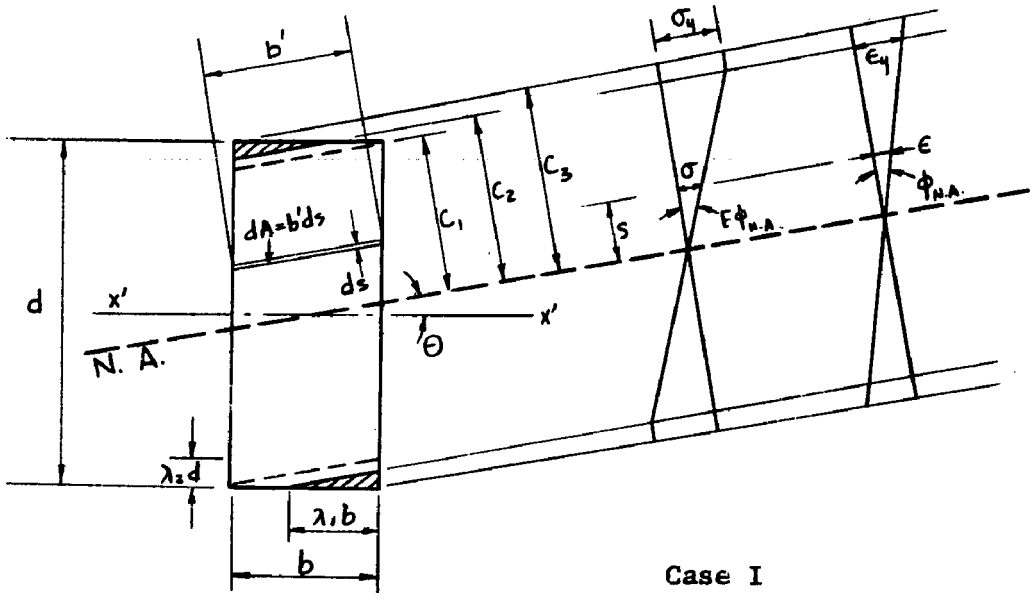

Case I

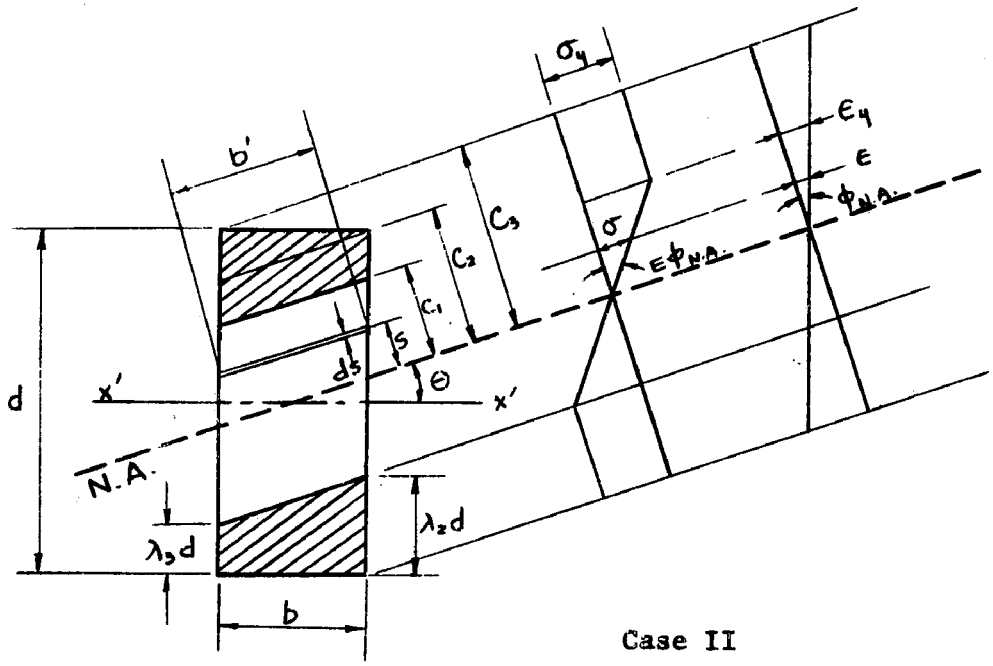

Case II

Fig. 5.9 STRESS AND STRAIN VARIATIONS ABOUT THE NEUTRAL AXIS OF PARTIALLY YIELDED SECTIONS

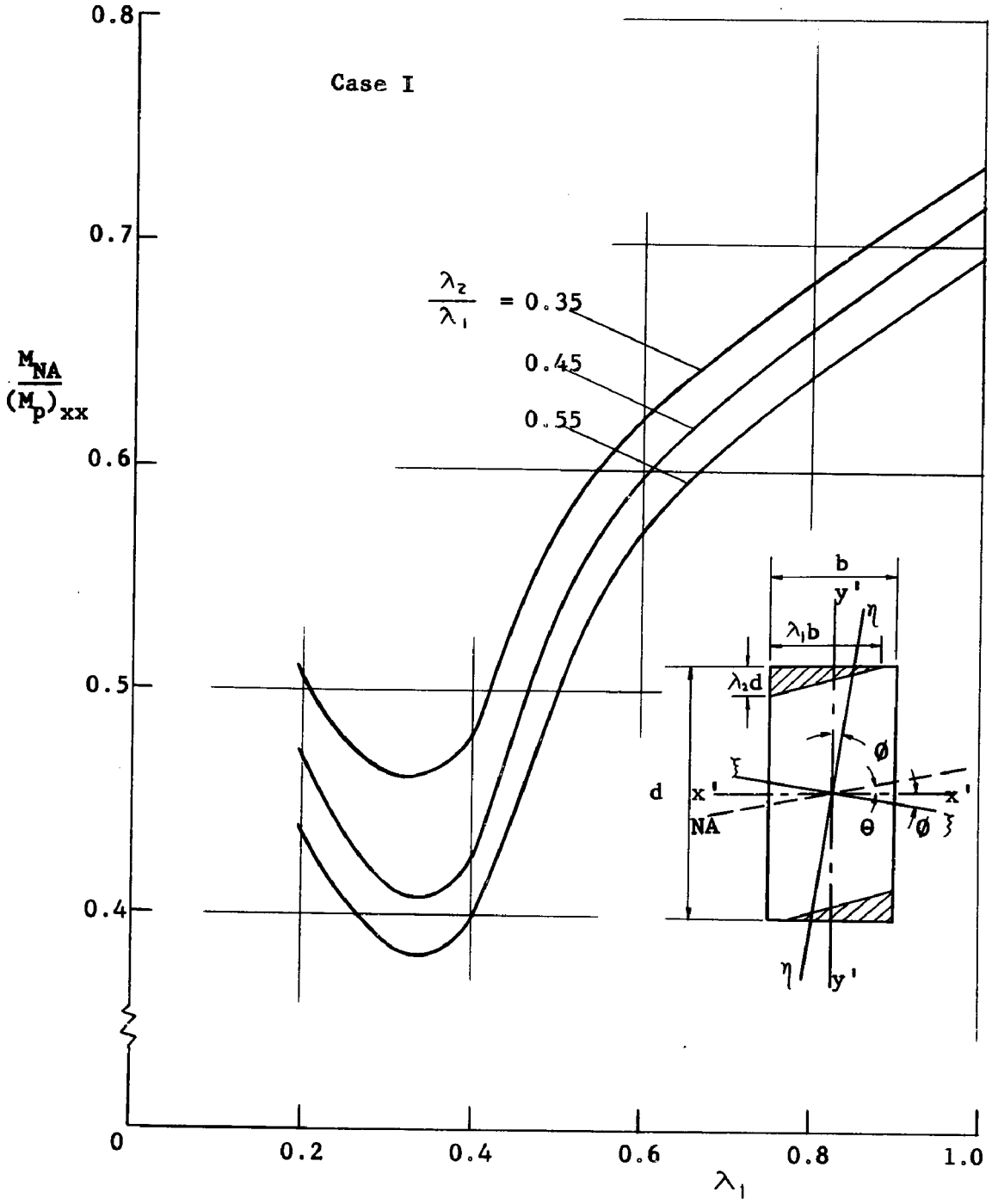

Fig. 5.10 VARIATION OF MOMENT ABOUT THE NEUTRAL AXIS IN PARTIALLY YIELDED SECTIONS

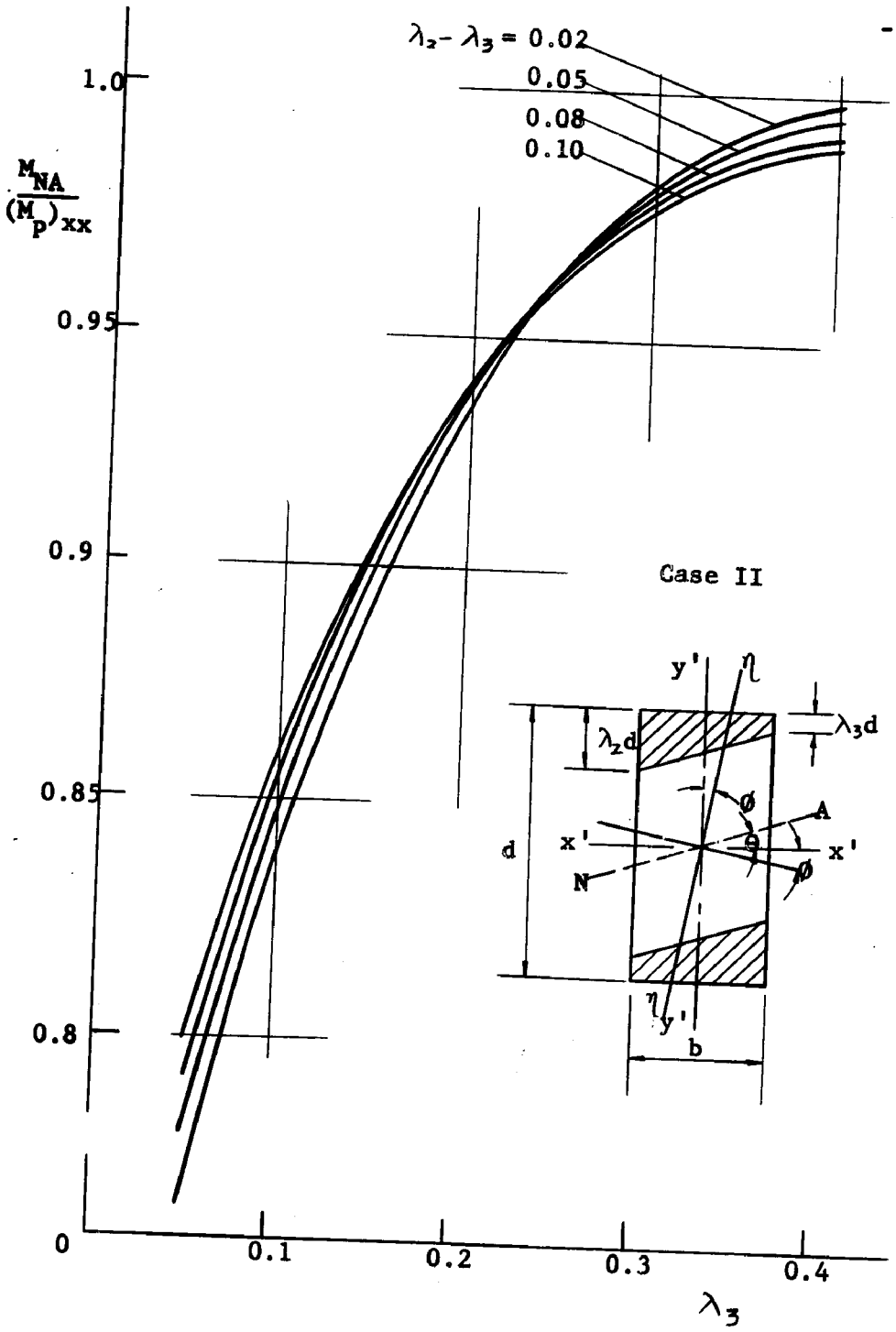

Fig. 5.11 VARIATION OF MOMENT ABOUT THE NEUTRAL AXIS IN PARTIALLY YIELDED SECTIONS

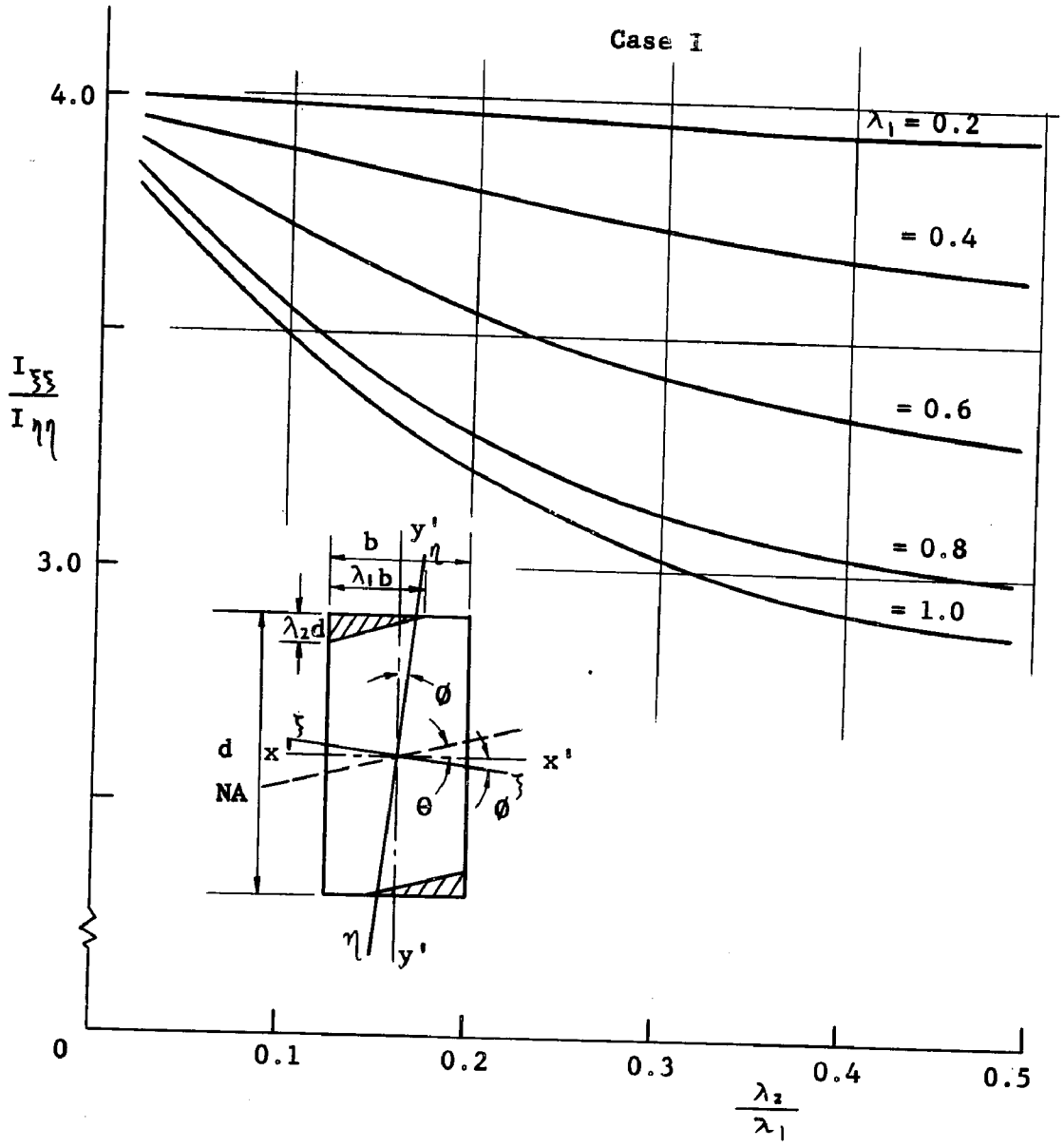

Fig. 5.12 RELATIONSHIP BETWEEN THE RATIO OF THE PRINCIPAL MOMENT OF INERTIA AND THE YIELDING PARAMETERS

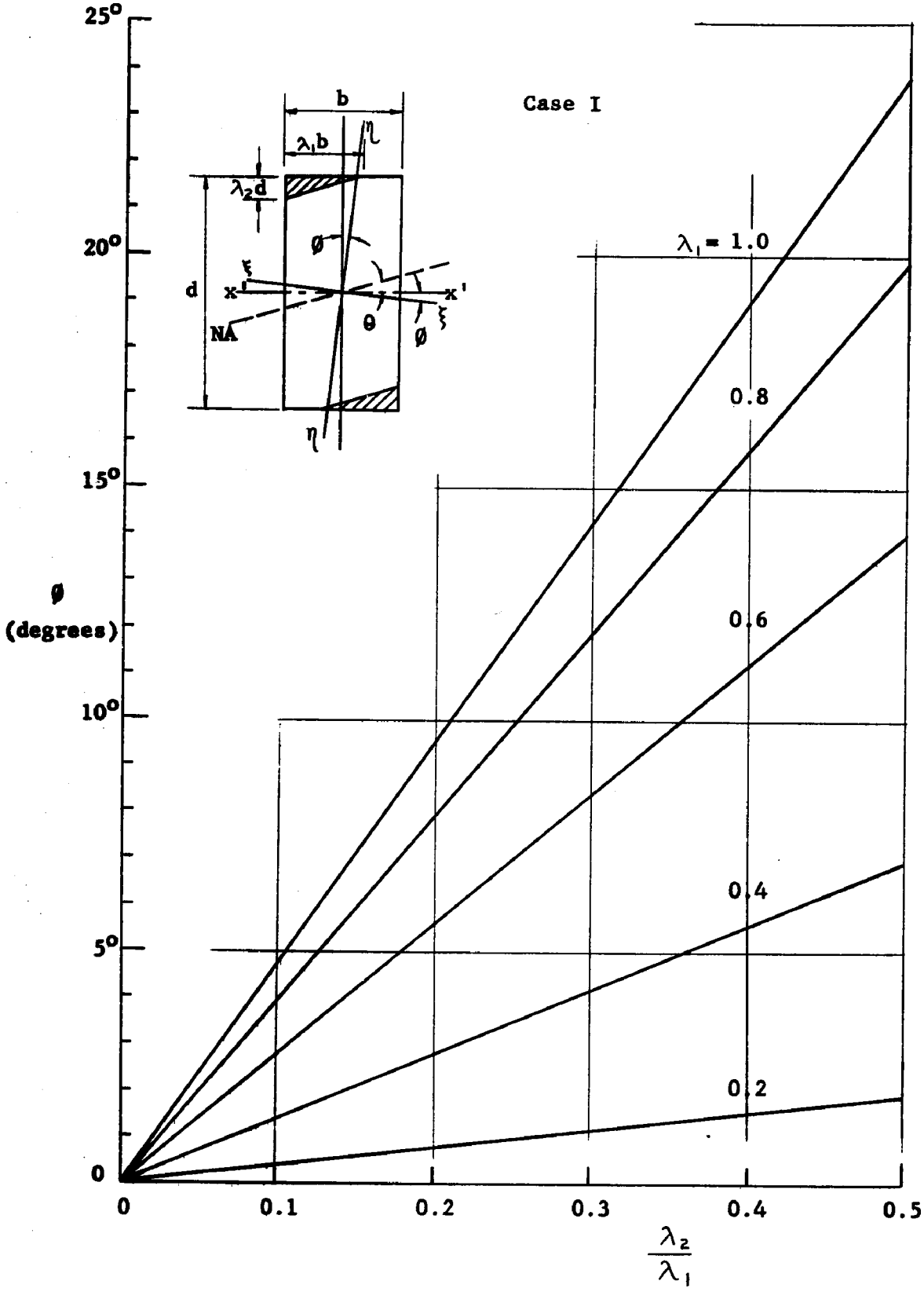

Fig. 5.13 INCLINATION OF THE PRINCIPAL AXES OF A PARTIALLY YIELDED RECTANGULAR SECTION

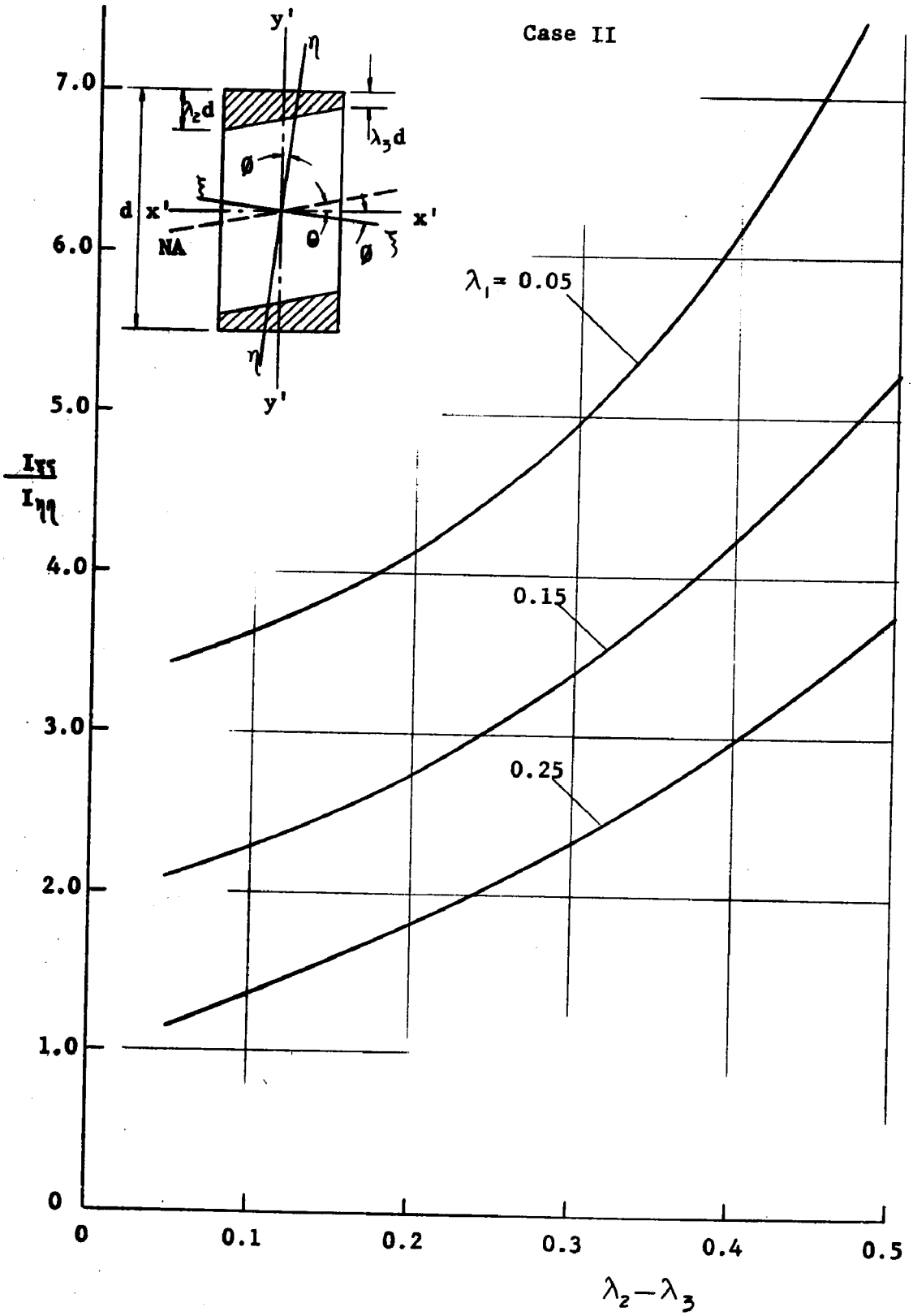

Fig. 5.14 RELATIONSHIP BETWEEN THE RATIO OF THE PRINCIPAL MOMENT OF INERTIA AND THE YIELDING PARAMETERS

Case II

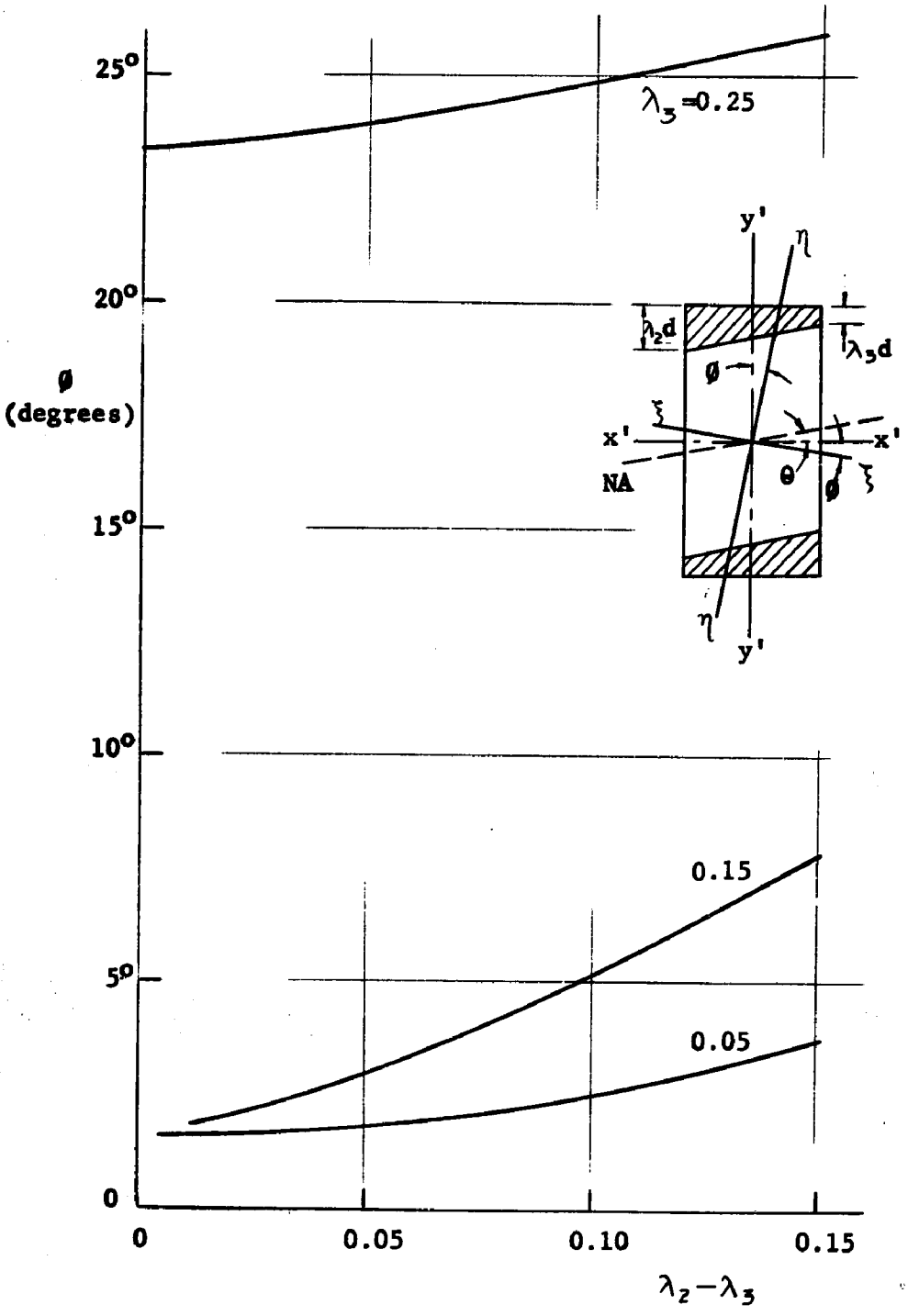

Fig. 5.15 INCLINATION OF THE PRINCIPAL AXES OF A PARTIALLY YIELDED RECTANGULAR SECTION

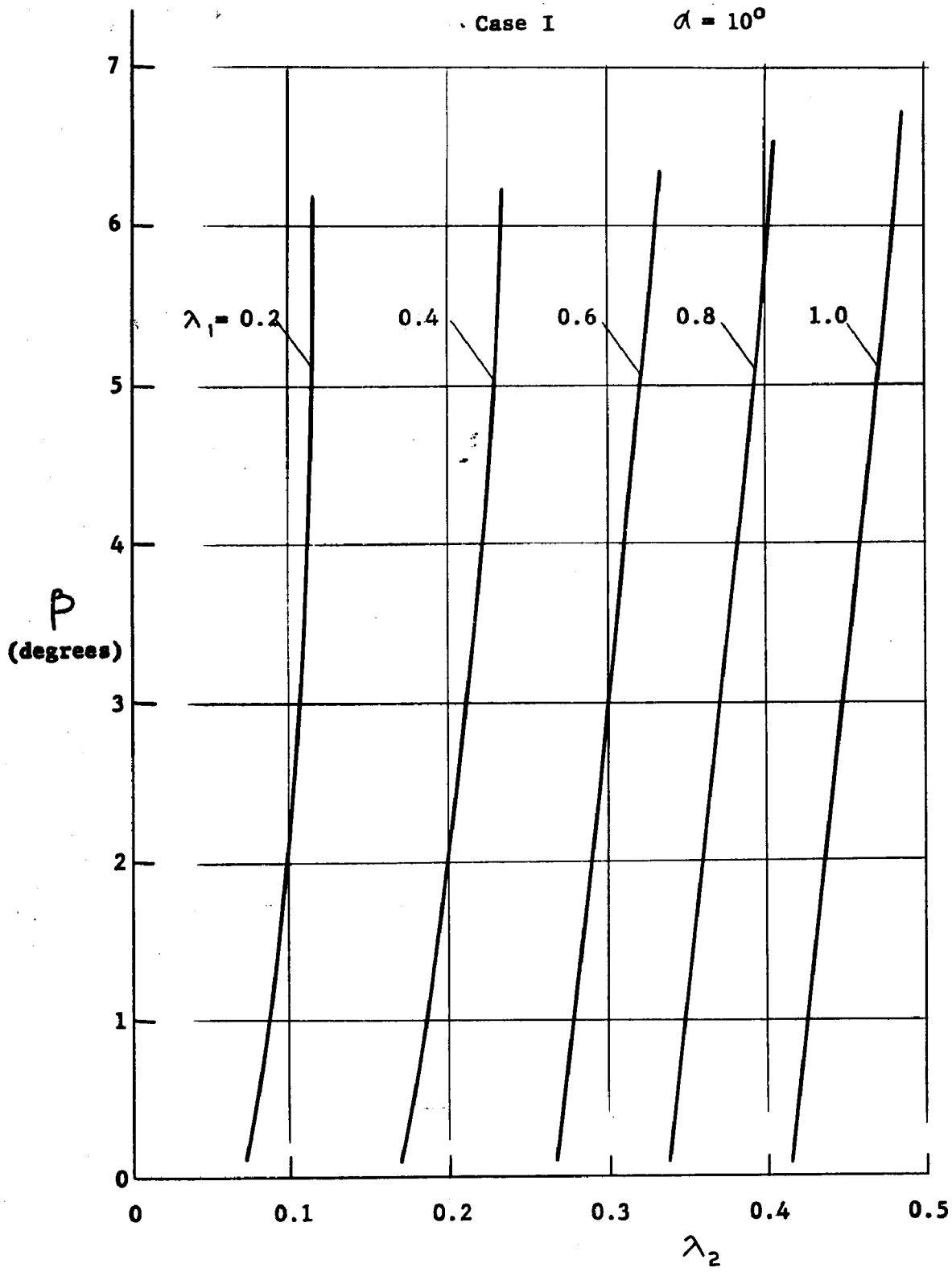

Fig. 5.16 VARIATION OF TWISTING ANGLE β WITH THE YIELDING PARAMETERS

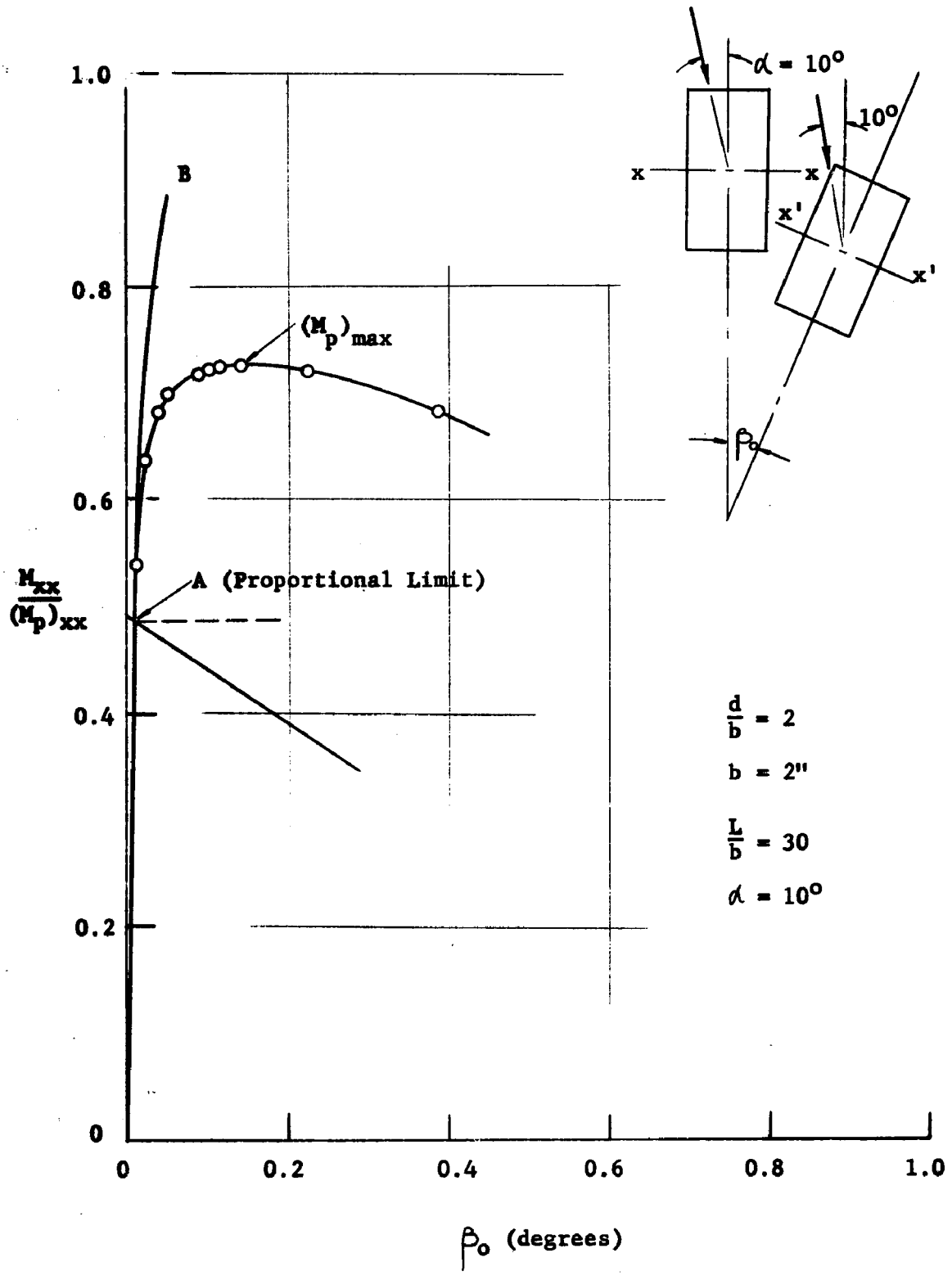

Fig. 5.17 THEORETICAL MEMENT VERSUS TWISTING RELATIONSHIP

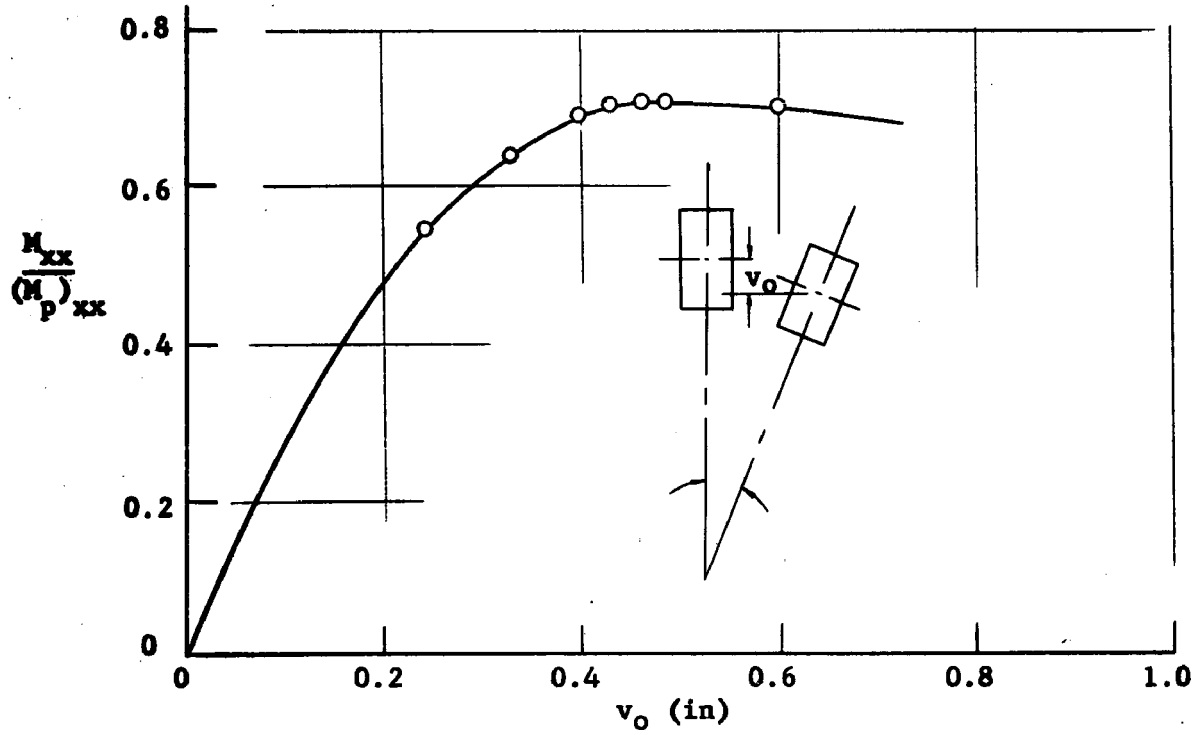

Fig. 5.18 THEORETICAL MOMENT VERSUS VERTICAL DEFLECTION RELATIONSHIP

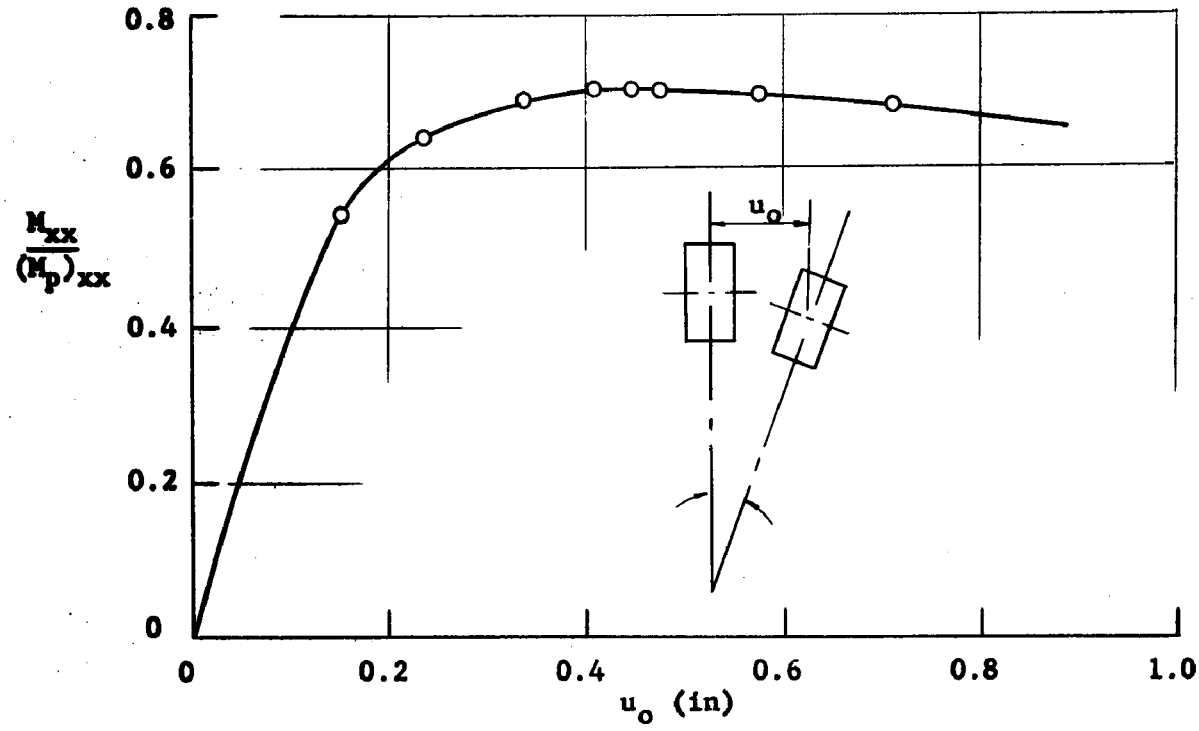

Fig. 5.19 THEORETICAL MOMENT VERSUS LATERAL DEFLECTION RELATIONSHIP

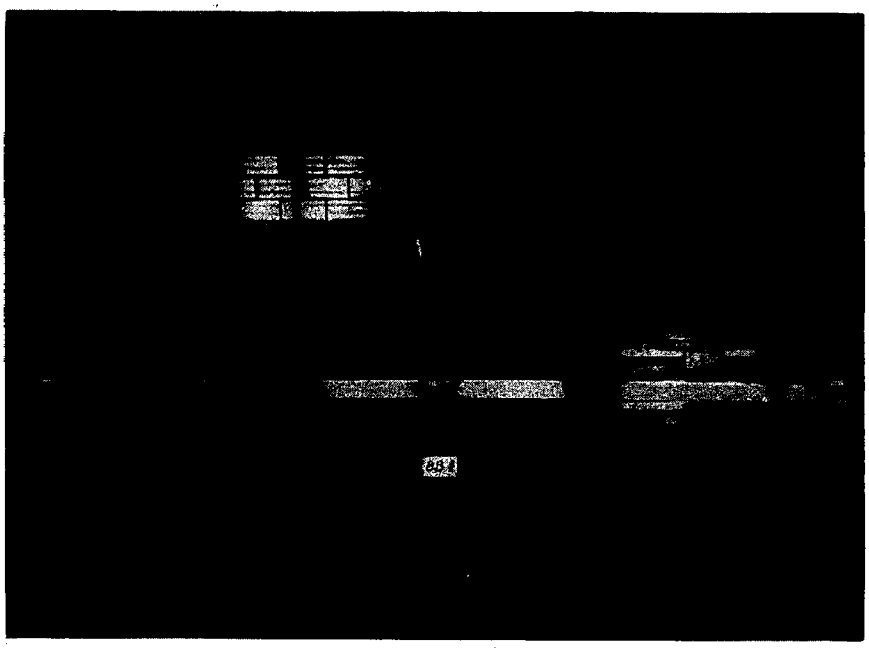

Fig. 5.20 BIAXIAL BENDING TEST ASSEMBLY - I

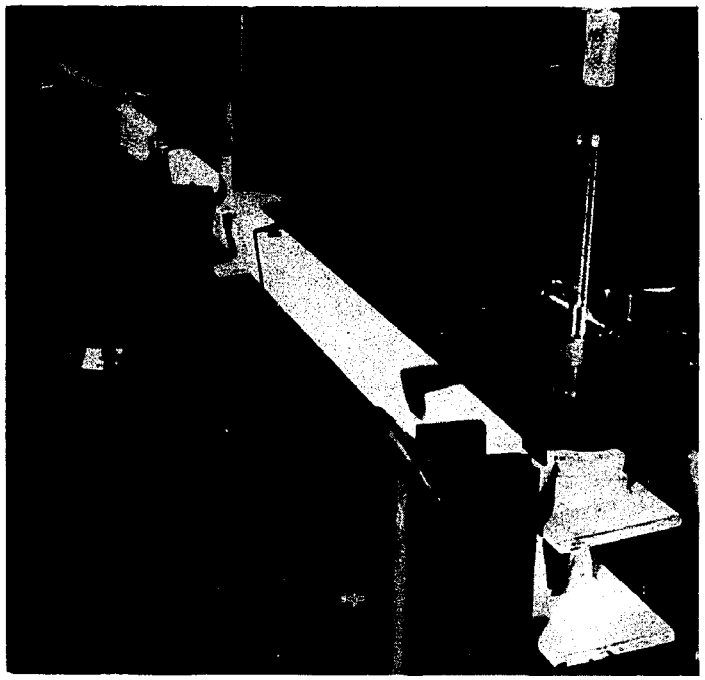

Fig. 5.21 BIAXIAL BENDING TEST ASSEMBLY - II

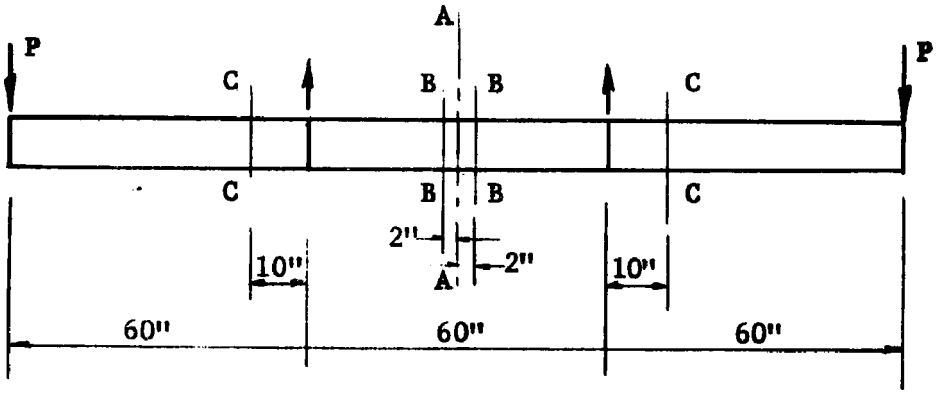

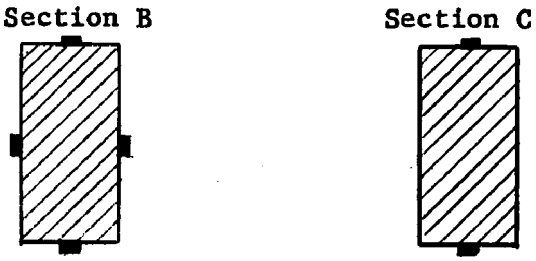

(a) SR-4 Strain Gage Locations

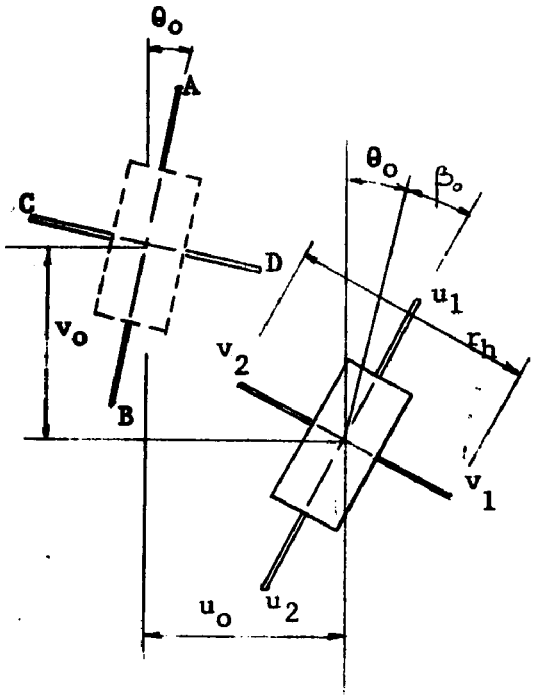

$$u_o = \frac{u_1 + u_2}{2}$$

$$v_o = \frac{v_1 + v_2}{2}$$

$$\beta_o = \frac{v_2 - v_1 - r_h \sin\theta_o}{r_h \cos\theta_o}$$

(b) Deformation Measurements

Fig. 5.22 INSTRUMENTATIONS FOR BIAXIAL BENDING TEST

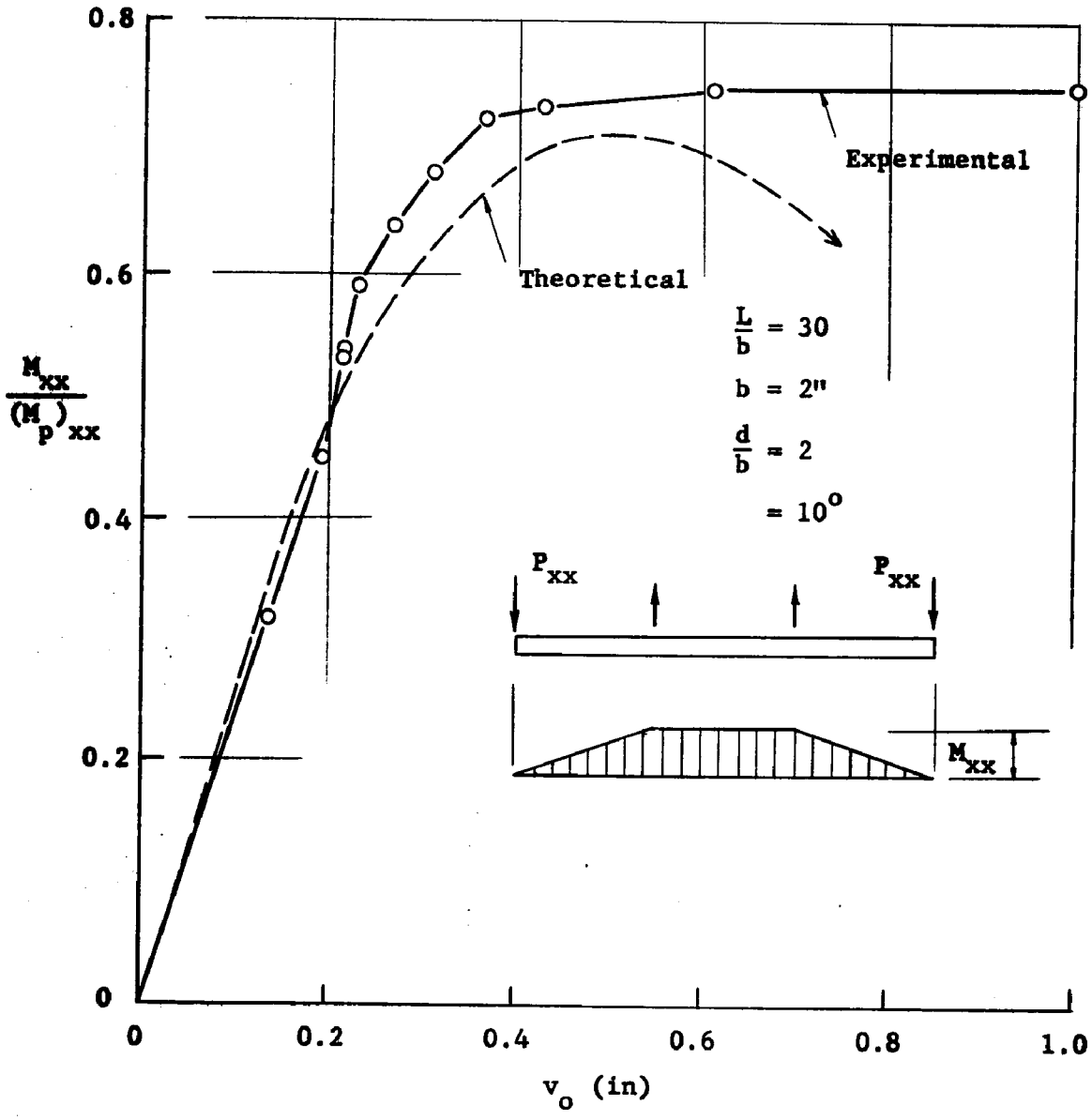

Fig. 5.23 COMPARISON BETWEEN THEORY AND TEST RESULTS

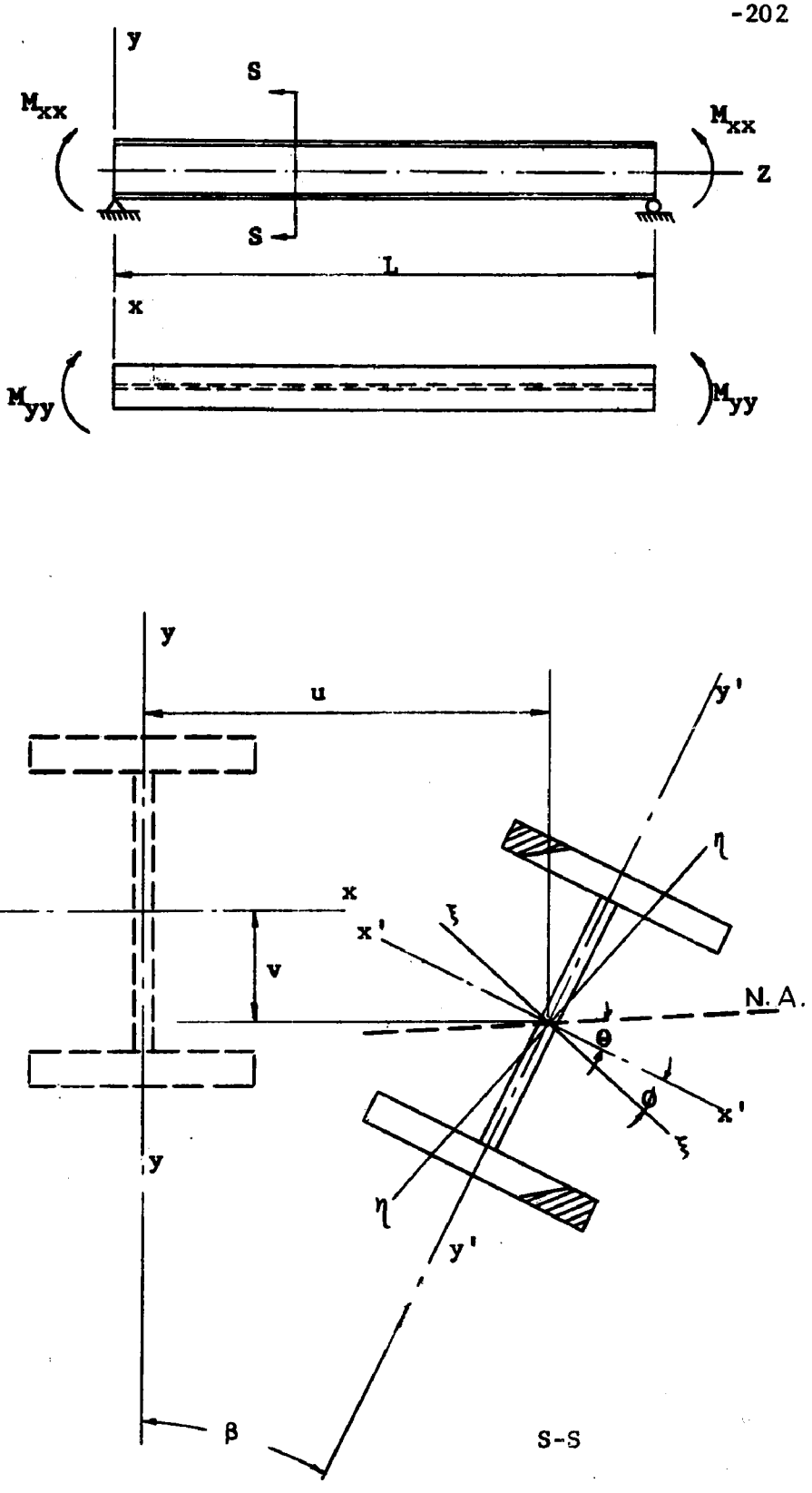

Fig. 5.24 SYMBOLS AND DEFINITIONS FOR A PARTIALLY YIELDED SECTION HAVING DEFORMATIONS u, v and β

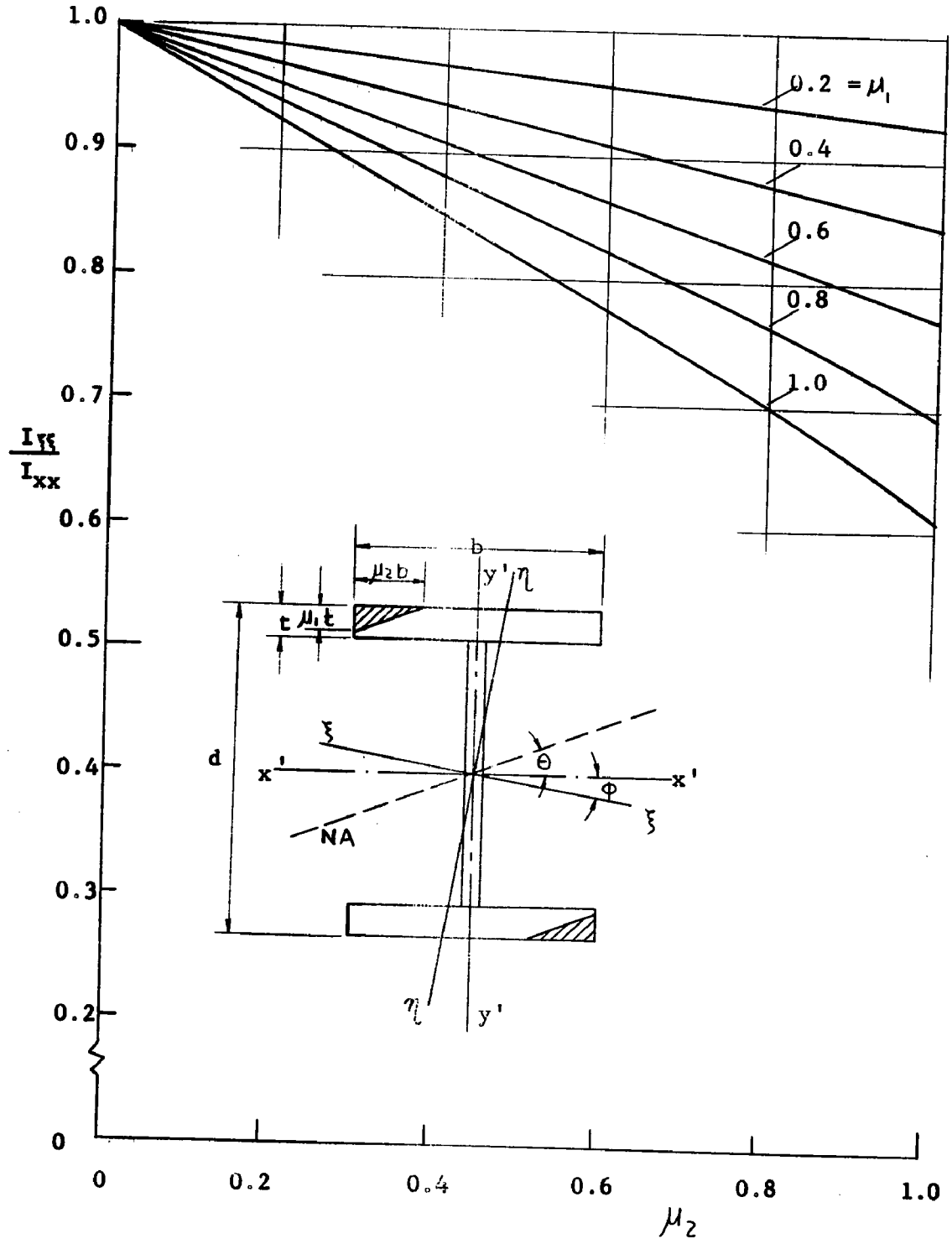

Fig. 5.25 REDUCTION OF MOMENT OF INERTIA ABOUT THE STRONG AXIS OF A WIDE-FLANGE SHAPE

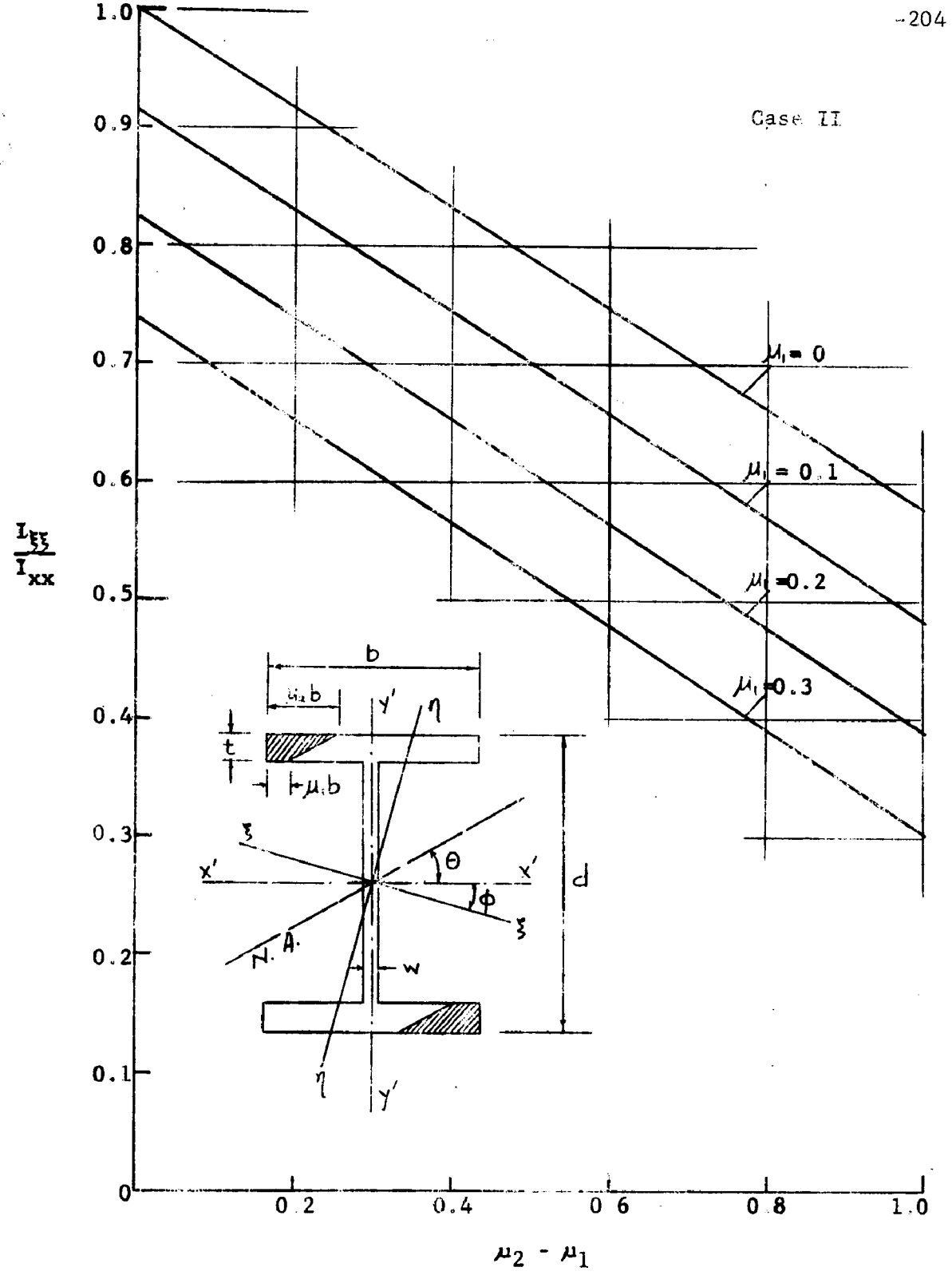

Fig. 5.26 REDUCTION OF MOMENT OF INERTIA ABOUT THE STRONG AXIS OF A WIDE-FLANGE SHAPE

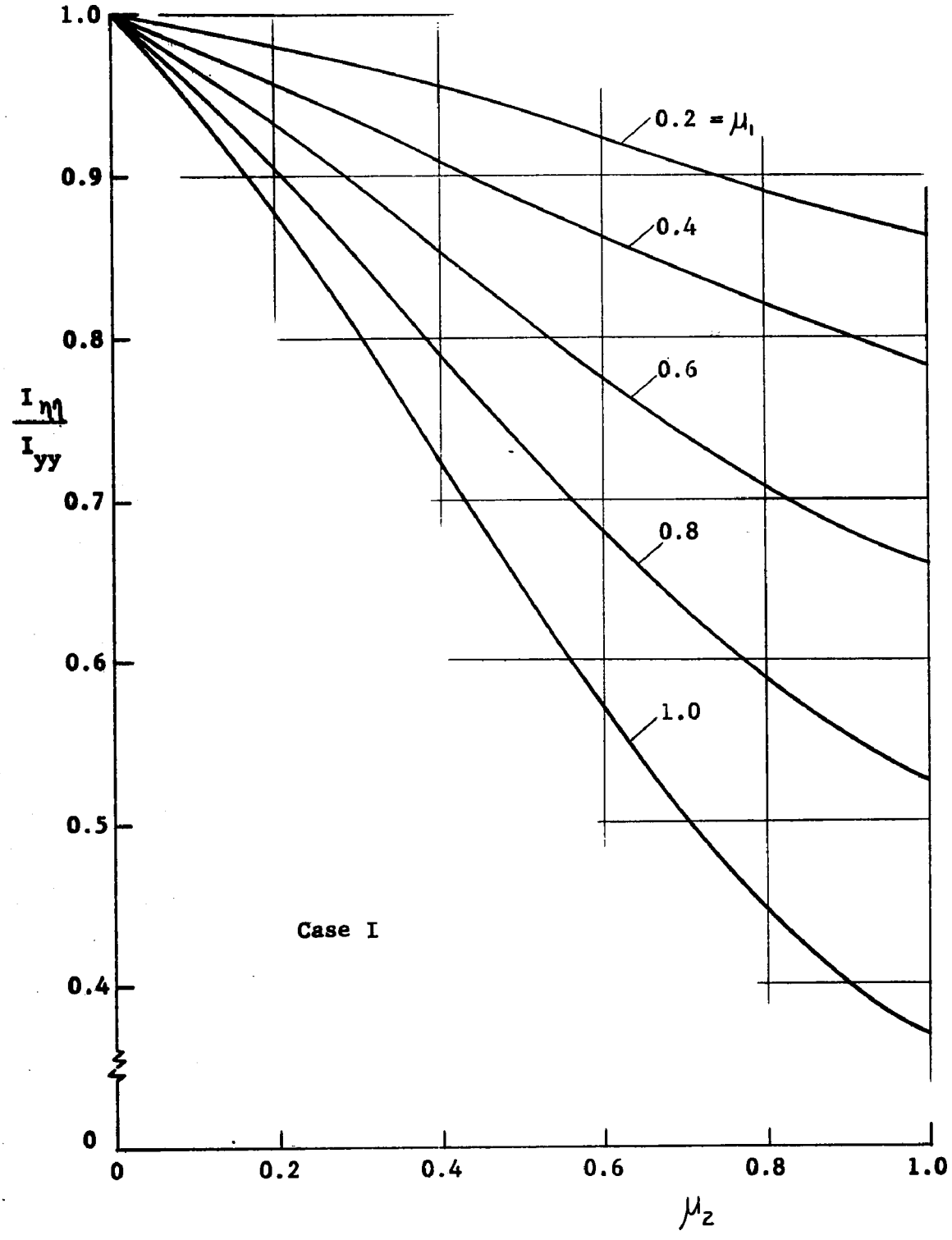

Fig. 5.27 REDUCTION OF MOMENT OF INERTIA ABOUT THE WEAK AXIS OF A WIDE-FLANGE SHAPE

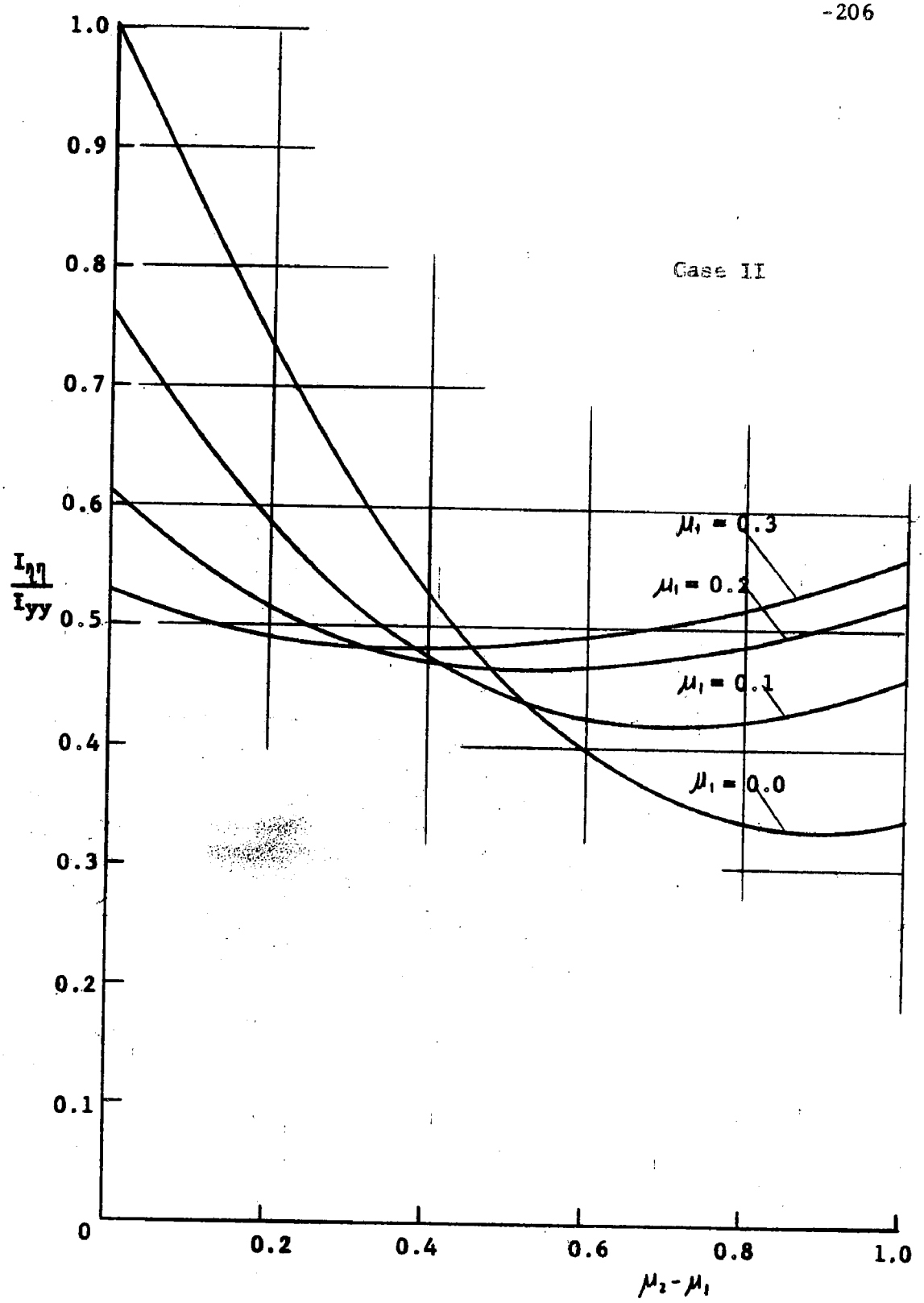

Fig. 5.28 REDUCTION OF MOMENT OF INERTIA ABOUT THE WEAK AXIS OF A WIDE-FLANGE SHAPE

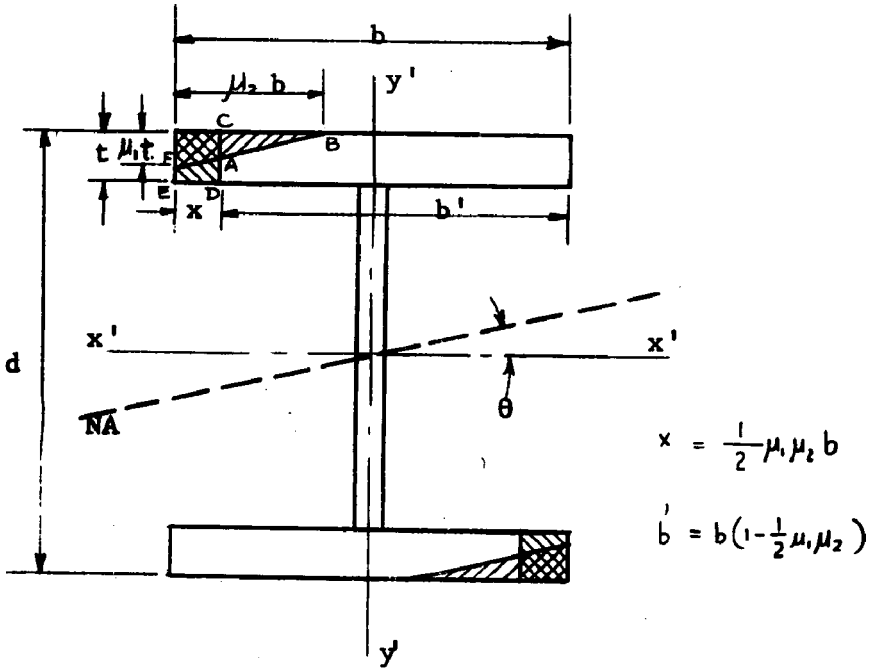

Case I

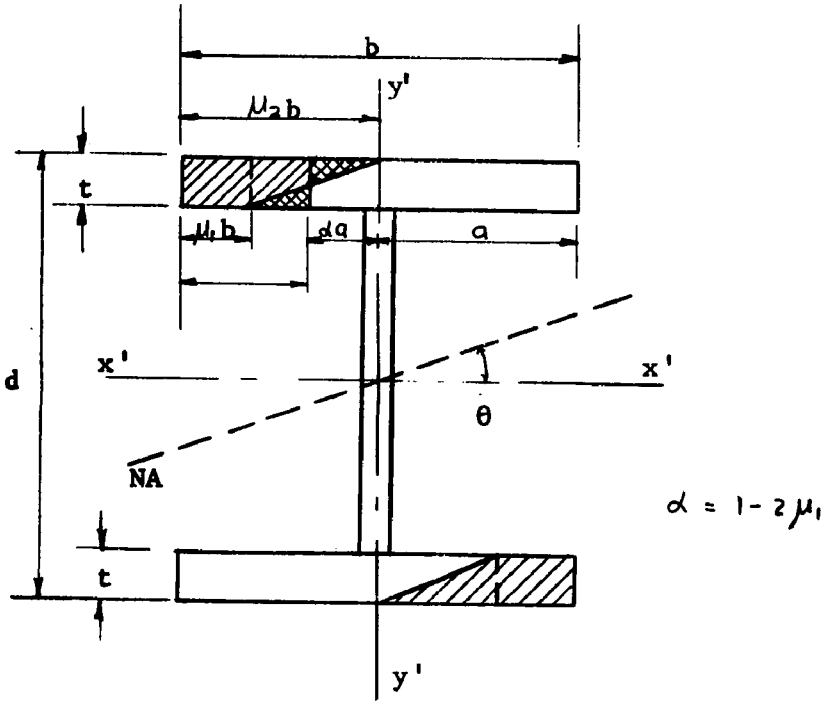

Case II

Fig. 5.29 APPROXIMATIONS OF ST. VENANT'S TORSIONAL CONSTANT FOR PARTIALLY YIELDED WF SECTION

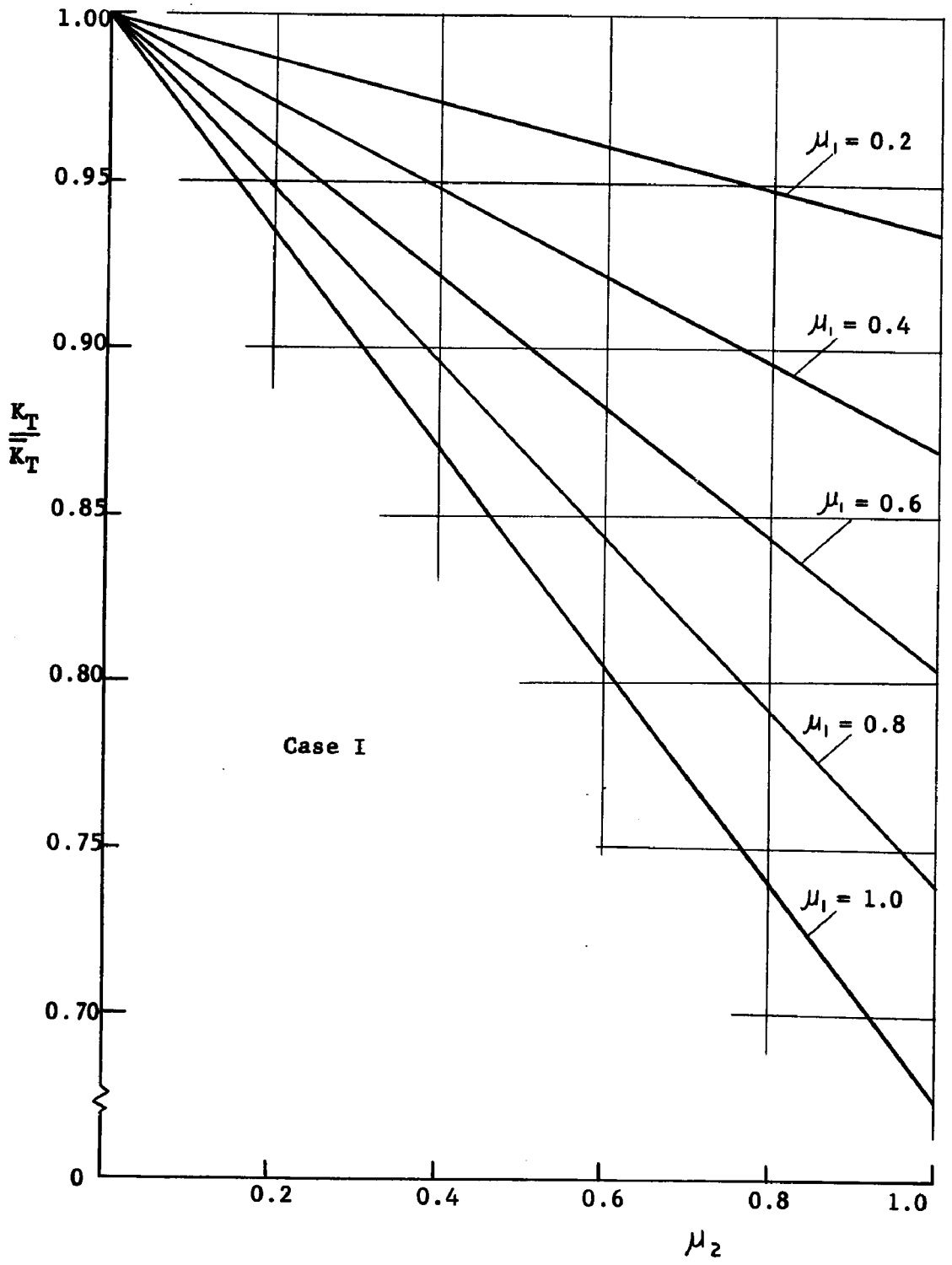

Fig. 5.30 REDUCTION OF ST. VENANT'S TORSIONAL CONSTANT OF A PARTIALLY YIELDED WF SECTION

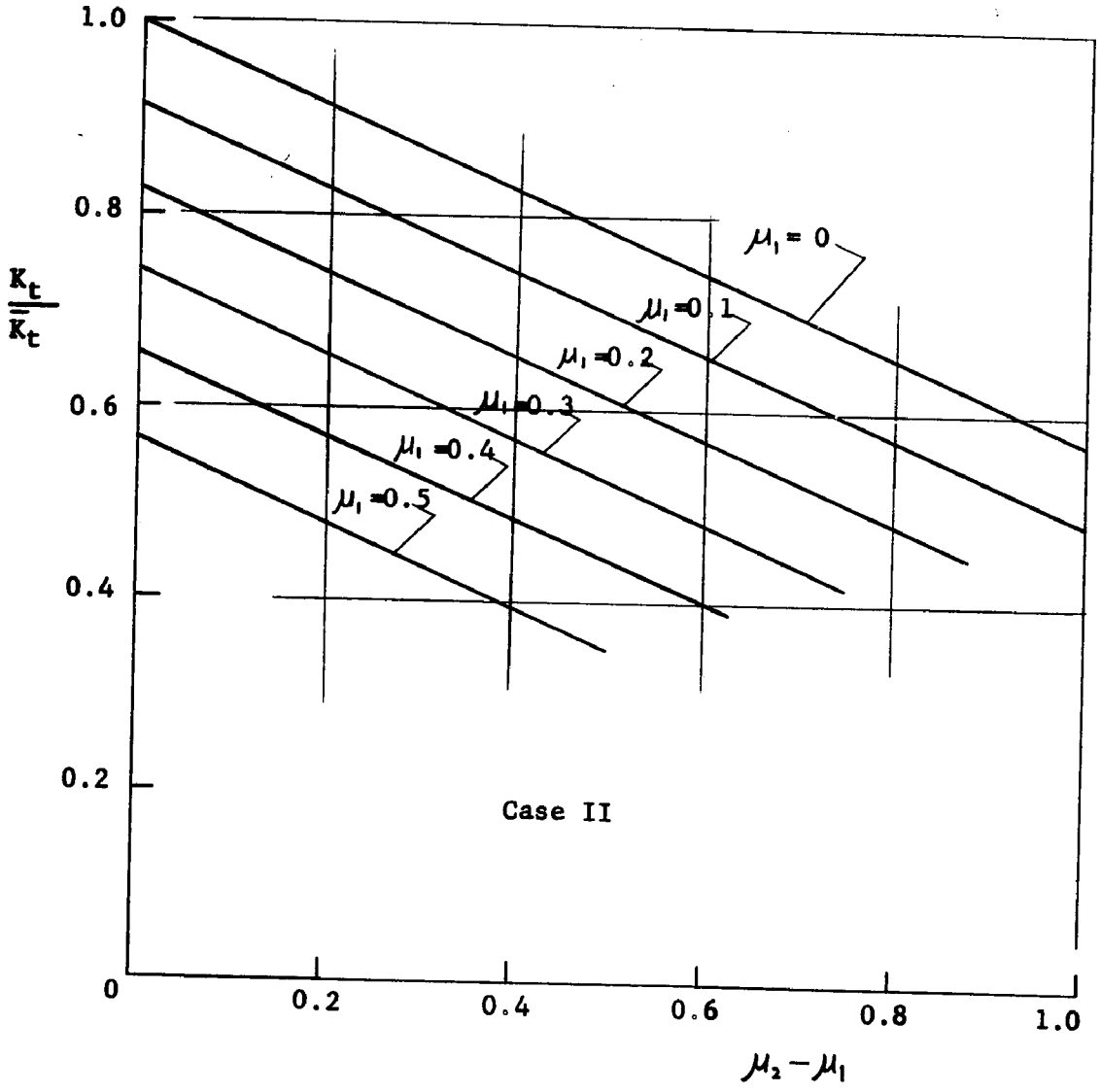

Fig. 5.31 REDUCTION OF ST. VENANT'S TORSIONAL CONSTANT OF A PARTIALLY YIELDED WF SECTION

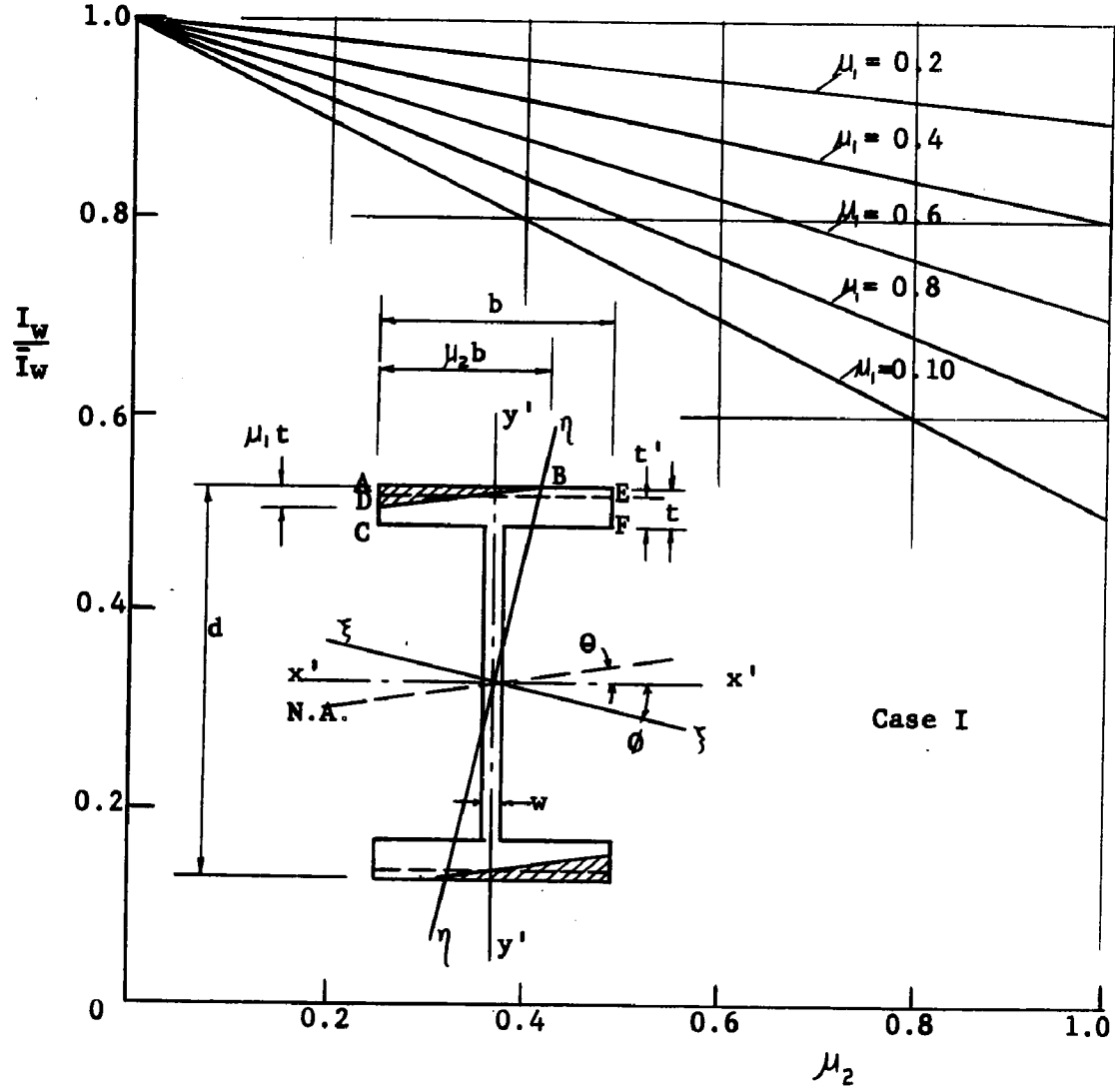

Fig. 5.32 REDUCTION OF THE WARPING CONSTANT OF A PARTIALLY YIELDED WF SECTION

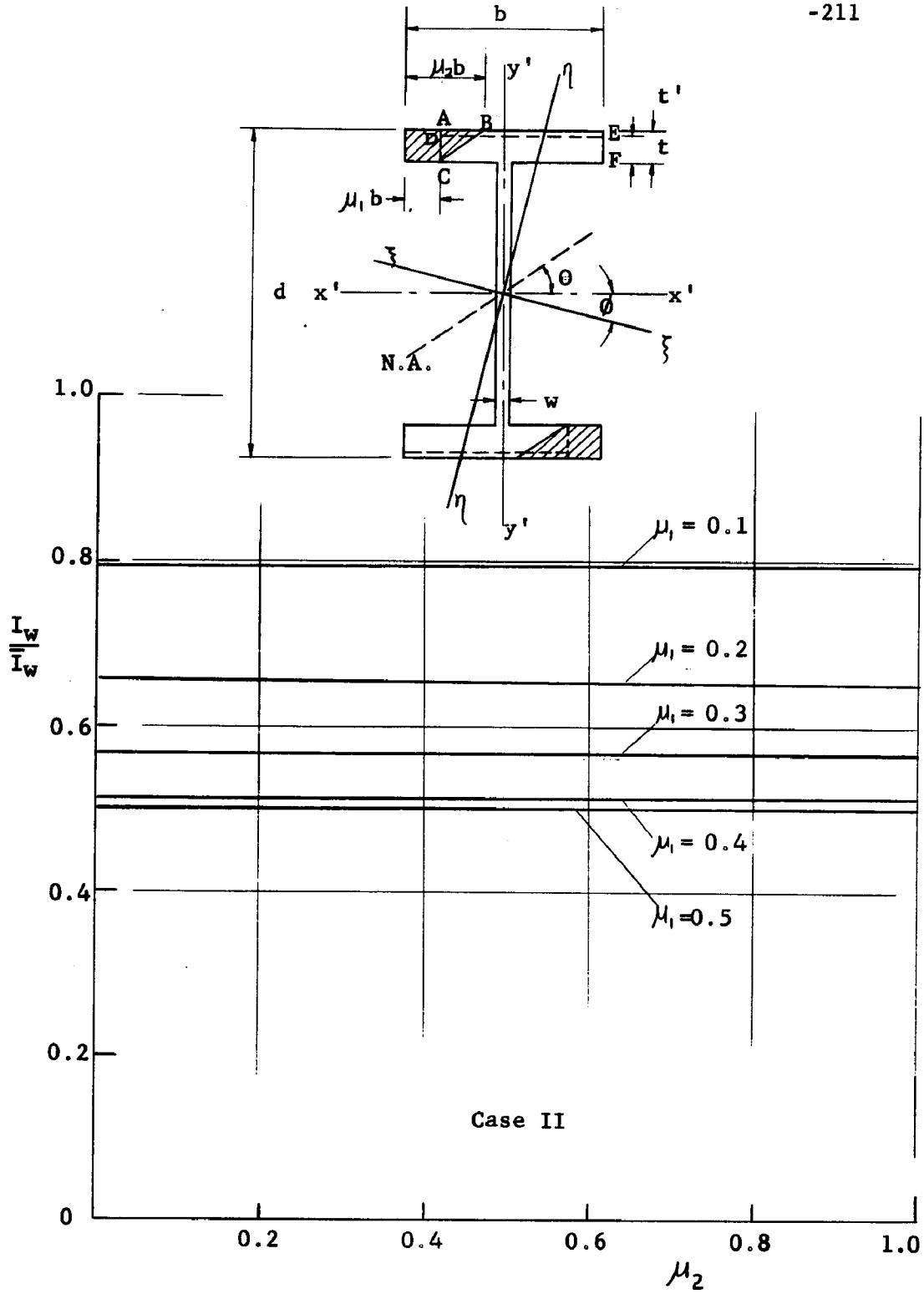

Fig. 5.33 REDUCTION OF THE WARPING CONSTANT OF A PARTIALLY YIELDED WF SECTION

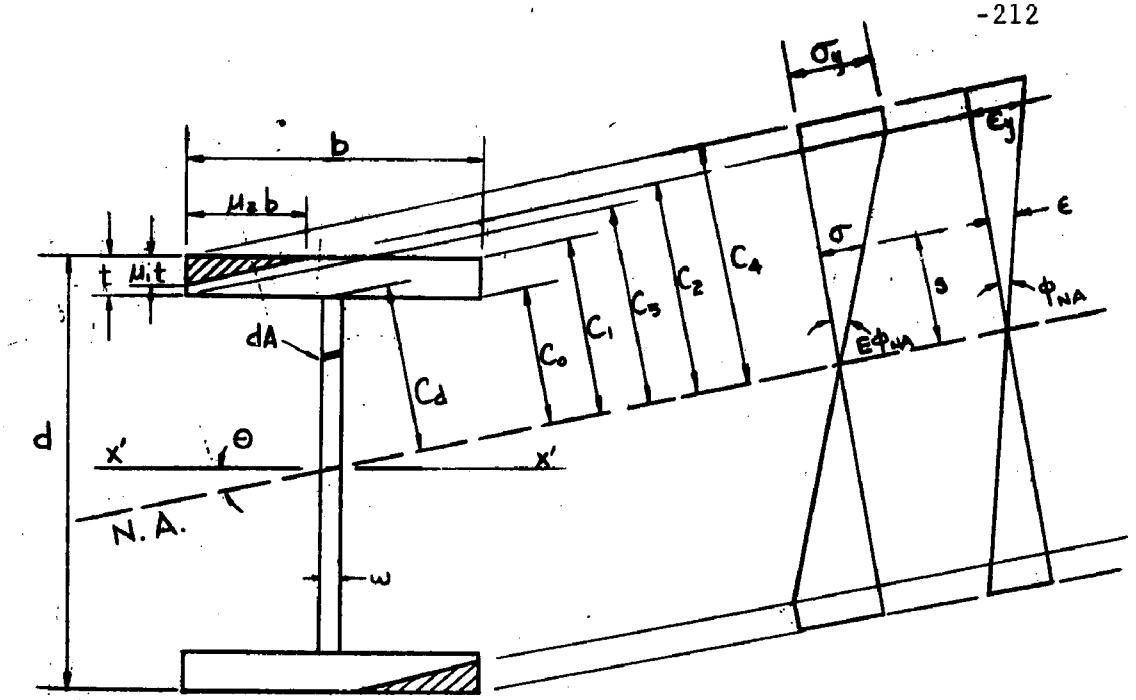

Case I

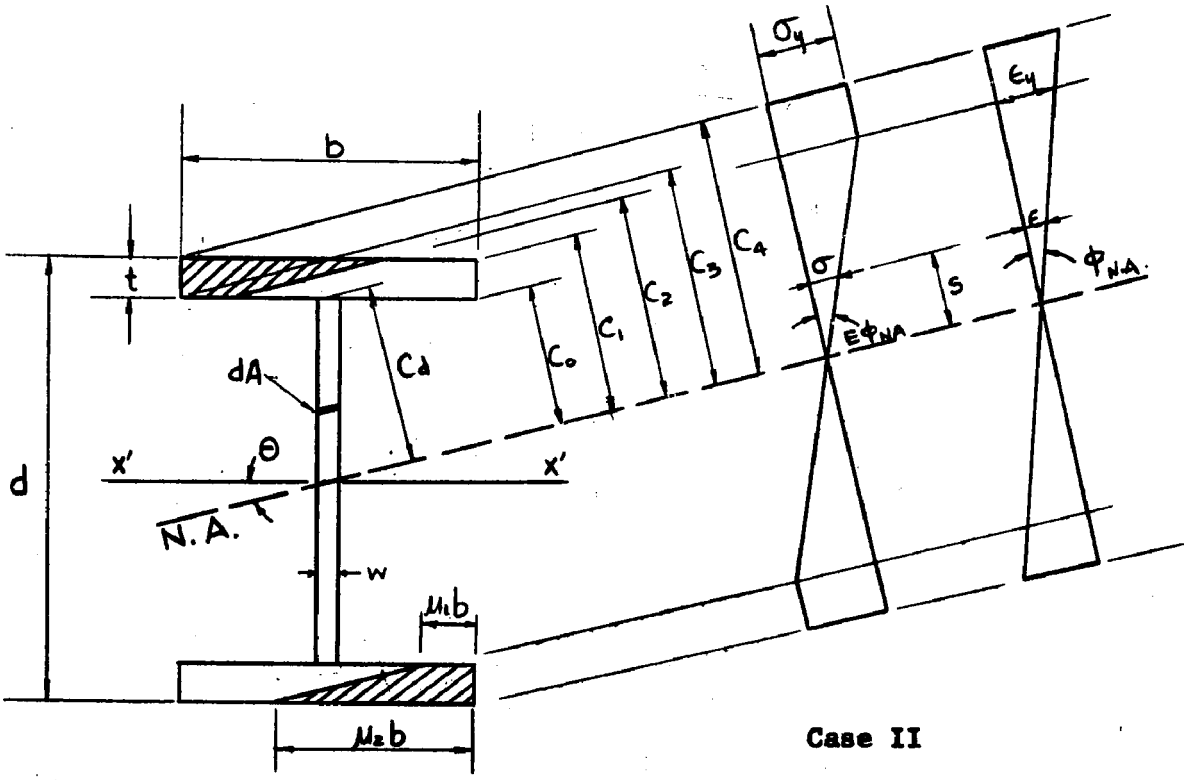

Case II

Fig. 5.34 STRESS AND STRAIN VARIATIONS ABOUT THE NEUTRAL AXIS OF A PARTIALLY YIELDED WF SECTION

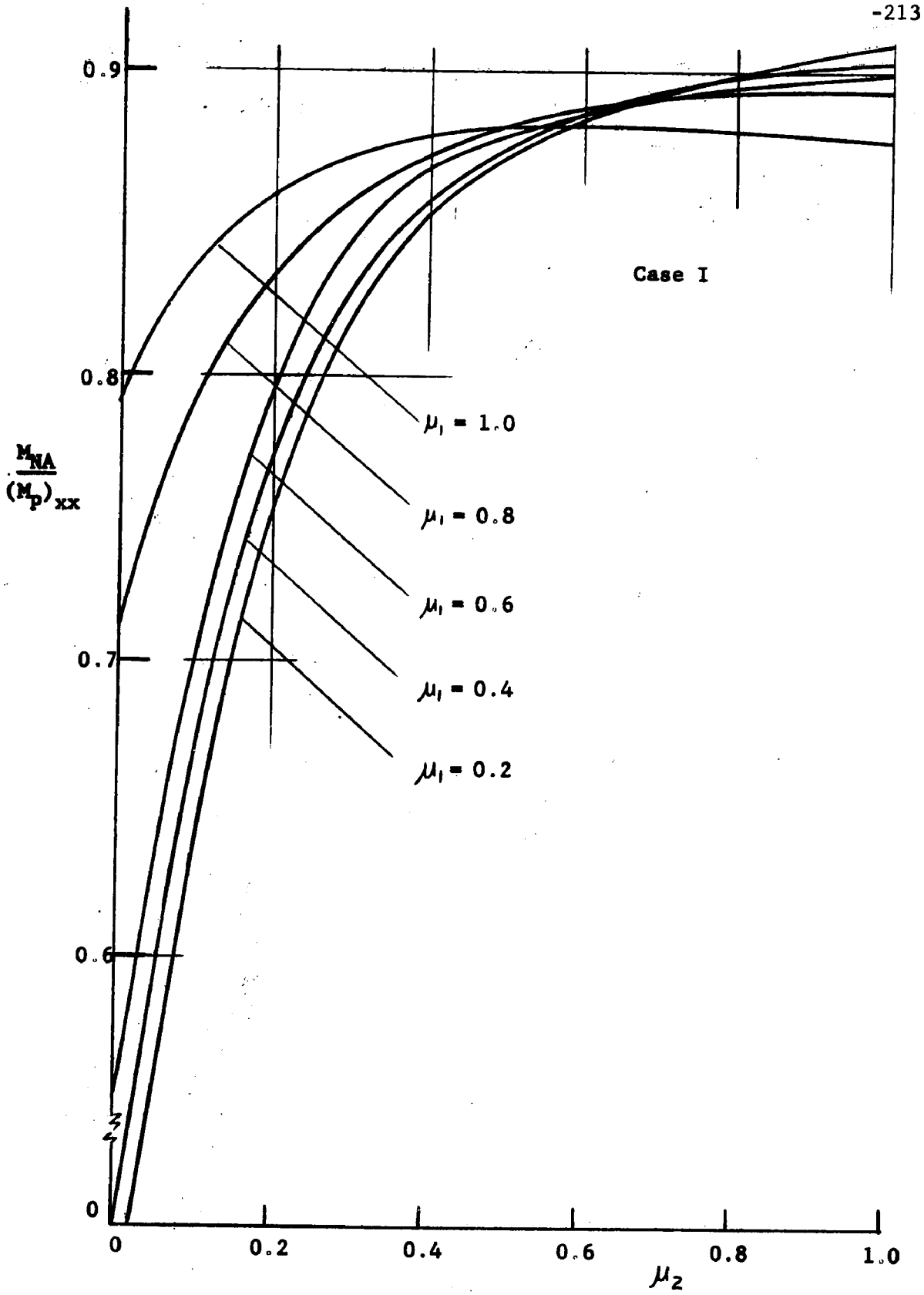

Fig. 5.35 VARIATIONS OF THE MOMENT ABOUT THE NEUTRAL AXIS OF A PARTIALLY YIELDED WF SECTION

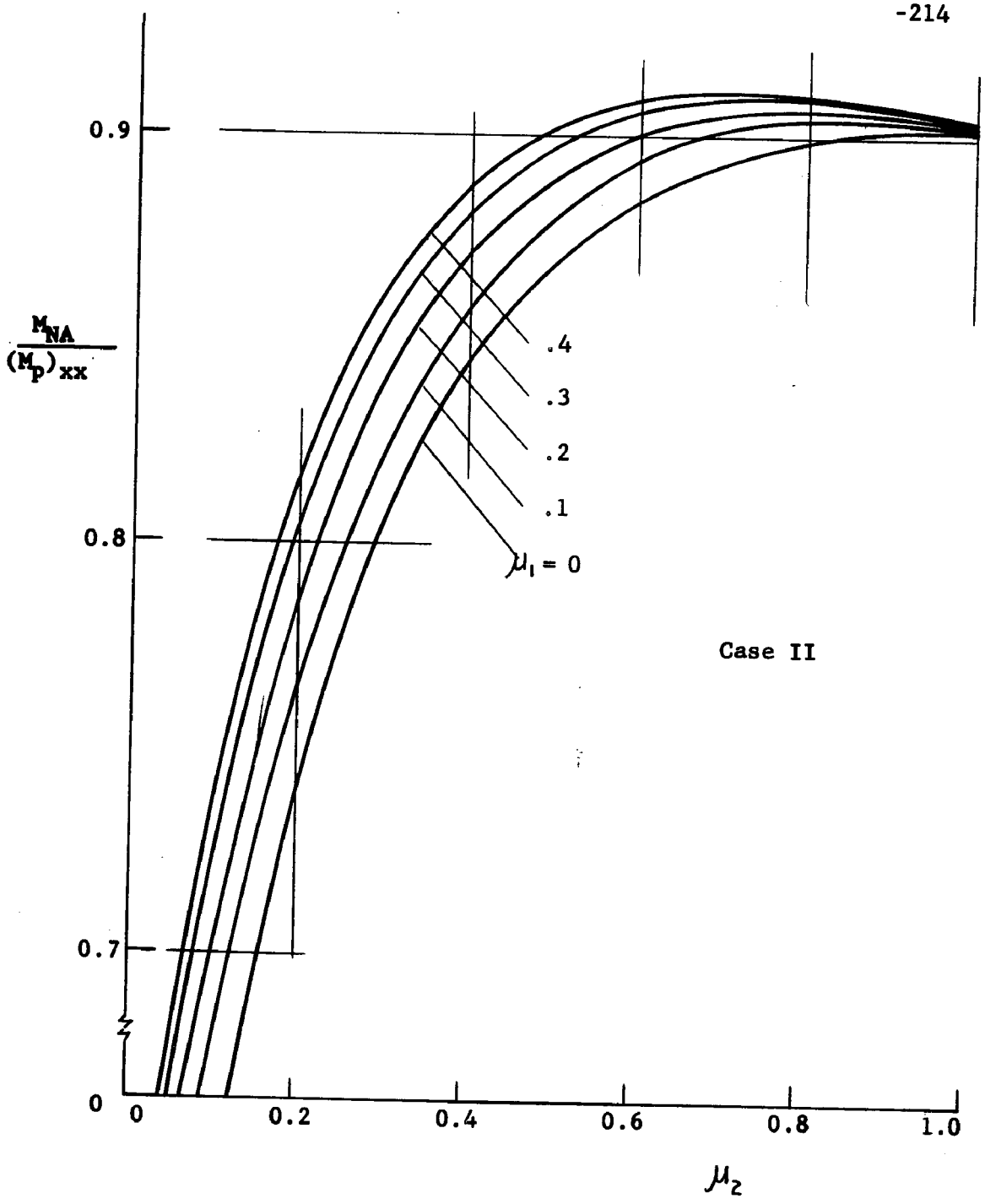

Fig. 5.36 VARIATIONS OF THE MOMENT ABOUT THE NEUTRAL AXIS OF A PARTIALLY YIELDED WF SECTION

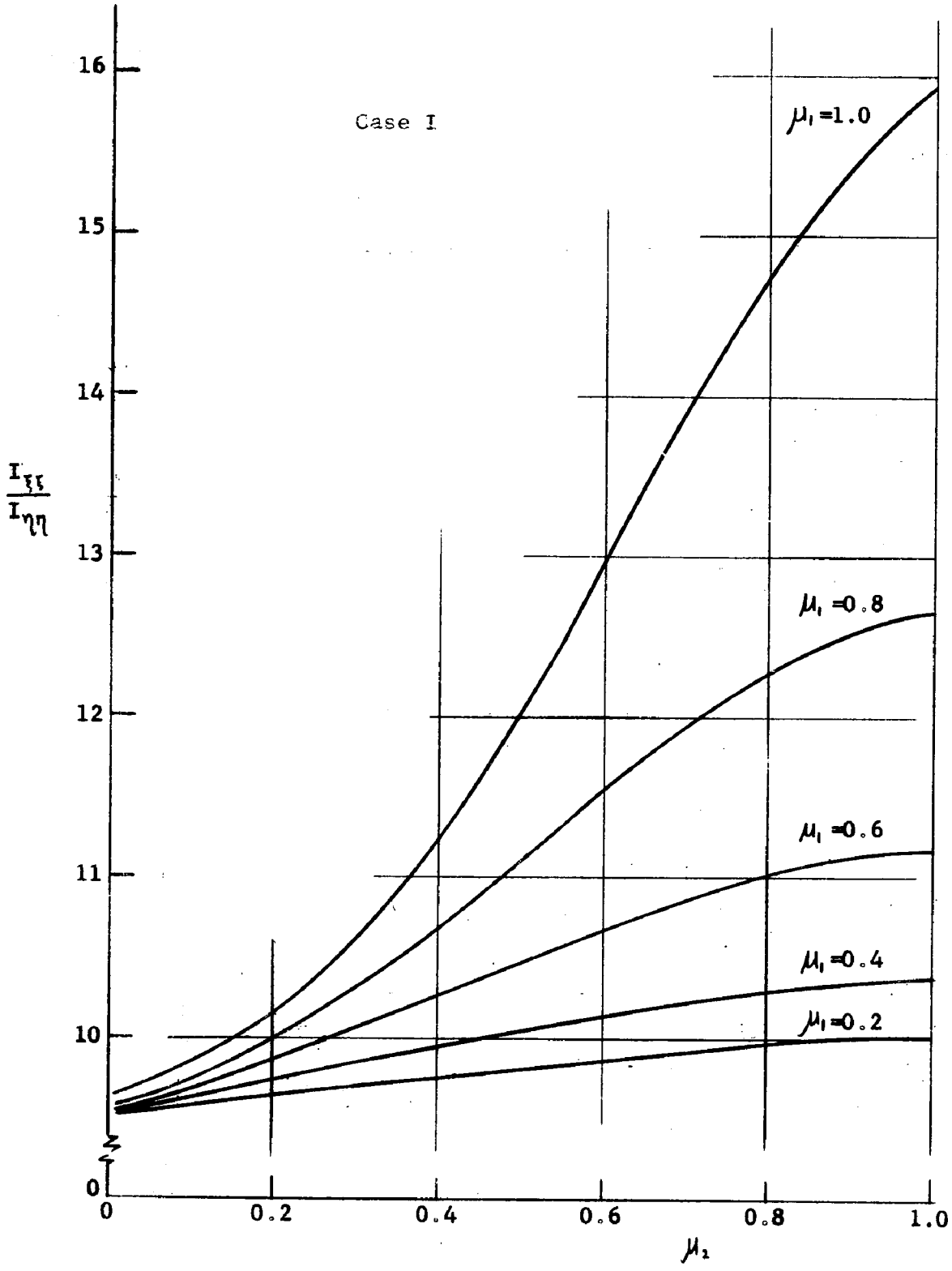

Fig. 5.37 RELATIONSHIPS BETWEEN THE RATIO OF THE PRINCIPAL MOMENT ON INERTIA AND THE YIELDING PARAMETERS

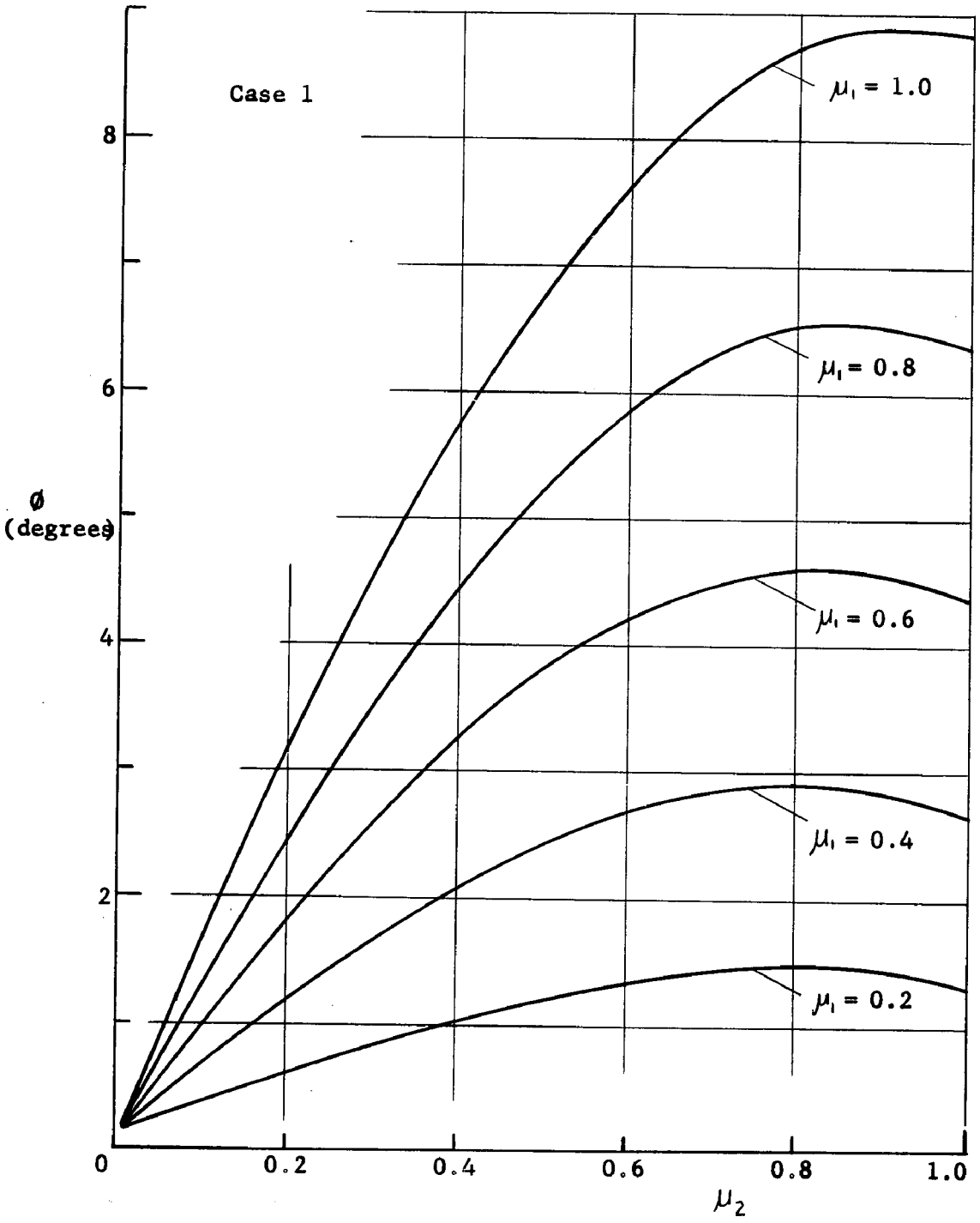

Fig. 5.38 INCLINATION OF THE PRINCIPAL AXES OF A PARTIALLY YIELDED WF SECTION

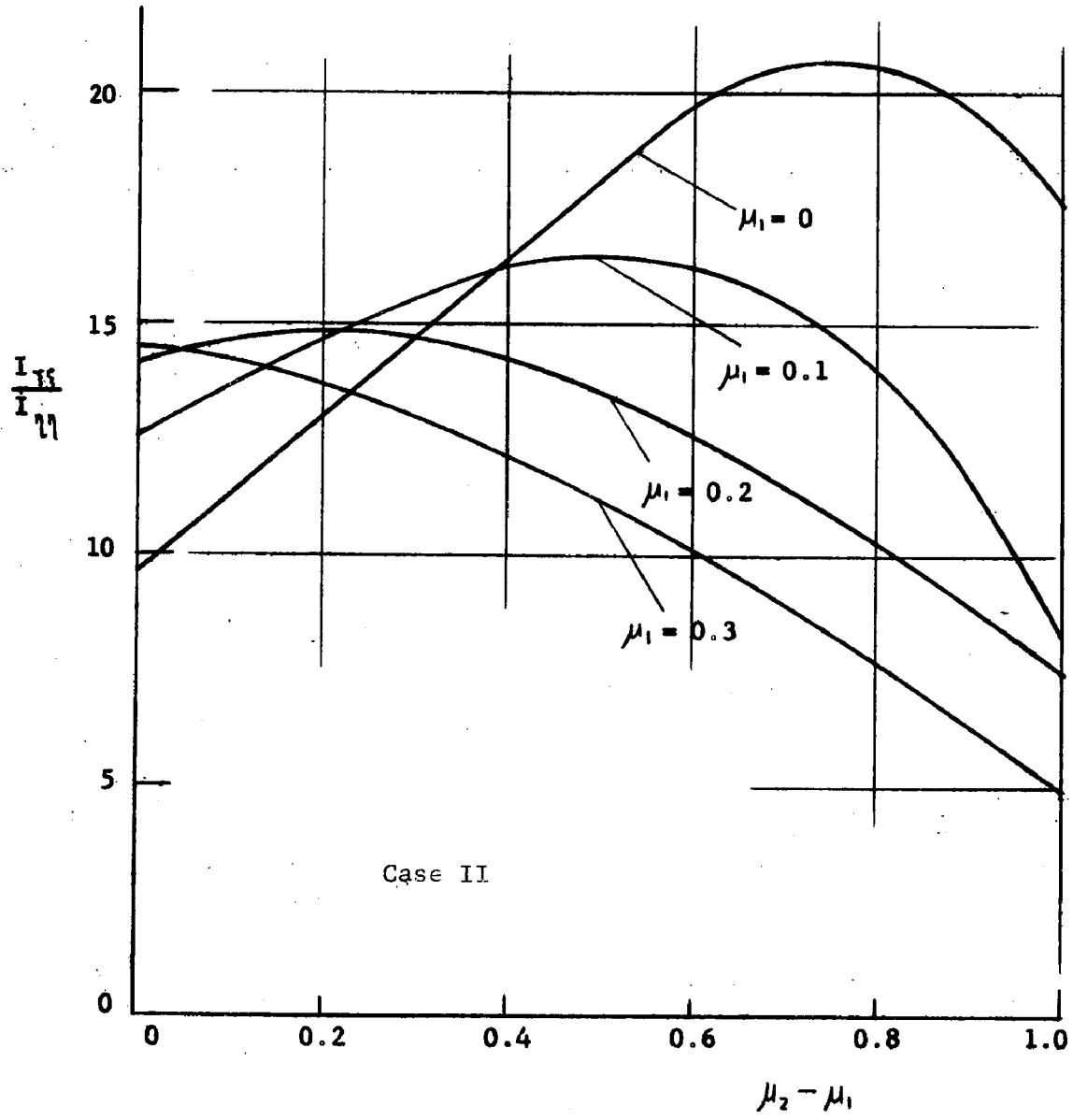

Fig. 5.39 RELATIONSHIPS BETWEEN THE RATIO OF THE PRINCIPAL MOMENT OF INERTIA AND THE YIELDING PARAMETERS

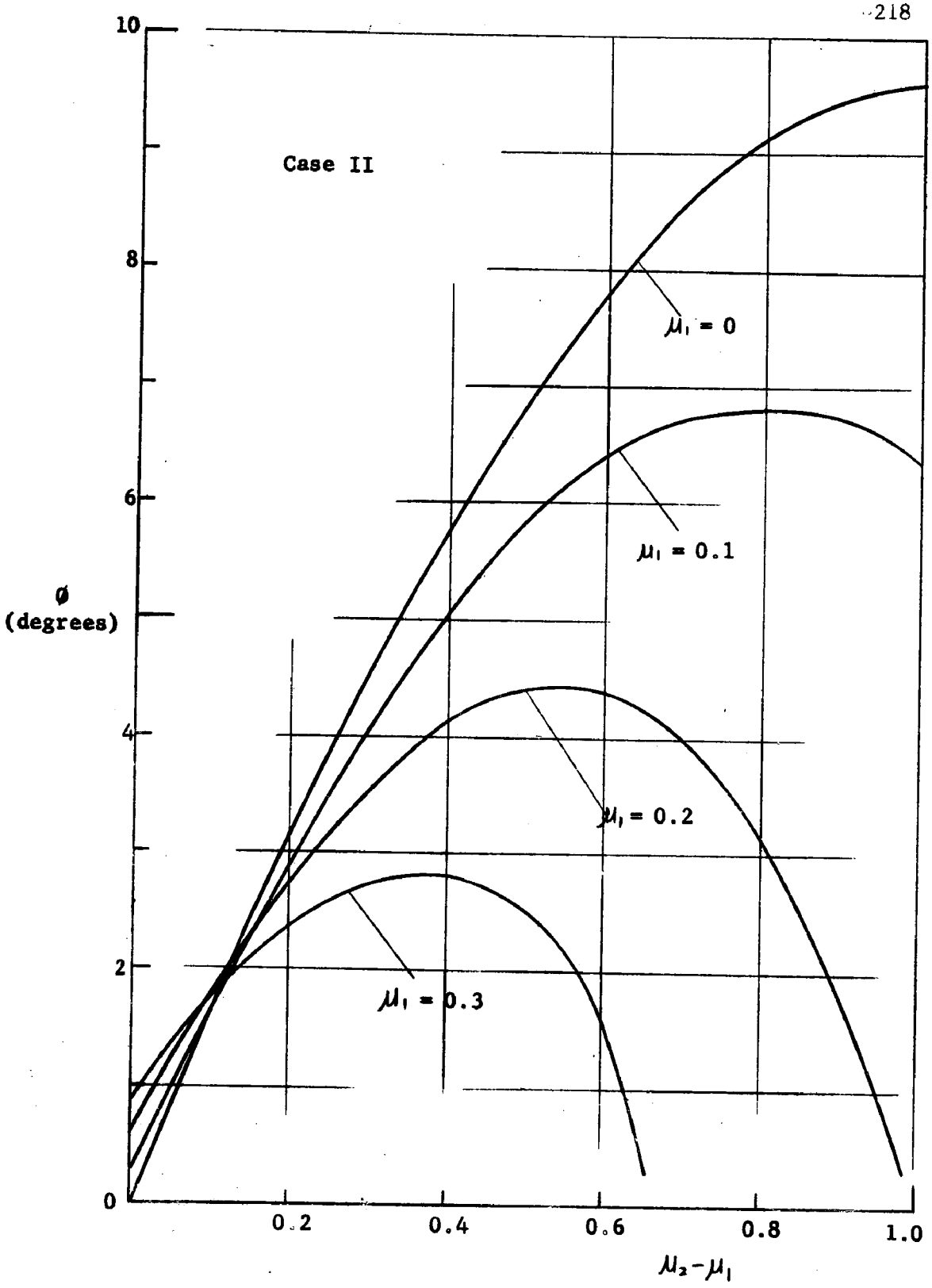

Fig. 5.40 INCLINATION OF THE PRINCIPAL AXES OF A PARTIALLY YIELDED WF SECTION

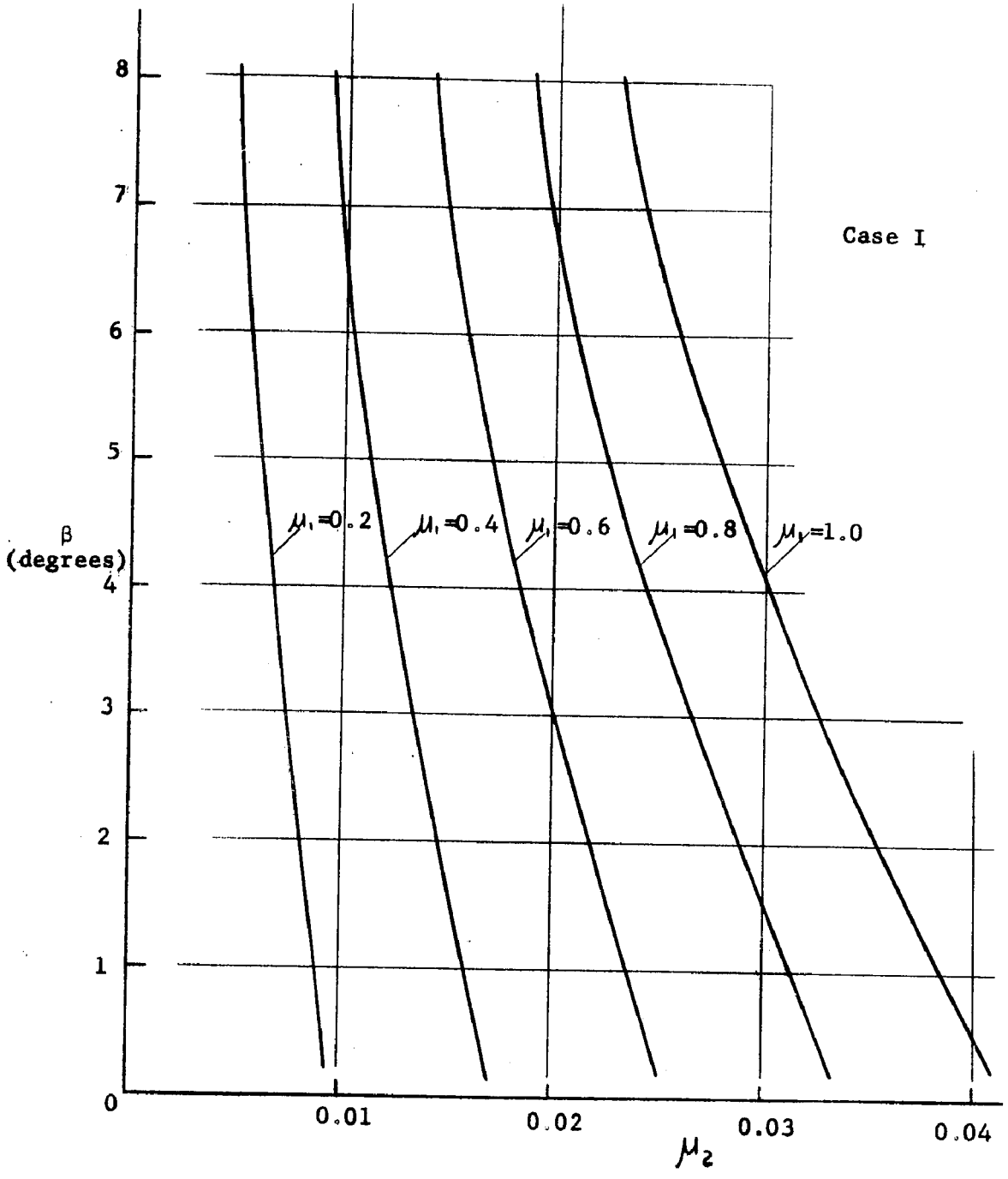

Fig. 5.41 THE RELATIONSHIPS BETWEEN THE TWISTING ANGLE AND THE YIELDING PARAMETERS

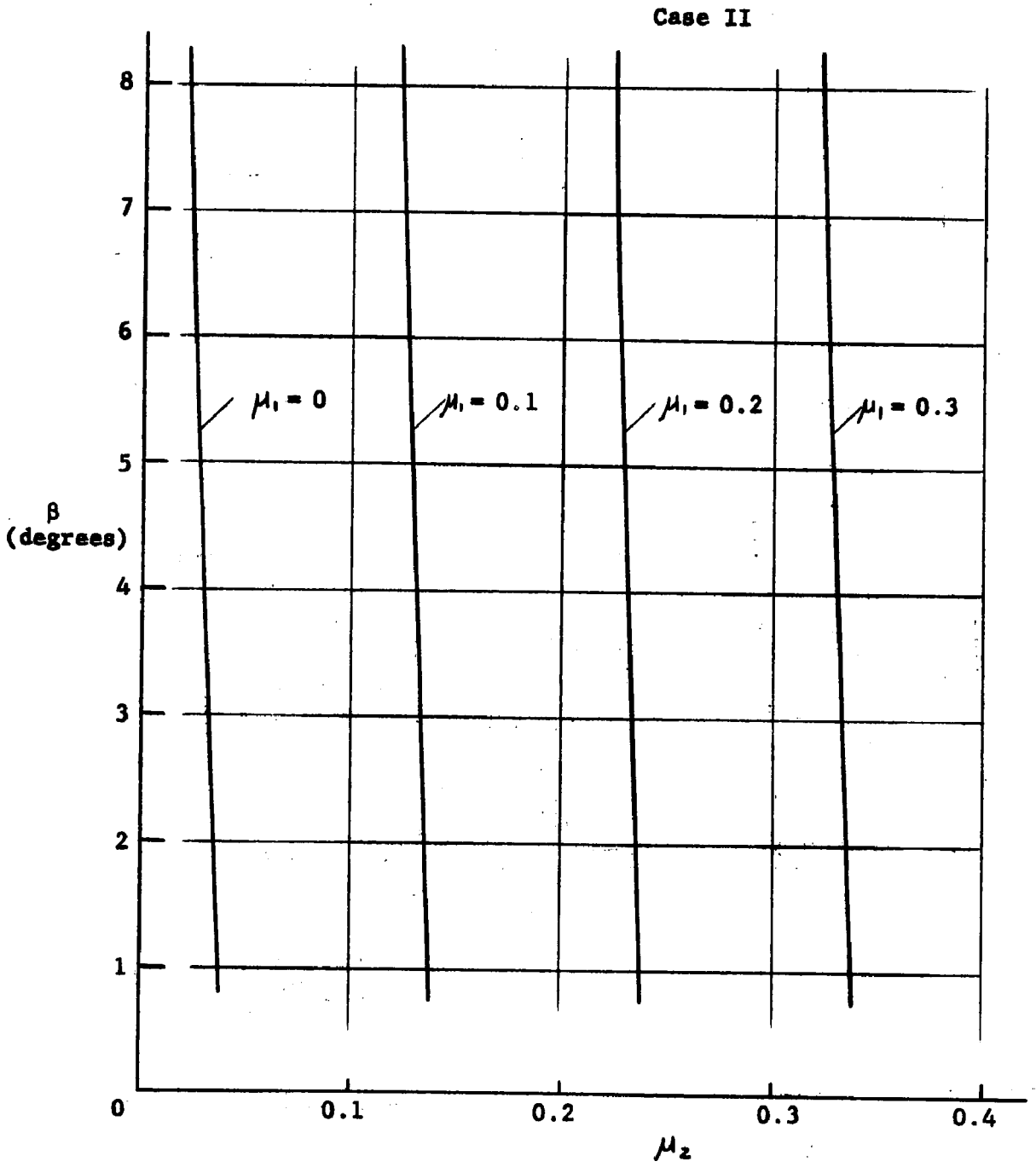

Fig. 5.42 THE RELATIONSHIPS BETWEEN THE TWISTING ANGLE AND THE YIELDING PARAMETERS

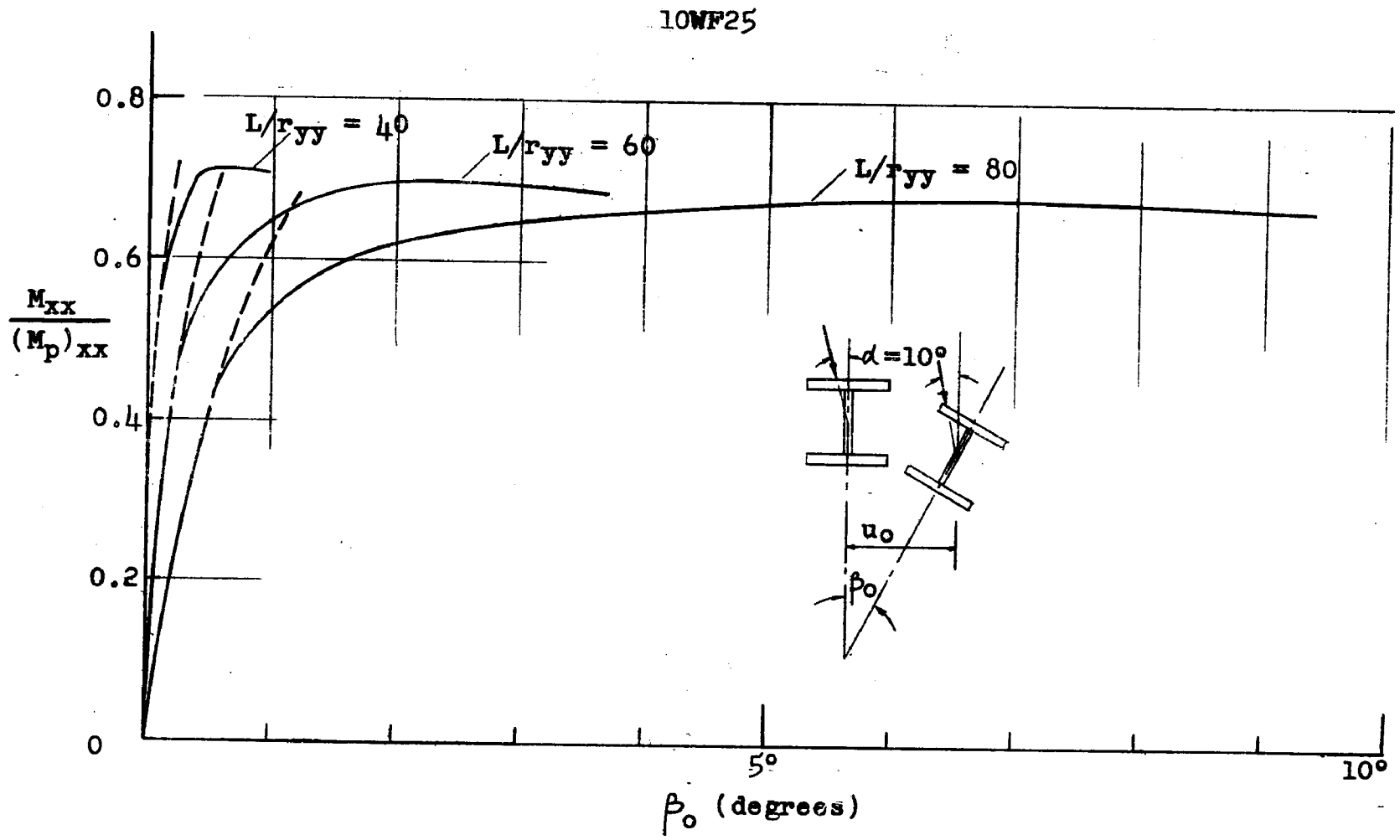

Fig. 5.43 - THE MOMENT VS. TWISTING RELATIONSHIPS OF 10WF25 BEAMS

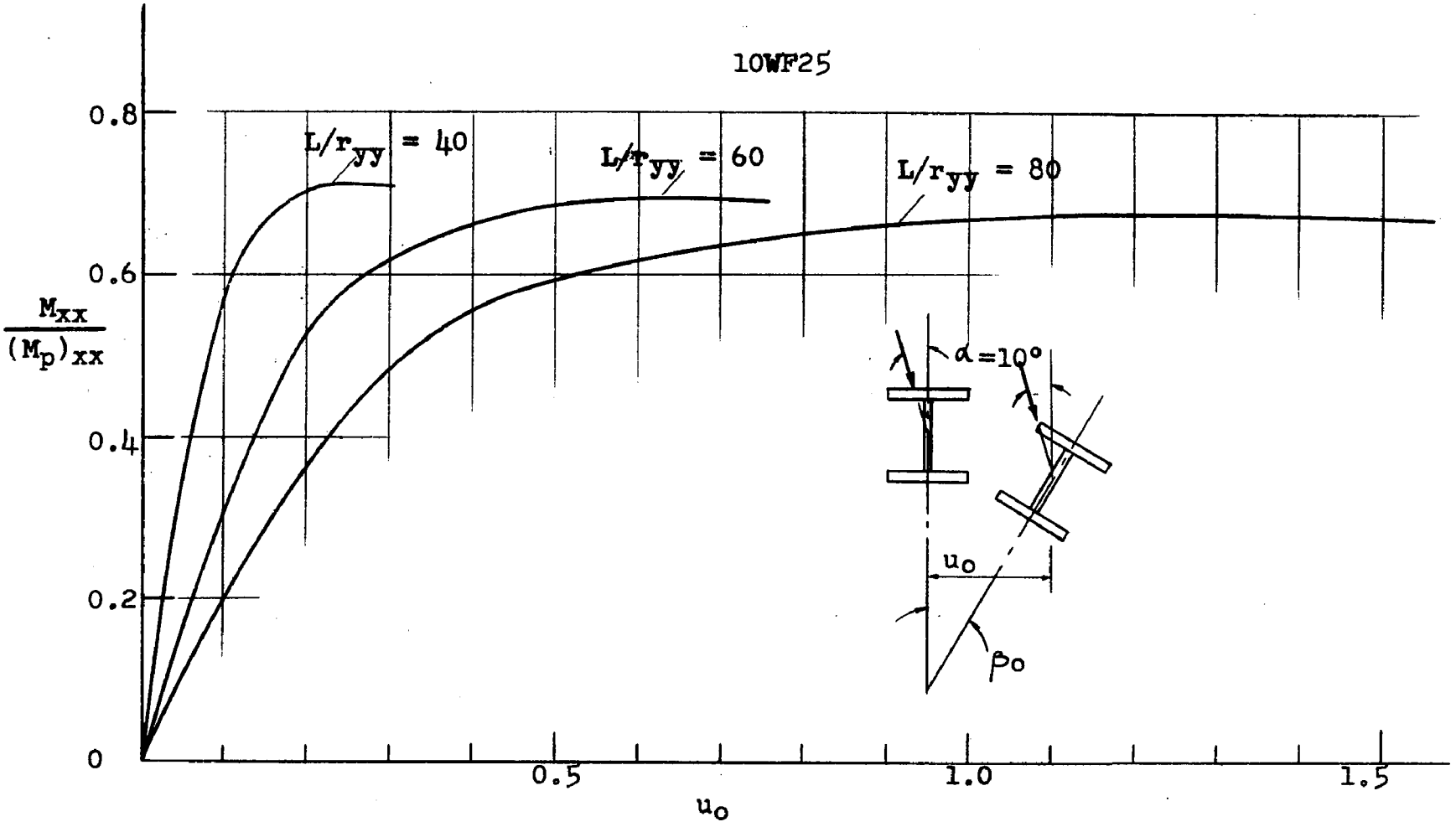

Fig. 5.44 - THE MOMENT VS. LATERAL DEFLECTION RELATIONSHIPS OF 10WF25 BEAMS

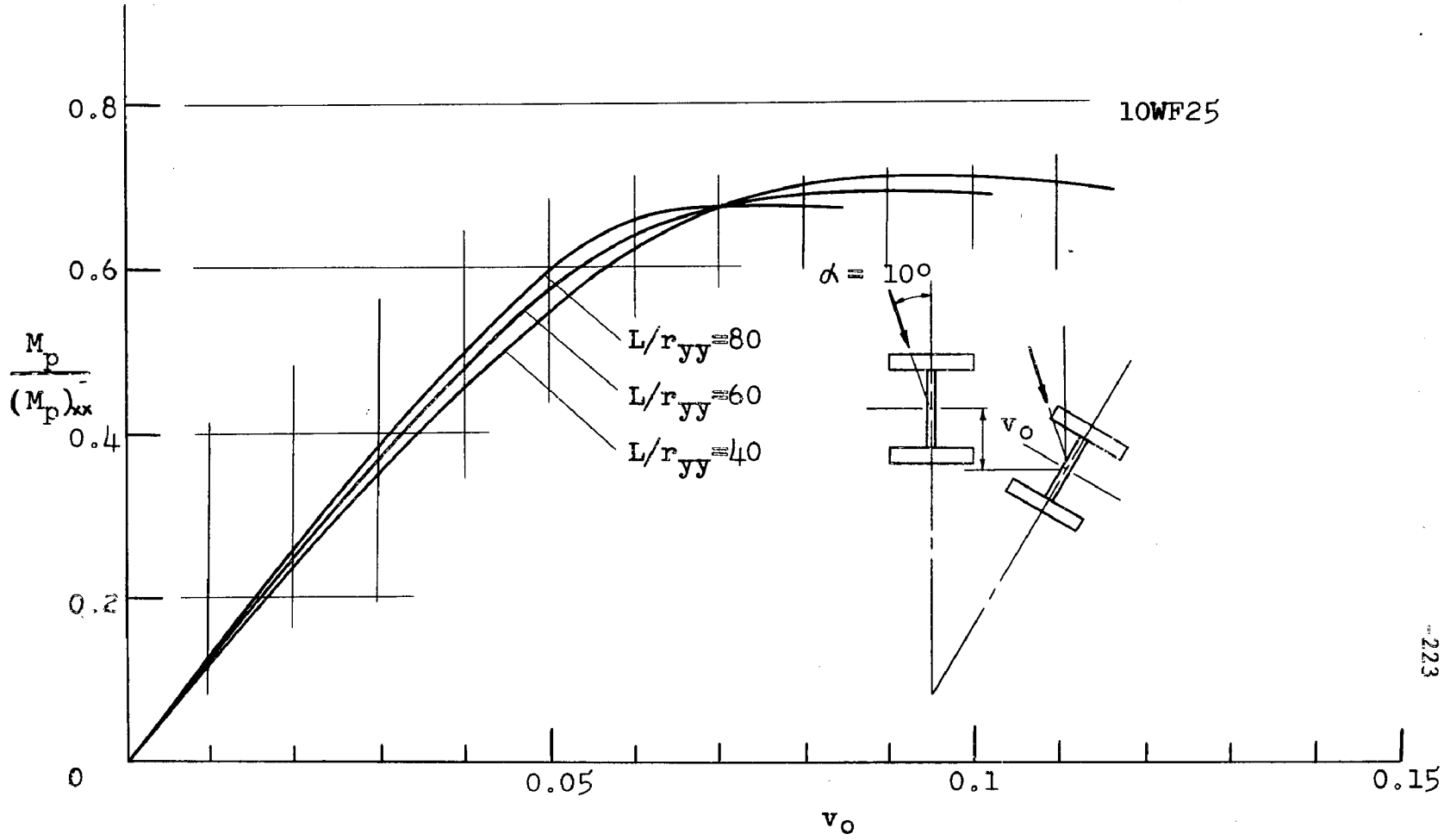

Fig. 5.45 - THE MOMENT VS. VERTICAL DEFLECTION RELATIONSHIPS OF 10WF25 BEAMS

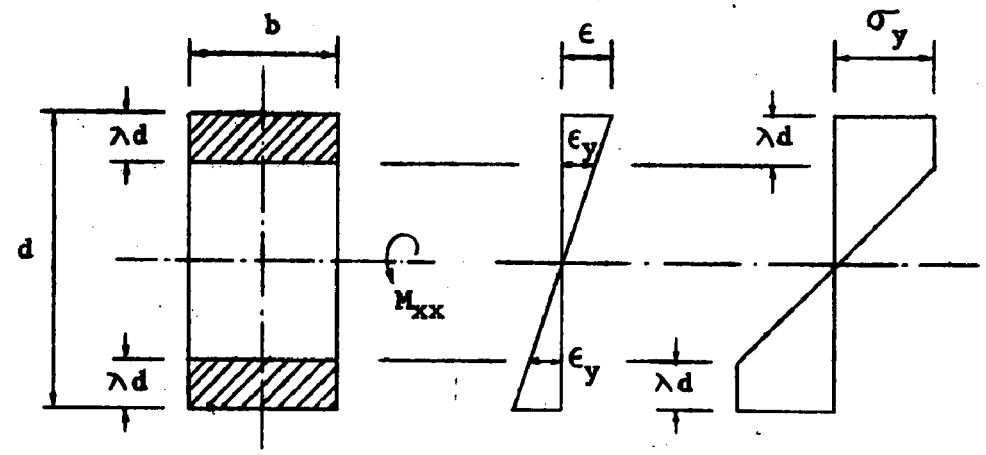

Fig. 5.46 STRESS DISTRIBUTION OF A PARTIALLY YIELDED CROSS SECTION AT THE INCEPTION OF LATERAL BUCKLING

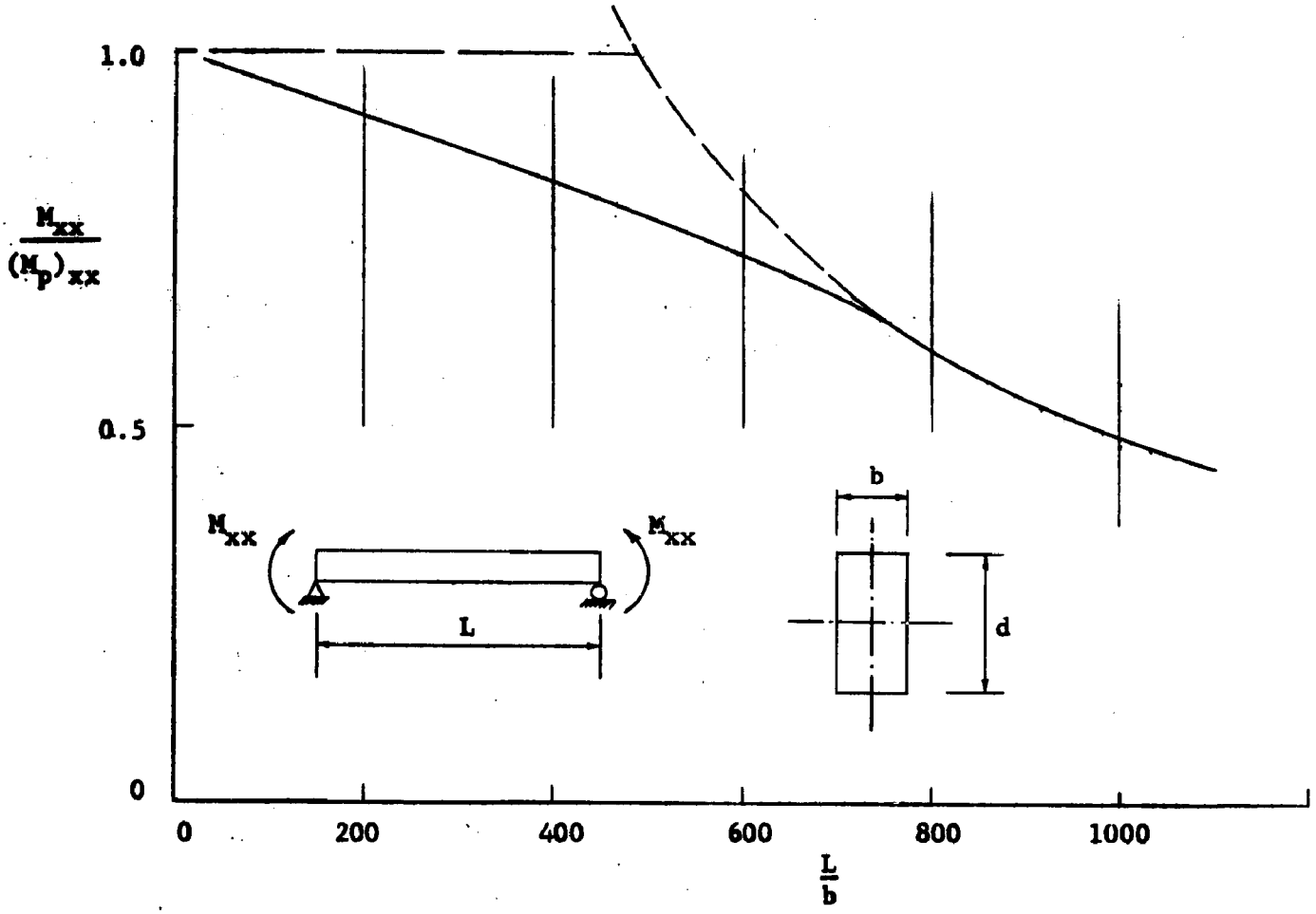

Fig. 5.47 LATERAL BUCKLING CURVE OF RECTANGULAR BEAMS WITH THE ASPECT RATIO EQUAL TO 2

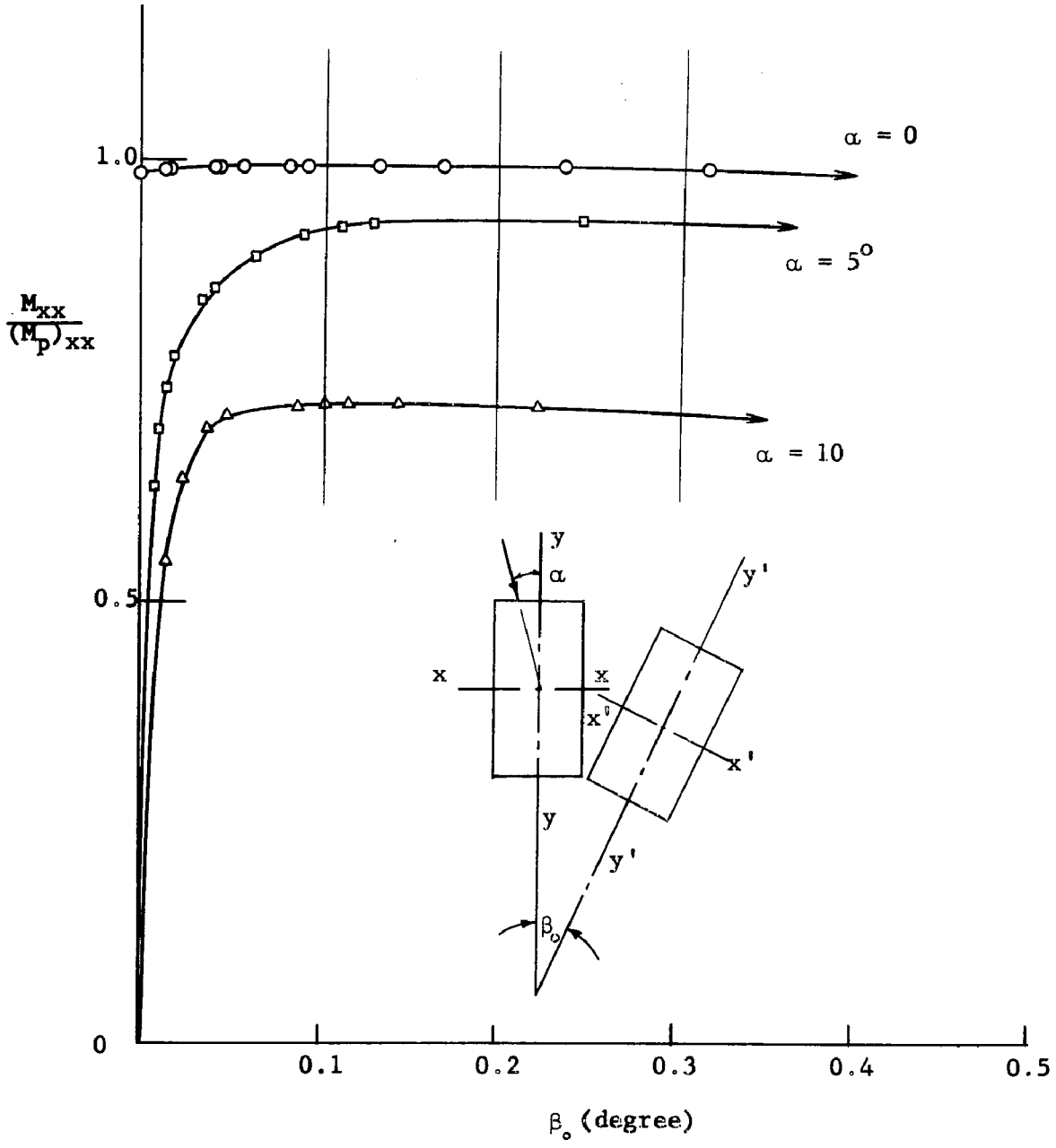

Fig. 5.48 POST-BUCKLING BEHAVIOR OF BEAMS

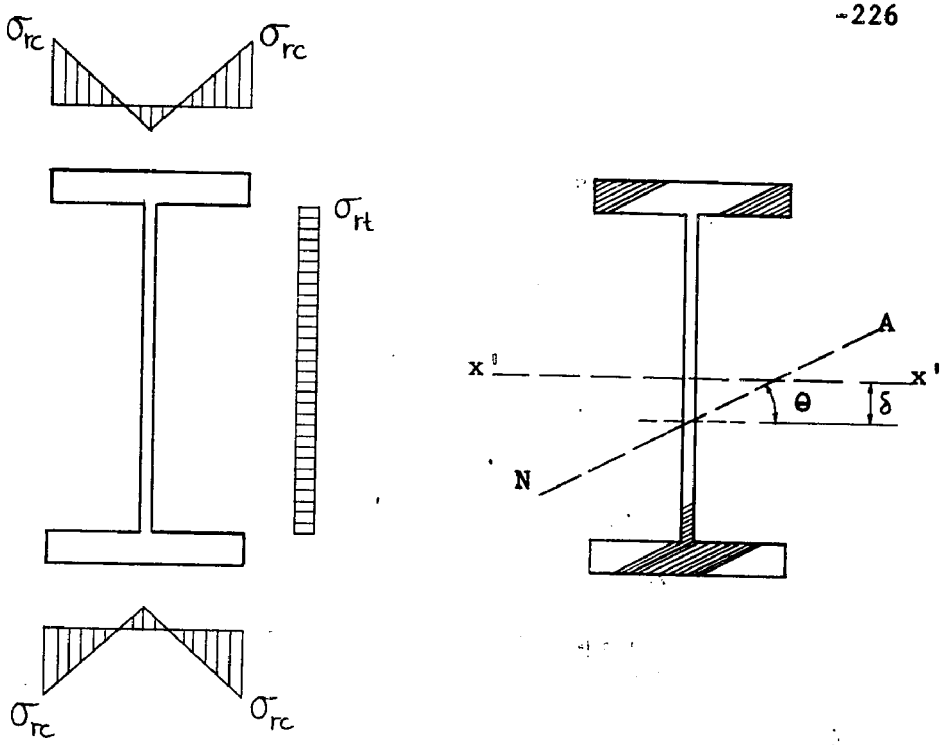

Fig. 5.49 THE YIELDED CONFIGURATIONS OF A WIDE-FLANGE SECTION CONSIDERING RESIDUAL STRESSES

10. REFERENCES

1. Bleich F.
   BUCKLING STRENGTH OF METAL STRUCTURES, McGraw-Hill Book Co., Inc., 1952.

2. Lee, G. C.
   A SURVEY OF LITERATURE ON THE LATERAL INSTABILITY OF BEAMS, Welding Research Council Bulletin 63, August 1960.

3. Galambos, T. V.
   INELASTIC LATERAL-TORSIONAL BUCKLING OF ECCENTRICALLY LOADED WF COLUMNS, Ph.D. Dissertation, Lehigh University, 1959.

4. Horne, M. R.
   CRITICAL LOADING CONDITIONS IN ENGINEERING STRUCTURES, Ph.D. Dissertation, Cambridge University, England, 1950.

5. White, M. W.
   THE LATERAL-TORSIONAL BUCKLING OF YIELDED STRUCTURAL STEEL MEMBERS, Ph.D. Dissertation, Lehigh University, 1956.

6. Timoshenko, S.
   ELASTIC STABILITY, Chapter V, McGraw-Hill Book Co., Inc., 1936.

7. Goodier, J. N.
   FLEXURAL TORSIONAL BUCKLING OF BARS OF OPEN SECTION, UNDER BENDING, ECCENTRIC THRUST OR TORSIONAL LOADS, Cornell University Engineering Experimental Station, Bulletin No. 28, (January 1942).

8. Timoshenko, S.
   THEORY OF BENDING, TORSION AND BUCKLING OF THIN-WALLED MEMBERS OF OPEN CROSS SECTION, Journal, Franklin Institute, 239, pp. 201, 249, 343, (March 1945).

9. Collatz, L.
   EIGENVERTAUFGABEN MIT TECHNISCHER ANWENDUNG, Akademische Verlagsgesellshaft M.G.H., Leipzig, p. 126 (1949).

10. Winter, G.
    STRENGTH OF SLENDER BEAMS, Transactions of the American Society of Civil Engineers, 109, p. 1321 (1944).

11. Pettersson, O.
COMBINED BENDING AND TORSION OF I-BEAM OF MONOSYMMETRICAL CROSS SECTION, Bulletin No. 10, Division of Building Statics and Structural Engineering, Royal Institute of Technology, Stockholm, Sweden, 1952.

12. Green, G. G.; Winter, G.; Cuykendall, T. R.
LIGHT GAGE STEEL COLUMNS IN WALL-BRACED PANELS, Cornell University Engineering Experimental Station Bulletin No. 35/2, 1947.

13. Zuk, W.
LATERAL BRACING FORCES ON BEAMS AND COLUMNS, Proceedings of the American Society of Civil Engineers, Journal of Engineering Mechanics Division, EM3, Paper 1032, (July 1956).

14. Winter, G.
LATERAL BRACING OF COLUMNS AND BEAMS, Proceedings of the American Society of Civil Engineers, 84 (ST2) Journal of the Structures Division, Paper No. 1561, (March 1958).

15. Beedle, L. S.
PLASTIC DESIGN OF STEEL FRAMES, John Wiley & Sons, New York, 1958.

16. WRC-ASCE
COMMENTARY ON PLASTIC DESIGN IN STEEL, Proceedings of the American Society of Civil Engineers

Progress Reports No. 1 and No. 2	85 (EM3) (July 1959)
Progress Reports No. 3 and No. 4	85 (EM4) (Oct. 1959)
Progress Report No. 5	86 (EM1) (Jan. 1960)
Progress Reports No. 6 and No. 7	86 (EM2) (April 1960)

17. Driscoll, G. C., Jr.
ROTATION CAPACITY REQUIREMENTS FOR BEAMS AND PORTAL FRAMES, Ph.D. Dissertation, Lehigh University, 1958.

18. AISC
PLASTIC DESIGN IN STEEL, American Institute of Steel Construction, New York, 1959.

19. Kusuda, T.; Sarubbi, R.G.; Thürlimann, B.
THE SPACING OF LATERAL BRACING IN PLASTIC DESIGN, Fritz Engineering Laboratory Report No. 205E.11, Lehigh University, 1960.

20. Tall, L.; Ketter, R. L.
ON THE YIELD PROPERTIES OF STRUCTURAL STEEL SHAPES, Fritz Engineering Laboratory Report No. 220A.33, Lehigh University, 1958.

21. Haaijer, G.; Thürlimann, B.
ON INELASTIC BUCKLING IN STEEL, Proceedings of the American Society of Civil Engineers, 84, (EM2), (April 1958).

22. AISC
STEEL CONSTRUCTION HANDBOOK, American Institute of Steel Construction, N.Y., 1955.

23. Huber, A. W.; Beedle, L. S.
RESIDUAL STRESS AND THE COMPRESSIVE STRENGTH OF STEEL, Welding Journal, Vol. 33, No. 12 p. 589-s (1954).

24. Fujita, Y.
BUILT-UP COLUMN STRENGTH, Ph.D. Dissertation, Lehigh University, 1956.

25. Huber, A. W.
THE INFLUENCE OF RESIDUAL STRESS ON THE INSTABILITY OF COLUMNS, Ph.D. Dissertation, Lehigh University, 1956.

26. Beedle, L. S.; Tall, L.
BASIC COLUMN STRENGTH, Proceedings of the American Society of Civil Engineers, Vol. 86, No. ST7, (July 1960).

27. Ketter, R. L.
INFLUENCE OF RESIDUAL STRESS ON THE STRENGTH OF STRUCTURAL MEMBERS, Welding Research Council, Bulletin No. 44, Nov. 1958.

28. Feder, D. K.; Lee, G. C.
RESIDUAL STRESSES IN HIGH STRENGTH STEEL, Fritz Engineering Laboratory Report No. 269.2, Lehigh University, April 1959.

29. Beedle, L. S.
ON THE APPLICATION OF PLASTIC DESIGN, Paper presented at the Second Symposium of Naval Structural Mechanics, Brown University, (April 1960).

30. Ketter, R. L.; Kaminsky, E. L., Beedle, L. S.
PLASTIC DEFORMATION OF WIDE-FLANGE BEAM-COLUMNS, Transactions of the American Society of Civil Engineers, Vol. 120, p. 1028 (1955).

31. Neal, B. G.
THE LATERAL INSTABILITY OF YIELDED MILD STEEL BEAMS OF RECTANGULAR CROSS SECTION, Philosphical Transactions of the Royal Society, 242, (846) pp. 197-242, (January 1950).

32. Shanley, F. R.
APPLIED COLUMN THEORY, Transactions of the American Society of Civil Engineers, Vol. 115, p. 698 (1950).

33. Column Research Council
GUIDE TO DESIGN CRITERIA FOR METAL COMPRESSION MEMBERS, Column Research Council,(September 1960).

34. Baker, J. F.; Horne, M. R.; Heyman, J.
THE STEEL SKELETON, Vol. II, Cambridge University Press, 1956.

35. Timoshenko, S.; MacCullough, G. H.
ELEMENTS OF STRENGTH OF MATERIALS, Van Nostrand, 3rd edition, 1949.

36. von Kármán, Th.; Chien, W. Z.
TORSION WITH VARIABLE TWIST, Journal of the Aeronautical Science, Vol. 13, 1946.

37. Niles, A. S.; Newell, J. S.
AIRPLANE STRUCTURES, Vol. II, 3rd edition, John Wiley & Sons, Inc., New York, 1943.

38. Thürlimann, B.
NEW ASPECTS CONCERNING INELASTIC STABILITY OF STEEL STRUCTURES, Proceedings of the American Society of Civil Engineers, Vol. 86, No. ST1 (January 1960).

39. Prager, W.; Hodge, P. G., Jr.
THEORY OF PERFECTLY PLASTIC SOLIDS, John Wiley & Sons, Inc., New York, 1951.

40. Salvadori, M. G.
LATERAL BUCKLING OF I-BEAMS, Transactions of the American Society of Civil Engineers, 120, p. 1165, (1955).

41. Austin, W. J.; Yegian, S.; Tung, T. P.
LATERAL BUCKLING OF ELASTICALLY END-RESTRAINED I-BEANS, Transactions of the American Society of Civil Engineers, 122, (2866), p. 374, (1957).

42. Solvey, J.
THE LATERAL INSTABILITY IN THE ELASTIC RANGE OF BEAMS WITH MIXED END CONDITIONS, Department of Supply, Research and Development Branch, Aeronautical Research Laboratory Report SM, 256, Melbourne, Australia, January 1958.

43. Kerensky, O.A. ; Flint, A.R.; Brown, W.C.
THE BASIS FOR DESIGN OF BEAMS AND PLATE GIRDERS IN THE REVISED BRITISH STANDARD,Proceedings of the Institution of Civil Engineers, Part III, 5, p. 396, England, (1956).

44. Clark, J. W. ; Jombock, J.R.,Jr.
LATERAL BUCKLING OF I-BEAMS SUBJECTED TO UNEQUAL END MOMENTS, Proceedings of the American Society of Civil Engineers, Engineering Mechanics Division, 83, (EM3), (July 1957).

45. Dumont, C.; Hill, H.N.
THE LATERAL STABILITY OF EQUAL FLANGED ALUMINUM ALLOY I-BEAMS SUBJECTED TO PURE BENDING, Technical Note 279, National Advisory Committee for Aeronautics, 1940.

46. Flint, A. R.
THE STABILITY AND STRENGTH OF SLENDER BEAMS, Engineering, 170, p. 545, England, (1950).

47. Flint, A.R.
THE LATERAL STABILITY OF UNRESTRAINED BEAMS, Engineering, 173, pp. 65, 99, England, (1952).

48. Winter, G.; Lansing, W.; McCalley, R.B.
PERFORMANCE OF LATERALLY LOADED BEAMS, Engineering Structures Supplement Colston Papers, II, p. 179, London, (1949).

49. Hill, H.N.
LATERAL BUCKLING OF CHANNELS AND Z-BEAMS Transactions of the American Society of Civil Engineers, 119, (2700), p. 829, (1954).

50. Hill, H.N.
THE LATERAL INSTABILITY OF UNSYMMETRICAL I-BEAMS, Journal of Aeronautical Science, 9, p. 175, (March 1942).

51. Hechtman, R.A.; Hattrup, J.M.; Styer, E.F.; Tiedemann, J.L.
LATERAL BUCKLING OF ROLLED STEEL BEAMS, Proceedings of the American Society of Civil Engineers, (797), (September 1955).

52. de Vries, K.
STRENGTH OF BEAMS AS DETERMINED BY LATERAL BUCKLING, Transactions of the American Society of Civil Engineers, 112, p. 1245, (1947).

53. Winter, G.
Discussion on STRENGTH OF BEAMS AS DETERMINED BY LATERAL BUCKLING, Transactions of the American Society of Civil Engineers, 112, p. 1245, (1947).

54. Clark, J.W.; Hill, H.N.
LATERAL BUCKLING OF BEAMS, Proceedings of the American Society of Civil Engineers, Vol. 86, No. ST7 (July 1960).

55. Lee, G.C.; Ueda, Y.
SURVEY ON LATERAL BUCKLING EXPERIMENTS, Fritz Engineering Laboratory Report No. 205H.4, Lehigh University (in preparation).

56. Driscoll, G.C.,Jr.; Beedle, L.S.
THE PLASTIC BEHAVIOR OF STRUCTURAL MEMBERS AND FRAMES, Welding Journal 36 (6) Research Supplement 275-S (1957).

57. Sawyer, H.A.,Jr.; Weitsman, Y.
THE POST-ELASTIC BEHAVIOR OF ROLLED-STEEL SECTIONS SUBJECTED TO MOMENTS WITH CONSTANT GRADIENT, Progress Report, Department of Civil Engineering, University of Connecticut, Storrs, Connecticut, (November 1959).

58. Haaijer, G.
PLSTE BUCKLING IN THE STRAIN-HARDENING RANGE, Proceedings of the American Society of Civil Engineers, 83, (EM2), (April 1957).

59. Sproull, R.L.
MODERN PHYSICS, John Wiley & Sons, Inc., New York, 1956.

60. Nadai, A.
THEORY OF FLOW AND FRACTURE OF SOLIDS, McGraw-Hill Book Co., New York, 1950.

61. Bethlehem Steel Company
BETHLEHEM MANUAL OF STEEL CONSTRUCTION, Bethlehem Steel Co., Bethlehem, Penna., 1934.

62. Galambos, T.V.;Ketter, R.L.
COLUMNS UNDER COMBINED BENDING AND THRUST, Proceedings of the American Society of Civil Engineers, Vol. 85, No. EM2, (April 1959).

63. Lee, G.C.; Fisher, J.W., Driscoll, G.C.,Jr.
BEHAVIOR OF HAUNCHED CONNECTIONS, Presented at the National Fall Meeting of the American Welding Society, September 1960.

64. Stüssi, F.
DIE STABILITAT DES AUF BIEGUNG BEANSPRUCHTEN TRÄGERS, International Association for Bridge and Structural Engineering, 3, p. 401, (1935).

65. Engle, H.L.
LATERAL BUCKLING OF BARS OF MONO-SYMMETRIC OPEN CROSS SECTION, Division of Engineering Mechanics, Stanford University, Technical Report No. 8, 1950.

66. Winter, G.
LATERAL STABILITY OF UNSYMMETRICAL I-BEAMS AND TRUSS IN BENDING, Transactions of the American Society of Civil Engineers, 108, p. 247, (1943).

67. Schrader, R.E.
Discussion of LATERAL STABILITY OF UNSYMMETRICAL I-BEAMS AND TRUSS IN BENDING, Transactions of the American Society of Civil Engineers, 108, p.247, (1943).

68. Winter, G.; Zetlin, L.
UNSYMMETRICAL BENDING OF BEAMS WITH AND WITHOUT LATERAL BRACING, Proceedings of the American Society of Civil Engineers, 81, paper No. 774, (1955).

69. Flint, A. R.
THE STABILITY OF BEAMS LOADED THROUGH SECONDARY MEMBERS, Civil Engineering and Publishing Works Review, 46, p. 175, England, (March 1951).

70. Cozzone, F. P.
BENDING STRENGTH IN THE PLASTIC RANGE, Journal of Aeronautical Science, 10, (5) pp. 137-151, (May 1943).

71. Williams, H. A.
INVESTIGATION OF PURE BENDING IN PLASTIC RANGE WHEN LOADS ARE NOT PARALLEL TO PRINCIPAL PLANE, Technical Note 2287, National Advisory Committee for Aeronautics, 1951.

72. Barrett, A. J.
UNSYMMETRICAL BENDING AND BENDING COMBINED WITH AXIAL LOADING OF BEAM OF RECTANGULAR CROSS SECTION INTO THE PLASTIC RANGE, Journal of the Royal Aeronautical Society, London, 57, p. 503, (1953).

73. Holland, F. L.; Egger, W.; Mayerjak, R.J.; Munz, R.J.
STATIC AND DYNAMIC LOAD-DEFLECTION TESTS OF STEEL STRUCTURES, Civil Engineering Studies, Structural Research Series No. 92, University of Illinois, 1954.

74. Aghbabian, M.S.; Popov, E.P.
UNSYMMETRICAL BENDING OF RECTANGULAR BEAMS BEYOND THE ELASTIC LIMIT, Proceedings of the First U.S. National Congress of Applied Mechanics, p. 579, (1951).

75. Bethlehem Steel Company
TORSIONAL STRESSES IN STRUCTURAL BEAMS, Bethlehem Steel Company Booklet S-57, Bethlehem, Pennsylvania, 1950.

76. Basler, K.; Thűrlimann, B.
BUCKLING PROBLEMS IN PLATE GIRDERS SUBJECTED TO BENDING, Presented at the Annual Convention of the American Society of Civil Engineers in Washington D.C. (October 1959).

77. Basler, K.; Yen, B.T.; Mueller, J.A.; Thűrlimann, B.
WEB BUCKLING TESTS ON WELDED PLATE GIRDERS, To be published as a Welding Research Bulletin, 1960.

78. Ojalvo, M.
RESTRAINED COLUMNS, Ph. D. Dissertation, Lehigh University, 1960.

79. Wittrick, W.H.
LATERAL INSTABILITY OF RECTANGULAR BEAMS OF STRAIN-HARDENING MATERIAL UNDER UNIFORM BENDING, Journal of Aeronautical Science, 19, (12) p. 835, (Dec. 1952).

11. V I T A

The author was born in Peiping, China on July 17, 1933, the first child of Dr. and Mrs. S. C. Lee.

He graduated from the High School of the Taiwan Normal University in Taipei, Taiwan in June 1951. He then attened the National Taiwan University from September 1951 to June 1955. There he completed the requirements of the Department of Civil Engineering and was awarded the degree of Bachelor of Science in Engineering in June 1955.

Upon graduation he joined the Engineering Corps of the Air Force of the Republic of China for a period of one year, he was commissioned as a second lieutenant in September 1956.

He was appointed to a research fellowship at Fritz Engineering Laboratory, Lehigh University, Bethlehem, Pennsylvania in September 1956, and to a research assistantship in April, 1957 and was associated with the project on residual stresses and column instabilities. He was awarded the degree of Master of Science in Civil Engineering in February 1958.

He became a research associate at Fritz Engineering Laboratory in July 1959 and has been associated mainly with the research of lateral bracing requirements in plastic design.